

VOLUME 78 SEPTEMBER 26, 1974 NUMBER 20

JPCA X

THE JOURNAL OF

PHYSICAL
CHEMISTRY

PUBLISHED BIWEEKLY BY THE AMERICAN CHEMICAL SOCIETY

THE JOURNAL OF PHYSICAL CHEMISTRY

BRYCE CRAWFORD, Jr., *Editor*

WILMER G. MILLER, *Associate Editor*

ROBERT W. CARR, Jr., **FREDERIC A. VAN-CATLEDGE,** *Assistant Editors*

EDITORIAL BOARD: A. O. ALLEN (1970-1974), C. A. ANGELL (1973-1977), F. C. ANSON (1974-1978), V. A. BLOOMFIELD (1974-1978), J. R. BOLTON (1971-1975), L. M. DORFMAN (1974-1978), M. FIXMAN (1970-1974), H. S. FRANK (1970-1974), R. R. HENTZ (1972-1976), W. J. KAUZMANN (1974-1978), R. L. KAY (1972-1976), D. W. McCLURE (1974-1978), R. M. NOYES (1973-1977), J. A. POPLE (1971-1975), B. S. RABINOVITCH (1971-1975), H. REISS (1970-1974), S. A. RICE (1969-1975), F. S. ROWLAND (1973-1977), R. L. SCOTT (1973-1977), A. SILBERBERG (1971-1975), J. B. STOTHERS (1974-1978), W. A. ZISMAN (1972-1976)

AMERICAN CHEMICAL SOCIETY, 1155 Sixteenth St., N.W., Washington, D. C. 20036

Books and Journals Division

JOHN K CRUM *Director*

RUTH REYNARD *Assistant to the Director*

CHARLES R. BERTSCH *Head, Editorial Processing Department*

D. H. MICHAEL BOWEN *Head, Journals Department*

BACIL GUILLEY *Head, Graphics and Production Department*

SELDON W. TERRANT *Head, Research and Development Department*

©Copyright, 1974, by the American Chemical Society. Published biweekly by the American Chemical Society at 20th and Northampton Sts., Easton, Pa. 18042. Second-class postage paid at Washington, D. C., and at additional mailing offices.

All manuscripts should be sent to *The Journal of Physical Chemistry*, Department of Chemistry, University of Minnesota, Minneapolis, Minn. 55455.

Additions and Corrections are published once yearly in the final issue. See Volume 77, Number 26 for the proper form.

Extensive or unusual alterations in an article after it has been set in type are made at the author's expense, and it is understood that by requesting such alterations the author agrees to defray the cost thereof.

The American Chemical Society and the Editor of *The Journal of Physical Chemistry* assume no responsibility for the statements and opinions advanced by contributors.

Correspondence regarding accepted copy, proofs, and reprints should be directed to Editorial Processing Department, American Chemical Society, 20th and Northampton Sts., Easton, Pa. 18042. Department Head: CHARLES R. BERTSCH. Assistant Department Head: MARIANNE C. BROGAN. Assistant Editor: CELIA B. McFARLAND. Editorial Assistant: JOSEPH E. YURVATI.

Advertising Office: Centcom, Ltd., 50 W. State St., Westport, Conn. 06880.

Business and Subscription Information

Send all new and renewal subscriptions *with payment to* Office of the Controller, 1155 16th Street, N.W., Washington, D. C. 20036. Subscriptions should be renewed promptly to avoid a break in your

series. All correspondence and telephone calls regarding changes of address, claims for missing issues, subscription service, the status of records, and accounts should be directed to Manager, Membership and Subscription Services, American Chemical Society, P.O. Box 3337, Columbus, Ohio 43210. Telephone (614) 421-7230.

On changes of address, include both old and new addresses with ZIP code numbers, accompanied by mailing label from a recent issue. Allow four weeks for change to become effective.

Claims for missing numbers will not be allowed (1) if loss was due to failure of notice of change in address to be received before the date specified, (2) if received more than sixty days from date of issue plus time normally required for postal delivery of journal and claim, or (3) if the reason for the claim is "issue missing from files."

Subscription rates (1974): members of the American Chemical Society, \$20.00 for 1 year; to nonmembers, \$60.00 for 1 year. Those interested in becoming members should write to the Admissions Department, American Chemical Society, 1155 Sixteenth St., N.W., Washington, D. C. 20036. Postage to Canada and countries in the Pan-American Union, \$5.00; all other countries, \$6.00. Air freight rates available on request. Single copies for current year: \$3.00. Rates for back issues from Volume 56 to date are available from the Special Issues Sales Department, 1155 Sixteenth St., N.W., Washington, D. C. 20036.

Subscriptions to this and the other ACS periodical publications are available on microfilm. Supplementary material not printed in this journal is now available in microfiche form on a current subscription basis. For information on microfilm or microfiche subscriptions, write Special Issues Sales Department at the address above.

THE JOURNAL OF
PHYSICAL CHEMISTRY

Volume 78, Number 20 September 26, 1974

JPCHAx 78(20) 1979-2072 (1974)
ISSN 0022-3654

- Transfer of Vibrational Energy from Highly Excited Butyl Radicals. Relative Collision Diameters of Homologous *n*-Perfluoroalkane Bath Molecules. . . . R. C. Ireton and B. S. Rabinovitch* 1979
- Transfer of Vibrational Energy from Highly Excited Butyl Radicals. Structural Effects on the Magnitudes of Relative Collision Diameters R. C. Ireton, An-Nan Ko, and B. S. Rabinovitch* 1984
- Reaction of the Hydrated Electron with Benzene Studied by Pulse Radiolysis D. G. Marketos,* Anastasia Marketou-Mantaka, and Gabriel Stein 1987
- Catalyzed and Uncatalyzed Dissolution of Anhydrous Chromic Chloride in Aqueous Solutions A. Hendifar, W. F. Libby,* and George L. Zimmerman 1993 ■
- Equilibrium Vaporization Rates and Vapor Pressures of Solid and Liquid Sodium Chloride, Potassium Chloride, Potassium Bromide, Cesium Iodide, and Lithium Fluoride Curtis T. Ewing and Kurt H. Stern* 1998 ■
- Optical Saturation and Quenching Effects in the Triplet State of Rhodamine 6G at 77°K Mikio Yamashita* and Hiroshi Kashiwagi 2006
- Mechanism of Fluorescence Quenching by Acids in Poly(*N*-vinylcarbazole) G. Pfister, D. J. Williams,* and G. E. Johnson 2009
- Electron Spin Resonance Studies of Fluoroalkyl Radicals in Solution. I. Structures, Conformations, and Barriers to Hindered Internal Rotation Kuang S. Chen, Paul J. Krusic,* Paul Meakin, and Jay K. Kochi* 2014
- Electron Spin Resonance Studies of Fluoroalkyl Radicals in Solution. II. Adducts to Fluoroolefins Kuang S. Chen, Paul J. Krusic,* and Jay K. Kochi* 2030
- Electron Spin Resonance Studies of Fluoroalkyl Radicals in Solution. III. Photolysis to Perfluoroketones and Adduct Formation Paul J. Krusic,* Kuang S. Chen, Paul Meakin, and Jay K. Kochi* 2036
- Electron Spin Resonance Measurement of Ammonia Condensed at 77°K after Reaction with Discharge Products and after High-Frequency Discharge F. W. Froben 2047
- Computer-Recorded Gouy Interferometric Diffusion and the Onsager-Gosting Theory T. A. Renner and P. A. Lyons* 2050
- Structure, Energetics, and Dynamics of the Water Dimer Lester L. Shipman, John C. Owicki, and Harold A. Scheraga* 2055
- Charge Neutrality in Electrolytic Solutions and the Liquid Junction Potential. . . . Julius L. Jackson 2060
- Statistical Thermodynamic Consideration of Solvent Effects on Conformational Stability. The Supermolecule-Continuum Model David L. Beveridge* and Gary W. Schnuelle 2064

ห้องสมุด กรมวิทยาศาสตร์
20 ธ.ค. 2517

COMMUNICATIONS TO THE EDITOR

Surface Acidity of Co-Mo-Al ₂ O ₃ Catalysts	P. Ratnasamy,* D. K. Sharma, and L. D. Sharma	2069
Surface Acidity of Modified Alumina	L. Petrakis* and F. E. Kiviat	2070
2537-Å Mercury-Sensitized Photochemical Decomposition of Perfluorocyclobutane	Rodney L. Cate and T. C. Hinkson*	2071

■ Supplementary material for this paper is available separately, in photocopy or microfiche form. Ordering information is given in the paper.

* In papers with more than one author, the asterisk indicates the name of the author to whom inquiries about the paper should be addressed.

AUTHOR INDEX

Beveridge, D. L., 2064	Jackson, J. L., 2060	Marketos, D. G., 1987	Scheraga, H. A., 2055
Cate, R. L., 2071	Johnson, G. E., 2009	Marketou-Mantaka, A., 1987	Schnuelle, G. W., 2064
Chen, K. S., 2014, 2030, 2036	Kashiwagi, H., 2006	Meakin, P., 2014, 2036	Sharma, D. K., 2069
Ewing, C. T., 1998	Kiviat, F. E., 2070	Owicki, J. C., 2055	Sharma, L. D., 2069
Froben, F. W., 2047	Ko, A.-N., 1984	Petrakis, L., 2070	Shipman, L. L., 2055
Hendifar, A., 1993	Kochi, J. K., 2014, 2030, 2036	Pfister, G., 2009	Stein, G., 1987
Hinkson, T. C., 2071	Krusic, P. J., 2014, 2030, 2036	Rabinovitch, B. S., 1979, 1984	Stern, K. H., 1998
Ireton, R. C., 1979, 1984	Libby, W. F., 1993	Ratnasamy, P., 2069	Williams, D. J., 2009
	Lyons P. A., 2050	Renner, T. A., 2050	Yamashita, M., 2006
			Zimmerman, G. L., 1993

THE JOURNAL OF PHYSICAL CHEMISTRY

Registered in U. S. Patent Office © Copyright, 1974, by the American Chemical Society

VOLUME 78, NUMBER 20 SEPTEMBER 26, 1974

Transfer of Vibrational Energy from Highly Excited Butyl Radicals. Relative Collision Diameters of Homologous *n*-Perfluoroalkane Bath Molecules^{1a}

R. C. Ireton^{1b} and B. S. Rabinovitch*

Department of Chemistry, University of Washington, Seattle, Washington 98195 (Received May 2, 1974)

Publication costs assisted by the Office of Naval Research

Vibrationally excited *n*-butyl-2 radicals at an average energy of ~ 43 kcal mol⁻¹ were prepared by chemical activation. Collisional deexcitation by a homologous series of perfluoro-*n*-alkane bath molecules, CF₄ to C₈F₁₈, as well as by CH₄ and *cis*-C₄H₈-2 was studied at 298 and 195°K. Increments in collision diameter $\Delta s(\text{CF}_2)$ were determined per CF₂ group. Relative collision diameters referenced to *cis*-butene-2 were measured. Comparison of results at both temperatures indicates that collisional deactivation efficiencies, $\beta_c(M)$, are less than unity for the smallest molecules. The temperature dependence of collision diameters does not follow the prediction based on the Lennard-Jones 6-12 potential.

Introduction

This paper is part of a continuing study of vibrational energy transfer between highly excited complex polyatomic molecules and various types of heat bath species. Our earliest efforts involved the use of chemical activation to produce vibrationally excited species having energies within a relatively narrow, well-defined region of energy. In these systems, a reaction event is in competition with vibrational deactivation by collisional transfer of energy to a bath gas. From a theoretical knowledge of the reaction event, and from measured values of the decomposition/stabilization ratio, information can be obtained concerning the nature of the deactivation process, including relative collision cross sections, collisional efficiency, and the form of the collisional transition probability distribution. Results have been obtained by this method both from single-channel unimolecular decomposition systems² and from competitive multichannel systems.³

The second principal source of information we have pursued has been collisional activation in low-pressure thermal unimolecular systems. Much of the work in this area (which has actually been active for almost 50 years) has tended to be incomplete and has been disconnected from cogent qualitative and quantitative considerations of experimental design and interpretation. A notable exception has been the pioneering contributions by Johnston and coworkers⁴ of the early 1950's which initiated quantitative examina-

tion of this subject. Recently, we have described theoretical^{5,6} and experimental⁷ studies of thermal systems which provide quantitative information concerning inert gas efficiencies. In particular, a method was devised for determining relative collision cross sections of bath molecules, for identifying the smallest member of a homologous series at and above which unit collisional efficiency (*i.e.*, satisfaction of the appropriate *operational* criteria for strong collision behavior) is attained, and for defining the relation between molecular geometry of structural isomers and collision cross sections.^{7a} This work involved highly polar methyl isocyanide ($\mu \approx 4$ D) substrate and various paraffinic alkane, alkene, alkyne, and perfluoroalkane bath molecules.^{7c}

In the present paper we have attempted to broaden the experimental basis of this phenomenon by measuring the cross sections of various fluoroalkane bath species for deactivation of an excited nonpolar substrate in a chemical activation system. In some of the earlier systems mentioned above, the activation was *via* H-atom addition to an olefin to form the relatively nonpolar, vibrationally excited alkyl radical. In order to minimize complications due to radical isomerization, and because *sec*-butyl decomposition has been very well studied, *cis*-butene-2 was chosen as the substrate olefin. This choice also eliminates the possibility of anti-Markovnikoff addition to the double bond. A series of bath gases has been examined. This series consists of the homologous perfluoro-*n*-alkanes, C₁ through C₈.

Experimental Section

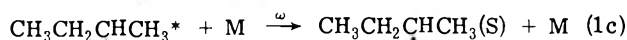
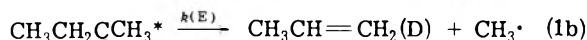
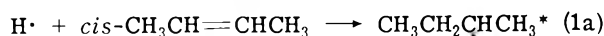
Materials. Phillips research grade *cis*-butene-2 was purified by gas chromatography until completely free of impurities. The perfluoroalkanes were obtained from P.C.R. Inc. and were further purified by gas chromatography. Ultrapure H₂ from Airco was passed through a silica trap at 77°K. The condensable gases were subjected to a freeze-pump-melt degassing procedure before use.

Apparatus and Procedure. A conventional greaseless Pyrex vacuum system was employed,⁸ and runs were carried out in a 12-l. reactor at 300°K and a 2-l. reactor at 195°K, each fitted with a Wood-Bonhoeffer discharge tube which carried a small slit through which H atoms effused into the reactor at a leak rate of ~15 μ/hr. Pressure in the discharge was maintained at ~0.8 Torr by a flow system. Mixtures of the substrate *cis*-butene-2 and perfluoroalkane bath molecules were made up in the proportion of ~1:80 for lighter molecules (C₁ to C₃) and ~1:25 for C₄ to C₈. The average run times varied from 0.25 to 2 hr, and average depletion of substrate was 6%.

Analysis. The reaction products were removed from the reactor with hydrogen sweep gas and were analyzed by gas chromatography using a flame ionization detection. The hydrocarbon products were separated from the bath gas on a 5% squalane column in series with a 40% AgNO₃ in glycol column. Two aliquots from each reaction were analyzed; the first on a 12-ft AgNO₃-ethylene glycol in series with a 12-ft squalane column 0.187 in. diameter; and the second on a 100-ft support-coated (SCOT) 0.02-in. squalane column, with temperature programming.

Results

The chemical activation system used is represented by the equations^{2a,9}



The minimum internal energy of the activated butyl radical (B) is 40.4 kcal mol⁻¹. This energy is sufficient to produce carbon-carbon bond rupture and leads to the decomposition product propylene (D) in (1b). The foregoing process is in competition with collisional energy transfer to heat bath molecules (M) which stabilizes the active butyl radical (S), as in (1c). Once stabilized, the radical undergoes typical disproportionation and combination reactions which provide a measure of S. The rate constant for the process characterized by reaction 1 is given by^{9a} $k_a = \beta_c(\text{M})\omega(\text{D}/\text{S})$, where $\beta_c(\text{M})$ is the effective collision efficiency on a collision-per-collision basis of collision partner M relative to the strong collider behavior of the 2-butene substrate for which $\beta_c(\text{B}) = 1$; ω is the collision frequency of B given by $p_{\text{M}}s_{\text{BM}}^2(8\pi/kT\mu_{\text{BM}})^{1/2}$; and s_{BM}^2 is the effective hard-sphere collision diameter of B and M. Then

$$S/D = 8\pi kT p_{\mu} \beta_c(\text{M}) s_{\text{BM}}^2 / k_a \quad (2)$$

where $p_{\mu} = p_{\text{M}}/(\mu_{\text{BM}})^{1/2}$ is a reduced mass-corrected pressure. Thus, a linear relationship exists (Figures 1 and 2) between S/D and p_{μ} , the slope of which is a measure of $\beta_c(\text{M})s_{\text{BM}}^2$. Relative to a suitable standard collision pair, taken as butyl-butene (BB), the cross section for any other pair s_{BM}^2 is found from the relation

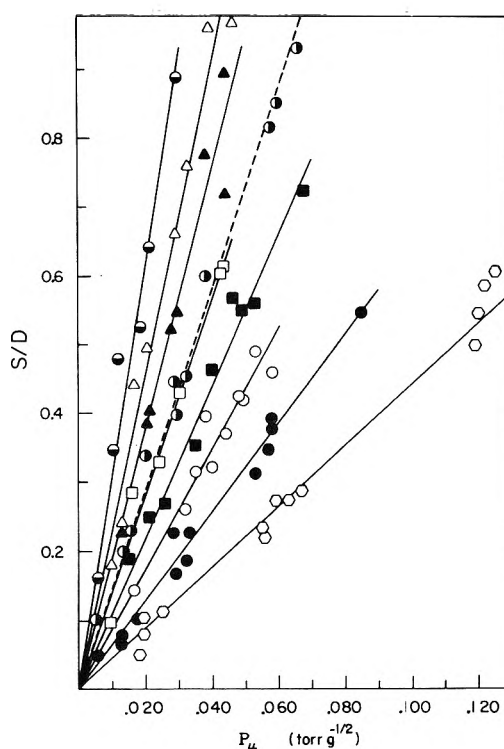


Figure 1. A plot of S/D vs. p_{μ} at 300°K for butyl radical decomposition in the presence of the following bath gases: CF₄ (●); C₂F₆ (○); C₃F₈ (■); C₄F₁₀ (□); C₅F₁₂ (▲); C₆F₁₄ (△); C₈F₁₈ (○); *cis*-C₄H₈ (○); and CH₄ (○). The lines represent least-squares fit constrained to have zero intercept; the dashed line gives the parent butene behavior.

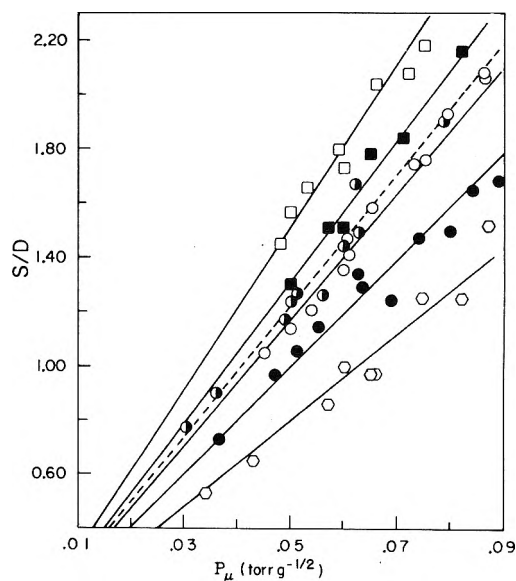


Figure 2. A plot of S/D vs. p_{μ} at 195°K for butyl radical decomposition. The symbols are as described in Figure 1.

$$s_{\text{BM}}^2 = s_{\text{BB}}^2 (\text{slope}_{\text{BM}} / \beta_c(\text{M}) \text{slope}_{\text{BB}}) \quad (3)$$

provided $\beta_c(\text{B}) = 1$. This condition seems the case at room temperature and below, as shown by earlier studies of alkylbutyl radicals,^{1b} and from related thermal energy transfer systems which utilized several homologous series as bath gases.⁷ Georgakakos, *et al.*,¹⁰ have given $\beta_c(\text{M}) = 0.85$ for CF₄, so that $\beta_c(\text{M}) \approx 1.00$ would be expected for C₂F₆

TABLE I: Summary of Experimental Quantities (Å) at 298°K

Bath gas	Slope _{BM} /slope _{BB}	This work		Ref 7c ^a		Viscosity values σ _M
		s _{BM} ^b	σ _M ^b	s _{AM}	σ _M	
CF ₄	0.443 ± 0.049	4.89 (5.39) ^c	3.23 (4.10) ^c			4.20 ^d
C ₂ F ₆	0.602 ± 0.059	5.21 (5.91) ^c	3.63 (4.81) ^c	5.59 ^e	4.28	5.01 ^d
C ₃ F ₈	0.760 ± 0.075	5.86 (6.17) ^c	4.63 (5.16) ^c	6.08	4.99	
C ₄ F ₁₀	0.991 ± 0.018	6.69	5.89	6.51	5.59	
C ₅ F ₁₂	1.304 ± 0.089	7.67	7.39	6.87	6.08	7.36 ^d
C ₆ F ₁₄	1.571 ± 0.220	8.43	8.58	7.27	6.67	8.05 ^d
C ₈ F ₁₈	2.102 ± 0.32	9.74	10.56			
<i>cis</i> -C ₄ H ₈	(1.00)	(6.72)	(5.51)	6.75	5.56	5.51 ^f
CH ₄	0.313 ± 0.046	4.86 (5.32) ^c	3.08 (3.86) ^c	5.26	3.77	3.76 ^g

^a As corrected in text. ^b Obtained using β_c(CH₄) = 0.60, β_c(CF₄) = 0.85, and β_c(M) = 1.00 for C₂ and higher homologs to determine s_{BM}, together with the Lennard-Jones values for Ω_{BM}^{22*}(T*) at 298°K (Appendix I) to obtain σ_{BM}. ^c Obtained using the value of β_c(M) determined as in footnote b, Table II, together with the value of Ω_{BM}^{22*} (Appendix I) to obtain σ_{BM}. ^d Reference 9. ^e Extrapolated from higher homologs in this series. ^f L. W. Flynn and G. Thodos, *AIChE J.*, 8, 362 (1962). ^g R. A. Svehla, NASA Technical Report No. R-132, p 34, 1962.

TABLE II: Experimental Slopes and Collision Diameters (Å) Measured at 195°K and Collisional Efficiencies β_c(M)(298°K) Based on Eq 6

Bath gas	Slope _{BM} /slope _{BB}	s _{BM}	β _c (M)	s _{BM} ¹⁹⁵ /s _{BM} ²⁹⁸
CF ₄	0.807 ± 0.073	6.74	0.55 ^a (0.70) ^b	1.109 ^c (1.244) ^b
C ₂ F ₆	0.961 ± 0.047	7.35	0.63 (0.80) ^b	1.110 (1.244)
C ₃ F ₈	1.073 ± 0.027	7.78	0.71 (0.90) ^b	1.114 (1.244)
C ₄ F ₁₀	1.227 ± 0.040	8.30	0.81 (1.00) ^b	1.112 (1.244)
<i>cis</i> -C ₄ H ₈	(1.00)	7.50	1.00	1.116
CH ₄	0.646 ± 0.034	6.03	0.50	1.109

^a β_c(M) values determined from eq 6 using the Lennard-Jones ratio of Ω_{BM}^{22*} integrals and β_c(M) = 1 at 195°K. ^b β_c(M) values determined from eq 6 using a corrected value for Ω_{BM}^{22*} at 195°K such that the ratio of Ω_{BM}^{22*} integrals makes β_c(C₄F₁₀) equal to 1.00 at both temperatures; this ratio is the parenthetic quantity in the adjoining column and is, of course, also the resulting value of the s² ratio. ^c Based on theoretical Ω integral ratio.

and higher members. These values of β_c(M) were used in the determination of the room temperature values of s_{BM} given in Table I. However, in order to test the validity of these values of β_c(M), studies were also performed at 195°K and the experimental s_{BM}, as well as calculated room temperature values of β_c(M), are given in Table II.

Discussion

Room Temperature Data. In order to compare more directly the present experimental results for the butyl radical (B) with those obtained at 553°K for fluoroalkane bath gases in the thermal methyl isocyanide (A) system,^{7c} it is desirable to apply a correction factor to the data in ref 7c which takes into consideration the temperature difference between the two systems, as well as changes in the ε_{AM} and σ_{AM} constants due to the different substrates A and B employed as references. Using the relation,^{2a,11} s² = σ²Ω^{22*}(T*), then

$$s_{AM}(\text{corr}) = s_{AM} \left[\frac{\Omega_{BM}^{22*}(T_{BM}^*)}{\Omega_{AM}^{22*}(T_{AM}^*)} \right]^{1/2} \sigma_{BM} / \sigma_{AM} \quad (4)$$

where the Ω^{22*} integrals are a tabulated function¹¹ of the reduced temperature, T_{AM}* = kT/ε_{AM} and T_{BM}* = kT/ε_{BM}, and ε_{AM} = (ε_Aε_M)^{1/2} and ε_{EM} = (ε_Bε_M)^{1/2}. (A discussion of the selection of ε_M values is given in the Appendix). The

σ_{BM} and σ_{AM} were found from the values in ref 7c with use of the relation

$$\sigma_{AM} = (\sigma_A + \sigma_M)/2 \text{ and } \sigma_{BM} = (\sigma_B + \sigma_M)/2 \quad (5)$$

σ_B for butyl was arbitrarily assigned the same value as for butane, 5.23 Å.

The values of s_{AM}(corr) are found in Table I; the value for C₂F₆ is our estimate based on extrapolation down to n = 2 of the available experimental s_{AM} values for higher homologs, C_nF_{2n+2}. Agreement may be seen to be fairly good between s_{AM}(corr) from ref 7c and the present work with regard to magnitudes of the several values; so that no gross change results, nor need be expected for polar-nonpolar molecular interaction upon passage from MeNC (μ ~ 4 D) to C₄H₉ (μ ~ 0).

The incremental changes Δs(CF₂) from member to member in both series are more disparate; the average increment Δs_{BM} is 0.75 Å (excluding the CF₄-C₂F₆ difference) while Δs_{AM}(corr) is 0.42 Å. However, an amelioration of the discrepancy can be made: the correction applied to s_{AM} to reduce the experimental values to room temperature does not reflect adequately the temperature variation for fluoro-carbon species; indeed, it will be evident from the present low-temperature results (below) that the temperature dependence of s_{BM} is not accurately predicted by the Lennard-Jones correlation, and a somewhat larger correction is expected based on our experimental low-temperature data.

Using this factor in the treatment applied to transpose the data in ref 7c to room temperature, Δs_{AM} then becomes¹² ~ 0.50 Å, which, although low, is in better agreement with the present data. Moreover, if the values of $\beta_c(M)$ determined with the aid of the low-temperature data are used, a new set of s_{BM} (Table I, parenthetic quantities) is obtained for which the average increment is only $\Delta s_{BM} = 0.60$. The disparity of values for Δs_{CF_2} in these two systems lies within the uncertainty of the overall precision available in the two experimental techniques.

Low-Temperature Data. Experiments at 195°K were performed for two reasons: first, to help eliminate uncertainties in the choice of the room temperature values of $\beta_c(M)$ for the less efficient gases, CH₄, CF₄, and C₂F₆; second, to obtain an experimental measure of the variation with temperature of the collision diameter for energy transfer by the more efficient gases.

The hydrocarbons studied at low temperature were CH₄ and C₄H₈. The reference collision diameter at 195°K, s_{BB} for the butyl-butene pair, was assigned a value of 7.50 Å, based on a Lennard-Jones extrapolation from room temperature, $s_{BB}^{195} = s_{BB}^{298}[\Omega_{BB}^{22^*}(195)/\Omega_{BB}^{22^*}(298)]^{1/2}$, assumed valid for hydrocarbons. The requirement that the Lennard-Jones predicted collision diameter should equal the experimental quantity for these species leads to the following relation between $\beta_c(M)$ at 298 and at 195°K,

$$\beta_c^{298}(M)/\beta_c^{195}(M) = (R_{298}/R_{195})(\Omega_{BM}^{22}(195)/\Omega_{BM}^{22}(298))/(\Omega_{BB}^{22}(195)/\Omega_{BB}^{22}(298)) \quad (6)$$

where $R_{298} = \text{slope}_{BM}/\text{slope}_{BB}$ at 298°K, and $R_{195} = \text{slope}_{BM}/\text{slope}_{BB}$ at 195°K, and are the experimental quantities measured at the two temperatures. The ratio of Ω integrals for BM and BB give the temperature dependence of s_{BM} and s_{BB} , respectively. From this, a value of $\beta_c^{298}(M)/\beta_c^{195}(M) = 0.50$ for CH₄ is obtained.

Previous workers^{2b} have shown that $\beta_c(M)$ for the noble gases increases with decreasing temperature in the butyl-2 system. This suggests a plausible choice of $\beta_c(\text{CH}_4) = 1.0$ at 195°K; *a fortiori*, $\beta_c(M) = 1.00$ for C₄H₈ at 195°K.

An absolute value of $\beta_c(M)$ for CH₄ has been measured at 298°K in the pentyl-2 chemical activation system by the low-pressure turn up method;¹⁰ this technique is independent of the value of the collision diameter and gave the result that $0.52 < \beta_c(\text{CH}_4) < 0.72$. The value for CH₄ in the present work (0.5) is easily within experimental error of the range of values for this gas in ref 10.

Predicted values of s_{BM} at 195°K were also calculated from the room temperature results, as above, with $s_{BM}^{195} = s_{BM}^{298}[\Omega_{BM}^{22^*}(195)/\Omega_{BM}^{22^*}(298)]^{1/2}$, and uniformly gave s_{BM} quantities less than the experimentally measured ones. For the lower members of the series, as we saw for CH₄, this comparison also depends on the choice of $\beta_c(M)$ used in the determination of the room temperature s_{BM} values, as well as on the Ω integral ratio.

If the value of $\beta_c(\text{CH}_4)$, the least efficient gas for this series, is unity at 195°K then $\beta_c(M)$ for CF₄, C₂F₆, etc., are expected also to be unity at 195°K. Efficiencies at 298°K can then be deduced from eq 6 (Table II) and result in $\beta_c(\text{CF}_4) = 0.55$, $\beta_c(\text{C}_2\text{F}_6) = 0.63$, $\beta_c(\text{C}_3\text{F}_8) = 0.71$, and $\beta_c(\text{C}_4\text{F}_{10}) = 0.81$. These values of $\beta_c(M)$ lead to $s_{B,CF_4} = 6.04$ Å, $s_{B,C_2F_6} = 6.57$ Å, $s_{B,C_3F_8} = 6.95$ Å, and $s_{B,C_4F_{10}} = 7.43$ Å, all of which appear too large in relation to s_{AM} and to the next member of the series, *i.e.*, $s_{B,C_5F_{12}} = 7.67$ Å. Indeed, there is

no reason to believe that $\beta_c(M)$ for C₄F₁₀ should be less than unity at 298°K.^{7c}

This discrepancy can be explained on the basis that although the assumed variation of s_{BM} with temperature, namely, $\Omega_{BM}^{22^*}(195)/\Omega_{BM}^{22^*}(298)$, is valid for hydrocarbons, the same is not true for fluorocarbons. Given that $\beta_c(M) = 1.0$ for C₄F₁₀, then $[\Omega_{BM}^{22^*}(195)/\Omega_{BM}^{22^*}(298)]^{1/2}$, must have the value 1.244, rather the theoretical value 1.109. We proceed from here as before but using the quantity 1.244 in the relation for $[\beta_c^{298}(M)/\beta_c^{195}(M)]^{1/2}$. The resulting values of efficiency are $\beta_c(\text{CF}_4) = 0.70$, $\beta_c(\text{C}_2\text{F}_6) = 0.80$, and $\beta_c(\text{C}_3\text{F}_8) = 0.90$ with, of course, $\beta_c(M) = 1.00$ for C₄F₁₀. These values correlate well with the results and expectation of ref 7c and 10 in terms of correct overall magnitude and are reasonable within the limitation of the present experimental accuracy.

It will come as no surprise that the Lennard-Jones 6-12 potential model seems not well suited to interactions of nonspherical fluorocarbon hydrocarbon species; notwithstanding, the use of the Ω integrals at constant temperature, based on the present set of ϵ/k values (see the Appendix), leads to plausible values of σ constants (Table II) for the gases studied, and which compare well with viscosity derived σ_M constants.

Comparison with Photoactivation Data. Recently, Luu and Troe¹³ studied the photoisomerization of cycloheptatriene (CHT) to toluene at 2600 Å in the presence of a number of bath gases. Overlap with bath gases in the present series occurs for CH₄, CF₄, C₂F₆, and C₃F₈. Their experimental quantities, Stern-Volmer constants, $a(M)$, were related to the ratio $k_{\text{iso}}/k_{\text{deact}}$ through an absolute efficiency factor γ , namely, $\gamma^{LJ}(M) = a(M)k_{\text{iso}}/k_{\text{deact}}$, in their notation, where k_{iso} is the RRKM calculated isomerization rate constant at 2600 Å (110 kcal/mol); k_{deact} is given by the gas kinetic collision number $\omega(M)$, evaluated with use of the same relation as used by us, $s_{\text{CHT},M}^2 = \sigma_{\text{CHT},M}^2 \Omega_{\text{CHT},M}^{22^*}$. Their quantity $\gamma^{LJ}(M)$ is an absolute average efficiency for bath gas M and would be the same as our $\beta_c(M)$ if $\beta_c(M)$ for the reference molecule CHT were unity. With the data analyzed in this manner, their values of γ varied from 0.078 for CF₄ to 0.17 for C₃F₈, with $\gamma(\text{CHT}) = 0.16$. However, these values depend directly on the choice of the σ_M values, chosen by them to be $\sigma_{CF_4} = 4.66$ Å, $\sigma_{C_2F_6} = 5.10$ Å, and $\sigma_{C_3F_8} = 5.03$ Å, with $\sigma_{\text{CHT}} = 8.0$ Å. Since there is no reason to believe that $\sigma_{C_2F_6}$ is greater than $\sigma_{C_3F_8}$, we will adopt more appropriate estimates, namely, $\sigma_{CF_4} = 4.10$ Å, $\sigma_{C_2F_6} = 4.81$ Å, $\sigma_{C_3F_8} = 5.16$ Å, and $\sigma_{\text{CHT}} = 5.90$ Å. Then we find from their data $\gamma^{LJ}(\text{CF}_4) = 0.13$, $\gamma^{LJ}(\text{C}_2\text{F}_6) = 0.18$, $\gamma^{LJ}(\text{C}_3\text{F}_8) = 0.23$, and $\gamma^{LJ}(\text{CHT}) = 0.30$. Obviously, the values of $\gamma^{LJ}(M)$ are strongly dependent on the choice of a σ_M basis set as well as the value of the RRKM calculated magnitude of k_{iso} .

In order to use the data of Luu and Troe for comparison with the present results, a recasting of their relation for $\sigma^{LJ}(M)$ is desirable, relative to their reference chosen as CHT. Their equation as modified is

$$\gamma^{LJ}(M)/\gamma^{LJ}(\text{CHT}) = (a(M)/a(\text{CHT}))\omega_{\text{CHT},\text{CHT}}/\omega_{\text{CHT},M} \quad (7)$$

and thus

$$s_{\text{CHT},M} = s_{\text{CHT},\text{CHT}}[(a(M)/a(\text{CHT}))(1/\beta_c'(M)) \times (\mu_{\text{CHT},M}^{1/2}/\mu_{\text{CHT},\text{CHT}}^{1/2})]^{1/2} \quad (8)$$

TABLE III: Some Collision Cross-Section Parameters for the 6-12 Potential

Bath gas	ϵ_M/k , °K	ϵ_{BM}/k , °K	$[(\Omega_{BM}^{22*})]^{1/2}$ (298°K)	σ_M , Å ^a
CF ₄	134	209	1.156	3.23
C ₂ F ₆	155	224	1.175	3.63
C ₃ F ₈	173	237	1.189	4.47
C ₄ F ₁₀	188	247	1.203	5.89
C ₅ F ₁₂	202	256	1.215	7.39
C ₆ F ₁₄	214	264	1.220	8.58
C ₈ F ₁₈	234	276	1.233	10.56
CH ₄	149	220	1.170	3.08
<i>cis</i> -C ₄ H ₈	259	290	1.251	5.51
C ₄ H ₉	325	325	1.249	5.23

^a See footnote *b*, Table I.

where $\beta_c'(M) = \gamma^{LJ}(M)/\gamma^{LJ}(\text{CHT})$. Here, the choice of $\gamma_c'(M)$ and $s_{\text{CHT,CHT}}$ determines $s_{\text{CHT,M}}$ from the experimental results for $\alpha(M)$. With use of $\beta_c'(M)$ values of Georgakakos, Rabinovitch, and McAlduff¹⁰ of $\beta_c(\text{CF}_4) = 0.85$ and $\beta_c(\text{C}_2\text{F}_6) = 1.00$ etc. as well as $s_{\text{CHT,CHT}} = \sigma_{\text{CHT,CHT}}(\Omega^{22})^{1/2}$ as 8.0 Å, then $s_{\text{CHT,CF}_4} = 4.09$ Å, $s_{\text{CHT,C}_2\text{F}_6} = 4.92$ Å, and $s_{\text{CHT,C}_3\text{F}_8} = 5.89$ Å. These s quantities give back $\sigma_{\text{CF}_4} = 1.10$ Å, $\sigma_{\text{C}_2\text{F}_6} = 2.37$ Å, and $\sigma_{\text{C}_3\text{F}_8} = 3.85$ Å. These results are clearly not the correct magnitudes for these gases compared to known viscosity results. However, if lesser values of β_c' such as may apply here are used, namely, $\beta_c''(\text{CF}_4) = 0.70$, $\beta_c''(\text{C}_2\text{F}_6) = 0.80$, and $\beta_c''(\text{C}_3\text{F}_8) = 0.90$, then $\sigma_{\text{CF}_4} = 1.80$, $\sigma_{\text{C}_2\text{F}_6} = 3.35$, and $\sigma_{\text{C}_3\text{F}_8} = 4.42$ Å in better, although not acceptable, agreement with the present work (Table I) as well as with the results and expectation from ref 7c. It seems that for the photoactivation system of Troe, substantially smaller efficiencies (β') may apply, at least for CF₄ (0.43) and C₂F₆ (0.60). Nonetheless, before accepting this conclusion, we need remember, as was pointed out by Luu and Troe, that the estimation of k_{iso} from RRKM theory, which affects the apparent value of γ , might be in error by a factor of 2-3; this could then raise the experimental results for $\gamma^{LJ}(\text{CHT})$ to ~ 1.0 . The relative efficiencies β_c would become absolute efficiencies which would be in the range 0.5-1.0, *i.e.*, approximately the same as found in the present work.

Appendix

The parameters needed to relate s_{BM} quantities to the Lennard-Jones force constants σ_M are a consistent set of ϵ/k values for the gases studied. Since no such set is available, three different prescriptions for assigning ϵ/k were considered. The first, similar to that of ref 7c, used a constant value of ϵ/k of 160° for all members greater than C₂F₆ and leads to an upper limit for σ_M . The second utilized a

simple theoretical relation based on the Lennard-Jones potential model, namely, $\epsilon/k = 1.15T_b$. Results obtained from this method give the smallest σ_M values and represent a lower limit for σ_M . Finally, the third method, and the one selected, used a correlation of existing experimental data¹⁴ ($\epsilon/k = 72^\circ + 0.43T_b$) and gives a consistent set of values as well as good agreement with existing viscosity data for C₅F₁₂ and C₆F₁₄ which are beyond any β_c uncertainties. These values are summarized in Table III, and those for the first two methods are given in ref 12.

References and Notes

- (1) (a) This work was supported by the Office of Naval Research. (b) NASA Graduate Trainee.
- (2) (a) R. E. Harrington, B. S. Rabinovitch, and M. R. Hoare, *J. Chem. Phys.*, **33**, 744 (1960); G. H. Kolmaier and B. S. Rabinovitch, *ibid.*, **38**, 1962, 1709 (1963); (b) J. D. Rynbrandt and B. S. Rabinovitch, *J. Phys. Chem.*, **74**, 1679 (1970); (c) see H. W. Chang, N. L. Craig, and D. W. Setser, *ibid.*, **76**, 954 (1972), for references to a series of papers on collisional deactivation of excited haloethanes.
- (3) (a) D. C. Tardy, C. W. Larson, and B. S. Rabinovitch, *Can. J. Chem.*, **46**, 341 (1968); (b) C. W. Larson and B. S. Rabinovitch, *J. Chem. Phys.*, **51**, 2293 (1969).
- (4) H. S. Johnston, *J. Amer. Chem. Soc.*, **75**, 1567 (1953).
- (5) D. C. Tardy and B. S. Rabinovitch, *J. Chem. Phys.*, **45**, 3720 (1966).
- (6) Y. N. Lin and B. S. Rabinovitch, *J. Phys. Chem.*, **74**, 5151 (1970).
- (7) (a) Y. N. Lin, S. C. Chan, and B. S. Rabinovitch, *J. Phys. Chem.*, **72**, 1932 (1968); (b) S. C. Chan, J. T. Bryant, L. D. Spicer, and B. S. Rabinovitch, *ibid.*, **74**, 2058 (1970); (c) S. C. Chan, B. S. Rabinovitch, J. T. Bryant, L. D. Spicer, T. Fujimoto, Y. N. Lin, and S. P. Pavlou, *ibid.*, **74**, 3160 (1970).
- (8) E. A. Hardwidge, B. S. Rabinovitch, and R. C. Ireton, *J. Chem. Phys.*, **58**, 340 (1973).
- (9) (a) B. S. Rabinovitch and R. W. Diesen, *J. Chem. Phys.*, **30**, 735 (1959); (b) R. F. Kubin, B. S. Rabinovitch, and R. E. Harrington, *ibid.*, **37**, 937 (1962).
- (10) J. H. Georgakakos, B. S. Rabinovitch, and E. J. McAlduff, *J. Chem. Phys.*, **52**, 2143 (1970); **56**, 5921 (1972).
- (11) J. O. Hirschfelder, C. F. Curtis, and R. B. Bird, "Molecular Theory of Gases and Liquids," Wiley, New York, N. Y., 1964, p 245.
- (12) R. C. Ireton, Ph.D. Thesis, University of Washington, 1974.
- (13) S. H. Luu and J. Troe, *Ber. Bunsenges. Phys. Chem.*, **77**, 325 (1973).
- (14) T. M. Reed, III, "Fluorine Chemistry," Vol. 5, J. H. Simons, Ed., Academic Press, New York, N. Y., 1964, p 150.

Transfer of Vibrational Energy from Highly Excited Butyl Radicals. Structural Effects on the Magnitudes of Relative Collision Diameters^{1a}

R. C. Ireton,^{1b} An-Nan Ko, and B. S. Rabinovitch*

Department of Chemistry, University of Washington, Seattle, Washington 98195 (Received May 2, 1974)

Relative collision diameters for energy transfer have been measured at room temperature in the butyl-2 radical chemical activation system for various substituted and cyclic fluorocarbon molecules. Three generalizations are supported and illustrated by the data. (1) Branching of fluoroalkanes causes a decrease of the collision diameter relative to the straight chain perfluoroalkane of the same carbon number. (2) Cyclization of the fluoroalkane chain decreases the effective size of the molecule. (3) Introduction of a terminal double bond decreases the size relative to the straight chain perfluoroalkane. A simple equivalent sphere model based on the strongest end-to-end carbon chain systematizes the relative collision diameters of related molecules. These results support similar considerations for hydrocarbon bath molecules found previously in the thermal methyl isocyanide system.

Introduction

Intermolecular vibrational energy transfer during the collision process in a gas-phase reaction is the primary mechanism of activation in thermal unimolecular systems, and of deactivation of vibrationally excited species. A knowledge of relative collision diameters of bath gas molecules for the energy transfer process in systems of highly vibrationally excited polyatomic molecules is of importance. For the most part, assumed collision diameters derived from transport properties (viscosity measurements, usually) have been used in the literature for the calculation of gas kinetic collision diameters, of rate constants, and for the evaluation of energy transfer data. In some cases, errors or irregularities in σ_M are carried directly into the corresponding $\beta_c(M)$ values, the efficiencies for transfer of vibrational energy upon collision between substrate and bath molecule. It is apparent, then, that a consistent set of collision diameters is important for the determination of $\beta_c(M)$ and for comparison with theoretical predictions when applicable.

Previously, we have made an extensive investigation of this phenomenon for the thermal low-pressure unimolecular isomerization of methyl isocyanide in the presence of several homologous series of hydrocarbon and fluorocarbon polyatomic bath molecules.^{2,3} It was possible to determine relative values of effective hard-sphere collision diameters for substrate-bath molecule pairs, s_{AM} ; incremental changes Δs_{AM} were also determined with increase in the number of structural units, *i.e.*, $\Delta s_{AM}(\text{CH}_2)$ and $\Delta s_{AM}(\text{CF}_2)$ were measured.² The relation between the molecular geometry of structural isomers and their effective collision diameters for energy transfer was also examined in this thermal system. In particular, it was found that increased branching of alkanes having constant carbon number entailed a progressive decrease in the collision diameters; cyclization of the alkane also decreased the effective size of the bath molecule.

In order to broaden the experimental basis of this phenomenon, we have previously reported⁴ a study of vibrational energy transfer in the chemically activated butyl-2 system and have measured the collision diameters of some fluorocarbon bath gases. In particular, a simple method

was devised for measuring the increments, $\Delta s_{BM}(\text{CF}_2)$, and the relative collision diameters, s_{BM} , of bath molecules for a homologous series of perfluoroalkanes (C_1 to C_8); also, by comparison of apparent collision diameters at 298 and 195°K, the relative collisional energy transfer efficiencies, $\beta_c(M)$, could be surmised for the less efficient gases. The experimentally determined values of $\beta_c(M)$ for inefficient bath gases are dependent directly on the choice of the equivalent hard-sphere collision diameter for the collider species.

In the present study, we extend our earlier studies on use of the nonpolar butyl-2 species in a chemical activation system. A series of perfluoro-1-alkenes, as well as selected cyclic fluoroalkanes and cyclic fluoroolefins, has been studied for comparison with the corresponding alicyclic compounds.

Experimental Section

The fluorocarbon compounds were obtained from P.C.R. Inc. and were further purified by gas chromatographic techniques until free of impurities. The *cis*-butene-2 was Phillips Research Grade, and was also chromatographically purified until the impurity level was less than 0.001%. Mixtures of the fluorocarbon with *cis*-butene-2 were made in the ratio of 20:1 on a pressure basis for all but the C_2F_4 -butene (10:1) system. The reactants were subjected to a vessel. The details of the run procedure and analytical techniques are given in ref 2 and 4.

Results

Description of the calculation of the effective hard-sphere collision diameters, s_{BM} , has been given earlier and need only be described briefly here. The relevant quantities measured in chemical activation systems are the ratio of stabilization to decomposition, S/D , and the collision frequency, $\omega = Zp$. The apparent rate constant for decomposition is $k_a = \beta_c(M)\omega(D/S)$. Then, $S/D = \beta_c(M)\omega/k_a = \beta_c(M)Zp/k_a$, and plots of S/D vs. p yield a linear relation whose slope is $\beta_c(M)Z/k_a$; the specific collision rate Z is a function of s_{BM}^2 , and a ratio of the slope of the butyl- M collision pair relative to the butyl-butene reference pair yields a relation for s_{BM} in terms of s_{BB}

TABLE I: Experimental Quantities and Lennard-Jones Constants at 300°K

Bath gas	Slope _{BM} /slope _{EB}	s _{BM} ^a	s _{BC_nF_{2n+2}} ^b	Δ ^c	ε _{BM} /R	[Ω _{BM} ^{22*} (T*)] ^{1/2}	σ _M , Å	σ _{MC_nF_{2n+2}}
C ₂ F ₄	0.620 ± 0.037 ^d	5.52	5.83	0.31	157	1.178	4.14	4.81
C ₃ F ₆	0.757 ± 0.033	5.88	6.18	0.30	176	1.193	4.62	5.16
<i>i</i> -C ₄ F ₁₀	0.894 ± 0.060	6.35	6.69	0.34	185	1.200	5.35	5.89
<i>cis</i> -C ₄ F ₈	1.092 ± 0.082	7.02	6.69	-0.33	189	1.204	6.43	5.89
C ₅ F ₁₀	1.284 ± 0.089	7.61	7.67	0.06	202	1.214	7.31	7.39
<i>c</i> -C ₄ F ₈	0.896 ± 0.110	6.36	6.69	0.33	187	1.203	5.32	5.81
<i>c</i> -C ₅ F ₈	1.040 ± 0.040	6.85	7.67	0.82	201	1.214	6.06	7.39
<i>c</i> -C ₆ F ₁₂	1.195 ± 0.064	7.35	8.43	1.08	212	1.220	6.82	8.58
<i>c</i> -C ₆ F ₁₀	1.148 ± 0.020	7.20	8.43	1.23	212	1.220	6.57	8.58
C ₆ F ₆	1.245 ± 0.114	7.50	8.43	0.93	224	1.230	6.97	8.58
<i>c</i> -CF ₃ C ₆ F ₁₁	1.325 ± 0.038	7.74			222	1.230	7.36	
<i>cis</i> -C ₄ H ₈	1.00	6.72			259	1.251	5.51	

^a Collision diameter obtained using $\beta_c(\text{C}_2\text{F}_4) = 0.88$, $\beta_c(\text{C}_3\text{F}_6) = 0.99$, and $\beta_c(\text{M}) = 1.0$ for $\text{M} \geq \text{C}_4\text{F}_8$. ^b Collision diameter from ref 5 for the corresponding straight chain alkanes. ^c Decrement between the collision diameter s_{BM} and the corresponding straight chain diameter. ^d Standard deviation.

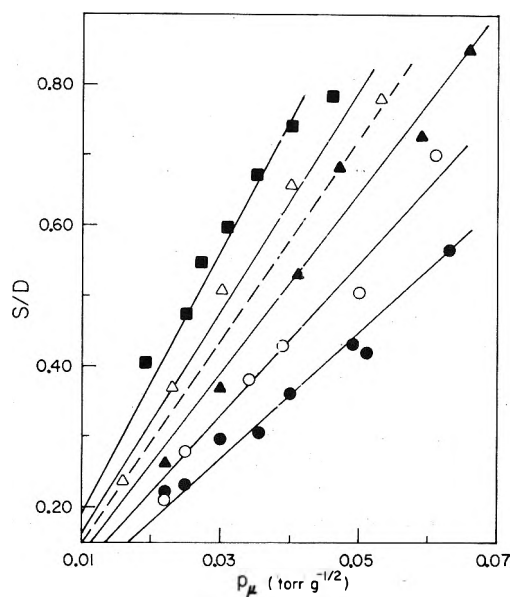


Figure 1. Plots of S/D vs. p_μ for butyl radical decomposition in the presence of the following bath gases at 300°K: *c*-C₄F₈ (●); *c*-C₅F₈ (○); *c*-C₆F₁₀ (▲); C₆F₆ (Δ); *c*-C₆F₁₂ (■); *c*-(CF₃)C₆F₁₁ (□). Dashed line represents the data for the reference *cis*-C₄H₈.

$$s_{\text{BM}} = s_{\text{BB}} (\text{slope}_{\text{BM}} / \beta_c(\text{M}) \text{slope}_{\text{BB}})^{1/2} \quad (1)$$

with the assertion that $\beta_c(\text{B})$ is unity.⁵

Of the present collision partners studied, C₂F₄ and C₃F₆ may have $\beta_c(\text{M})$ less than unity. Previously,⁵ $\beta_c(\text{M})$ for C₂F₆ was found to be 0.8, and $\beta_c(\text{M})$ for C₃F₈ was 0.9. Chan, *et al.*,² found an increase in $\beta_c(\text{M})$ in going from perfluoroethane to perfluoroethylene, from $\beta_c(\text{C}_2\text{F}_6) = 0.64$ to $\beta_c(\text{C}_2\text{F}_4) \geq 0.71$. This represents an increase of 10%. This seems a reasonable choice for the present system, also, and yields $\beta_c(\text{C}_2\text{F}_4) = 0.88$ and $\beta_c(\text{C}_3\text{F}_6) = 0.99$. For the remainder of the bath gases studied, $\beta_c(\text{M})$ equal to unity was used in the evaluation of s_{BM} . The Lennard-Jones constants ϵ/k (and the integrals Ω_{BM}^{22*}) were found as in ref 5. The results are summarized in Table I and the data are shown in Figures 1 and 2.

Discussion

Fluoroolefins. Hydrogen atoms add to the olefin to give

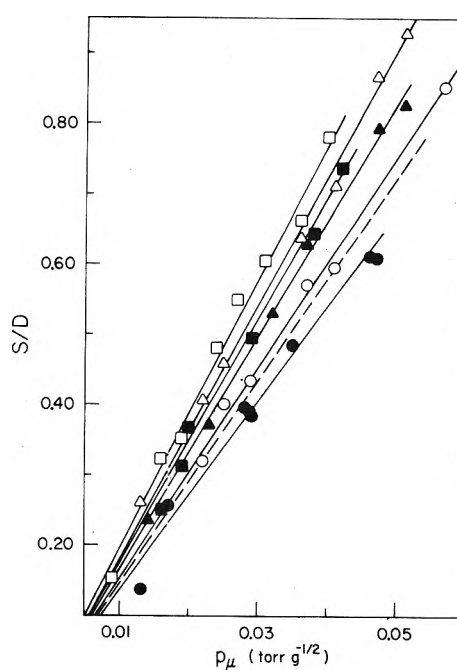


Figure 2. Plots of S/D vs. p_μ for butyl radical decomposition in the presence of the following bath gases at 300°K: C₂F₄ (●); C₃F₆ (○); *i*-C₄F₁₀ (▲); *cis*-C₄F₈ (Δ); C₅F₁₀ (■). Dashed line represents the data for the reference *cis*-C₄H₈.

the excited fluoroalkyl radical.⁵ For C₂F₄H·, as well as C₃F₆H·, evidence of radical addition to the stabilized butyl radical was confirmed by mass spectrometric identification. Where mass spectrometric identification was not feasible, chromatographic retention data provided identification of the radical combination products. These products accounted for a maximum of 20% of the stabilization product for the C₂F₄ system, ~10% of S for C₃F₆, ~1% of S for *cis*-C₄F₈, and ~5% for C₅F₁₀.

The C₂F₄, C₃F₆, and C₅F₁₀ bath gases show a decrease in collision diameter in comparison with the corresponding alkanes (see Table I), but the *cis*-C₄F₈ diameter is larger than that of perfluoro-*n*-butane.

The general trends here are consistent with the findings for hydrocarbon-olefin compounds in ref 2, where contrac-

tion in diameter occurred on going from alkane to olefinic species, except for interior olefins such as *cis*-butene-2 where the reverse was obtained. C₅F₁₀ data appear to give the smallest contraction.

These results apparently reflect the contraction of bond length encountered on going from a single to a double bond in the α position of the carbon skeleton. When interior double bonds are considered, the planar configuration of the fluoromethyl groups seems to lead to a larger effective diameter, as for *cis*-C₄F₈-2.

Cyclic Fluoroalkanes. The results of Spicer and Rabinovitch³ in the isocyanide system revealed that cyclic hydrocarbon bath gases behaved like straight chain molecules with an effective length equal to the longest end-to-end distance in the ring, and with the remaining CH₂ moieties to be taken as CH₃ branching substituents; such branching adds an increment to the effective collision diameter which is less than 0.4 Δs (CH₂) for the interval in question. On applying this model to fluorocarbon species, *c*-C₄F₈ simulates a C₃ compound having one CF₃ substituent, or effectively has the same size as *i*-C₄F₁₀; likewise, *c*-C₅ represents an effective chain of four carbons with one side CF₃ group; and a C₆ cyclic compound is effectively *n*-perfluorobutane in length with two methyls attached. These considerations are summarized in Table II, where the equivalent carbon number chain length and side CF₃ groups are given. The collision diameter s_{BM} for perfluorocyclobutane is 6.36 Å, almost identical with that of perfluoroisobutane, s_{BM} = 6.35 Å, as anticipated. Also, the increase in diameter from C₃F₈ to *i*-C₄F₁₀ was measured as 0.17 Å, in agreement with the prediction of ≤ 0.22 Å obtained from $\leq 0.4\Delta s$ (CF₂), for the C₃-C₄ pair. For *c*-C₆F₁₂, the longest chain is a C₄, equivalent, from Table II, to 6.69 Å, while the additional two CF₃ groups predict an additional ≤ 0.8 Å, since the Δs (CF₂) value between C₄ and C₅ is 0.99; thus, $s_{BM} \leq 7.49$ Å is expected, as compared to the experimental value 7.35 Å. The same comparison yields a predicted s_{BM} of ≤ 8.47 Å for perfluoromethylcyclohexane while the experimental value is 7.74 Å.

The only irregularity in this pattern is found for perfluoromethylcyclohexane, in which the longest chain is five carbons with two equivalent side methyls, and which has a diameter only a little larger than that of *n*-C₅F₁₂. This behavior may possibly be characteristic of cyclic compounds with exterior branching, since Spicer and Rabinovitch³ found that methylcyclopentane, which should behave like an effective C₄ with two side methyl groups, had a diameter of the same size as *n*-butane with s_{AM} = 5.53 Å. This phenomenon also appears for toluene in ref 3. This molecule can be considered as an effective C₅ with an additional increment for two effective methyls; what was found was a collision diameter s_{AM} = 5.66 Å, less than that of *n*-pentane, s_{AM} = 5.83 Å.

Cyclic Fluoroolefins. Perfluorocyclopentene, perfluorocyclohexene, and perfluorobenzene were examined in order to ascertain the effects of cyclization and, also, of olefinic bonding on the collision diameter. Due to the double bonding, the previous considerations for predicting the effective diameter of cyclic molecules are expected to be slightly modified, but they do hold in general. For example, perfluorocyclopentene has a longest chain of C₃ (6.18 Å), with two side methyls for a predicted collision diameter s_{BM} = 6.62 Å, slightly less than the measured value of 6.85 Å. Perfluorocyclohexene has an effective longest chain length of a C₄, or 6.69 Å, with again two side methyls, for a predicted

TABLE II: Effective Chain Length of Cyclic Compounds in Comparison with Straight Chain Molecules

Bath gas	s_{BM} , Å	Effective straight chain carbon no.	Effective no. of CF ₃ branching units	Fraction ^b Δs (CF ₂)
C ₂ F ₄	5.52	2	0	
C ₃ F ₆	5.88	3	0	
C ₃ F ₈ ^a	6.18			
<i>i</i> -C ₄ F ₁₀	6.35	3	1	0.23
<i>c</i> -C ₄ F ₈	6.36	3	1	0.24
<i>n</i> -C ₄ F ₁₀	6.69	4	0	
<i>c</i> -C ₅ F ₈	6.85	3	2	0.45
<i>cis</i> -C ₄ F ₈	7.02	4	0	
<i>c</i> -C ₆ F ₁₀	7.20	4	2	0.34
<i>c</i> -C ₆ F ₁₂	7.35	4	2	0.38
C ₆ F ₆	7.50	4	2	0.54
<i>n</i> -C ₅ F ₁₀	7.61	5	0	
<i>n</i> -C ₅ F ₁₂ ^a	7.67	5	0	
<i>c</i> -CF ₃ C ₆ F ₁₁	7.74	5	2	(0.05)
<i>n</i> -C ₆ F ₁₄ ^a	8.43	6	0	

^a Values for the perfluoroalkane member are those from ref 5.

^b Expressed as the fractional incremental increase in Δs (CF₂) per effective CF₃ branching unit with use of the average value Δs (CF₂) = 0.75 Å, as in ref 4.

length of 7.49, a little larger than the measured value of 7.20 Å.

From the last column in Table II the individual experimental incremental increases per equivalent side substituent CF₃ are seen to fluctuate due, at least in part, to experimental error. They have an average value of 0.36 Δs (CF₂) (excluding the anomalous methylcyclohexane), similar to the value of Spicer and Rabinovitch.

There are insufficient data for a detailed comparison of these cyclic alkenes with the corresponding perfluorocycloalkane compounds. However, for the one pair for which experimental evidence is at hand, perfluorocyclohexane-perfluorocyclohexene, the evidence is for a slight contraction in size of the latter.

The situation for perfluorobenzene is not well understood. In the methyl isocyanide thermal system,³ it was found upon comparison of the hydrocarbon species, cyclohexane and benzene, that benzene was much the smaller of the two. The present result gives an increase in size for perfluorobenzene relative to perfluorocyclohexane. If the data are correct, evidently perfluorobenzene does not follow the behavior of its hydrogen counterpart.

Summary

Some qualitative generalizations are supported and demonstrated by the data. (1) Branching of fluoroalkanes causes a decrease of the collision diameter relative to the straight chain alkane. (2) Cyclization of the fluoroalkane chain decreases the effective size of the molecule. (3) Introduction of terminal double bonds decreases the size relative to the fluoroalkanes. The quantitative magnitudes associated with each of these effects are revealed by the data of Tables I and II.

These results emphasize again^{3,6,7} that the drop model central force treatment which predicts a cross-section de-

pendence on carbon number⁶ does not apply, and collision diameters for energy transfer are a strong function of the detailed molecular structure; molecules may be treated as equivalent spheres whose diameters are related to their end-to-end molecular geometric lengths.

References and Notes

(1) (a) Abstracted in part from the Ph.D. Thesis of R.C.I., University of Wash-

ington, 1974. This work was supported by the Office of Naval Research. (b) NASA Graduate Trainee.

- (2) S. C. Chan, B. S. Rabinovitch, J. T. Bryant, L. D. Spicer, T. Fujimoto, Y. N. Lin, and S. P. Pavlou, *J. Phys. Chem.*, **74**, 3160 (1970).
- (3) L. D. Spicer and B. S. Rabinovitch, *J. Phys. Chem.*, **74**, 2445 (1970).
- (4) R. C. Ireton and B. S. Rabinovitch, *J. Phys. Chem.*, **78**, 1979 (1974).
- (5) R. D. Penzhorn and H. L. Sandoval, *J. Phys. Chem.*, **74**, 2065 (1970).
- (6) W. H. Duewer, G. J. Williams, C. F. Aten, and B. S. Rabinovitch, *J. Phys. Chem.*, **75**, 727 (1971).
- (7) R. D. Levine, *Chem. Phys. Lett.*, **4**, 309 (1969).

Reaction of the Hydrated Electron with Benzene Studied by Pulse Radiolysis

D. G. Marketos,^{*}† Anastasia Marketou-Mantaka,

Nuclear Research Center "Demokritos," Radiation Chemistry Laboratory, Aghia Paraskevi-Attikis, Athens, Greece

and Gabriel Stein

The Hebrew University of Jerusalem, Department of Physical Chemistry, Jerusalem, Israel (Received March 11, 1974)

Publication costs assisted by the Greek Atomic Energy Commission

The reaction of the hydrated electron with benzene has been studied by the technique of pulse radiolysis. The rate constant of this reaction was found $(1.3 \pm 0.5) \times 10^7 M^{-1} \text{ sec}^{-1}$ by following the pseudo-first-order disappearance of e_{aq}^- at 600 nm, in Ar-saturated aqueous benzene solutions, at pH 11 and 13, in the presence of OH radical scavengers (*tert*-butyl and isobutyl alcohol). The bimolecular rate constants of the disappearance of $C_6H_7\cdot$ and $C_6H_6OH\cdot$ have also been determined as $(1.25 \pm 0.22) \times 10^9$ and $(7.05 \pm 0.35) \times 10^8 M^{-1} \text{ sec}^{-1}$, respectively. The absorption maxima of the transient species $C_6H_6^-$, $C_6H_7\cdot$, and $C_6H_6OH\cdot$ were found at 312, 311, and 313 nm, respectively, and their molar extinction coefficients were calculated as $\epsilon_{C_6H_6^-}$ ³¹² 2450 ($\pm 13\%$), $\epsilon_{C_6H_7\cdot}$ ³¹¹ 5350 ($\pm 10\%$), and $\epsilon_{C_6H_6OH\cdot}$ ³¹³ 4700 ($\pm 13\%$) $M^{-1} \text{ cm}^{-1}$. The observed absorption at 312 nm, under conditions where mostly electrons are present (pH neutral to 13, Ar-saturated, *tert*-butyl alcohol present), is consistent with the assumption that this absorption is due to the formation of $C_6H_6^-$ (B^-), which, under the present experimental conditions, rapidly disappears by bimolecular radical reactions before protonation.

Introduction

The reactions of the simple free radicals, H atoms, OH radicals, and hydrated electrons with benzene in aqueous solutions is an interesting problem from the point of view of physical organic chemistry, in that it shows the reactivity of the simplest aromatic molecule toward free radicals. This problem has been studied using the technique of pulse radiolysis. In particular, the reactions of OH radicals and H atoms have been elucidated² and the rate of formation, absorption spectra, and further reactions of the intermediate free-radicals $C_6H_6OH\cdot$ (BOH) and $C_6H_7\cdot$ (BH) have been established.²⁻⁸

By contrast, the reaction of e_{aq}^- with benzene is still not fully elucidated. A number of researchers, and in particular Hart and coworkers,^{7,9} have convincingly shown that e_{aq}^- reacts with benzene and leads to the formation of products. The suggested mechanism of the reaction is the attachment of e_{aq}^- to benzene, as a first step, followed by rapid protonation leading to the formation of BH, which is the intermediate claimed to have been observed. This radical then reacts further.

The absorption spectrum of B^- has not yet been studied. However, it is reported¹⁰ that in γ -irradiation of benzene in

MTHF, at -196° , two small bands were observed at 290 and 390 nm, which were assigned to B^- .

An interesting fact is the difference between the high rate constants of OH and H addition to benzene (of the order of $10^9 M^{-1} \text{ sec}^{-1}$) and the relatively low apparent rate constant of the reaction of e_{aq}^- with benzene, which is nearly two orders of magnitude smaller.^{7,11,12}

We therefore reinvestigated the reaction of e_{aq}^- with benzene in some detail, using the technique of fast pulse radiolysis.

Experimental Section

Materials. The reagents [benzene (Mallinckrodt), *tert*-butyl alcohol (Fluka), isobutyl alcohol (BDH), NaOH (Riedel de Haën), and HClO_4 (Merck)] were of analytical grade and were used without further purification. Ultra-high-purity N_2O and Ar (Matheson Co.), also Ar (Oxygen Center, Israel), were further purified by passing them through two bubblers of alkaline pyrogallol solution, followed by two additional bubblers containing 50% H_2SO_4 and water, respectively.

Solutions. All solutions were prepared just before irradiation in triply distilled water, saturated with Ar or N_2O

in 100-ml syringes. The pH was adjusted either with HClO_4 or with NaOH , as required, and measured with a Radiometer PHM52 digital pH meter. Saturated benzene solutions were prepared by adding a slight excess of liquid benzene to a syringe containing the aqueous solution of solute (*tert*-butyl and isobutyl alcohol), while purified Ar or N_2O gas was flushed for 15 min through the syringe. To avoid loss of solute, an additional bubbler, containing an aqueous solution of the corresponding alcohol of the same concentration was inserted before the syringe. Then the excess gas was expelled and after a few minutes of standing the excess benzene was discharged. The concentration of benzene in this solution was taken equal to $2.02 \times 10^{-2} M$.⁷ Solutions of benzene of the desired concentrations were then prepared by injecting the proper amount of the saturated benzene solution into another syringe containing a blank solution of *tert*-butyl alcohol similarly prepared. The syringes were kept without gas space, ground stoppered, to avoid volatilization of solutes. The concentration of benzene in these solutions was determined on a Hilger Uvispek spectrophotometer or on a Cary 14 spectrophotometer, using $\epsilon_{254\text{nm}} 177.4 M^{-1} \text{cm}^{-1}$.¹³ This value is in good agreement with a recently reported one⁷ of $180 M^{-1} \text{cm}^{-1}$. We believe that the accuracy in the determination of benzene concentration is within $\pm 5\%$, including a correction for the loss of benzene occurring during the transfer of the solution to the spectrophotometric cell.

Pulse Irradiation. All experiments were carried out by pulse radiolysis using a Varian-7715 linear accelerator with electron pulses of 5-MeV energy and 200-mA current. Pulse durations varied between 0.2 and 1.5 μsec . The dose ranged from 950 to 3500 rads/pulse. The pulse intensity was monitored by using the inductive current of the electron beam in a coil. A rectangular, 4 cm long, Spectrosil cell equipped with a multiple reflection arrangement served as the irradiation vessel. A threefold pass of the analyzing light was used with a total optical path of 12.4 cm. An automatic syringe sample changer was used to provide fresh solution in the absence of a gas phase. The analyzing light source was a 150-W Osram xenon arc lamp. Two Bausch and Lomb grating monochromators were used, one for the region below and the other for above 400 nm. Suitable light filters (Schott or Corning) were used between the light source and the irradiation cell to avoid photochemical reactions, also in front of the entrance slit of the monochromator to reduce scattered light. Regardless of this, scattered light below 290 nm was observed and allowed for. An RCA 1P28 photomultiplier was used in the range from 270 to 600 nm and a Tektronix 556 dual-beam oscilloscope with selected (1A1 and/or 1A5) plug-in units was employed. Changes in light transmittance through the sample after delivery of the pulse were displayed on the oscilloscope and photographed. A split analyzing light beam was used to record spectra. One beam at the maximum of the absorption served to monitor the pulse intensity, the other being varied.

Dosimetry. The total dose per pulse was determined using an argon saturated 10 mM aqueous methanol solution of pH 9.5 as a dosimeter, and measuring the transient optical densities at 578 nm. The dose was then calculated by extrapolating the optical density to "zero time" and assuming $\epsilon_{\text{e}_{\text{aq}}^-} 1.06 \times 10^4 M^{-1} \text{cm}^{-1}$ ¹⁴ and $G_{\text{e}_{\text{aq}}^-} = 2.75$. The reproducibility of the dose per pulse was found to be of the order of $\pm 10\%$.

Data Treatment. A CDC 6400 computer was employed

for the kinetic analysis of the photographs of the oscillographic traces.

Results

Reaction of e_{aq}^- with Benzene. The rate constant of this reaction was determined directly by following the decay of the absorption of e_{aq}^- at 600 nm, in Ar-saturated solutions of benzene, at pH's 11 and 13, in the presence of OH radical scavengers at relatively high concentrations (*tert*-butyl alcohol 0.8 and 2 M, or isobutyl alcohol 0.6 M). By using 500-nsec and 1.5 μsec pulses and appropriate concentrations of benzene (3.5×10^{-3} , 1.01×10^{-2} , and $2.02 \times 10^{-2} M$), in different combinations, the ratio of the initial concentration of e_{aq}^- to that of benzene was 0.002 or less. Under these conditions pseudo-first-order kinetics prevail; indeed, strictly first-order plots were obtained (shown in Figure 1) from which, after corrections for the reactions of e_{aq}^- with impurities, the value $(1.3 \pm 0.5) \times 10^7 M^{-1} \text{sec}^{-1}$ was calculated for the rate constant of the reaction of e_{aq}^- with benzene.

Reaction of H Atoms with Benzene. The transient absorption spectrum of the H-atom adduct of benzene (BH) was observed in pulse radiolysis of Ar-saturated aqueous solutions of $3.5 \times 10^{-3} M$ benzene, at pH 2, in the presence of 2 M *tert*-butyl alcohol. Under these conditions the e_{aq}^- , reacting with H^+ , are completely converted into H atoms, while 95.5% of the OH radicals are taken up by *tert*-butyl alcohol, the rest reacting with benzene. In the competition between benzene and *tert*-butyl alcohol for the H atoms 90.3% BH is formed. Taking the total $G_{\text{HT}} = G_{\text{H}} + G_{\text{e}_{\text{aq}}^-} = 3.50$ and $G_{\text{OH}} = 3.00$ at pH 2, we calculated $G(\text{BH}) = 3.16$, i.e., 96% of the benzene radicals formed and $G(\text{BOH}) = 0.13$, i.e., 4% of the benzene radicals formed. The maximum absorption was observed at 311 nm. Applying appropriate corrections for the interfering absorption due to BOH from the spectrum of BOH and the value of $\epsilon_{\text{BOH}}^{313}$ determined previously by us,⁸ and redetermined further in the present work, we calculated $\epsilon_{\text{BH}}^{311} 5350 (\pm 10\%) M^{-1} \text{cm}^{-1}$.

Kinetic analysis of the rate curve obtained with a slow (100 $\mu\text{sec}/\text{cm}$) sweep rate at 311 nm gave a second-order decay of BH. From the slope of the plot shown in Figure 2 and the value of the peak-molar extinction coefficient of BH, the rate constant of the bimolecular disappearance of BH was calculated $k_{\text{BH}+\text{BH}} = (1.25 \pm 0.22) \times 10^9 M^{-1} \text{sec}^{-1}$.

Reaction of OH Radicals with Benzene. The transient absorption spectrum of the OH-radical adduct of benzene (BOH) was observed in pulse radiolysis of neutral, N_2O -saturated, aqueous solutions of $3.5 \times 10^{-3} M$ benzene. Under these conditions the e_{aq}^- , reacting with N_2O , are completely converted into OH radicals, which subsequently react with benzene to form BOH. The H atoms add also to benzene with formation of BH. Taking the total $G_{\text{OHT}} = G_{\text{OH}} + G_{\text{e}_{\text{aq}}^-} = 5.45$ and $G_{\text{H}} = 0.55$ at neutral pH, we calculated $G(\text{BOH}) = 5.45$ (90%) and $G(\text{BH}) = 0.55$ (10%). The maximum absorption was observed at 313 nm. After corrections similar to those applied for the ϵ_{BH} , we obtained $\epsilon_{\text{BOH}}^{313} 4700 (\pm 13\%) M^{-1} \text{cm}^{-1}$.

Kinetic analysis of the rate curve obtained at 313 nm gave a second-order decay of BOH. The plot is shown in Figure 3. From this we calculated $k_{\text{BOH}+\text{BOH}} = (7.05 \pm 0.35) \times 10^8 M^{-1} \text{sec}^{-1}$.

Transient Spectra. Under conditions similar to the above, we observed the transient absorptions produced in the uv region from 280 to 330 nm. The transient absorption

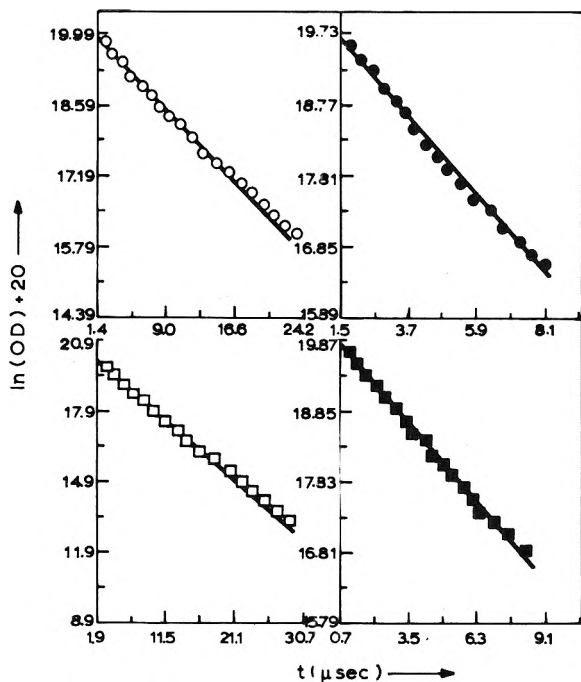


Figure 1. First-order decay of e_{aq}^- at 600 nm in Ar-saturated solutions: (O) 3.5×10^{-3} M benzene, 0.8 M *tert*-butyl alcohol, pH 11, 3500 rads/pulse; (●) 2.02×10^{-2} M benzene, 0.8 M *tert*-butyl alcohol, pH 11, 3500 rads/pulse; (□) 3.5×10^{-3} M benzene, 0.6 M isobutyl alcohol, pH 11, 3500 rads/pulse; (■) 1.01×10^{-2} M benzene, 2 M *tert*-butyl alcohol, pH 13, 1650 rads/pulse.

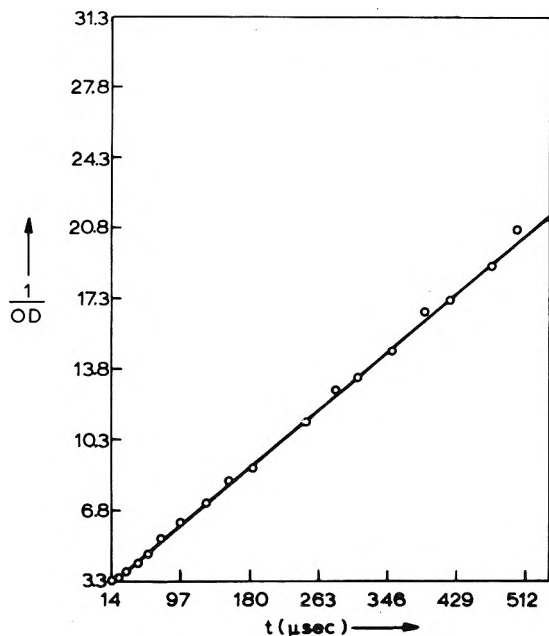


Figure 2. Second-order decay of the $C_6H_7^-$ radical at 311 nm in Ar-saturated solutions: 3.5×10^{-3} M benzene, 2 M *tert*-butyl alcohol, pH 2, 1650 rads/pulse.

spectrum obtained 3 μ sec after the pulse (Figure 6, curve b), when the maximum absorption has been built up, showed a maximum at 312 nm. Under these experimental conditions small percentages of the H atoms and OH radicals produced escape scavenging and react with benzene. The resulting concentrations of the species formed from these equaled $\sim 15\%$ for BH and $\sim 10\%$ for BOH, leaving $\sim 75\%$ of the total concentration of the radicals reacting

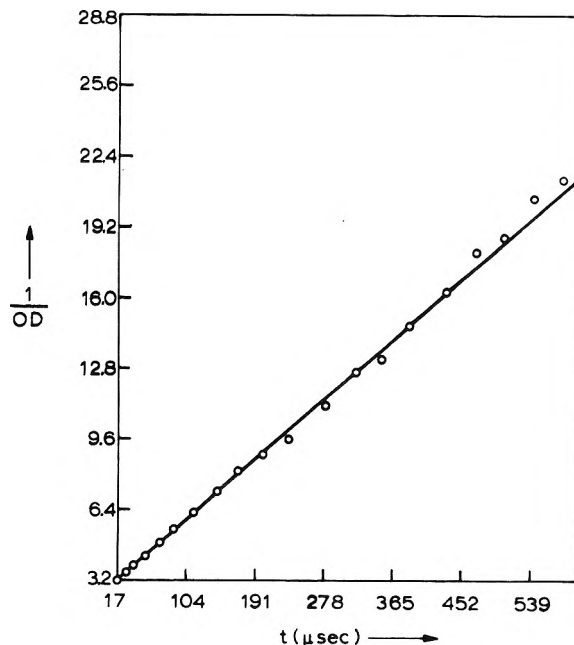


Figure 3. Second-order decay of the $C_6H_6OH^-$ radical at 313 nm in N_2O -saturated solutions: 3.5×10^{-3} M benzene, pH neutral, 1650 rads/pulse.

with benzene for the species resulting from the e_{aq}^- addition. The two known species formed have absorption maxima at 311 (BH) and 313 nm (BOH). We calculated the percent absorptions due to these species in the region 280–330 nm from their molar extinction coefficients and subtracted their sum from the experimentally observed total absorption. We used the value of $4700 M^{-1} cm^{-1}$ for ϵ_{BOH}^{313} determined previously by us⁸ and redetermined in the present work. We measured also the ϵ_{BH}^{311} $5350 (\pm 10\%) M^{-1} cm^{-1}$, using proper conditions, because of a disagreement in the reported values of $5400 (\pm 9.3\%)^{2b}$ and $3300 (\pm 6\%) M^{-1} cm^{-1}$.⁷ We found that, in optical densities, BH contributed $\sim 25\%$ and BOH $\sim 15\%$, leaving $\sim 60\%$ due to the species resulting from the e_{aq}^- addition to benzene. Another necessary correction further applied was the subtraction from the experimentally observed spectrum of the absorption due to the e_{aq}^- which had not reacted with benzene in 3 μ sec. We used the values of $\epsilon_{e_{aq}^-}$ $850\text{--}950 M^{-1} cm^{-1}$ for the region 280–330 nm. The resulting difference spectrum is shown in Figure 4. The absorption maximum of this spectrum is at 312 nm and the $\epsilon_{B^-}^{312}$ was calculated equal to $2450 (\pm 13\%) M^{-1} cm^{-1}$.

It could be argued that this excess absorption might be due to the *t*-BuOH radical adduct of benzene. We investigated this possibility by pulse radiolysis of aqueous solutions of benzene, in the presence of *tert*-butyl alcohol (a) Ar saturated and (b) N_2O saturated. In the first case, in which mostly electrons were present, an absorption was observed at 312 nm, which decreased in the second case, where electrons were taken up by the N_2O . This result showed that the excess absorption must be attributed to the product of e_{aq}^- addition to benzene. Our results should be compared with the spectrum attributed to BH in Figure 5 of ref 7 and with that of BH in Figure 2 of ref 2b, reproduced in our Figure 4. It will be seen from the present Figure 4, that neither our B^- spectrum nor that of ref 7 (which closely resembles it) could be compared with that of BH of

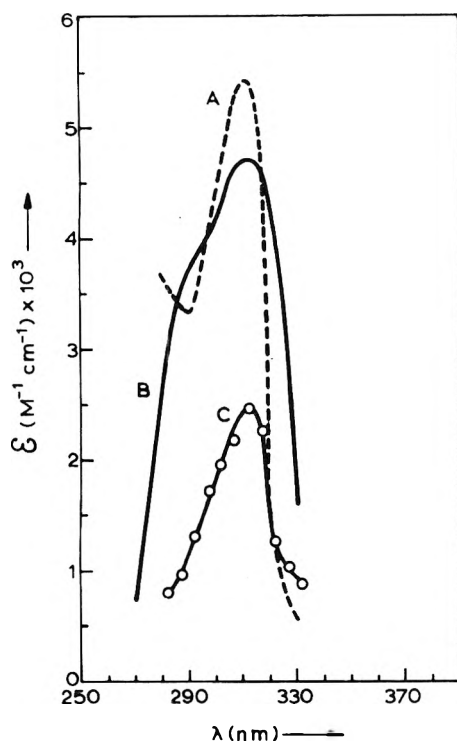


Figure 4. Transient absorption spectra of the H atom, OH radical, and e_{aq}^- adducts of benzene: (A) H-atom adduct, λ_{max} 311 nm (from ref 2b, converted by using ϵ_{BH}^{311} $5400 M^{-1} cm^{-1}$); (B) OH-radical adduct, λ_{max} 313 nm (from ref 8, converted by using ϵ_{BOH}^{313} $4700 M^{-1} cm^{-1}$); (C) e_{aq}^- adduct, corrected for the contribution of BH, BOH, and e_{aq}^- , λ_{max} 312 nm, ϵ_{B-}^{312} $2450 (\pm 13\%) M^{-1} cm^{-1}$.

ref 2b. There is no increase in ϵ for B^- below ~ 290 nm. There is an excess ϵ above ~ 325 nm.

Reaction Stages. Using slower sweep rates we calculated the half-lives of BH and BOH. In solutions where either only BH or BOH were present the half-life due to bimolecular disappearance was equal to about $130 \mu sec$. From the results in experiments where mixed absorptions were observed as mentioned before, the spectrum due to mixtures of BH, BOH, and B^- decays with a half-life of $\leq 60 \mu sec$. Figure 5 shows some representative results in neutral solution. We see the initial formation of the intermediates BH and BOH. We can also see, quite clearly, a third intermediate process proceeding on the time scale of the order of a few microseconds in Ar-saturated solutions, but not present in N_2O -saturated solutions. This intermediate stage overlaps both preceding step of H addition and subsequent step of radical decay and therefore exact kinetics could not be established for the rate of B^- formation, though it agrees in time scale with the rate of e_{aq}^- disappearance. The mixed spectrum does not show a further increase in the time range of ~ 3 to $\sim 10 \mu sec$ after the pulse, but begins to decay from ~ 3 – $4 \mu sec$ after the pulse. Figure 6 shows stages in the build up and the decay. No new intermediate is indicated.

Discussion

Under the experimental conditions of the present work the main species present, reacting with benzene, was e_{aq}^- . However, some H and OH radicals were also present and reacted with benzene. Therefore, we first evaluated exactly the contributions due to H and OH so as to establish the amount due to e_{aq}^- .

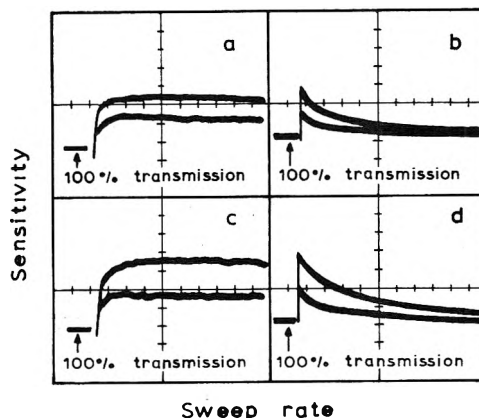


Figure 5. Transient absorptions obtained at 312 nm in pulse radiolysis of neutral, aqueous solutions of $1.01 \times 10^{-2} M$ benzene in the presence of $2 M$ *tert*-butyl alcohol: upper trace, Ar-saturated solutions; lower trace, N_2O -saturated solutions; (a) 500-nsec pulse, sweep rate $1 \mu sec/division$, sensitivity $50 mV/division$; (b) as in a, but sweep rate $100 \mu sec/division$; (c) 200-nsec pulse, sweep rate $1 \mu sec/division$, sensitivity $20 mV/division$; (d) as in c, but sweep rate $100 \mu sec/division$.

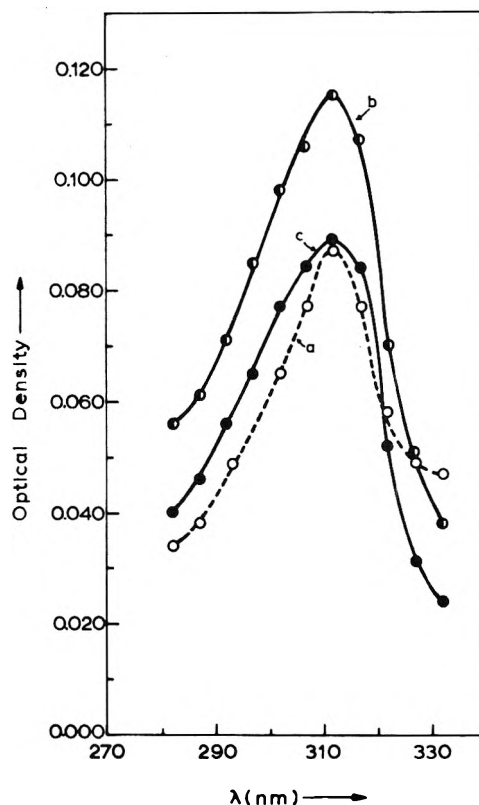


Figure 6. Experimentally observed transient absorption spectra obtained in Ar-saturated solutions of benzene of different concentrations (3.5×10^{-3} and $1.01 \times 10^{-2} M$), at different pH values (neutral, 11, and 13), in all cases with $2 M$ *tert*-butyl alcohol present. Dose 1650 rads/pulse. Every point is the mean value of similar measurements in six different experiments corresponding to various combinations of the conditions described above: (a) 500 nsec after the pulse; (b) $3 \mu sec$ after the pulse; (c) $35 \mu sec$ after the pulse.

Table I sums the results for BH. References 2b and 7 give different data for its ϵ . We find excellent agreement with that of ref 2b and propose that the value $5350 M^{-1} cm^{-1}$ be used. References 2b and 7 also differ on the rate constant of BH formation. Michael and Hart⁷ suggest that this may be connected with the different values of ϵ . If so,

TABLE I: Summary of Rate Constants for the Reaction of H Atoms with Benzene, for the Bimolecular Disappearance of the Resulting Radical C₆H₇· and Spectral Data for the Products

Reaction	$k, M^{-1} \text{sec}^{-1}$	Product	$\lambda_{\text{max}}^{\text{product}}, \text{nm}$	$\epsilon_{\text{max}}^{\text{product}}, M^{-1} \text{cm}^{-1}$	pH	Ref
B + H	$(1.1 \pm 0.1) \times 10^9$	BH	311	5400 ± 500	3	2b
B + H		BH	310		2	6
B + H	$(5.3 \pm 1.0) \times 10^{8a}$	BH	310 ^b	3300 ± 200^b	2, 4	7
B + H		BH	311	$5350 (\pm 10\%)$	2	This work
BH + BH	1.8×10^9				3	2b
BH + BH	$(0.8 \pm 0.15) \times 10^9$	(BH) ₂ (mainly)			4	7
BH + BH	$(1.25 \pm 0.22) \times 10^9$				2	This work

^a At pH 2. ^b At pH 4.**TABLE II: Summary of Rate Constants for the Reaction of OH Radicals with Benzene, for the Bimolecular Disappearance of the Resulting Radical C₆H₆OH·, and Spectral Data for the Products**

Reaction	$k, M^{-1} \text{sec}^{-1}$	Product	$\lambda_{\text{max}}^{\text{product}}, \text{nm}$	$\epsilon_{\text{max}}^{\text{product}}, M^{-1} \text{cm}^{-1}$	pH	Ref
B + OH	$(4.3 \pm 0.9) \times 10^9$	BOH	313		Neutral	2b
B + OH	$(4.3 \pm 0.9) \times 10^9$	BOH	313	3500 ± 800	Neutral	3
B + OH	$(3.3 \pm 0.8) \times 10^9$	BOH	313		3	4
B + OH	$(7.8 \pm 1.1) \times 10^9$	BOH	313		Neutral	5
B + OH	$(7.6 \pm 1.9) \times 10^9$	BOH			Neutral	7
B + OH		BOH	313	4700 ± 600	Neutral	This work, 8
BOH + BOH	$(7.0 \pm 0.9) \times 10^8$	(BOH) ₂ (mainly)	260	2300	Neutral	8
BOH + BOH	$(7.05 \pm 0.35) \times 10^8$	(BOH) ₂ (mainly)	260		Neutral	This work

TABLE III: Summary of Rate Constants for the Reaction of e_{aq}⁻ with Benzene and Spectral Data for the Products

Reaction	$k, M^{-1} \text{sec}^{-1}$	Product	$\lambda_{\text{max}}^{\text{product}}, \text{nm}$	$\epsilon_{\text{max}}^{\text{product}}, M^{-1} \text{cm}^{-1}$	pH	Ref
B + e _{aq} ⁻	$(1.2 \pm 0.2) \times 10^7$	$\xrightarrow{+H_2O}$ BH			13	7
B + e _{aq} ⁻	$(1.4 (\pm 10\%)) \times 10^7$				10.5–11.5	11
B + e _{aq} ⁻	$< 7 \times 10^6$				Neutral	12
B + e _{aq} ⁻		B ⁻	290, 390		<i>a</i>	10
B + e _{aq} ⁻	$(1.3 \pm 0.5) \times 10^7$	B ⁻	312	$2450 (\pm 13\%)$	11, 13	This work
B + e _{aq} ⁻		$\xrightarrow{H_2O}$ BH			13	9 ^b

^a γ irradiated organic glasses (benzene in MTHF) at -196° . ^b γ radiolysis.

then also the value of $k = 1.1 \times 10^9 M^{-1} \text{sec}^{-1}$ from ref 2b would be correct. We have no independent evidence on this point. For the bimolecular decay of BH our rate constant is between the values of ref 2b and 7. We believe our present rate constant ($k = 1.25 \times 10^9 M^{-1} \text{sec}^{-1}$) to be reliable. Note that all data concerning H atom reactions of all three researchers relate to the pH range 2–4.

Table II sums the results for BOH. The rate constant for its formation ($k = 7.7 \times 10^9 M^{-1} \text{sec}^{-1}$) is given in good agreement in ref 5 and 7, revising the previous values of ref 2a and 4. In the present work we confirmed the value of $\epsilon_{\text{BOH}}^{313} 4700 M^{-1} \text{cm}^{-1}$ in ref 8, correcting the previous value in ref 3, which, as has been pointed out,⁸ was derived from mixed spectra. For the bimolecular decay of BOH the present work is in excellent agreement with the value of $7.0 \times 10^8 M^{-1} \text{sec}^{-1}$ of ref 8. Note that all the data from the references referred to and the present work relate to neutral solutions.

In order to study the reaction of e_{aq}⁻ with benzene a pH of 11–13 was mainly used, though our results in neutral solution support our conclusions. In order to derive the results it is necessary to make the reasonable assumption that benzene itself in aqueous solution does not undergo any acid–base change in the pH range 2–13. Both H and OH do undergo such changes and we have included these exactly in our calculations, using the data in ref 16 and in previous work referred to therein. Table III sums the results. We obtained the rate constant of reaction between e_{aq}⁻ and benzene ($1.3 \times 10^7 M^{-1} \text{sec}^{-1}$) in very good agree-

ment with ref 7 and 11. As to the product of the reaction, which is observed under the experimental conditions employed, Michael and Hart⁷ argued that it is BH formed as a result of fast protonation subsequent to primary addition of e_{aq}⁻ to benzene. However, their conclusion was not based on direct experimental evidence but on analogy of the products obtained from e_{aq}⁻ and H reactions. Similar products of course can and do result in both cases. The question is at what stage does the required protonation occur. Our results are not in consonance with the assumption that BH is the first observable intermediate in the reaction of e_{aq}⁻ with benzene. They do agree with the alternative possibility that it is B⁻ itself that we observe. The evidence for this is the following. At the fast sweep rates of 1–5 $\mu\text{sec}/\text{cm}$ and using pulses of 500 nsec or shorter, we observed that the formation of the intermediate due to e_{aq}⁻ addition to benzene was complete in about 3 μsec . The growing in of its spectrum agreed in rate with the rate of disappearance of the e_{aq}⁻ spectrum. We did not observe any stage that could have been due to protonation and two-stage formation of BH. If we make the rather unlikely assumption that protonation is so fast as to be inseparable from e_{aq}⁻ addition, then the additional absorption due to the species will account for only about 35–40% of the amount of BH expected. If we assume that B⁻ is the species obtained and observed, the value of $\epsilon 2450 M^{-1} \text{cm}^{-1}$ shown in Table III is obtained. We observed the decay of the intermediate. At similar total concentrations of radicals, the half-life was shorter, $\sim 60 \mu\text{sec}$, under condi-

tions where some ~75% of the radicals were due to e_{aq}^- and some ~25% to (H + OH), than under conditions where either H or OH were the main species of radicals present. Under these latter conditions the half-life was ~130 μ sec. One has to consider that for H radical reactions the pH was ~3 and for OH a neutral pH was used, while for e_{aq}^- the pH was ~12. All these facts strengthen the view that, when the source of the radicals is mainly e_{aq}^- , B^- is the species observed and reacting. Reactions between charged and neutral forms of radicals are often faster than between two neutral forms. Thus $e_{aq}^- + H \rightarrow H_2 + OH^-$ is faster¹⁶ than $H_{aq} + H_{aq} \rightarrow H_2$ and $O_2^- + HO_2 \rightarrow HO_2^- + O_2$ is faster¹⁷ than $HO_2 + HO_2 \rightarrow H_2O_2 + O_2$. The faster decay observed here may be due to reactions $B^- + BH \rightarrow$ products, $B^- + BOH \rightarrow$ products being faster than $BH + BH \rightarrow$ products, and $BOH + BOH \rightarrow$ products. The reaction $B^- + B^-$ may have been observable at pH 13 under the conditions in ref 7, but no data are reported there. Under our conditions we could not isolate this process.

Our results do not conclusively prove the existence and reactions of B^- , but are entirely consistent with it. The question our work poses is one of time scale. Quite possibly in chemical systems, where B_{solv}^- is allowed to exist long enough, protonation may precede other chemical reactions. On our short time scale and under our experimental conditions B_{aq}^- appears to be observable and to react as such.

The general similarity and differences in details in the rates of reaction, absorption spectra, and further reactions of the product of e_{aq}^- and of H atoms reaction with benzene may be interpreted on the basis of the solvated anion model of e_{aq}^- ,¹⁶ in which the participation of the first hydration layer and partial electron density on water protons

is explicitly considered. These questions will be considered separately.

Acknowledgments. D. G. M. and A. M. M. thank the International Atomic Energy Agency for Fellowships during the tenure of which this work was carried out in Jerusalem.

This research was supported in part by the U. S. Atomic Energy Commission, Division of Biology and Medicine, under Contract with G. S. We thank Mr. Y. Ogdan and Mr. A. Shafferman for valuable advice and help.

References and Notes

- (1) On leave of absence from the Greek State Chemical Laboratories.
- (2) (a) L. M. Dorfman, R. E. Büchler, and I. A. Taub, *J. Chem. Phys.*, **36**, 549 (1962); (b) M. C. Sauer, Jr., and B. Ward, *J. Phys. Chem.*, **71**, 3971 (1967).
- (3) L. M. Dorfman, I. A. Taub, and R. E. Büchler, *J. Chem. Phys.*, **36**, 3051 (1962).
- (4) L. M. Dorfman, I. A. Taub, and D. A. Harter, *J. Chem. Phys.*, **41**, 2954 (1964).
- (5) P. Neta and L. M. Dorfman, *Advan. Chem. Ser.*, No. **81**, 222 (1968).
- (6) B. Chutny, *Nature (London)*, **213**, 593 (1967).
- (7) B. D. Michael and E. J. Hart, *J. Phys. Chem.*, **74**, 2878 (1970).
- (8) A. Mantaka, D. G. Marketos, and G. Stein, *J. Phys. Chem.*, **75**, 3886 (1971).
- (9) M. H. Studier and E. J. Hart, *J. Amer. Chem. Soc.*, **91**, 4068 (1969).
- (10) J. P. Guarino and W. H. Hamill, *J. Amer. Chem. Soc.*, **86**, 777 (1964).
- (11) M. Anbar and E. J. Hart, *J. Amer. Chem. Soc.*, **86**, 5633 (1964).
- (12) E. J. Hart, S. Gordon, and J. K. Thomas, *J. Phys. Chem.*, **68**, 1271 (1964).
- (13) D. G. Marketos, *Anal. Chem.*, **41**, 195 (1969).
- (14) M. S. Matheson and L. M. Dorfman, "Pulse Radiolysis," M.I.T. Press, Cambridge, Mass., 1969, p 74.
- (15) E. J. Hart and M. Anbar, "The Hydrated Electron," Wiley-Interscience, New York, N. Y., 1970, p 42.
- (16) G. Stein in "Hydrogen-Bonded Solvent Systems," A. M. Covington and P. Jones, Ed., Taylor and Francis, London, 1968, p 87.
- (17) D. Behar, G. Czapski, J. Rabani, L. M. Dorfman, and H. A. Schwarz, *J. Phys. Chem.*, **74**, 3209 (1970).

Catalyzed and Uncatalyzed Dissolution of Anhydrous Chromic Chloride in Aqueous Solutions¹

A. Hendifar,² W. F. Libby,*

Department of Chemistry, University of California, Los Angeles, California 90024

and George L. Zimmerman

Department of Chemistry, Bryn Mawr College, Bryn Mawr, Pennsylvania 19010 (Received October 9, 1973;

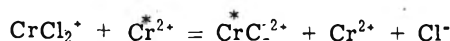
Revised Manuscript Received May 6, 1974)

Publication costs assisted by the U. S. Air Force Office of Scientific Research and the University of California, Los Angeles

The Cr(II)-catalyzed rate of solution of CrCl₃ in aqueous media is consistent with a mechanism analogous to that proposed by Taube and Myers³ for the Cr(II)-catalyzed dissociation of CrCl₂⁺ into CrCl²⁺ and Cl⁻, but after about 40 catalytic cycles, the rate of solution returns to a value somewhat larger than the uncatalyzed rate possibly as a result of the diffusion of Cr²⁺ into the CrCl₃ crystals. The uncatalyzed rate of dissolving of CrCl₃ is very low, increases with the total surface area, is independent of the nature of the cation but depends on the anion, depends little on acidity, and has an activation energy of 11.7 ± 1 kcal/mol and a large activation entropy. Perhaps surface defects with water entering to coordinate gradually the surface Cr³⁺ ions over a particular region to free Cl⁻ ions as well as Cr(H₂O)₆³⁺ constitute a possible mechanism. Insufficient data are at hand to settle the matter.

I. Introduction

The purpose of this work was to study quantitatively the rate of solution of anhydrous chromic chloride in aqueous solutions as a function of the concentration of H⁺, Cl⁻, Br⁻, and other selected ions, temperature, and CrCl₃ particle size in the presence and absence of Cr(II). Taube and Myers³ had studied the homogeneous reaction



and demonstrated that one of the chloride ions from the chromic dichloride ion was transferred to the chromous as the electron transfer occurred to form the nonlabile CrCl²⁺ ion. It seemed reasonable that the known fact that chromous ion catalyzes the dissolving of chromic chloride in aqueous solutions should involve analogs of this reaction. It was our purpose to test this point.

II. Experimental Procedure

A. Materials. 1. Ferrous ammonium sulfate (Baker AR grade used without further purification) solution was prepared and standardized according to a common procedure.^{4a} Diphenylamine was used as an indicator.^{4b,5}

A sample of anhydrous chromic chloride was ground and introduced into a series of sieves with the following openings:^{6,7} (a) 0.295, 0.246, 0.147, 0.124, .061 mm; (b) 0.250, 0.149, 0.074; (c) 0.38, 0.18, 0.117, 0.104, 0.084 mm.

The surface area (BET with N₂) was measured for four particle sizes and the results were as follows.

Particle size, mm	Surface area, m ² /g	Size × area
0.38	0.25	0.095
0.18	0.35	0.063
0.117	0.50	0.0595
0.084	0.64	0.0538

The sieves were arranged in series from the largest to the smallest openings. The sieves were shaken by a sieve shaker until a suitable sample of each particle size was collect-

ed. The CrCl₃ samples were identified by the size of the finest sieve they could pass. Thus, 0.124-mm samples will actually contain a distribution of sizes between 0.061 and 0.124 mm. We know little about the distribution of sizes within a given sample however. Microscopic examinations of particle sizes 0.38, 0.18, and 0.084 mm showed the particles to be platelike crystals. X-Ray diffraction patterns of the above three particle sizes show no change in the structure of CrCl₃ due to grinding.

2. A solution of 0.01 M chromous chloride was prepared by reduction of chromic chloride in a modified Jones reductor containing amalgamated zinc.

3. The amalgamated zinc was prepared according to the procedure given by Kolthoff and Sandell.⁸

B. Apparatus. The nitrogen used for purging was passed through a column maintained at 200° containing metallic copper obtained by H₂ reduction of CuO wire.

The spectrophotometer cell had quartz windows and an inlet and outlet for purging with nitrogen.

Two sets of bottles were used in this work. The first set, used for the measurement of the uncatalyzed rate, was made of 25-mm tubing, 20 cm long, capped with a ground joint. The second set was especially made for the measurement of the catalyzed rate of solution. This set has an inlet and outlet; nitrogen could be introduced to flush out the residual air.

A constant-temperature bath was made according to the design of Hildebrand, *et al.*⁹ The temperature was maintained at 32.8 ± 0.10, 42.5, and 50.8.

C. Procedures. 1. *Analysis.* Chromium in solution was determined according to a slight modification of the procedure given in Kolthoff and Sandell.¹⁰

To 1 ml of CrCl₃ solution was added 2 ml of 0.1 M AgNO₃ followed by 1.5 g of K₂S₂O₈ or (NH₄)₂S₂O₈ and 5 ml of 6 N H₂SO₄. The mixture was diluted to 50 ml and boiled vigorously for 45 min to 1 hr. The pale yellow solution was titrated with 0.1 N ferrous ammonium sulfate using diphenylamine as an indicator. At the end point the color

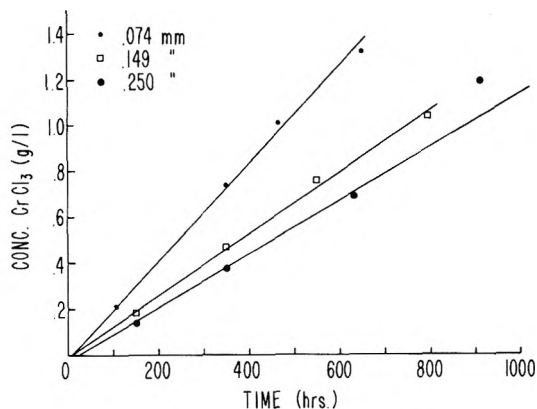


Figure 1. Dissolution of CrCl_3 in 10^{-1} M HCl at 32.8° .

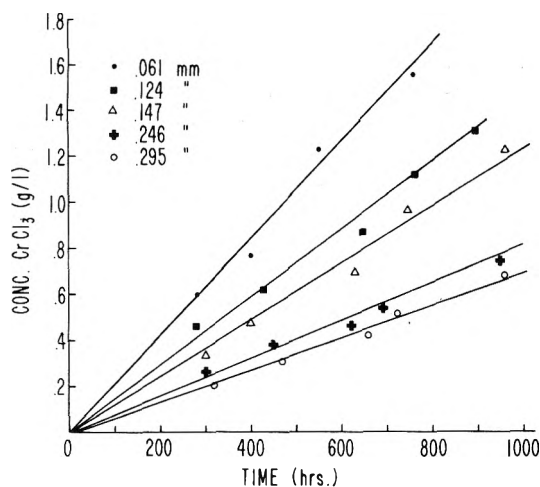


Figure 2. Dissolution of CrCl_3 in 10^{-2} M HCl at 32.8° .

changed from a deep red to a pale green. A few drops of concentrated H_3PO_4 was used to sharpen the end point.

2. *Preparation of CrCl_2 .* Chromous chloride was prepared by the reduction of chromic chloride in a modified Jones reductor. In order to exclude air, nitrogen was introduced into the system to flush out the residual air.

3. *Measurement of the Uncatalyzed Rate.* About 1.00 g of the salt of a given particle size was placed in a sample bottle and 70 ml of HCl or other aqueous solutions as indicated was added. No attempt was made to exclude air. The bottle was placed in a water bath shaking continuously for about 100 hr. A 1-ml sample was withdrawn through a pipet, the tip of which was attached by a small piece of gum rubber tubing to an 0.8-ml fine-fritted glass Büchner funnel which served to prevent any solid CrCl_3 from entering the pipet. Samples were taken and analyzed about every 100 hr for each of the particle sizes. Light was excluded intentionally.

4. *Measurement of the Catalyzed Rate.* One gram of chromic chloride was placed in the special bottle, and 50 ml of HCl solution was added to the salt. The bottle was flushed out with nitrogen for about 5 hr. It was then sealed at both ends and placed in the inert-atmosphere box. A known volume of 0.01 M CrCl_2 solution was added to the solution in the glove box. The bottle was removed from the box and placed in the water bath. The bottle was left in the water bath first for 1 hr. It was then placed in the air lock of the glove box, and the air was flushed out with nitrogen for 30 min. A small sample was taken for analysis, and the

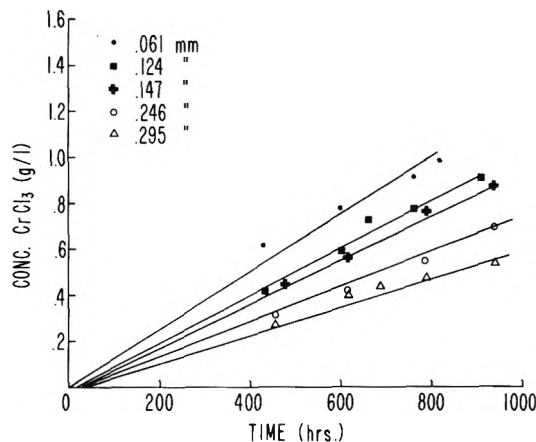


Figure 3. Dissolution of CrCl_3 in 10^{-3} M HCl at 32.8° .

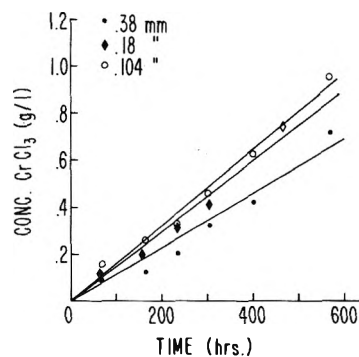


Figure 4. Dissolution of CrCl_3 in 10^{-1} M HCl at 42.5° .

bottle was returned to the water bath for a longer time (about 3 hr). This procedure was repeated at different intervals.

III. Results

A. *The Uncatalyzed Rate.* The uncatalyzed rate was first studied with particle sizes 0.061, 0.074, 0.124, 0.125, 0.147, 0.149, 0.246, and 0.295 mm in HCl concentrations of 10^{-1} , 10^{-2} , and 10^{-3} M at 32.8° with the results in Figures 1–3. Second, with particle sizes 0.38, 0.18, 0.117, 0.104, and 0.084 mm, at temperatures of 42.5° and 50.8° for various concentrations of HCl, NaCl, KCl, KBr, and HClO_4 solutions, the rate was studied with the results shown in Figures 4–7.

These results indicate that (1) the rate is very slow and over a period of 1000 hr shows no signs of changing when something less than 10% has dissolved, (2) the rate increases with total surface area exposed (Table I, Figure 8), (3) the activation energy is low at about 11.7 ± 1 kcal/mol (Table II), (4) Na^+ and K^+ give the same rates (Table III), (5) a tenfold increase (0.01 to 0.1 M) in NaCl or KCl concentration decreases the rate 17% at 42.5° with 0.084-mm ($0.64\text{-m}^2/\text{g}$) powder (Table III), (6) H^+ behaves nearly the same as Na^+ and K^+ at 42.5° but increases the rate slightly as its concentration is increased at 32.5° (Table IV), (7) Br^- rates are 21% larger than Cl^- rates at 42.5° and 0.01 M; at 0.1 M, they are 22% larger (Table V), and (8) the rate is increasing somewhat as the concentration of HClO_4 is decreasing (0.01 to 0.1 M) at 42.5° (Figure 7).

B. *The Catalyzed Rate.* In the case of the catalyzed rate of solution of CrCl_3 in 0.1 M HCl the rate was studied for the particle sizes 0.072, 0.125, and 0.245 mm, using two dif-

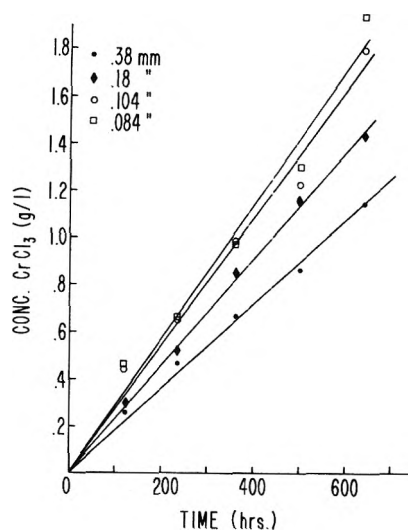


Figure 5. Dissolution of CrCl₃ in 10⁻¹ M HCl at 50.8°.

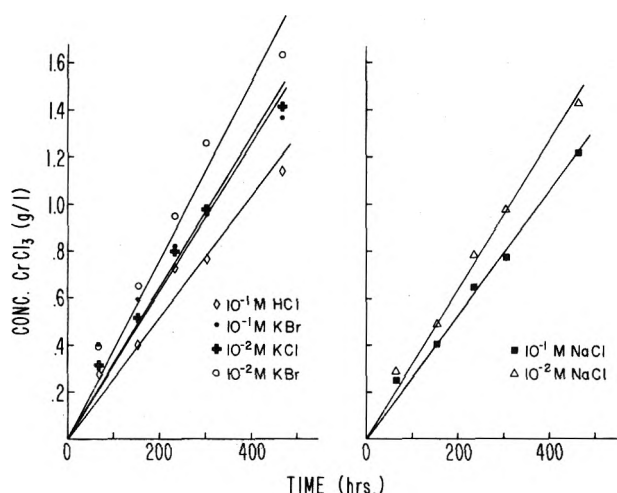


Figure 6. Dissolution of CrCl₃ in 10⁻¹ and 10⁻² M KCl, KBr, and NaCl at 42.5°; particle size 0.084 mm.

ferent concentrations of the catalyst (Cr²⁺): 2.38×10^{-4} and 4.80×10^{-4} M. The results are given in Figures 9 and 10.

These results indicate that (1) after two to four dozen catalytic cycles of the Cr²⁺ the catalytic rate diminishes dramatically (we call this the "turnover" point), (2) the process is a surface phenomenon since the rate is higher for finer material, (3) the rate increases with increasing concentration of Cr²⁺ and the total CrCl₃ dissolved before turnover is nearly proportional to the square of the initial Cr²⁺ concentration, (Cr²⁺)₀, (4) there is very rapid initial rate of dissolving over a period of about 1 hr when the turnover takes place. After that, the rate of solution is slower but still considerably larger than the uncatalyzed rate. The ratio of the rate of solution after turnover for the catalyzed systems to the rate of the uncatalyzed systems both for the same particle size increases with particle size.

IV. Discussion

A. *The Uncatalyzed Dissolving.* The activation energy of the uncatalyzed dissolving of CrCl₃ in aqueous solutions is about 11.7 kcal/mol (Table II). This low value taken with the very low rate shows that the reaction has a large negative entropy of activation.

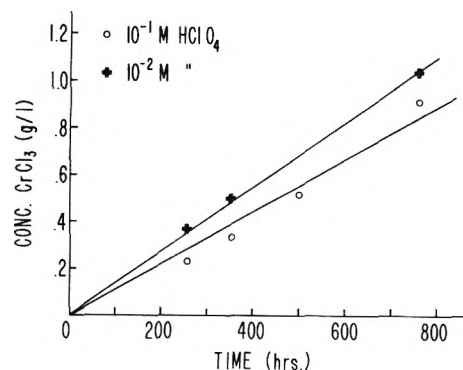


Figure 7. Dissolution of CrCl₃ in 10⁻¹ and 10⁻² M HClO₄ at 42.5°; particle size 0.084 mm.

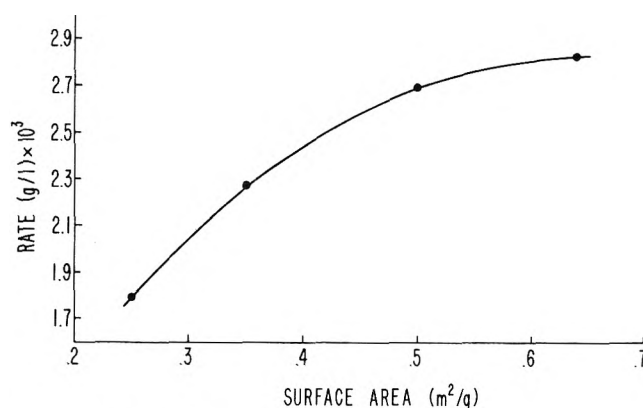


Figure 8. Rate of dissolution of CrCl₃ vs. surface area.

TABLE I: Surface Area Effects^a

Particle size, mm	Surface area, m ² /g	Rate × 10 ³ , g/(l. hr)
0.38	0.25	1.79
0.18	0.35	2.27
0.117	0.50	2.69
0.084	0.64	2.82

^a Rates at 50.8°; HCl concentration 0.1 M.

TABLE II: Temperature Coefficient (0.1 M HCl)

Temp, °C	Rate × 10 ³ , g/(l. hr)	ΔH*, kcal/mol	Particle size, mm
42.5	1.15	10.8 ± 1	0.38
50.8	1.79		
32.8	0.7		0.25
50.8	2.0	11 ± 1	
42.5	1.49	10.4 ± 1	0.18
50.8	2.27		
42.5	1.60		0.084
50.8	2.82	13.9 ± 1	

TABLE III: Cation Effects—Na⁺ and K⁺ Concentrations^a

(NaCl), M	Rate × 10 ³ , g/(l. hr)	(KCl), M	Rate × 10 ³ , g/(l. hr)
0.1	2.6	0.1	2.6
0.01	3.2	0.01	3.2

^a Temperature 42.5°; particle size 0.084 mm.

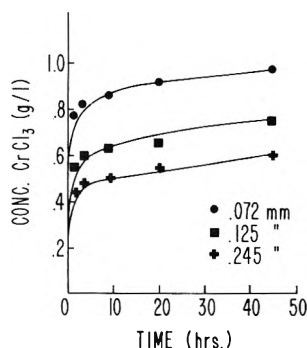
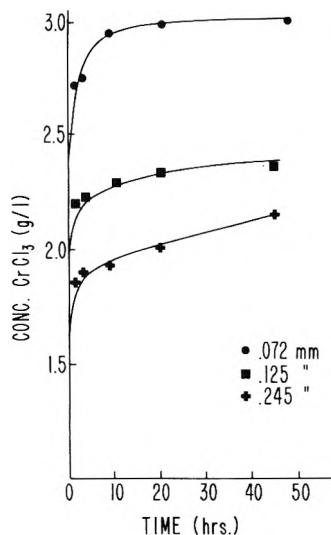
The rate increases nonlinearly with surface area (Table I, Figure 8). The nature of cation has little effect and the rates are somewhat faster at lower salt concentrations.

TABLE IV: Cation Effects—H⁺ Concentration^a

(HCl), M	Rate × 10 ³ , g/(l. hr)
0.1	1.1
0.01	0.90
0.001	0.80

^a Temperature 32.8°; particle size 0.25 mm.TABLE V: Anion Effects—Cl⁻ vs. Br⁻^a

Salt	Concn, M	Rate × 10 ³ , g/(l. hr)
KCl	0.1	2.58
KBr	0.1	3.14
KCl	0.01	3.15
KBr	0.01	3.8

^a Temperature 42.5°; particle size 0.084 mm.Figure 9. Dissolution of anhydrous CrCl₃ in 10⁻¹ M HCl catalyzed by 2.3 × 10⁻⁴ M CrCl₂.Figure 10. Dissolution of anhydrous CrCl₃ in 10⁻¹ M HCl catalyzed by 4.80 × 10⁻⁴ M CrCl₂.

Even H⁺ has little effect, the rate increasing slightly as the H⁺ concentration is increased from 0.001 to 0.100 M at 32.5°. On the other hand, the anions have larger effects.

Possibly surface defects which coalesce to free a CrCl₃ molecule is the general nature of the mechanism with anions from the solution playing an essential role. There are several possibilities but we have insufficient data to distinguish between them.

B. Mechanism for the Catalyzed Dissolving. The catalysis of the dissolving of CrCl₃ by Cr²⁺ can be understood as

TABLE VI: Rates after Turnover vs. Uncatalyzed Rates (32.8°)

Particle size, mm	Rates × 10 ³ , g/(l. hr)		
	Uncatalyzed	Catalyzed after turnover	
		2.3 × 10 ⁻⁴ M Cr ²⁺	4.8 × 10 ⁻⁴ M Cr ²⁺
0.072	2.3	3.0	1.2
0.125	1.5	3.4	4.7
0.245	1.2	2.9	12

TABLE VII: Turnover Points at 32.8°

Particle size, mm	g of Cr ²⁺ /l. in 0.1 M HCl		Ratio
	(Cr ²⁺) = 2.3 × 10 ⁻⁴ M	(Cr ²⁺) ₀ = 4.8 × 10 ⁻⁴ M	
0.074	0.8	2.8	3.5
0.125	0.55	2.2	4.0
0.245	0.45	1.8	4.0

being due to the lability of Cr(II) complexes and the nonlability of Cr(III) structures. Thus, CrCl₃ is slow to dissolve since the Cl⁻ ions are held to the surface Cr³⁺ ions. An approaching Cr²⁺, however, can be absorbed on the surface and share a Cl⁻ with the surface Cr³⁺. This immobilizes the shared Cl⁻ in the coordination sphere of the newly created Cr³⁺ now in aqueous solution as something like Cr(H₂O)₅Cl²⁺. The surface layer of the solid now has a Cl⁻ vacancy and a Cr²⁺ ion beneath it. Cr²⁺ ion is labile and can dissolve taking two Cl⁻ ions, thus completing the catalytic cycle. However, before this can happen, two neighboring Cl⁻ ions must be freed. This appears to require a certain minimum surface population of Cr²⁺ ions before the cycle can be completed.

After two or three dozen such trips, the Cr²⁺ seems to disappear, or at least the catalytic activity does, in a phenomenon we call the "turnover" corresponding to the sharp bend in Figures 9 and 10. The rate after turnover appears to be somewhat larger than the uncatalyzed rate (*cf.* Table VI), and the ratio of catalyzed rate after turnover to uncatalyzed rate appears to increase with particle size (*cf.* Table VII).

There is much evidence³ derived from studies of oxidation-reduction reactions involving Cr²⁺ and Cr³⁺ that, in the activated complex, there is a formation of a bridge between Cr³⁺ and Cr²⁺ by a ligand associated with the initial Cr³⁺. In the case under study, the ligand can only be chloride. Taube and Myers³ have observed this bridging mechanism in the case of catalysis of the reaction CrCl₂⁺ → CrCl₂²⁺ + Cl⁻ by Cr²⁺ where one ligand from CrCl₂⁺ acts as the bridging group between Cr³⁺ and Cr²⁺. These authors observed that the only ligands participating in bridging between Cr³⁺ and Cr²⁺ come from Cr³⁺ and not from the Cr²⁺ or other ions in the solution.

At first sight, one might think that the turnover phenomenon was due to oxidation by oxygen which was destroying the Cr²⁺ and the catalysis causing the "turnover." However, great care was taken to exclude oxygen, as described above, and this theory could hardly explain the increase of the ratio of the residual rate to that for the uncatalyzed system nor its increase with particle size as seen in Table VI.

Another possibility comes to mind, namely, that the CrCl₃ crystals are impure and contain oxidizing agents. No evidence for such impurities was found by analysis. How-

ever, the amounts required are quite small: 4.6×10^{-6} mol of Cr^{2+}/g of CrCl_3 for the $2.3 \times 10^{-4} M$ Cr^{2+} cases and twice this for the $4.8 \times 10^{-4} M$ cases. This theory, however, also cannot explain the rates after turnover being larger than those in the uncatalyzed cases nor the variation of the rate ratio with particle size.

Thus we seem to be driven to consider another explanation: the internal dissolving of the surface-adsorbed catalytic Cr^{2+} ions into the CrCl_3 crystals by diffusion so as to remove them from action.

While waiting for the necessary two labile neighbors to appear to free two Cl^- ions, the surface-exposed Cr^{2+} has a chance to diffuse inward and be replaced by a nonlabile $\text{Cr}^{3+}\text{Cl}^-$ on the surface, thus being removed from the catalytic cycle. The simultaneous movement inward of an electron to an underlying Cr^{3+} neighbor converts it into labile Cr^{2+} and the outward movement of a Cl^- to transfer to the empty surface site would accompany this change. The formerly surface-exposed labile Cr^{2+} would then have been converted to a nonlabile Cr^{3+} with a surface Cl^- bound to it.

C. Tests of the Proposed Mechanism. Observations show that the total CrCl_3 catalytically dissolved before the "turnover" is proportional to the square of the initial Cr^{2+} concentration, $(\text{Cr}^{2+})_0$, as set forth in Table VII.

Our solid solution theory explains this as being due to the inward diffusion of Cr^{2+} being essentially independent of the concentration of Cr^{2+} in the solution because of the requirement that a large fraction of the surface be covered by Cr^{2+} before the catalytic cycle can be completed. This makes the rate of inward diffusion independent of the Cr^{2+} concentration and requires that the total time elapsed until complete Cr^{2+} removal from the solution be proportional to the total Cr^{2+} present originally, $(\text{Cr}^{2+})_0$. The rate of catalyzed dissolving also will be proportional to $(\text{Cr}^{2+})_0$ so the total CrCl_3 dissolving before turnover should be proportional to $(\text{Cr}^{2+})_0^2$.

Now it is clear from Table VI that the rates after turnover are larger than the uncatalyzed rates. This is explained as being due to the exposure of Cr^{2+} as the crystal

dissolves and exposes Cr^{2+} on the surface until the necessary fraction of the monolayer is present when it will dissolve and catalyze the dissolving of CrCl_3 until it once again diffuses into the crystal, after which the process repeats. For larger crystals, the surface area is smaller and the diffused Cr^{2+} will be more concentrated and therefore will be more likely to be freed for use when a given fraction of the total standard 1.00 g of CrCl_3 has dissolved. This explains qualitatively the fact that the ratio of the rates increases with particle size.

Acknowledgments. The authors wish to thank Mr. Selig Cynman (UCLA, Department of Chemistry) for assisting in the experimental work by measuring the uncatalyzed rate of dissolution at different temperatures. Ms. Rima Christianson's help in the laboratory is also appreciated.

Supplementary Material Available. The preparation of CrCl_2 and the apparatus used (Figure 11) will appear following these pages in the microfilm edition of this volume of the journal. Photocopies of the supplementary material from this paper only or microfiche (105 × 148 mm, 24× reduction, negatives) containing all of the supplementary material for the papers in this issue may be obtained from the Journals Department, American Chemical Society, 1155 16th St., N.W., Washington, D. C. 20036. Remit check or money order for \$3.00 for photocopy or \$2.00 for microfiche, referring to code number JPC-74-1993.

References and Notes

- (1) This research was sponsored by the Air Force Office of Scientific Research, United States Air Force, under Grant No. 71-2019.
- (2) On leave from The National University of Iran.
- (3) H. Taube and H. Myers, *J. Amer. Chem. Soc.*, **76**, 2103 (1954).
- (4) I. M. Kolthoff and E. B. Sandell, "Text Book of Quantitative Inorganic Analysis," 3rd ed, Macmillan, New York, N. Y., 1952: (a) pp 579-580; (b) p 474.
- (5) A. R. Pray, *Inorg. Syn.*, **5**, 154 (1957).
- (6) The Tyler Standard Screen Scale, The W. S. Tyler Co., Cleveland, Ohio.
- (7) U. S. Standard Sieve Series, Dual Manufacturing Co., Chicago, Ill.
- (8) See ref 4, pp 568-570.
- (9) J. H. Hildebrand, *et al.*, *J. Phys. Colloid Chem.*, **53**, 886 (1946).
- (10) See ref 4, p 690.

Equilibrium Vaporization Rates and Vapor Pressures of Solid and Liquid Sodium Chloride, Potassium Chloride, Potassium Bromide, Cesium Iodide, and Lithium Fluoride

Curtis T. Ewing and Kurt H. Stern*

Electrochemistry Branch, Naval Research Laboratory, Washington, D. C. 20375 (Received December 17, 1973; Revised Manuscript Received May 30, 1974)

Publication costs assisted by the Naval Research Laboratory

Equilibrium vaporization rates of solid and liquid NaCl, KCl, KBr, CsI, and LiF have been measured, using Knudsen cells, with orifice flows in the molecular, hydrodynamic, and transitional regions. Observed rates in the latter two regions are always greater than those predicted by the Hertz-Knudsen theory for molecular flow. Methods for calculating equilibrium vapor pressures from rates in the transitional and hydrodynamic regions have been developed, and vapor pressures calculated in this way agree well with those derived from standard thermodynamic procedures. The ratio, actual flow/(hypothetical) Knudsen flow, in the transition regime depends only on the mean free path and is independent of the diameter of the orifice.

Introduction

In a previous paper¹ we reported measurements of the free (vacuum) vaporization rate of solid NaCl up to the melting point and have now also completed a similar (unpublished) study for liquid NaCl. In order to interpret these and similar data for other alkali halides in terms of a vaporization mechanism it is necessary to compare free vaporization rates with those obtained under equilibrium conditions, *e.g.*, from Knudsen cells. In our earlier paper¹ we accepted the thermodynamic data for NaCl given in the JANAF tables,² However, the experimental data on which these tables are based show a gap of several hundred degrees over which, for the high-temperature solid and the low-temperature liquid, no experimental data are available. The authors of the tables therefore had to extrapolate the solid data upward and the liquid data downward, adjusting them so as to yield the same vapor pressure for the solid and liquid at the melting point. Although the results thus obtained seem quite reasonable, it appeared to be useful to actually make measurements over this range to verify the JANAF calculation.

There is also a more important reason for extending Knudsen cell measurements to higher temperatures. The equation which was derived by Hertz³ and Knudsen⁴ for calculating the equilibrium vapor pressure from the mass flux through an orifice assumes that the flow is molecular, *i.e.*, intermolecular collisions near the orifice are negligible. In that case the only corrections which need be applied are those derived by Clausing⁵ for finite-length holes.

As the mean free path decreases, the problem of calculating vapor pressure from flux becomes more complicated because the flow regime changes from molecular to hydrodynamic and the Knudsen equation is no longer valid. Therefore most Knudsen cell measurements have been restricted to the molecular region. However, because the Knudsen cell method is very attractive for determining vapor pressures it seemed worthwhile to find out if it is possible to calculate these from measurements of flow in the transitional and hydrodynamic regions. Much of the relevant theory for high flow rates has been developed by gas dynamicists interested in flow through orifices and pipes. The phenomena encountered are dependent on the magnitude of the

mass flow and independent of the nature of the effusing substance. Thus, if our interpretation of the mass flux in terms of the equilibrium vapor pressure is correct it should hold for any substance.

To test experimentally the usefulness of the Knudsen method at high flow rates, we selected five alkali halides. The particular salts were selected to provide materials which vaporize over a wide temperature range and for which the molecular compositions of the vapors are well known.

Theory

A. Flow of Gases Through Thin-Edge Orifices. The problem of total mass flow of gases through orifices for flows extending from the molecular to the hydrodynamic region has been experimentally investigated by Knudsen,⁶ Smetana, *et al.*,⁷ Liepmann,⁸ Carlson, *et al.*,⁹ and Bianco and Boridy.¹⁰ The field in general has been reviewed and summarized by Bianco¹⁰ and Shapiro.¹¹

For the measurements reported in this article, a saturated vapor flows from a constant temperature source and, therefore a constant pressure source, through a thin-edged orifice into an evacuated chamber. Since the flow characteristics of a saturated vapor should be analogous to those of a "permanent" gas (as long as the effusing vapor does not condense at the orifice), the mass flow per unit area J for a single species is related to the pressure P of the gas in the cell by

$$J = \Gamma P(M/RT)^{1/2} \quad (1)$$

where T is the temperature of the vapor in the cell, M is the molecular weight, and Γ is a factor which depends according to several references^{8,10,11} on the Knudsen number λ/D and the specific-heat ratio $\gamma = C_p/C_v$.

Measurements of flow through an orifice are generally made under conditions permitting variation of the pressures upstream and downstream of the orifice, and the value of Γ in eq 1 will also depend¹⁰ on the pressure ratio. However, Γ will reach its asymptotic limit¹⁰ (or its maximum value) when the ratio of the upstream to downstream pressure exceeds approximately 200. For flow measurements of the type performed in this study, where the space

external to the orifice is under evacuation, pressure ratios are always greater than 10^3 and the value of Γ will have its maximum value at all flow conditions.

Equation 1 is strictly applicable only for flow through a vanishingly thin orifice. Practical orifices generally have effective thicknesses in the neighborhood of 0.001 in. and the flow through the orifice is reduced by a small, but well-characterized, Clausing⁵ effect. The magnitude of this correction for the types of flows encountered in this study is discussed in a subsequent section.

The flow of gases is characteristically divided into three regions: molecular, transition, and hydrodynamic.

Molecular Flow. Where the mean free path of the molecules is relatively large compared to the diameter of the orifice, we have from kinetic theory the well-known expression for molecular effusion

$$J_K = 1/4\rho\bar{c} = (2\pi)^{-1/2}P(M/RT)^{1/2} \quad (2)$$

where ρ is the density and \bar{c} is the average velocity of the molecule. This represents a limiting case of eq 1 with $\Gamma = \Gamma_K = 0.399$.

Hydrodynamic Flow. It has been well established experimentally by Liepmann,⁸ Smetana, *et al.*,⁷ Bianco and Boridy,¹⁰ and Carlson, *et al.*,⁹ that at high pressures the average velocity of the gas at an orifice approaches the sonic limit and that above this limit in the hydrodynamic region mass flow is dependent only on the density of the gas and the coefficient Γ . The coefficient above the limit is theoretically constant and its magnitude is determined by the specific-heat ratio γ and a discharge coefficient C_D . The equation¹⁰ relating these quantities at high pressure ratios is

$$\Gamma = C_D[\gamma/2(\gamma + 1)]^{(\gamma+1)/(\gamma-1)} \quad (3)$$

The coefficient Γ determined from eq 1 and, therefore, the ratio Γ/Γ_K was found to be constant, within experimental error, for potassium chloride (see Figures 1 and 2) and for the other alkali halides measured in this study. The flow range over which Γ exhibits constancy has been shown^{8,10} to extend for at least one order of magnitude change in the pressure or in the flow rate.

The alkali halides exhibit association in the vapor state, and reliable values of the pressure and the molecular composition of a vapor are required to accurately define the value of the coefficient Γ from observed orifice flows in the hydrodynamic region. For KCl there is excellent agreement over a wide temperature range² between existing measurements of both vapor pressure and molecular composition, and the average observed value of Γ for this salt is 0.574. If it is assumed that KCl vapor is essentially diatomic with one degree of vibrational freedom ($\gamma = 1.29$), eq 3 predicts a value of 0.86 for C_D . (Equation 3 is not sensitive to small changes in γ .) Dimers in the alkali halide would have a γ of approximately 1.11, and the neglect of the dimer content in calculating C_D introduces an error of only 1–2%.

There are several existing measurements of the value of C_D at high pressure ratios for the flow of monoatomic and diatomic gases through thin orifices. Perry¹² found a value of 0.84 for air; Liepmann⁸ a value of 0.81–0.84 for Ar, N₂, and CO₂; Bianco¹⁰ a value of 0.82 to 0.88 for N₂; and Smetana, *et al.*,⁷ a value of 0.858–0.89 for N₂. Frankl¹³ computed a theoretical value of 0.85 for the flow of a diatomic gas through a thin two-dimensional slit, and as a first approximation it can be assumed that a slit and an orifice should have the same value¹⁰ of the coefficient.

Transition Flow. In this region the value of the coefficient Γ in eq 1 progressively changes from 0.399 to its value at the hydrodynamic limit. The region is generally believed to be limited to the range $0.1 < \lambda/D < 10$.

B. Mass Flow, Vapor Pressure, and Molecular Association. At saturation the vapors of the five alkali halides under study contain substantial amounts of dimer and, in the case of LiF, trimer. Even so, the total vapor pressure is readily obtained from the observed flux in the molecular region by treating the gas as an ideal mixture of molecular species. Using this principle and taking into account the preferential escape of light molecules through the orifice, the weight fraction X of each molecular species i in the effusing vapor is related to the equilibrium mole fractions N in the vapor by

$$X_i = N_i\sqrt{i}/\sum(N_i\sqrt{i}) \quad (4)$$

where $i = 1$ for monomer, 2 for dimer, etc. and the equilibrium vapor pressure P_{eq} is the sum of the partial pressures for the individual molecular species, such that

$$P_{eq} = \sum P_i = \sum[X_i J_K (2\pi RT/M_i)^{1/2}] \quad (5)$$

A problem of interpreting flux information arises for the hydrodynamic and transition regions. If the orifice were of sufficient length to maintain streaming conditions within its length, the weight fraction of a species in the vapor would be that in the equilibrium vapor and the equations above would have to be modified. However, it will be shown (Table I) from observations of flow at high pressures through orifices of varying lengths that the major portion of the pressure drop appears to occur within the cell and that the flow through the thin orifice is principally free molecular. On the basis of this evidence, eq 4 and 5 were used to compute compositions and pressures in the hydrodynamic and transition regions. It will be shown later that in the high-flow regimes, J_K represents the hypothetical Knudsen value, *i.e.*, the mass flow which would be observed if molecular flow conditions existed at all temperatures.

For the purpose of comparing observed mass flows in this study with those computed from existing partial pressure and composition information in the JANAF² tables, the following equation, based on the same principles used to derive eq 5, was used.

$$J_K = \sum J_i = \sum[P_i(2\pi RT/M_i)^{-1/2}] \quad (6)$$

Experimental Method

Equilibrium vaporization rates for the alkali halides were obtained isothermally with small Knudsen cells by observing the loss in weight against time with a recording Mettler thermoanalyzer.¹

The Knudsen cell was surrounded by a larger chamber maintained at an apparent vacuum of 10^{-5} Torr or lower. Temperatures were precisely measured with a platinum–platinum–10% rhodium thermocouple, the junction of which was in direct thermal contact with the base of the cell. The thermobalance and the associated experimental system were previously used for a free-evaporation study on sodium chloride.¹ The extensive precautions taken in that study to assure furnace isothermality and reliability of the temperature measurement were repeated in the present work.

The balance is provided with 1- and 0.1-g standard

weights for internal calibration of both ranges. To supplement this, all traces were periodically calibrated by adding and removing standard weights from a large crucible serving as balance pan. The recorded weight differences observed were generally within 0.03 mg of the standard weight for the 0.1-g range and within 0.3 mg for the 1.0-g range, and no correction factors were required. The chart speed was also periodically checked and no calibration or adjustment was required.

All vaporization runs for a particular salt in both its solid and liquid phases were made using single lots of optical grade single crystals procured from the Harshaw Chemical Co. Cation impurities in all lots, when analyzed spectroscopically, were found in concentrations sufficiently low to have no effect on the observed rates. In an effort to reduce surface impurities to a minimum, single crystals were shaped and loaded into the cells under a controlled dry atmosphere. In addition, the Mettler apparatus itself afforded a means of cleaning exposed crystal surfaces. Prior to the actual rate measurements, a sample and cell were always preheated under high vacuum to constant weight at a temperature of 400–500°. This procedure removes many of the surface-adsorbed volatile impurities such as water. It was also customary, before performing any experiment above the melting point of the salt, to premelt the sample under vacuum in order to improve thermal contact between the salt and crucible.

Knudsen Cell. The typical cell was of high-purity Poco graphite which was a suitable container for all the salts except CsI. This salt, with its low surface tension, formed a wetting contact angle with graphite and diffused into the pores of the crucible, so that it was necessary for containment to use a thin palladium liner cemented with gold paste¹ into the graphite. All crucibles and metal covers, prior to filling with a salt sample, were pre-fired in the Mettler system to constant weight at a temperature of 900–1200°.

Each cell was designed for a positive gasket seal of 1-mil thick platinum or palladium sheet in which the small orifice was formed. Nominal orifice sizes were $\frac{1}{32}$, $\frac{1}{16}$, and $\frac{3}{32}$ in. in diameter. Each salt was measured in at least two cells of different orifice sizes, and, for NaCl, in six different cells of these three nominal sizes. No difference in the normalized mass flows ($\text{mg cm}^{-2} \text{min}^{-1}$) was ever observed. The integrity of the seal was always maintained, and periodically was checked by comparing mass flows obtained with the gasket seal against those obtained with the same size orifice cemented to the graphite with gold paste. The paste and the procedure for using it were described in our previous study.¹

The forming of satisfactory holes in the thin sheet was initially a problem and machining techniques had to be developed for rigidly supporting the sheet and forming clean round holes. The size of each orifice was measured with a traveling microscope before and after each experiment, and dimensions were generally reproducible to better than 0.0002 in. Thermal expansion corrections were applied to obtain the orifice size at the temperature of the experiment.

The cylindrical hole in the graphite cell used to contain the salt was always 0.3 in. in diameter or larger so that the ratio of surface area of the salt to that of the orifice was at least 100 for the $\frac{1}{32}$ in. size and 25 for the $\frac{1}{16}$ in. size. Even so, due to the presence of the hole in the cell, there is a departure from true equilibrium pressure, and the magnitude

of the effect should be considered. Many investigators^{14–18} have studied the problem in detail, but the most rigorous analysis and treatment is that by Carlson, *et al.*¹⁸ From that work it can be reliably shown that for those salts which have relatively high vaporization coefficients the deviation of the observed rate from the true equilibrium value is not great for $\frac{1}{32}$ - and $\frac{1}{16}$ -in. orifices. Undersaturation should not exceed 1% for the $\frac{1}{32}$ in. diameter and 3% for the $\frac{1}{16}$ in. However, an undersaturation of 7% is predicted for the $\frac{3}{32}$ -in. orifice, and for this reason only a few measurements with NaCl were made with the larger orifice size.

Even though the experiences of other investigators seemed to preclude any large error from undersaturation, the authors believed that experimental evidence for each salt was necessary. Consequently, comparable flow measurements for each salt were routinely made to as high a temperature as possible with cross-sectional areas differing by at least a factor of 4 to 1. No systematic difference in observed flow rate per unit area was ever found for any of the salts, supporting the conclusion that significant undersaturation with either the $\frac{1}{32}$ - or the $\frac{1}{16}$ -in. orifice did not occur.

Heat Transfer Processes. Vaporization is an endothermic process, and for the rapid evaporation rates encountered in this study it was necessary to make certain that the rate was not controlled by some heat-transfer process. The heat-transfer problem was considered in some detail in a previous paper.¹ It was pointed out above that the possibilities of cell undersaturation required that flow measurements for each salt be made with at least two orifices, of $\frac{1}{32}$ and $\frac{1}{16}$ in. in diameter. Therefore, for high evaporation rates with each salt, it was possible to directly compare the mass flow per unit area at the same temperature for experiments with observed vaporization rates (and thus required heat transfer rates) differing by at least a factor of 4 to 1. Since no significant differences in absolute rates were ever observed, we conclude that the heat-transfer rate to each salt is sufficient to offset the heat-loss due to vaporization.

Another possible source of error, also directly related to poor heat transfer, is self-cooling of the salt at the vaporizing surface. However, it was consistently demonstrated experimentally that even at the highest vaporization rates the steady-state isothermal rate remained constant while vaporizing at least 95% of the salt added to the cell. This, we believe, eliminates the possibility of significant self-cooling.

Treatment of Experimental Data

The application of the Knudsen method to determine vapor pressure under conditions where the flow through an orifice is in the continuum region is new. Techniques to analyze and interpret the data had to be developed and are presented here in some detail.

It has already been established^{8–10} for flows in the hydrodynamic and transition regions that the mass flow J is always higher than, but characteristically related to, the corresponding flow J_K which would be predicted from the Knudsen equation. In general, to obtain vapor-pressure information from mass-flow observations in the high-flow regions, one must generate values of the normalized flow J_K from known relationships between J_K and J . The procedures used for all three regions are discussed below.

Molecular Region. For free-molecular flow, J_K was measured directly and smoothed data in this region for each salt were obtained by fitting the least-squares equation to the data in the form $\log J_K$ vs. $1/T$. The approach of Γ in

the transition region to the free-molecular limit Γ_K is slow and the linearity of the plot of $\log J_K$ vs. $1/T$ in this region was carefully analyzed to make certain that no data from the lower part of the transition region were inadvertently used in deriving the molecular-region curve.

Hydrodynamic Region. Experimental flow data extending into the hydrodynamic region were obtained for four of the alkali halides. Information on LiF was not obtained in this region due to an apparatus-limiting temperature of 1100° . The interpretation of the flow information required first that the lower limit of the hydrodynamic region for each salt be clearly established. For three of the salts (KCl, NaCl, and CsI) experimental flows were observed well into the hydrodynamic region, and the limit was defined by the change in slope of $\log J$ vs. $1/T$. It will be shown later that this limit occurs at roughly the same mean free path for all the salts, and this fact permitted us to establish that the higher flows observed for KBr were in the hydrodynamic region even though the temperature range with flows in this region was short.

The experimental constancy of the coefficient Γ (and therefore the ratio Γ/Γ_K) in the hydrodynamic region for the alkali halides and for other materials was discussed in the theory section of this report. It was assumed in our treatment of the data in this region that Γ/Γ_K is a constant for all the salts, and that J_K for flow rates above the hydrodynamic limit is equal to $J/(\Gamma/\Gamma_K)$. The KCl experimental value ($\Gamma = 0.754$), which has already been shown to be within a few per cent of theoretical, was selected as being the best available value. This was selected, rather than one slightly different which might have been generated from either theoretical or observed values of the discharge coefficient C_D , for the following reason. The vapors of alkali halides are known to be moderately associated, and the KCl experimental value of Γ/Γ_K should incorporate any influence from this effect. The assumption that the value of the ratio does not change for NaCl, KBr, and CsI appears justified since the dimer contents of the four alkali halide vapors are surprisingly similar, differing by only a few per cent; and, in addition, eq 3 is rather insensitive to a change in γ .

Transition Region. For four of the salts the hydrodynamic limit of the transition region occurs at saturation pressures some 70 – 100° above the melting point and the free-molecular limit at pressures some 80 – 110° below the melting point. If an extrapolation procedure is to be used to obtain J_K in the transition region, the question arises as to the expected deviation from linearity of $\ln J_K$ vs. $1/T$ for temperature ranges of the order of 100° . The activation energy E_a for the equilibrium vaporization process is proportional to $d \ln J_K/d(1/T)$ and theoretically is expected to exhibit the same temperature dependence as does the standard thermodynamic enthalpy of vaporization ΔH_v° . From data in the JANAF tables² $d \ln J_K/d(1/T)$ is expected to decrease 1–2% per 100° temperature rise. This change of slope is within the expected experimental error in J_K and therefore an extrapolation procedure is justified.

For all the alkali halides, with the exception of LiF, values of J_K in the transition region were generated by linear extrapolation of $\ln J_K$ vs. $1/T$ from known values of $\ln J_K$ at the hydrodynamic and free-molecular limits to that value at the melting point which gives a change in slope equal to the theoretical value. It can be readily shown by differentiating the Hertz–Knudsen equations for the solid and the liquid at the melting point, that the difference in

slope of $\ln J_K$ vs. $1/T$ at the melting point is related to the standard enthalpy change for the melting process and compositional changes in the molecular state of the vapor above the two phases in the following way

$$[E_a^s/R - E_a^l/R] = [\Delta H_f/R] \Sigma(iN_i) +$$

$$\left[\frac{d \ln \Sigma(\sqrt{iN_i})}{d(1/T)} \right]^l - \left[\frac{d \ln \Sigma(\sqrt{iN_i})}{d(1/T)} \right]^s \quad (7)$$

The theoretical change in the slope at the melting point for each salt was computed numerically with this equation. JANAF² figures for the heat of fusion and the molecular composition of the vapor are available for all the salts except CsI. For this salt the heat of fusion was that reported by Dworkin and Bredig¹⁹ and the vapor compositions were those selected and discussed in the next section of this article.

A different extrapolation procedure was required for LiF since J_K at the hydrodynamic limit could not be experimentally obtained. This salt also differed in that free-molecular flow occurred over the entire solid range and extended several degrees above the melting point. So, the required values of J_K in the liquid region were generated by a linear extrapolation from known values in the molecular region at the melting point using the theoretical change in slope obtained from eq 7.

Results

The Clausung Effect at High Flows. Since the thickness of a real orifice cannot be infinitesimally small, some of the molecules in free-molecular flow are reflected back into the Knudsen chamber. Clausung⁵ calculated and tabulated values of a factor K which is the ratio of the number of molecules escaping to those entering the orifice. Two diameters, $1/32$ and $1/16$ in., were generally used in our experiments, and these had Clausung factors⁵ of 0.970 and 0.984, respectively.

It followed directly that an observed rate in the molecular region should be corrected with the appropriate Clausung factor to give the desired rate for the same orifice size at zero thickness. However, it was not apparent as to whether or not one should apply the same factor in the hydrodynamic and transition regions. Therefore, a series of Knudsen-type experiments with NaCl were carried out in the high-flow regions to measure directly the magnitude of the Clausung effect. Orifices with nominal diameters of $1/32$ and $1/16$ in. were made in sheets of varying thickness to give length-to-radius ratios from 0.033 to 1.656. The results of the flow measurements with these orifices are presented in Table I. The observed Clausung factor K' in the third column is the ratio of the observed mass flow to that for the same size orifice at zero thickness. The base value at zero thickness for each diameter was obtained by applying a small theoretical Clausung factor to the mass flow observed for the same size in 0.001-in. thick sheet.

In general there is agreement between the experimental and theoretical factors. One must conclude that there is an effect of the Clausung type at orifice walls even in the hydrodynamic region. This is not too surprising. The velocity distribution in this region cannot be Maxwellian, but one would expect long mean free paths at and downstream of the orifice. It is possible in the hydrodynamic region that the major part of the pressure gradient at the orifice occurs upstream and that the flow in the plane of the thin orifice is effectively molecular. Consequently, all mass rates re-

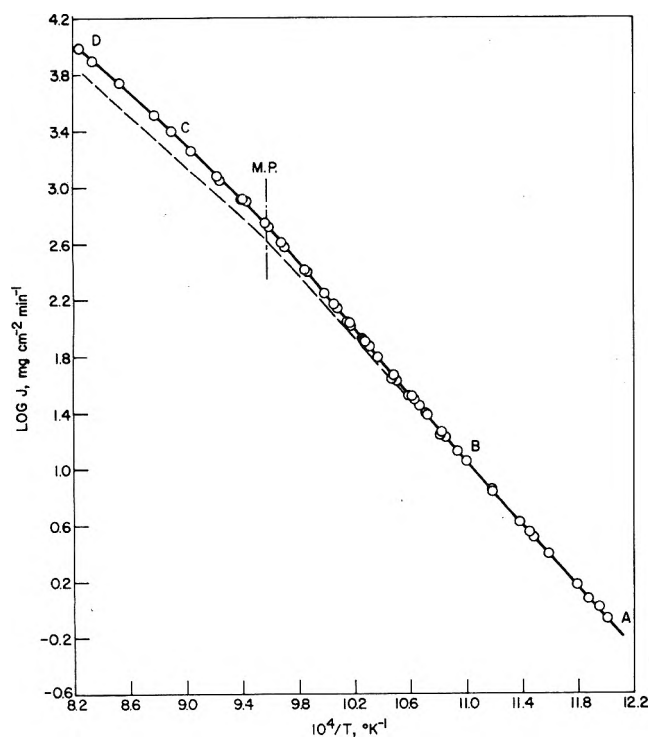


Figure 1. Experimental values of the mass flow J vs. the reciprocal of the absolute temperature for potassium chloride vapor.

TABLE I: Experimental Evidence of Clausing Effect for Orifice Flow in the Hydrodynamic and Transition Regions (NaCl)

Length-to-radius ratio (L/R)	Flow regions of measurements	Experimental factor (K')	Clausing ^a factor (K)
0.033	Both molecular and hydrodynamic		0.984
0.067	Both molecular and hydrodynamic		0.970
0.154	Molecular	0.94	0.93
0.157	Higher transition	0.90	0.93
0.458	Molecular	0.77	0.81
0.458	Molecular	0.79	0.81
0.458	Higher transition	0.73	0.81
0.458	Hydrodynamic	0.73	0.81
1.656	Molecular	0.56	0.56
1.656	Molecular	0.54	0.56
1.656	Higher transition	0.56	0.56
1.656	Higher transition	0.57	0.56

^a Reference 5.

ported in this article are corrected for small Clausing effects. Three orifice diameters ($\frac{3}{32}$, $\frac{1}{16}$, and $\frac{1}{32}$ in.) were used in our experiments, and these had Clausing factors of 0.990, 0.984, and 0.970, respectively.

All mass flow observations for sodium chloride are listed in Table II²⁰ along with the corresponding nominal size of the orifice. Each reported point represents a single experimental determination, but not necessarily a single filling of the cell. The time for a determination depended on the temperature and the vaporization rate. At lower temperatures, time periods of 1–2 hr were not unusual, and several determinations were obtained with a single filling. In contrast, at higher temperatures, a period of only a few minutes was often sufficient to completely empty the cell.

TABLE II: Experimental Values of the Mass Flow of Saturated Sodium Chloride Vapors

t , °C	J , ^a mg cm ⁻² min ⁻¹	t , °C	J , ^a mg cm ⁻² min ⁻¹
587.1	0.8037 (c)	718.6	53.76 (a)
610.5	1.832 (c)	729.4	69.43 (b)
611.4	1.880 (b)	732.3	78.74 (a)
629.3	3.463 (b)	732.6	78.62 (b)
630.7	3.365 (c)	733.8	82.87 (b)
631.6	3.609 (b)	738.4	97.07 (a)
639.2	5.005 (a)	750.2	127.2 (a)
639.3	5.092 (a)	752.6	129.1 (b)
647.6	6.640 (b)	753.5	150.8 (a)
651.0	6.892 (b)	753.6	143.8 (b)
651.5	6.703 (b)	758.7	167.8 (a)
651.6	6.919 (a)	763.5	184.8 (b)
651.6	7.066 (b)	770.2	219.5 (a)
653.2	7.242 (c)	772.4	234.5 (a)
653.3	7.254 (c)	772.9	249.5 (a)
657.6	8.763 (a)	773.3	239.4 (b)
670.9	13.05 (a)	783.2	320.7 (a)
671.1	12.59 (b)	786.9	346.0 (a)
671.2	12.94 (b)	788.1	361.7 (b)
671.3	12.33 (c)	790.1	376.7 (a)
671.3	13.13 (b)	808.0	541.8 (b)
674.5	15.04 (b)	813.6	658.0 (a)
677.8	16.56 (a)	828.6	811.5 (b)
691.6	23.84 (b)	830.1	878.8 (a)
691.7	24.06 (a)	830.7	895.3 (a)
691.8	24.47 (b)	830.2	822.1 (b)
691.9	24.38 (b)	846.8	1232 (a)
693.0	26.17 (b)	853.8	1338 (b)
698.1	29.46 (a)	868.4	1695 (b)
710.3	42.14 (b)	872.3	1875 (a)
711.6	42.55 (b)	887.0	2426 (a)
712.0	44.09 (b)	909.6	3373 (a)
712.2	43.07 (b)	940.5	5116 (a)
713.0	46.82 (b)	960.3	6805 (a)

^a Nominal orifice size as follows: (a) 0.0794 cm, (b) 0.159 cm, (c) 0.238 cm.

Characteristics of the flow through a thin-edge orifice in the three flow regimes are illustrated for potassium chloride in Figure 1. The logarithm of the observed mass flow J is plotted vs. the reciprocal of the absolute temperature. For potassium chloride, the molecular region extends from the temperature point A to B, the transition region from B through the melting point to C, and the hydrodynamic region from C to the measured limit D. In order to more clearly show the transition from free-molecular to hydrodynamic flow, smoothed values of $\log J_K$ are presented on the same figure and are represented by the dashed curve. It should be recognized that J_K is the hypothetical flow which would be calculated from the Hertz-Knudsen equation (see eq 2) using the free-molecular value of Γ for the entire flow range.

The typical dependence of the coefficient Γ for an alkali halide on the mean free path of the vapor and orifice size is illustrated in Figure 2, again with the results for KCl. Orifice diameters of $\frac{1}{32}$ and $\frac{1}{16}$ in. were used. The value of the coefficient ratio Γ/Γ_K is readily obtained for each experimental determination since Γ/Γ_K is numerically equal to the corresponding mass-flow ratio J/J_K . The required value of J_K in the transition region may be generated in two ways: either by the extrapolation method outlined in the section on Treatment of Experimental Data or from eq 6 using partial pressures and molecular compositions from the JANAF² tables. The first method was arbitrarily selected for KCl since essentially the same values of J_K are generated by either method. Values of the mean free path λ

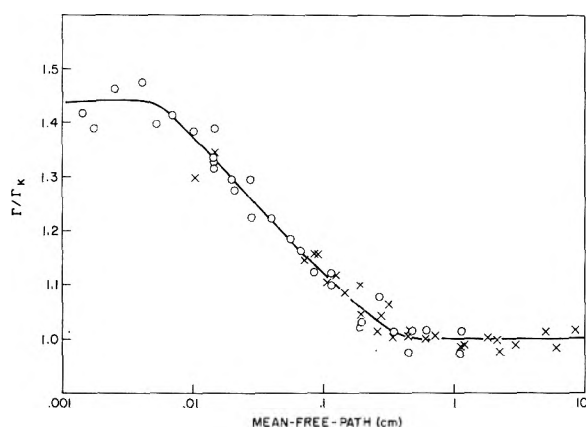


Figure 2. Experimental values of the coefficient ratio Γ/Γ_K vs. mean free path for potassium chloride: O, $\frac{1}{32}$ in. orifice; X, $\frac{1}{16}$ in. orifice.

were computed from standard kinetic equations^{21a} using collision diameters from diffraction studies^{21b} and vapor pressures from the JANAF² tables.

An important fact emerges from Figure 2. The free-molecular limit and the value of the coefficient Γ in the transition region are independent of the diameter of the orifice. This is true for all the alkali halides. In fact, for sodium chloride the free-molecular limit was also defined by an orifice of $\frac{3}{32}$ in. diameter, and there was still no effect of the diameter. The expected dependency of the limit and of $\Gamma^{7,8,10}$ on the dimensionless number λ/D was not found, and possible reasons for this are discussed in the next section. The experimental observations of Γ for two orifice sizes in the transition region do not show any dependency on the diameter, but it is unfortunate that flow observations could not be made with the larger diameter orifice into the hydrodynamic region.

As might be expected, all the alkali halides exhibited the same flow characteristics. This is illustrated in Figure 3 where smoothed values of the coefficient ratio Γ/Γ_K are plotted against mean free path. Since vapor pressures are not reliably known for several of the salts, the required values of J_K and λ are based on the vapor pressures obtained in this study. The dependence of the two limits on the mean free path is surprisingly similar for all the alkali halide vapors; and, within the reliability limits of the quantities involved, the two limits occur at the same absolute value of the mean free path for all five salts. The average value of λ at the molecular limit is 0.7 cm, and at the hydrodynamic limit is 0.005 cm.

Vapor Pressure

One purpose of this study was to measure vapor pressures for the alkali halides at intermediate pressures between about 0.1 and 5 Torr where measurements are practically nonexistent. The paucity of information in this region exists because Knudsen studies are generally confined to lower pressures where flows are in the free-molecular region, and direct vapor pressure studies are necessarily confined to pressures high enough to permit manometric determination. The determination of vapor pressures from Knudsen cell measurements requires, in addition to the Knudsen fluxes (actual or hypothetical molecular), a knowledge of the vapor composition, as indicated by eq 5. The method for reducing hydrodynamic and transitional to molecular fluxes has been described. For all the salts ex-

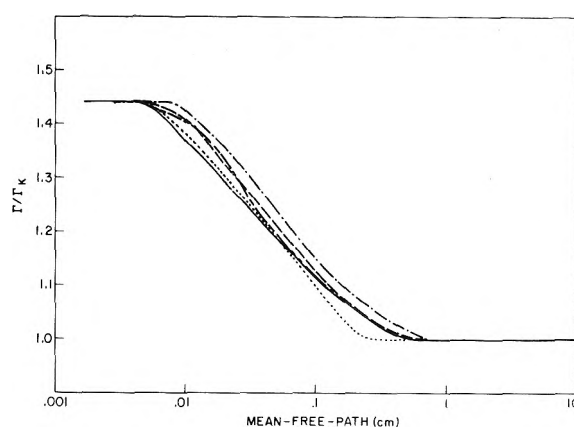


Figure 3. The coefficient ratio Γ/Γ_K vs. mean free path for five alkali halide vapors: (—) KCl, (.....) KBr, (- - - -) NaCl, (- - - -) LiF, and (- - - -) CsI.

cept CsI compositions were calculated from data in the JANAF tables.² The procedure for CsI is described below. Flux measurements can generally be made to four significant figures. We have therefore listed vapor pressures to the same number of significant figures although the absolute values of the vapor pressures are probably no better than $\pm 3\%$. This procedure, which avoids rounding errors, is similar to the one used by JANAF. Smoothed pressures for sodium chloride are presented in Table III.²⁰ Values of vapor pressure, and the mass flows upon which they are based, are tabulated at 20° intervals covering the experimental ranges. These values are compared with those obtained from JANAF.

KCl. The vapor pressure of solid KCl has been measured by several investigators²²⁻²⁵ and the total spread of the values is $\sim 30\%$. The JANAF evaluation closely follows the data of Zimm and Mayer²⁴ and Mayer and Wintner.²³ In the liquid state all reported measurements²⁶⁻³¹ agree closely.

The maximum deviation of our vapor pressures from those of JANAF is $\sim 3\%$, which occurs in the solid near the melting point. This means that our ΔH_v° for the solid is slightly less than that of JANAF and for the liquid it is slightly greater.

KBr. The vapor pressure of the solid has only been measured in two studies: Zimm and Mayer²⁴ covered a range of nearly 270° , while Mayer and Wintner²³ covered a much shorter range. The JANAF evaluation (which considers other thermodynamic data as well) lies approximately 30% below the Zimm and Mayer data, whereas, our data are from 4 to 12% above JANAF.

Four groups have measured the vapor pressure of the liquid.^{26-28,32} Three of these are reasonably consistent and have been adopted by JANAF. Only Ruff and Mugdan²⁷ report values a factor of 2 lower. Our data deviate increasingly from JANAF as the temperature rises, from less than 1% near the melting point to nearly 9% at 1240°K .

NaCl. Experimental vapor-pressure measurements in both the solid²³⁻²⁵ and liquid state^{26-29,33} are consistent, except for the data of Miller and Kusch²⁵ for the solid which are lower than the others and scatter considerably. Our data are $1-8\%$ greater than the JANAF evaluation.

LiF. The only vapor-pressure data for the solid are those of Hildenbrand, *et al.*,³⁴ but they covered only a 30° range, and a similar range in the liquid just above the melting point. These values are moderately consistent with values

TABLE III: Experimental Vapor Pressures of Sodium Chloride and Comparison Vapor Pressures Selected by JANAF^a

$T, ^\circ\text{K}$	$J_K, \text{mg cm}^{-2} \text{min}^{-1}$	$P_{\text{expt}}, \text{Torr}$	P_J, Torr	% dev
860	0.7943	8.003×10^{-4}	8.223×10^{-4}	-2.68
880	1.613	1.637×10^{-3}	1.674×10^{-3}	-2.20
900	3.173	3.244	3.297	-1.62
920	6.062	6.241	6.302	-0.97
940	11.27	1.168×10^{-2}	1.171×10^{-2}	-0.21
960	20.34	2.123	2.117	+0.28
980	35.50	3.731	3.733	-0.04
1000	60.59	6.413	6.426	-0.21
1020	101.3	0.1079	0.1081	-0.21
1040	166.0	0.1780	0.1782	-0.08
1060	266.9	0.2883	0.2879	0.12
1080	411.3	0.4478	0.4454	0.55
1100	590.6	0.6502	0.6431	1.10
1120	837.0	0.9315	0.9153	1.77
1140	1172	1.318	1.285	2.60
1160	1622	1.844	1.779	3.65
1180	2220	2.550	2.435	4.72
1200	3007	3.490	3.295	5.92
1220	4032	4.728	4.410	7.20
1240	5357	6.344	5.839	8.64

^a Reference 2.

determined for the high-temperature liquid.³⁴⁻³⁶ The JANAF evaluation also takes into account the vapor composition (containing appreciable concentrations of dimer and trimer) and enthalpies. Our vapor pressures for the solid are ~30% lower than those selected by JANAF, and 10-20% lower for the liquid.

CsI. The vapor pressure of the solid has been measured by several workers.^{22,37,38} The extremes are represented by the low values of Dietz²² and the high values of Scheer and Fine³⁸ which differ by a factor of 2. The Scheer and Fine data are more consistent with most of the high-temperature liquid values^{27,33,36} (except those of Ruff and Mugdan²⁷ whose slope is obviously incorrect).

Since these data had not yet been evaluated by JANAF and since the vapor composition above the solid was unknown, a different procedure was used than for the other salts; the partial vapor pressures of monomer and dimer above the high-temperature liquid, as given by Topor,³³ were extrapolated to the melting point. The corresponding curves for the solid were determined by adding the heat of fusion.¹⁹ The resulting curves were used *only* to determine the monomer/dimer *ratio*. The actual vapor pressures were then determined from this composition and our experimental fluxes. The results lie ~20% below the data of Scheer and Fine.³⁸

In order to evaluate the reliability of the vapor pressures reported in Table III we rely heavily on a comparison with literature values. Of the salts used in this study, only for KCl is there virtually complete agreement among the various reported investigations. In the molecular-flow region (<930°K) our vapor pressures, calculated from flux measurements with the Hertz-Knudsen equation and the Clausing correction, are within 1% of the JANAF evaluation² of previous studies. In the temperature range corresponding to flows in the transition region (930 → 1130°K), the vapor pressures obtained in this study depend on the extrapolation procedures developed to obtain values of J_K from observed values of J . Similarly, the vapor pressures reported by JANAF in the same temperature range depend essentially on the extrapolation of observed vapor pressures from the two temperature limits. Nevertheless, the maximum difference between vapor pressures calculated

from JANAF tables and our values is only ~3%. We therefore conclude that the procedures developed in this work are valid and can be used to determine vapor pressures from Knudsen cell measurements even if the flow from the orifice is not molecular.

For the other salts, differences between our vapor pressures and those obtained from JANAF are somewhat greater. Nevertheless, they are not large, generally within 5% for NaCl, and within 10% for KBr. For LiF, literature data are very few and scattered so that the larger differences between our values and the JANAF evaluation is not surprising. In fact, since our data on LiF now constitute the most systematic and complete vapor pressure study on this salt, a reevaluation of LiF would probably be appropriate. CsI has not previously been critically evaluated, but our data are consistent with previous studies.

Discussion

The transition-flow measurements made in this study with the microbalance are of higher precision than those which have generally been made, so the experimental fact that Γ at the molecular limit and in the transition region is independent of orifice size takes on added significance. Only a few measurements at high flows have been made with thin-edge orifices (or short tubes), and the authors believe that dependency of the free-molecular limit on λ/D has not been established. The flow pattern at an orifice and the effects of interactions between the molecules themselves and between the molecules and the edge of the orifice are unquestionably complex, but it can be speculated in a general way that the lack of molecular reflections and of operative viscous forces at the hole for a thin-edge orifice compensates for the diameter dependence observed^{6,10} in the transition region for long tubes.

Fluid mechanics conditions one to expect a flow limit to occur at some dimensionless number, and the use of the absolute mean free path as a correlation factor for the molecular and hydrodynamic limits is perhaps controversial. In any event, the results for the alkali halides with different size orifices have shown that the molecular limits (and perhaps even the hydrodynamic limits) do not occur at the same Knudsen number, but at roughly the same mean free

path. The degree of generality which can be attached to this is not known. It is interesting that in several flow studies with permanent gases, the observed molecular limits occur at mean free paths which are close to those found for the salts. For example, both Liepmann⁸ and Smetana⁷ experimentally studied the approach of Γ to the free-molecular limit. Liepmann used an orifice with a diameter of 0.150 cm and Smetana a much larger one with a diameter of 1.15 cm. Even with this large difference in diameter, the observed limit in each case occurred at a mean free path near 1 cm which agrees satisfactorily with the average value of 0.7 cm observed for the five salts.

With the exception of some questions related to the flow limits and their dependence on orifice size, the general characteristics of flow through a thin-edge orifice have been experimentally established and this includes the fact that the flow in the hydrodynamic region is systematically higher than that which would be predicted from Hertz-Knudsen equations. This conclusion, however, is in conflict with the work of Johnson³⁹ who reported that the mass flow for mercury through a tube is proportional to pressure up to an actual pressure of 35 Torr ($\lambda/D = 0.002$). Searcy and Schulz⁴⁰ concluded from torsion-effusion studies of flow through thin orifices that the force exerted by escaping vapors are identical with those predicted by molecular-flow equations.

We believe that our work demonstrates that flows through a thin-edged orifice in the transition and near hydrodynamic regions are well characterized and that reliable vapor pressures may be obtained by the Knudsen method over pressure ranges extending from about 0.005 to 5 Torr. The extension of the method to pressures in the intermediate range between 0.1 and 5 Torr provides a tool where none now exists.

Acknowledgment. The authors appreciate the generous and helpful discussions with Professor Hans W. Liepmann of the California Institute of Technology.

Supplementary Material Available. Parts of Tables II and III, containing data for KCl, KBr, LiF, and CsI, will appear following these pages in the microfilm edition of this volume of the journal. Photocopies of the supplementary material from this paper only or microfiche (105 × 148 mm, 24X reduction, negatives) containing all the supple-

mentary material for the papers in this issue may be obtained from the Journals Department, American Chemical Society, 1155 16th St., N.W., Washington, D. C. 20036. Remit check or money order for \$3.00 for photocopy or \$2.00 for microfiche, referring to code number JPC-74-1998.

References and Notes

- (1) C. T. Ewing and K. H. Sterr, *J. Phys. Chem.*, **77**, 1442 (1973).
- (2) D. R. Stull and H. Prophet, *Nat. Stand. Ref. Data Ser., Nat. Bur. Stand.*, **No. 37** (1971).
- (3) H. Hertz, *Ann. Phys.*, **17**, 177 (1882).
- (4) M. Knudsen, *Ann. Phys.*, **47**, 697 (1915).
- (5) P. Clausing, *Ann. Phys.*, **12**, 961 (1932).
- (6) M. Knudsen, *Ann. Phys.*, **23**, 999 (1909).
- (7) F. O. Smetana, W. A. Sherrill, and D. R. Schort, Jr., *Rarefied Gas Dyn., Proc. Int. Symp.*, **5th**, 1966, **2**, 1243 (1967).
- (8) H. W. Liepmann, *J. Fluid Mech.*, **10**, 65 (1961).
- (9) K. D. Carlson, P. W. Gilles, and R. J. Thorn, *J. Chem. Phys.*, **38**, 2725 (1963).
- (10) W. D. Bianco and E. Boridy, *Nucl. Instr. Meth.*, **92**, 111 (1971).
- (11) A. H. Shapiro, *Vacuum*, **13**, 83 (1963).
- (12) J. A. Perry, *Trans. Amer. Soc. Mech. Eng.*, **71**, 757 (1949).
- (13) F. I. Frankl, *Trans. Acad. Sci. USSR*, **58**, No. 3 (1947).
- (14) E. W. Balson, *J. Phys. Chem.*, **65**, 1151 (1961).
- (15) K. Motzfeldt, *J. Phys. Chem.*, **59**, 139 (1955).
- (16) C. I. Whitman, *J. Chem. Phys.*, **20**, 161 (1952); **21**, 1407 (1953).
- (17) M. G. Rossmann and Y. Yarwood, *Brit. J. Appl. Phys.*, **5**, 7 (1954).
- (18) K. D. Carlson, P. W. Gilles, and R. J. Thorn, *J. Chem. Phys.*, **38**, 2064 (1963).
- (19) A. S. Dworkin and M. A. Bredig, *J. Phys. Chem.*, **64**, 264 (1960).
- (20) See paragraph at end of text regarding supplementary material.
- (21) (a) M. Barrow, "Physical Chemistry," McGraw-Hill, New York, N. Y., 1966, pp 42-44; (b) P. A. Akishin, N. G. Rambidi, and V. P. Spiridonov, "The Characteristics of High-Temperature Vapors," J. L. Margrave, Ed., Wiley, New York, N. Y., 1957, Chapter 12.
- (22) V. Deitz, *J. Chem. Phys.*, **4**, 575 (1936).
- (23) J. E. Mayer and I. H. Wintner, *J. Chem. Phys.*, **6**, 301 (1938).
- (24) B. H. Zimm and J. E. Mayer, *J. Chem. Phys.*, **12**, 362 (1944).
- (25) R. C. Miller and P. Kusch, *J. Chem. Phys.*, **25**, 860 (1956).
- (26) H. V. Wartenberg and P. Albrecht, *Z. Elektrochem.*, **27**, 162 (1921).
- (27) O. Ruff and S. Mugdan, *Z. Anorg. Chem.*, **117**, 147 (1921).
- (28) E. F. Fock and W. H. Rodebush, *J. Amer. Chem. Soc.*, **48**, 2522 (1926).
- (29) J. L. Barton and H. Bloom, *J. Phys. Chem.*, **60**, 1413 (1956).
- (30) C. Beusman, ORNL-2323 (1957).
- (31) G. I. Novikov and O. G. Polyachenkov, *Russ. J. Inorg. Chem.*, **6**, 996 (1961).
- (32) K. Hagemark, M. Blander, and E. B. Luchsinger, *J. Phys. Chem.*, **70**, 276 (1966).
- (33) L. Topor, *J. Chem. Thermodyn.*, **4**, 739 (1972).
- (34) D. L. Hildebrand, W. F. Hall, Jr., F. Ju, and N. D. Potter, *J. Chem. Phys.*, **40**, 2882 (1964).
- (35) O. Ruff, G. Schmidt, and S. Mugdan, *Z. Anorg. Chem.*, **123**, 83 (1922).
- (36) H. v. Wartenberg and H. Schulz, *Z. Elektrochem.*, **27**, 568 (1921).
- (37) G. E. Cogin and G. E. Kimball, *J. Chem. Phys.*, **16**, 1035 (1948).
- (38) M. D. Scheer and J. Fine, *J. Chem. Phys.*, **36**, 1647 (1962).
- (39) T. H. Johnson, *Phys. Rev.*, **31**, 103 (1928).
- (40) A. W. Searcy and D. A. Schulz, *J. Chem. Phys.*, **38**, 772 (1961).

Optical Saturation and Quenching Effects in the Triplet State of Rhodamine 6G at 77°K

Mikio Yamashita* and Hiroshi Kashiwagi

Laser Research Section, Radio- and Opto-Electronics Division, Electrotechnical Laboratory, Tanashi, Tokyo, Japan (Received January 2, 1974; Revised Manuscript Received May 6, 1974)

Publication costs assisted by Electrotechnical Laboratory

X-Band esr measurements at 77°K during Ar ion laser excitation are conducted to directly monitor the dependence of the Rhodamine 6G (R6G) triplet state (T_1 state) on pumping laser power and on the concentration of cyclooctatetraene (COT) as a quencher. The experimental results indicate that the intersystem crossing rate K_{ST} and triplet lifetime τ_T of R6G in ethanol are $1.1 \times 10^5 \text{ sec}^{-1}$ and 1.7 sec at 77°K, respectively. Furthermore, using Perrin's model, the quenching mechanism of R6G T_1 state in glassy solution of COT is explained in terms of triplet-triplet energy transfer by an electron exchange process.

Introduction

With developments in tunable continuous wave dye lasers, physical properties related to the T_1 state of the laser medium have been investigated by the observation of triplet quenching, T-T absorption, photobleaching, etc., in order to improve performance of the laser.¹⁻¹⁰ We recently reported the first observation of the triplet esr and two-microwave-photon absorption of R6G during laser excitation.¹¹ Furthermore, $\Delta m = \pm 2$ esr signals of some dye molecules have been recently observed under mercury arc excitation by Antonucci and Tolley.¹² This paper gives a new method for measuring intersystem crossing rates which are obtained by combining the optical saturation curve in the R6G T_1 state observed at 77°K during laser excitation with calculation of triplet concentration derived from rate equations. Furthermore, a mechanism of quenching of R6G triplet molecules by COT molecules is discussed in terms of Perrin's model¹³ of triplet-triplet energy transfer due to electron exchange in rigid media.

Experimental Section

Materials. The R6G used in our experiments was obtained from the Eastman Kodak Co.¹¹ and the COT from Aldrich Chemical and Tokyo Chemical Industry Co. The dye was dissolved in ethanol with or without COT. Oxygen-free R6G solution was outgassed and sealed in individual 4.5- or 2.5-mm i.d. quartz tubes which were kept at 77°K in a quartz dewar vessel.

Apparatus. The esr spectrometer, used for the investigation of the effects of the laser pumping power and COT concentration on the triplet concentration, was of a conventional X-band homodyne detection type with 100-kHz field modulation.¹¹ The R6G glassy solution was excited with the unfocused 5145-Å beam of an Ar ion laser, Spectra Physics Model 165-03. The long triplet lifetime was measured for each sample at 77°K by the following method. After laser irradiation of a sample in the esr cavity, the decay of the derivative H_{\min} line ($\Delta m = \pm 2$ transition) was displayed on an oscilloscope. Fluorescent lifetimes of 77°K R6G, pumped by an Avco C950 pulsed N_2 gas laser, were determined by using an Optics Corp. F-11-20 monochromator followed by an RCA 8645 photomultiplier connected to a Tektronix 7904 oscilloscope. Optical absorption spectra of $5 \times 10^{-4} M$ R6G in ethanol with and without $2 \times 10^{-2} M$

COT added were measured at 77°K with a Cary Model 14 spectrophotometer with a cell length of 0.1 cm.

Results

Optical Saturation in the T_1 State. The dependence of the esr spectra corresponding to the $\Delta m = \pm 2$ transition in the randomly oriented T_1 state on the laser pumping power for circular polarized 5145-Å beam was examined for each R6G concentration (4×10^{-5} , 1×10^{-4} , 4×10^{-4} , 1×10^{-3} , and $5 \times 10^{-3} M$). The observed saturation curves for the R6G triplet molecular concentration that are proportional to the esr signal intensity¹⁴ are shown in Figure 1a-c for different R6G concentrations. From these curves, we find that triplet molecular concentrations for R6G solutions of concentrations from 4×10^{-5} to $1 \times 10^{-3} M$ in 2.5-mm i.d. tubes begin to saturate above 1.5 W/cm², and for the $5 \times 10^{-3} M$ solution the triplet concentration begins to saturate above 6 W/cm². The difference is possibly caused by the fact that in the case of the high concentration of $5 \times 10^{-3} M$ all R6G molecules are not homogeneously excited by the laser beam since only some molecules near the irradiated surface of the sample tube absorb most of the laser power. In Figure 1c, the saturation curve for $5 \times 10^{-3} M$ R6G samples in the quartz tubes with different diameters (the results for 2.5- and 4.5-mm i.d. tubes correspond to open and closed points in the figure, respectively) is shown. The optical saturation hardly depends on the tube diameter. The transmittance of the quartz tube was measured for the 5145-Å laser beam. The quartz tube without R6G solution was inserted into the dewar vessel which contained liquid nitrogen. From the results, the attenuations of the laser pumping power due to air, liquid nitrogen, and the cylindrical quartz sheets of the dewar vessel and sample tube were about 60 and 50%, and the laser beam diameter at the surface of the rigid solution matched the diameter of the tube.

From the decay curve of H_{\min} line, we found that the triplet lifetime τ_T of R6G cooled to 77°K was $1.7 \pm 0.1 \text{ sec}$.¹² The fluorescent lifetime τ_S and singlet absorption cross section σ of R6G at 5145 Å were $8.3 \pm 0.3 \text{ nsec}$ and $1.5 \times 10^{-16} \text{ cm}^2$ at 77°K, respectively. These measured values at 77°K are summarized in Table I.

Quenching of the T_1 State. The effects of the COT concentration on the signal intensity of the H_{\min} line were ex-

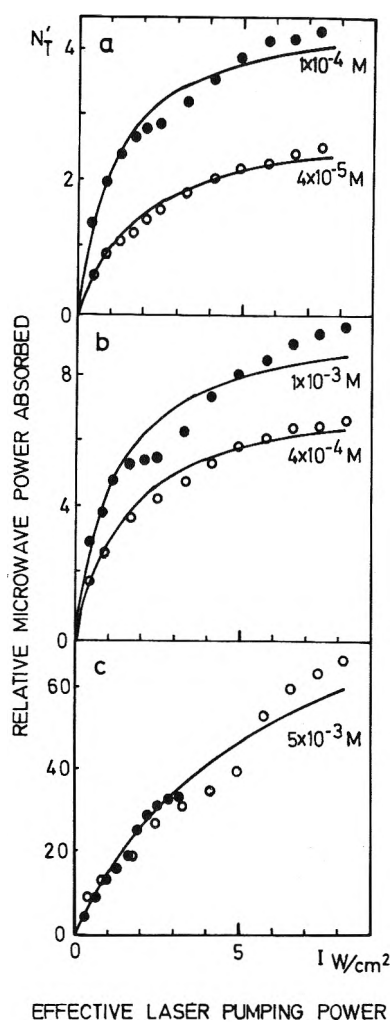


Figure 1. Dependence of the relative intensities of the H_{\min} lines in the R6G T_1 state on the effective laser pumping power. a, b, and c show the optical saturation curves at 77°K for R6G concentrations 4×10^{-5} and 1×10^{-4} M, 4×10^{-4} and 1×10^{-3} M, and 5×10^{-3} M, respectively. Open and closed points in c represent the saturation curves for 5×10^{-3} M solution in 2.5- and 4.5-mm i.d. tubes, respectively. The curves calculated from a rate-equation analysis using values K_{ST} obtained in our method are shown by solid lines. Concentrations are values measured at room temperature.

amined for each 5×10^{-3} M R6G glassy sample, with different COT concentrations. The average values of the ratio of the R6G T_1 state population at COT concentration N_A to that at zero COT concentration are plotted as a function of N_A in Figure 2. The triplet population decreased with the addition of COT to the R6G solution and could not be detected at COT concentrations greater than 0.5 M. In spite of the addition of 0.3 M COT to the solution, the triplet lifetime hardly changed at 77°K.

Both the fluorescent lifetime and singlet absorption cross section at 77°K were independent of COT concentration. From the measurements of the absorption spectra, we found that the absorption peaks of R6G and COT molecules lay at 5280 and 3620 Å, respectively, and the energy level of the first singlet state (S_1 state) of COT lay above that of R6G.

The concentrations measured at room temperature must always be corrected for about 25% reduction in the volume of ethanol on freezing to 77°K.¹⁵

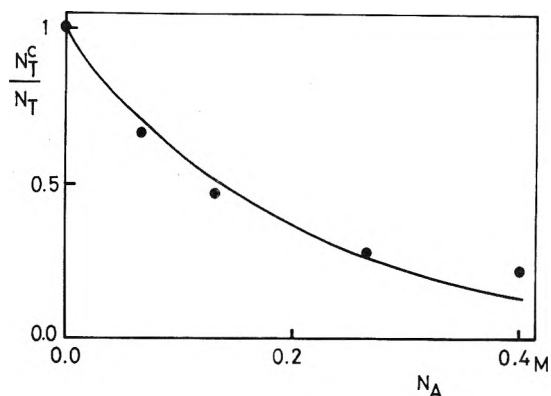


Figure 2. Dependence on COT concentration N_A of the ratio of the R6G triplet population at COT concentration N_A to that at zero COT concentration. The solid line is the curve calculated from Perrin's model. The COT concentrations are corrected for the shrinkage of the solution on freezing.

Discussion

Optical Saturation in T_1 State. Dye molecules excited to the S_1 state by laser light may decay by a nonradiative process to the lowest triplet state (T_1 state). This process proceeds at a rate designated as the intersystem crossing rate constant K_{ST} . Molecules in the T_1 state may decay to the S_0 state at a rate very much smaller than that of the strong fluorescence transition. Therefore, as the power of the pumping laser light increases many dye molecules accumulate in this metastable T_1 state and are at equilibrium.

Describing this population behavior of dye molecules using a rate-equation analysis under the steady-state conditions of continuous constant excitation, we obtain the following equation for the molecular concentration in T_1 state¹⁶

$$N_T = \frac{\tau_S \tau_T K_{ST} N(\sigma/h\nu)I}{1 + \tau_S(\tau_T K_{ST} + 1)(\sigma/h\nu)I} \quad (1)$$

In this equation, τ_S and τ_T are the lifetimes of the S_1 and the T_1 state at 77°K, respectively, N is the total molecular concentration, σ is the singlet absorption cross section at pumping frequency ν and 77°K, and I is the effective power per unit area of the excitation laser. We find from this equation that the population of the T_1 state approaches the optical saturation region as pumping power of the laser is increased. The experimentally obtained plots in Figure 1 show that, for Ar ion laser excitation power of 1.5 W/cm², R6G molecules from the S_1 state begin to be saturated by intersystem crossing in the metastable T_1 state, which possesses a long lifetime.

The intersystem crossing rate constant K_{ST} of R6G may now be estimated by using the saturation curves shown in Figure 1 and the data of Table I in conjunction with eq 1. Since the vertical axis in Figure 1 represents the relative values of N_T , the observed saturation curves of the triplet R6G are exactly described by the following equation under the assumption $\tau_T K_{ST} \gg 1$

$$N_T' = \frac{a\tau_S \tau_T K_{ST} N(\sigma/h\nu)I}{\tau_S \tau_T K_{ST} (\sigma/h\nu)I + 1} \quad (1')$$

where $N_T' = aN_T$ and a is a constant depending on the experimental apparatus. The reciprocal of this equation is as follows

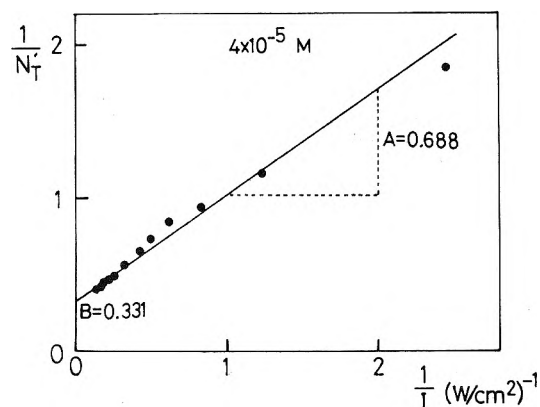
$$1/N_T' = (A/I) + B \quad (2)$$

TABLE I: Optical and Lifetime Parameters of R6G in Ethanol at 77°K Used for Calculation of K_{ST}

Dye	ν , sec ⁻¹	τ_S , nsec	τ_T , sec	σ , cm ²
R6G in EtOH	5.827×10^{14}	8.3 ± 0.3	1.7 ± 0.1	1.5×10^{-18}

TABLE II: Intersystem Crossing Rate Constants K_{ST} at 77°K Obtained from R6G Optical Saturation Curves for Different Concentrations

N, M	4×10^{-5}	1×10^{-4}	4×10^{-1}	1×10^{-3}	5×10^{-3}
K_{ST} , sec ⁻¹	0.9×10^5	1.6×10^5	1.1×10^5	1.5×10^5	0.3×10^5

Figure 3. The reciprocal of the relative triplet concentration $1/N_T'$ as a function of $1/I$ in the case of the 4×10^{-5} M R6G rigid solution.

where $A = 1/[\tau_{ST}K_{ST}(\sigma/h\nu)aN]$ and $B = 1/aN$. Then the slope and intercept in the graph of the linearly plotted $1/N_T'$ as a function of $1/I$ give A and B , respectively. (As an example, the dependence of $1/N_T'$ on $1/I$ for the 4×10^{-5} M R6G solution is shown in Figure 3.) Therefore, the value K_{ST} at 77°K is obtained from the relation $K_{ST} = B/[\tau_{ST}(\sigma/h\nu)A]$ using A , B , and the data in Table I. The values K_{ST} of rigid R6G solutions, obtained in this method, are given in Table II for different concentrations, and we find that the average value K_{ST} is 1.1×10^5 sec⁻¹. The reason why the value K_{ST} in the case of the high concentration of 5×10^{-3} M is less than the lower concentrations is probably that, as mentioned previously, the concentration is too high for all R6G in ethanol to be homogeneously excited with the laser beam. The calculated curves are shown as solid lines in Figure 1. The value at 77°K is reasonable in comparison with the order of limiting values of K_{ST} of various aromatic molecules.¹⁷ However, the value of K_{ST} for R6G solution measured at room temperature by Buettner, *et al.*,² is two orders of magnitude larger than our value. The increase of K_{ST} in their case may be caused by the paramagnetic effect of oxygen molecules dissolved in the solution and an increase in the temperature-dependent component of the intersystem crossing rate.¹⁸

Quenching of the T_1 State. Since the R6G triplet molecular concentration decreases exponentially with increasing COT concentrations at 77°K, as shown in Figure 2, COT molecules are regarded as quenchers of R6G triplet molecules. The energy of the S_1 state of COT molecules, which cannot be directly excited to the S_1 state or the T_1 state by the absorption of 5145-Å laser light, is greater than that of R6G. The quenching of the R6G triplet may be due to energy transfer from R6G triplet molecules (donor) to COT triplet molecules (acceptor), where the energy level of the former T_1 state ($E_{T_1} = 15.3 \times 10^3$ cm⁻¹) probably lies

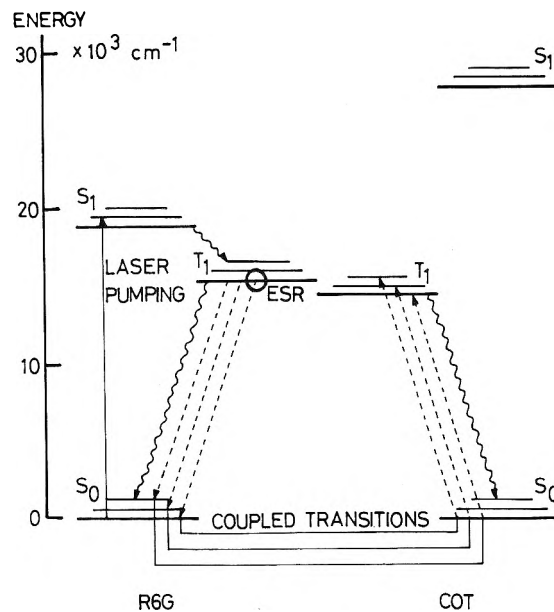


Figure 4. Energy diagram for triplet-triplet excitation transfer in R6G-COT pair.

above that of the latter.^{5,19} The occurrence of triplet-triplet energy transfer is described by the relation $D_T + A_0 \rightarrow A_T + D_0$, whose energy diagram is given in Figure 4. It is already known that triplet-triplet transfer in rigid media is due to an electron exchange mechanism on the basis of spin allowedness, long triplet lifetime of donor, etc.¹⁷ The exchange mechanism occurs only when the donor in the T_1 state and the acceptor in the S_0 state are essentially in molecular contact. According to a model suggested by Perin,^{13,20} the quenching of donor triplet obeys the equation $N_T^c/N_T = \exp(-\frac{4}{3}\pi R^3 n N_A)$, where N_T^c is the triplet molecular concentration at quencher concentration N_A , R the radius in ångströms of a quenching sphere, which depends only on the donor-acceptor pair but not on their concentrations, and $n = 6.02 \times 10^{-4}$. If an acceptor molecule happens to fall within the critical radius R , the occurrence of energy transfer is assumed. Acceptor molecules outside the sphere have no effect on the decay of the donor. The experimental value of R obtained from the plot in Figure 2 is 13 Å, which agrees approximately with the order of the van der Waals dimensions of the molecule.

The donor lifetime in the rigid solution in our experiments hardly changes as the acceptor concentration is increased, in contrast to the case of fluid solutions at room temperature where the transfer rate constant depends noticeably on the rate of molecular diffusion, and a shortening of the lifetime apparently occurs.⁵ The slight shorten-

ing of the mean lifetime may be ascribed to poor solubility of COT-R6G pair in the frozen ethanol solution.^{21,22}

Conclusions

On the basis of the data from the esr spectra corresponding to the $\Delta m = \pm 2$ transition in the R6G T_1 state, it was shown that the triplet population at 77°K began to be saturated at a pumping power of about 1.5 W/cm². A intersystem crossing rate of $1.1 \times 10^5 \text{ sec}^{-1}$ was obtained by a new technique where the experimental saturation curve was described by the equation for the triplet concentration calculated from a rate equation analysis. A triplet lifetime of 1.7 sec at 77°K was observed from the decay curve of the esr signal. Quenching of the R6G T_1 state by COT molecules in a rigid media was well explained in terms of triplet-triplet energy transfer by an electron exchange mechanism using Perrin's model.

Acknowledgment. We thank Dr. K. Sakurai for continuing guidance, T. Sato for experimental advice, and S. Nakajima and K. Hosomura for help with the experiments. The absorption spectra were measured by Dr. S. Inowaki and Y. Tan-no.

References and Notes

- (1) R. A. Keller, *IEEE J. Quantum Electron.*, **6**, 411 (1970).
- (2) A. V. Buettner, B. B. Snavely, and O. G. Peterson in "Molecular Luminescence," E. C. Lim, Ed., W. A. Benjamin, New York, N. Y., 1969, p 403.
- (3) O. G. Peterson, W. C. McColgin, and J. H. Eberly, *Phys. Lett.*, **29A**, 399 (1969).
- (4) C. V. Shank, J. Edighoffer, A. Dienes, and E. P. Ippen, *Opt. Commun.*, **7**, 176 (1973).
- (5) J. B. Marling, Ph.D. Thesis, University of California, 1971.
- (6) R. Pappalardo, H. Samelson, and A. Lempicki, *Appl. Phys. Lett.*, **16**, 267 (1970).
- (7) F. C. Strome, Jr., and S. A. Tuccio, *Opt. Commun.*, **4**, 58 (1971).
- (8) J. Weber, *Opt. Commun.*, **7**, 420 (1973).
- (9) A. D. Britt and W. B. Moviz, *IEEE J. Quantum Electron.*, **8**, 912 (1972).
- (10) D. Beer and J. Weber, *Opt. Commun.*, **5**, 307 (1972).
- (11) M. Yamashita and H. Kashiwagi, *J. Chem. Phys.*, **59**, 2156 (1973).
- (12) F. R. Antonucci and L. G. Tolley, *J. Phys. Chem.*, **77**, 2712 (1973).
- (13) F. Perrin, *Compt. Rend.*, **178**, 1978 (1924).
- (14) S. P. McGlynn, T. Azumi, and M. Kinoshita, "Molecular Spectroscopy of the Triplet State," Prentice-Hall, Englewood Cliffs, N. J., 1969.
- (15) A. I. P. Handbook, "Coordinating," 3rd ed, D. E. Gray, Ed., McGraw-Hill, New York, N. Y., 1972.
- (16) S. A. Tuccio and F. C. Strome, Jr., *Appl. Opt.*, **11**, 64 (1972).
- (17) N. J. Turro, "Molecular Photochemistry," W. A. Benjamin, New York, N. Y., 1967.
- (18) J. B. Birks and I. H. Munro, *Progr. React. Kinet.*, **4**, 249 (1967).
- (19) J. M. Drake, Ph.D. Thesis, Clark University, 1973.
- (20) S. Siegel and H. Judeikis, *J. Chem. Phys.*, **41**, 648 (1964).
- (21) A. N. Terenin and V. L. Ermolaev, *Trans. Faraday Soc.*, **52**, 1042 (1956).
- (22) M. Inokuti and F. Hirayama, *J. Chem. Phys.*, **43**, 1978 (1965).

Mechanism of Fluorescence Quenching by Acids in Poly(*N*-vinylcarbazole)

G. Pfister, D. J. Williams,* and G. E. Johnson

Xerox Corporation, Rochester Research Center, Webster, New York 14580 (Received December 20, 1973)

Publication costs assisted by Xerox Corporation

The electrical properties of poly(*N*-vinylcarbazole) (PVCA) have been found to be extremely sensitive to the presence of acidic impurities in the polymer. In order to identify the role of acids in the carrier generation and trapping processes, a detailed study of the excited state reactions of PVCA with various acids was undertaken. The acid concentration and wavelength dependence of the PVCA emission spectrum were examined in solution (tetrahydrofuran) and in the solid state. At 4600 Å the emission is entirely due to excimer fluorescence and is quenched more efficiently by acids than at 3600 Å where the emission is thought to be predominantly due to monomer fluorescence. It is shown that the more efficient quenching of the excimer band reflects the competition between the excimer formation reaction and the quenching of the 1L_b monomer state. The quenching of the excimer state is shown to be less efficient than the quenching of the excited 1L_b monomer state.

Introduction

Acidic impurities play an important role in the electrical characteristics of the polymer poly(*N*-vinylcarbazole) (PVCA). Enhanced photogeneration efficiency and trapping can be directly correlated with the presence of acid in this polymer.¹ When acids are present in PVCA in conjunction with nitroaromatic acceptors a thermally reversible persistent conductive state²⁻⁴ is observed. This effect has been attributed to an efficient excited state protonation of the acceptor molecule.² These results prompted us to in-

vestigate the excited state properties of PVCA alone in the presence of acids. In a previous study quenching of the fluorescence of *N*-isopropylcarbazole (NIPCA) was described.⁵ These experiments revealed a definite correlation between the strength of the acid (pK_a value) and the degree of quenching. It was also noted that excitation of the carbazole ring results in a shift of electron density from the nitrogen to the ring which produces a substantial increase in basicity of the ring. Quenching of carbazole fluorescence in strongly acidic aqueous media was attributed to proton-

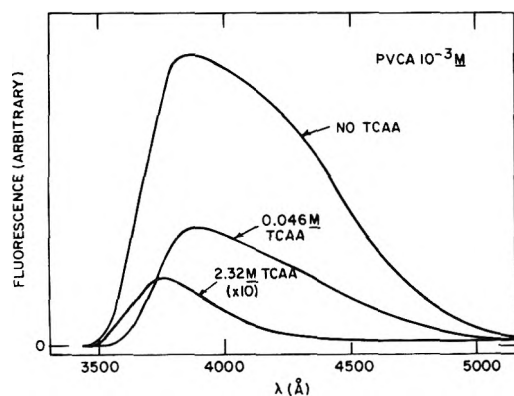


Figure 1. Fluorescence spectrum of PVCA $10^{-3} M$ in THF in the absence and presence of TCAA (λ_e 3000 Å).

ation of one of the benzenoid positions of the excited carbazole.⁶ In view of these facts a similar mechanism was proposed to account for the quenching of the NIPCA fluorescence in aprotic media by trichloroacetic acid (TCAA), maleic acid (MA), and bromoacetic acid (BAA).

A closer examination of the organic acids employed in this and the earlier investigation⁵ suggests that all of the acids can function as electron acceptors as well as proton donors and that their electron-accepting ability may parallel their proton-donating strengths. This prompted additional experiments to be carried out in an attempt to reveal the role of the acid in the fluorescence quenching mechanism. The ethyl esters of TCAA and MA were found to be slightly more efficient quenchers than the acids themselves. Furthermore it was shown that sulfuric acid, a much stronger proton donor than TCAA, is approximately two orders of magnitude less effective as a fluorescence quencher. These and the results of additional fluorescence quenching experiments will be reported in detail elsewhere.⁷ In view of these results it appears that the quenching of NIPCA fluorescence by TCAA, MA, and BAA is dominated by an excited state electron exchange mechanism rather than by excited state protonation. The quenching can still be considered to result from an acid-base interaction but only in the more general Lewis sense rather than the more restrictive Brønsted sense.

In this report the results of acid quenching experiments on PVCA will be discussed. In the polymer it is necessary to consider additional excited state processes in the kinetic analysis. Klopffer⁸ has reported the solution emission spectrum of PVCA and in contrast to NIPCA two overlapping emission bands were observed.

The higher energy emission is attributed to "monomer emission" while the longer wavelength broad structureless band is attributed to "excimer emission." Offen⁹ has observed emission from a dimer state formed from exciton coupling between neighboring chromophores in films of PVCA at 77°K. It is expected that the efficiency of the quenching reactions involving different excited states would be somewhat different and therefore the wavelength dependence of the quenching efficiency should reflect the different states contributing to the PVCA emission spectrum.

Experimental Section

A. Materials. Poly(*N*-vinylcarbazole) PVCA was obtained from BASF under the trade name Luvicon. The polymer was purified by seven reprecipitations from te-

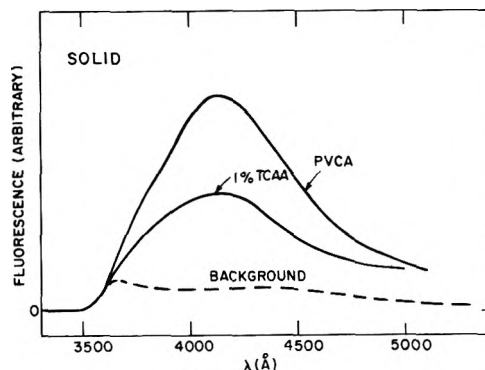


Figure 2. Fluorescence spectrum of PVCA films in the absence and presence of TCAA (λ_e 3000 Å).

trahydrofuran (THF) with methanol and a final freeze drying from benzene. The resulting polymer which visibly discolors on prolonged exposure to light and air was dried on a vacuum line and stored in evacuated ampoules until ready for use. The molecular weight of the polymer was determined from gel permeation chromatography on a 0.5% solution of polymer in THF ($M_w = 240,000$, $M_n = 113,000$). Trichloroacetic acid (TCAA) and bromoacetic acid (BAA) (EK White Label) were used without further purification. The THF was obtained from Burdick and Jackson and was treated as described previously.⁵ Films were prepared by dissolving an appropriate amount of acid in 15% solution of PVCA in THF and spreading the solution on a tin oxide coated conductive glass substrate (NESA) with a doctor blade. The films were dried slowly in a solvent atmosphere and for an additional 24 hr *in vacuo*. The resulting films had a smooth surface and were approximately 10 μ thick. NESA glass was used so that subsequent electrical measurements could be made.

B. Spectra. Emission spectra were measured on an Aminco Bowman spectrophotofluorometer in which the optical axis of the excitation and detection monochromators are fixed at 90° to one another. The excitation wavelength was held constant at 3000 Å (xenon arc light source). The solution emission spectra were obtained in a 1-cm quartz cell. Fluorescent light from films was obtained by monitoring the emission from the illuminated surface. In all experiments the excitation wavelength was λ_e 3000 Å.

Results

The absorption spectrum of PVCA in THF is essentially identical with those of PVCA in methylene chloride and of PVCA films which were discussed by Klopffer.⁸ The solution absorption spectrum of the polymer is very similar to NIPCA indicating that in the electronic ground state the mixing with neighboring chromophores is weak.

The emission spectrum of a $10^{-3} M$ solution of PVCA is shown in Figure 1 for several acid concentrations. The compound shape of the spectrum has been attributed⁸ to fluorescence from the 1L_b state of the individual or "monomer" chromophore at short wavelengths and fluorescence from an excimer state at longer wavelengths. The acid quenches the emission band nonuniformly (in contrast to the NIPCA emission⁵) and at 2.32 M TCAA the excimer band appears to be completely quenched. The position of the remaining monomer emission maximum occurs at 3750 Å whereas in the $10^{-3} M$ PVCA solution in the absence of acid the maximum is at 3870 Å, indicating that there is appreciable excimer emission at this wavelength.

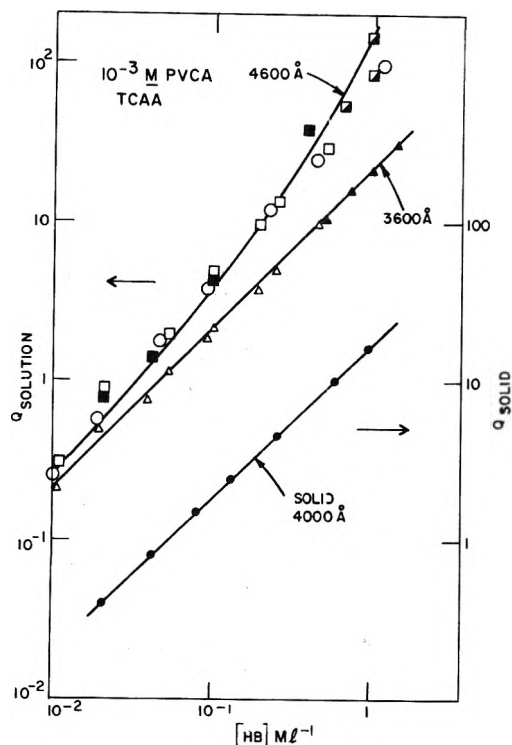


Figure 3. Quenching factor vs. TCAA concentration for PVCA 10^{-3} M in THF at λ_f 4600 Å and λ_f 3600 Å and quenching factor vs. TCAA concentration. The solid line was calculated using the parameters in Table I and eq 17 and 18 (λ_e 3000 Å).

The emission spectrum from PVCA films has been attributed to pure excimer emission with negligible contribution from the monomer chromophores.⁸⁻¹⁰ The excimer fluorescence spectrum of a PVCA film and a film with 0.6 M TCAA as well as the reflectance from the NESAslide is shown in Figure 2. Unlike the solution spectrum the solid spectrum is quenched uniformly which by analogy to Figure 1 indicates emission from only one state.

From the data in curves similar to Figures 1 and 2 the quenching factor Q

$$Q(\lambda) = [F_0(\lambda) - F(\lambda)]/F(\lambda)$$

(F_0 and F are the fluorescent intensities at the wavelength λ in the absence and presence of acid respectively) was calculated as a function of acid concentration at several wavelengths. The result for TCAA is shown in Figure 3. It is easily seen that the fluorescence quenching efficiency is larger at 4600 Å than at 3600 Å. The functional dependence of Q on acid concentration at 4600 Å is linear at low acid concentrations and approaches a square law at higher acid concentrations. At 3600 Å in solution and 4000 Å in the film the functional dependence is linear. Similar plots are shown for solutions of the weaker acid BAA and PVCA in Figure 4. The transition from linear to square law dependence at 4600 Å is less evident but a change in slope is definitely occurring at higher acid concentrations than for TCAA. The overall quenching is also less efficient than for TCAA at a given acid concentration.

The dependence of the quenching factor Q upon the wavelength of the emitted light is shown in Figure 5 for various TCAA concentrations. The excitation wavelength was λ_e 3000 Å. The quenching factors appear to approach a constant values at short ($\lambda < 3600$ Å) and long wavelengths ($\lambda > 4500$ Å) with $Q(4500 \text{ Å}) > Q(3600 \text{ Å})$. A very broad

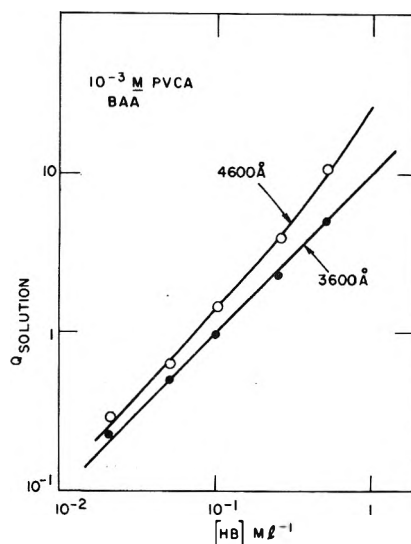


Figure 4. Quenching factor vs. BAA concentration for PVCA 10^{-3} M in THF at λ_f 3600 Å and λ_f 4600 Å, λ_e 3000 Å. The solid lines were calculated using the parameters in Table I and eq 17 and 18.

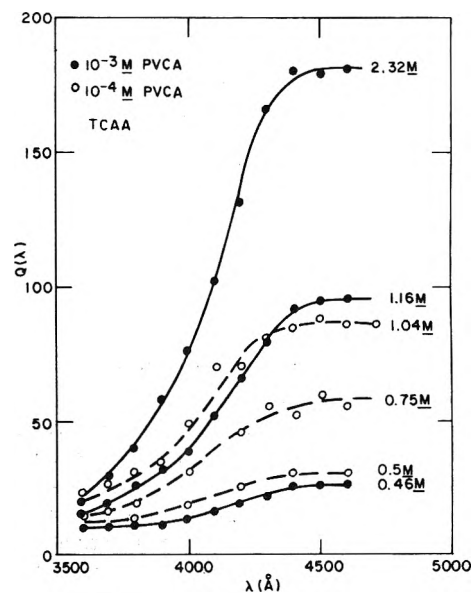


Figure 5. Quenching factor vs. fluorescence wavelength for PVCA 10^{-3} and 10^{-4} M in THF at a series of TCAA concentrations (λ_e 3000 Å).

transition between the two values occurs over the region from 3500 to 4500 Å. On the basis of Figure 2 of ref 5 the monomer fluorescence should be negligible for $\lambda > 4150$ Å so that it is somewhat surprising that Q has a spectral dependence that extends to 4500 Å. A similar plot for BAA is shown in Figure 6. The shape of the curve is very similar to the TCAA curves but ratio of $Q(>4500 \text{ Å})/Q(<3600 \text{ Å})$ is smaller at a given acid concentration.

Discussion

The fluorescence spectrum of PVCA has been analyzed by several authors as consisting of overlapping monomer and excimer emission bands. On the basis of this assignment and the experimental results in the previous section it is proposed that the quenching of the monomer and ex-

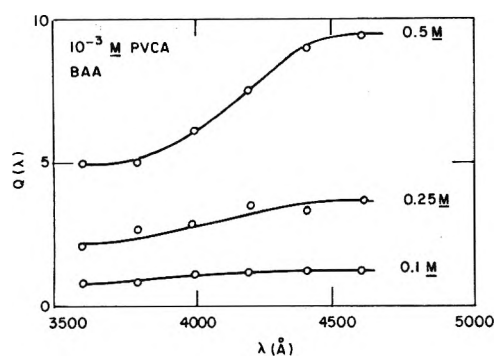
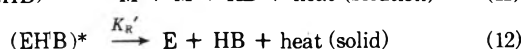
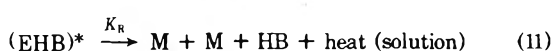
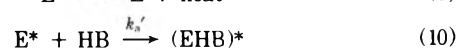
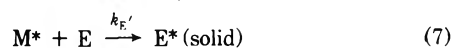
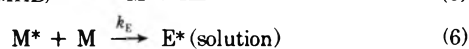
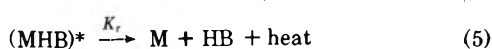
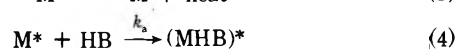
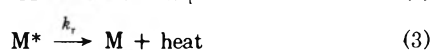


Figure 6. Quenching factor vs. fluorescence wavelength for 10^{-3} M PVCA in THF at several BAA concentrations (λ_0 3000 Å).

cimer fluorescence can be described by the following reaction scheme.



M^* and E^* are the excited monomer and excimer states and E is a site in the solid polymer where two rings form sandwich-like pairs and energy trapping by excimer formation can take place.⁸ $(\text{MHB})^*$ and $(\text{EHB})^*$ are transient species resulting from an electron transfer from the excited PVCA monomer and excimer states respectively to the acid quencher. I is proportional to the light absorbed by the PVCA. The rate constants are defined by their respective equations. Since the absorption of light by TCAA and BAA is negligible at the excitation wavelength, the wavelength dependence of the quenching factor due to attenuation of the incident light does not need to be treated explicitly (compare corresponding equations of ref 5).

Expressions for the monomer fluorescence ($f_M = k_f[M^*]$) and excimer fluorescence ($f_E = k_f'[E^*]$) can be obtained from eq 1–12 by assuming steady-state conditions ($d[M^*]/dt = d[E^*]/dt = 0$). With the further assumption that the nominal “monomer” and acid concentrations, $[M]_0$ and $[\text{HB}]_0$, are not appreciably depleted in the photostationary state one obtains for the “monomer” fluorescence

$$f_M = \frac{I k_f [M]_0}{k_f + k_r + k_E + k_a [\text{HB}]_0} \quad (13)$$

and for the excimer fluorescence

$$f_E = \frac{I k_f' k_E [M]_0}{(k_f + k_r + k_E + k_a [\text{HB}]_0)(k_f' + k_r' + k_a' [\text{HB}]_0)} \quad (14)$$

Quenching factors can be defined for the “monomer” fluorescence

$$q_M = \frac{f_M(0)}{f_M(\text{HB}_0)} - 1 \quad (15)$$

and for the excimer fluorescence

$$q_E = \frac{f_E(0)}{f_E(\text{HB}_0)} - 1 \quad (16)$$

where $f_M(0)$, $f_M(\text{HB}_0)$, $f_E(0)$, and $f_E(\text{HB}_0)$ are the monomer and excimer fluorescence intensities at a given wavelength for an acid concentration of $[0]$ and $[\text{HB}_0]$, respectively. Substituting eq 13 and 14, into eq 15 and 16, respectively, yields

$$q_M = K_M [\text{HB}_0] \quad (17)$$

$$q_E = (K_M + K_E) [\text{HB}_0] + K_M K_E [\text{HB}_0]^2 \quad (18)$$

where $K_M = k_a/(k_f + k_r + k_E)$ and $K_E = k_a'/(k_f' + k_r')$. It is noted that q_M exhibits a linear dependence on acid concentration whereas q_E contains an additional quadratic term, and that q_M and q_E are independent of the wavelength of the emitted light.

Since the monomer and excimer fluorescence overlap, the measured fluorescence intensity $F(\lambda, \text{HB}_0)$ may be written as

$$F(\lambda, \text{HB}_0) = f_E(\lambda, \text{HB}_0) + f_M(\lambda, \text{HB}_0) \quad (19)$$

The observed quenching factor ($Q(\lambda) = F_0(\lambda)/F(\lambda) - 1$) can be expressed in terms of the contributions of the individual components q_M and q_E as follows

$$\frac{f_M(\lambda, 0) + f_E(\lambda, 0)}{Q(\lambda) + 1} = \frac{f_M(\lambda, 0)}{q_M + 1} + \frac{f_E(\lambda, 0)}{q_E + 1} \quad (20)$$

The contribution of the monomer fluorescence f_M to the observed fluorescence F becomes negligible above 4400 Å^{7,8} and eq 20 reduces to

$$Q(\lambda) \sim q_E \quad \lambda > 4400 \text{ Å} \quad (21)$$

Therefore, the data shown in Figures 3 and 4 for λ_F 4600 Å and in Figures 5 and 6 for $\lambda_F > 4400$ Å approximately represent the quenching factor q_E as defined in eq 18. In agreement with the theoretical prediction for both cases, the quenching factors increase linearly at low acid concentrations and change to a square law dependence at higher acid concentrations (Figures 3 and 4) and for $\lambda > 4400$ Å become independent of wavelength (Figures 5 and 6). The observed approach to a wavelength independent value for $\lambda < 3700$ Å (Figures 5 and 6) indicates the observed quenching factor approaches the quenching of the monomer fluorescence, *viz.*

$$Q(\lambda) \sim q_M \quad \lambda \lesssim 3700 \text{ Å} \quad (22)$$

The “monomer” quenching factor eq 17 is consistent with the observed linear dependence of the quenching factor upon acid concentration at λ 3600 Å (Figures 3 and 4). From Figures 5 and 6 and eq 17 and 18 the values of K_M and K_E can be calculated. The results, which are given in Table I, indicate that for both acids the quenching reaction is much more efficient for monomer than excimer. It is well known that the properties of excited molecular states differ in many respects from those of the ground state. One property which by necessity is changed significantly is the ionization potential. It is invariably reduced favoring a charge transfer interaction between the excited donor (PVCA) and the acid quencher functioning as an electron acceptor.

TABLE I: Experimental Values for K_M and K_E Defined Following Eq 18 (M^{-1})

	TCAA	BAA
K_M	20	10
K_E	6	1.6
$(K_M + K_E)_{\text{solid}}$	18	

Since the 1L_b state of the monomer pendant group lies higher in energy than the excimer state the excited monomer should be the stronger electron donor. The relative values of K_M and K_E reflect this difference in the strength of the charge transfer interaction.

For BAA the excimer quenching is smaller relative to the monomer quenching than for TCAA. One might expect that the quenching efficiency would fall off faster for the weaker "base (donor)/(acceptor)" (*i.e.*, the excimer) as the acidic (acceptor) strength of the quencher decreases.

In films of PVCA the emission is due entirely to excimer fluorescence and the observed quenching factor is the sum ($K_M + K_E$) = 18 M^{-1} . From the smaller value of the quenching factor and the failure to observe a square law at higher acid concentrations it is evident that $K_M \gg K_E$ in the solid. Hence the decrease in excimer fluorescence intensity is largely due to excited "monomer" quenching.

It is also interesting to note that the value of q_M at a given concentration is approximately a factor of 4 lower than for the monomer quenching factor in NIPCA.⁵ The term k_E in the expression for K_M could account for this difference and is consistent with the competition between the acid and excimer formation for the excitation. An additional manifestation of this competition is the apparent value of q_M (*i.e.*, <18) for films of PVCA where the value of k_E is probably quite large. The less efficient quenching in the polymer may also result from the high degree of steric hindrance in the polymer.

References and Notes

- (1) G. Pfister and D. J. Williams, *J. Chem. Phys.*, in press.
- (2) D. J. Williams, M. Abkowitz, and G. Pfister, *J. Amer. Chem. Soc.*, **94**, 7970 (1972).
- (3) G. Pfister, M. Abkowitz, and D. J. Williams, *J. Chem. Phys.*, **57**, 2979 (1972).
- (4) D. J. Williams, G. Pfister, and M. Abkowitz, *TAPPI J.*, **56**, 129 (1973).
- (5) G. Pfister and D. J. Williams, *J. Chem. Phys.*, **59**, 2683 (1973).
- (6) A. C. Capomachia and S. G. Schulman, *Anal. Chim. Acta.*, **59**, 471 (1972).
- (7) G. E. Johnson, to be submitted for publication.
- (8) W. Klopffer, *J. Chem. Phys.*, **50**, 1689 (1969).
- (9) P. C. Johnson and H. W. Offen, *J. Chem. Phys.*, **55**, 2945 (1972).
- (10) C. David, M. Piens, and G. Geuskeins, *Europ. Polym. J.*, 1291 (1972).

Electron Spin Resonance Studies of Fluoroalkyl Radicals in Solution. I. Structures, Conformations, and Barriers to Hindered Internal Rotation

Kuang S. Chen, Paul J. Krusic,*^{1a} Paul Meakin, and Jay K. Kochi*^{1b}

Department of Chemistry,^{1c} Indiana University, Bloomington, Indiana 47401 and The Central Research Department,^{1d} E. I. du Pont de Nemours and Company, Wilmington, Delaware 19898 (Received January 2, 1974; Revised Manuscript Received April 23, 1974)

Publication costs assisted by E. I. du Pont de Nemours and Company

Methods are described for the production and esr study in solution of a variety of alkyl radicals which are substituted with one or more fluorines in the α , β , γ , and δ positions. Analysis of the isotropic ^1H and ^{19}F coupling constants and their temperature dependence together with the selective line broadening in the esr spectra provide information about the configuration at the α -carbon center, the stable conformation, and barriers to hindered internal rotation in fluoroalkyl radicals. Thus, the presence of two α -fluorines promote a pyramidal radical center in $\text{CH}_3\text{CF}_2\cdot$, $\text{CF}_3\text{CF}_2\cdot$, $\text{CF}_3\text{CF}_2\text{CF}_2\cdot$, and $\text{CF}_3(\text{CF}_2)_5\text{CF}_2\cdot$ and line broadening studies show that the rotation barrier about the $\text{C}_\alpha\text{-C}_\beta$ bond is raised to 2–3 kcal/mol in comparison to <1 kcal/mol in planar alkyl radicals. Bending at the radical center also causes decreased hyperconjugative interactions to β protons and fluorines. Moreover, the presence of α -fluorine induces a viscosity-dependent line width effect which is due to a relaxation process brought about by the modulation of the relatively large anisotropic fluorine splitting by the tumbling motion of the radical in solution. The conformation effects of fluorine substituted in the α and β positions of alkyl radicals are discussed in detail for $\text{CH}_3\text{CF}_2\cdot$, $\text{CF}_3\text{CF}_2\cdot$ and $\text{CF}_3\text{CF}_2\text{CF}_2\cdot$, as well as $\text{FCH}_2\text{CH}_2\cdot$ and $\text{F}_2\text{CHCH}_2\cdot$ by considering the selective line broadening in the esr spectra and the temperature dependence of the β -proton and -fluorine coupling constants. The unusual line broadening observed in $\text{FCH}_2\text{CH}_2\cdot$ and $\text{F}_2\text{CHCH}_2\cdot$ is discussed in terms of a dominant fourfold potential function involving equilibration among two pairs of conformers differing in energy by <300 cal/mol and separated by a barrier <1500 cal/mol. With the aid of INDO calculations, the angular dependence of the β -proton and fluorine hfs in these radicals can be described by a $(A + B \cos^2 \theta)$ function in which the values of A and B depend on the number of fluorine substituents. Long-range and conformational effects of γ -fluorine substituents are also observed.

Introduction

Electron spin resonance (esr) spectroscopy has provided a wealth of structural information on hydrocarbon radicals both in the solid state as well as in solution. The correlation of the structure of reactive intermediates such as free radicals with their chemical properties is an important objective of these studies.²

The introduction of fluorine or fluorinated groups causes changes in the chemical reactivity and properties of hydrocarbons.³ Since fluorinated alkyl radicals are common intermediates in a variety of preparative reactions, it would be desirable to examine systematically the effect which fluorine substitution has on the structures of alkyl radicals.⁴

Esr studies of organic fluorine compounds irradiated in the crystalline or polycrystalline state have provided valuable information on the anisotropic hyperfine and g tensors of fluoroalkyl radicals.⁵ Unfortunately, single crystal studies are limited to a narrow class of carboxylic derivatives while studies in the polycrystalline or amorphous solid state lead to powder spectra of great complexity which are difficult to interpret. Esr studies in solution are needed, since most reactions are carried out under these conditions and the structures of radicals derived from solid-state esr need not coincide with those in solution. More importantly, isotropic components of the nuclear couplings can be determined with great precision from solution esr spectra, and their temperature dependences as well as selective variations of line widths can provide valuable information on dynamic processes involving the radicals in solutions.⁶

For transient species, the generation of radicals in sufficiently high concentrations for esr study represents an experimental problem. In this study we wish to present various chemical techniques for the photolytic generation of fluoroalkyl radicals in solution. The structures, conformations and barrier to rotations of fluoroalkyl radicals deduced from their esr parameters are compared with the hydrocarbon analogs.

Results

Photolytic Generation of Fluoroalkyl Radicals in Solution. The general techniques developed for the selective production of alkyl radicals⁷ in solution for esr study can be applied to fluoroalkyl radicals. The basic method employs a static solution of the reactive substrate contained in a small quartz tube which is irradiated by uv light (254 nm) directly in the cavity of the esr spectrometer. The small tube utilizes only a small amount of critical substrate, and it allows the temperature of the sample to be readily controlled over a wide range. The chemical methods utilized in this technique are enumerated below, together with specific examples.

Diacyl Peroxides and Peresters. Diacyl peroxides are readily prepared from the corresponding carboxylic acid via the acid chloride and hydrogen peroxide. Photolysis of diacyl peroxides in solution with 254-nm light proceeds with unit quantum yield.⁸ For example, perfluoropropionyl peroxide in cyclopropane or difluorodichloromethane (Freon-12) affords an intense and well-resolved spectrum

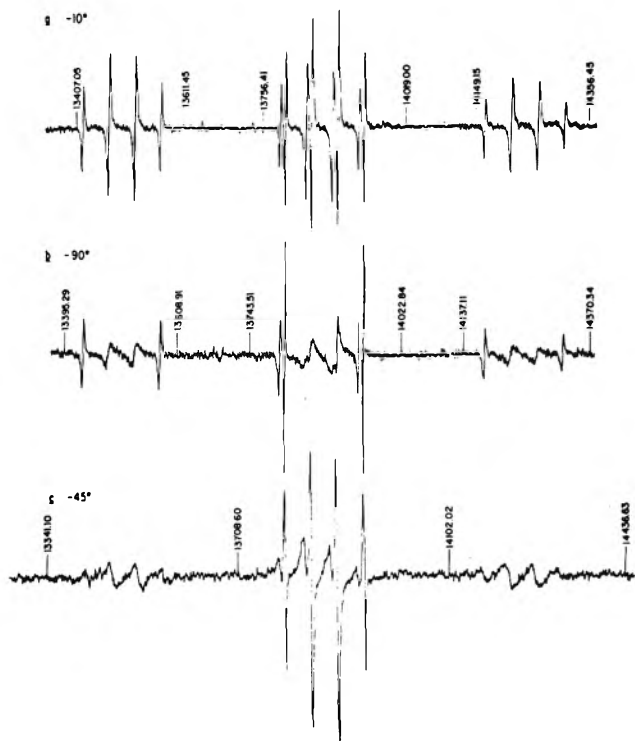
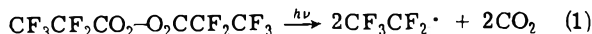


Figure 1. ESR spectra of the perfluoroethyl radical obtained by photolysis of perfluoropropionyl peroxide (a) in dichlorodifluoromethane at -10° , (b) in dichlorodifluoromethane at -90° , and (c) in a completely halogenated fluorocarbon oil of high viscosity (see text) at -45° . In the absence of unusual relaxation processes, the spectrum should consist of four identical 1:3:3:1 quartets (the doubling of the central quartet is due to second-order effects).

of perfluoroethyl radical⁹ (eq 1) shown in Figure 1. This



method is limited only by the synthesis of the peroxide and

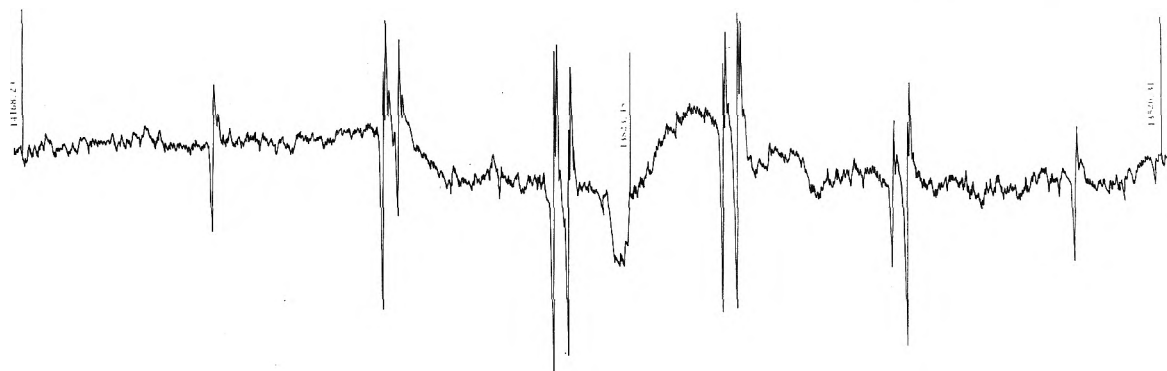


Figure 2. ESR spectrum of $(\text{CF}_3)_2\dot{\text{C}}\text{H}$ obtained during the photolysis of *tert*-butyl peroxyhexafluoroisobutyrate in pentane at -78° .

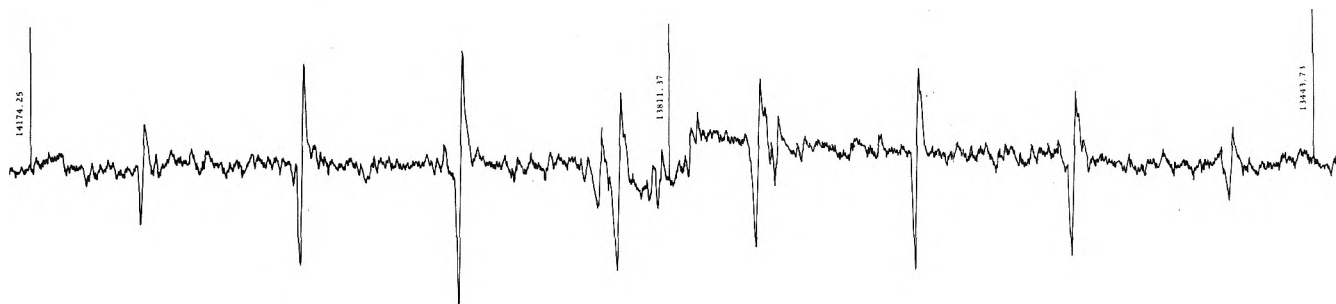
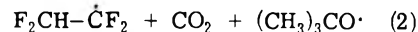
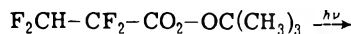
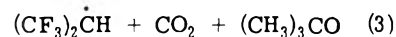
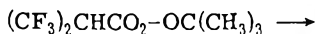


Figure 3. ESR spectrum of $(\text{CH}_3)_2\dot{\text{C}}\text{F}$ obtained during the reaction of 2-fluoropropane and bis(trifluoromethyl) peroxide in Freon 12 solution at -45° . Proton nmr field markers are in kHz.

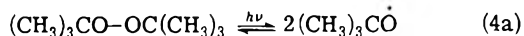
its solubility.¹⁰ In the latter regard, the readily synthesized *tert*-butyl peresters are generally more soluble in various media and thermally more stable than the corresponding diacyl peroxides and offer a convenient alternative precursor. The esr spectrum of the partially fluorinated $\alpha,\alpha,\beta,\beta$ -tetrafluoroethyl radical (eq 2) was obtained during the



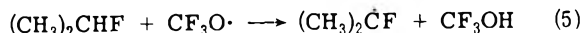
photolysis of *tert*-butyl peroxy- $\alpha,\alpha,\beta,\beta$ -tetrafluoropropionate in cyclopropane solution and similarly, the spectrum shown in Figure 2 of the 1,1,1,3,3,3-hexafluoro-2-propyl radical (eq 3) was produced under the same conditions from *tert*-butyl peroxy-hexafluoroisobutyrate.



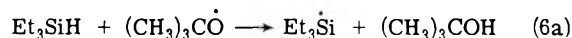
Fluoroalkanes. The generation of fluoroalkyl radicals from fluoroalkanes depends on the selective removal of a hydrogen atom by *tert*-butoxy or trifluoromethoxy radical generated photochemically from the peroxide in eq 4a and



4b.⁷ The esr spectrum in Figure 3 is associated with the 2-fluoro-2-propyl radical generated from 2-fluoropropane and bis(trifluoromethyl) peroxide in Freon-12.



Alkyl Halides. Alkoxy radicals generated from reactions 4a and 4b are also capable of selectively abstracting a hydrogen bonded to silicon or phosphorus in trialkylsilanes and dialkylphosphites, respectively.



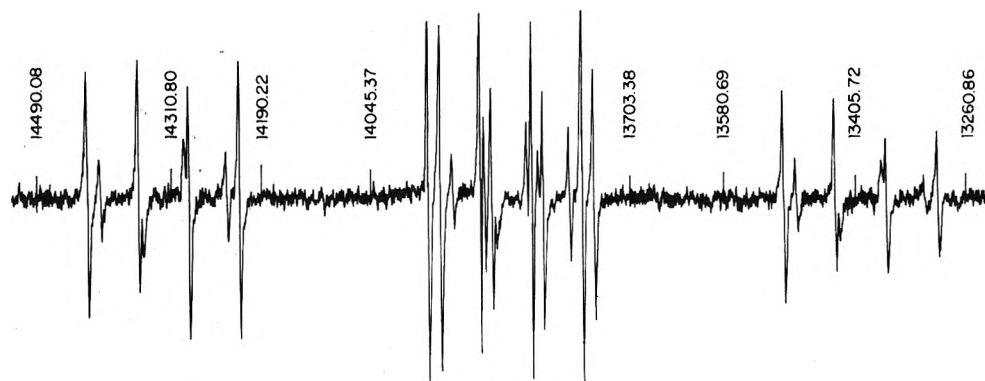
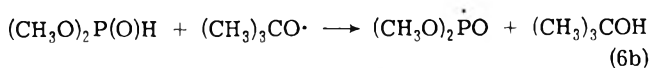
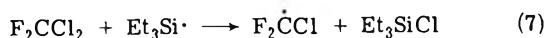


Figure 4. Esr spectrum of the chlorodifluoromethyl radical obtained by chlorine atom abstraction from Freon 12 at -90° .



Silicon- and phosphorus-centered radicals generated in this manner readily abstract halogen atoms from alkyl chlorides and bromides.¹¹ These facile reactions can be used to generate fluoroalkyl radicals by photolyzing a fluoroalkyl halide solution of the silane or phosphite and di-*tert*-butyl peroxide. The esr spectrum of the chlorodifluoromethyl radical generated from the photolysis of a Freon-12 solution of triethylsilane and di-*tert*-butyl peroxide is shown in Figure 4.



Perfluoroalkyl radicals have also been generated for esr studies by photolysis a 10% solution of perfluoroalkyl iodides in di-*tert*-butyl peroxide as solvent.¹² The reactions taking place under these conditions are not known.

Esr Parameters of Fluoroalkyl Radicals in Solution. Systematic replacement of the hydrogen atoms in ethyl radicals at the α - and β -carbon atoms leads to three series of fluoroalkyl radicals listed in Chart I. The isotropic esr parameters for these radicals are listed in Table I.

Chart I

I (α substituted)	II (β substituted)	III (α and β substituted)
$\text{CH}_3\dot{\text{C}}\text{H}_2$	$\text{FCH}_2\dot{\text{C}}\text{H}_2$	$\text{FCH}_2\dot{\text{C}}\text{F}_2$
$\text{CH}_3\dot{\text{C}}\text{HF}$	$\text{F}_2\text{CH}\dot{\text{C}}\text{H}_2$	$\text{F}_2\text{CH}\dot{\text{C}}\text{F}_2$
$\text{CH}_3\dot{\text{C}}\text{F}_2$	$\text{CF}_3\dot{\text{C}}\text{H}_2$	$\text{F}_3\text{C}\dot{\text{C}}\text{F}_2$

The esr spectra of the radicals listed in Table I were examined over a range of temperatures. The esr parameters and line widths in the spectra for $\text{CH}_3\dot{\text{C}}\text{H}_2$, $\text{CH}_3\dot{\text{C}}\text{HF}$, and $\text{CF}_3\dot{\text{C}}\text{H}_2$ showed no significant changes between -30 and -140° . The esr spectra of $\text{FCH}_2\dot{\text{C}}\text{H}_2$ and $\text{F}_2\text{CH}\dot{\text{C}}\text{H}_2$ showed pronounced selective line width variations at low temperatures ($< -100^\circ$) and changes in the β -fluorine and β -proton hfs. Both of these effects are due to hindered internal rotation about the $\text{C}_\alpha\text{-C}_\beta$ bond and are discussed in the next section. Line shape effects associated with hindered internal rotation were also displayed by $\text{CH}_3\dot{\text{C}}\text{F}_2$ and $\text{CF}_3\dot{\text{C}}\text{F}_2$ in addition to a selective line broadening caused by the modulation of the α -fluorine anisotropic hyperfine tensor by the rotational Brownian motion.^{9,13}

A series of fluorinated propyl radicals was also examined and their esr parameters are listed in Table II. The spectra of these radicals showed no exceptional changes in either

the hyperfine splittings or the line widths with changes in temperature except for the *n*-perfluoropropyl radical whose β -fluorine coupling constant is strongly temperature dependent. This dependence is again indicative of hindered internal rotation.

Discussion

Substitution of fluorine into the α and β positions of alkyl radicals gives rise to three principal structural questions: (i) the configuration at the α -carbon radical center, (ii) the stable conformation of the fluoroalkyl radical, and (iii) the barrier to hindered internal rotation about the $\text{C}_\alpha\text{-C}_\beta$ bond. Each of these structural points will be discussed separately in the following presentation.

Configuration at the α -Carbon Center and α -Fluorine Hyperfine Interactions. Particularly relevant to this question is the previous study carried out by Fessenden and Schuler¹⁴ on the fluoromethyl radicals. In Table III, the isotropic hyperfine splitting constants and *g* factors are summarized for this series of radicals. The exceptionally high ¹³C splittings in $\dot{\text{C}}\text{F}_3$ and $\dot{\text{C}}\text{HF}_2$ indicate that fluorine substitution in the methyl radical induces a pyramidal configuration at the carbon radical center. The extent of nonplanarity in the $\dot{\text{C}}\text{F}_3$ radical is given in Table III by ϕ , the angle between a C-F bond and a plane normal to the three-fold symmetry axis. These conclusions are supported by LCAO-SCF molecular orbital treatments.¹⁵

The proton and fluorine isotropic hyperfine coupling constants for fluorinated methyl radicals are also determined by the equilibrium geometries. For both nuclei these couplings become more positive as the departure from planarity increases (Table III). Therefore, α -proton and α -fluorine splittings can also be used as rough indicators of the geometry at the radical center. The similarities between the α -fluorine and α -proton hyperfine splittings in the series of fluoroethyl and fluoropropyl radicals in Tables I and II to the fluoromethyl radicals listed in Table III suggest the same trend of increasing pyramidal character at the radical center with successive fluorine substitution on the α carbon in all of these fluoroalkyl radicals.

The pronounced dependence of the α -proton coupling on the angle for out-of-plane bending is also responsible for the temperature dependence of this coupling as a result of vibrational motions.¹⁶ For the planar methyl radical a symmetric out-of-plane bending vibration produces a temperature coefficient of the α -proton coupling ($d|a^{\text{H}}|/dT$) of about -1.3 mG/deg.¹⁷ The fluorine coupling in the pyramidal $\dot{\text{C}}\text{F}_3$ radical is also temperature dependent with $d|a^{\text{F}}|/dT = +11.5$ mG/deg in the temperature range $-200^\circ < T$

TABLE I: Esr Parameters of Fluoroethyl Radicals in Solution

Fluoroethyl radical	T, °C	(g)	Hyperfine splitting, G				Gen ^a
			$a_{H\alpha}$	$a_{H\beta}$	$a_{F\alpha}$	$a_{F\beta}$	
CH ₃ ĊH ₂	-113	2.00260	22.37	26.99			PE(C)
CH ₃ ĊHF	-106	2.00366	17.31	24.48	59.21		PE(F)
FCH ₂ ĊH ₂	-94	2.00248	22.15	27.35		47.59	PE(C)
CH ₃ ĊF ₂	-78	2.00361		13.99	94.01		H,S(F)
F ₂ CHĊH ₂	-92	2.00243	23.16	12.05		49.28	S(C)
F ₂ CĊH ₂	-113	2.00234	23.77			29.61	S(C)
F ₃ CĊHF	-106	2.00363	21.47		66.18	25.25	S(C)
F ₃ CĊF ₂	-84	2.00386			87.26	11.36	S(F)

^a Gen = method of generation; P = diacyl peroxide, PE = perester, S = silyl radical abstraction, H = hydrogen abstraction in cyclopropane (C) or Freon-12 (F).

TABLE II: Esr Parameters of Fluoropropyl and Fluorobutyl Radicals in Solution

Fluoro-propyl radical	T, °C	(g)	Hyperfine splitting, G				Gen ^a
			$a_{H\alpha}$	a_{CH_3}	$a_{F\alpha}$	a_{CF_3}	
CH ₃ ĊHCH ₂	-113	2.00267	22.12	24.75			P(C)
CH ₃ ĊFCH ₃	-48	2.00360		21.11	60.85		H(F)
CF ₃ ĊHCF ₃	-113	2.00221	24.61			22.64	PE(F)
CF ₃ ĊFCF ₃	-60	2.0033			67.4	19.2	I
CF ₃ CF ₂ ĊF ₂	-60	2.0039			86.2	3.61	S(C)
(CH ₃) ₃ C·	-113	2.00270		22.93	15.09 ^b		S,P(C)
(CF ₃) ₃ C·	-60	2.0015				17.9	I

^a See footnote a, Table I. I = RFI see ref 12. ^b βF splitting.

TABLE III: Isotropic Esr Parameters for Fluoromethyl Radicals^a

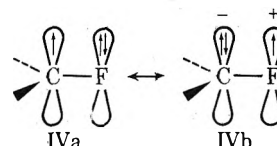
Radical	Hyperfine splitting, G			(g)	φ, deg
	a_H	a_F	a_C		
ĊH ₃	-23.0		38.5	2.0026	0
ĊH ₂ F	-21.1	64.3	54.8	2.0045	<5
ĊHF ₂	22.2	84.2	148.8	2.0041	12.7
ĊF ₃		142.4	271.6	2.0031	17.8

^a From ref 14.

< -130°. ¹⁴ This dependence must also be attributed to vibronic effects but, unlike the methyl radical, no detailed analysis of this problem has been carried out so far. In this case, a vibronic analysis must take into account the double-minimum potential function governing the umbrella inversion mode which is the most likely major source for the temperature dependence of the α-fluorine splitting. The existence of a substantial temperature coefficient for this splitting would seem to preclude a barrier to inversion in CF₃ of about 27 kcal mol⁻¹ which is predicted by INDO molecular orbital calculations. ¹⁵ It is of interest to note, however, that the same calculations for the CH₃CF₂ and the CF₃ĊF₂ radicals (*vide infra*) which formally result by replacing a fluorine atom in trifluoromethyl with a methyl or a trifluoromethyl group, predict the drastically reduced barriers to inversion to 7 and 3 kcal mol⁻¹, respectively.

Except for the temperature dependence of the fluorine, proton, and ¹³C splittings, pyramidal inversion in fluoromethyl radicals is not expected to cause any other temperature-dependent spectral effects such as selective line broadening. The spectrum of the difluoromethyl radical, however, does exhibit a line width effect below -100° (Figure 5). This effect has a strong viscosity dependence and is

due to a relaxation process brought about by the modulation of the anisotropic (dipolar) component of the hyperfine tensor by the tumbling motion in solution. ^{9,13} This component is very large for α fluorines because of contributions to the ground electronic state of configurations such as IVb which place unpaired spin density in fluorine 2p or-



bitals. This line shape effect is thus ubiquitous for radicals with α-fluorine atoms.

The dipolar contribution to the line width of each line of a hyperfine multiplet, $[T_{2d}(M_I, I)]^{-1}$, can be calculated as a function of the rotational correlation time τ_r using the Redfield relaxation matrix approach. ⁹ As an example, the calculated spectra for the trifluoromethyl radical are shown in Figure 6 for two rotational correlation times which give good fit to the experimental spectra. These spectra were calculated using Lorentzians with line widths given by

$$[T_2(M_I, I)]^{-1} = [T_{2d}(M_I, I)]^{-1} + T_{20}^{-1} \quad (8)$$

where T_{20} accounts for other relaxation processes. Identical results are also obtained using the explicit expression derived by McLachlan ^{13b} for the dipolar contribution to the line width of the (M_I, I) component of a hyperfine multiplet due to a set of completely equivalent nuclei. For an axially symmetric hyperfine tensor

$$2[T_{2d}(M_I, I)]^{-1} = (A_{II}^2/40)\{[3I(I+1) + 5M_I^2]J_0 + [7I(I+1) - M_I^2]J_\omega\} \quad (9)$$

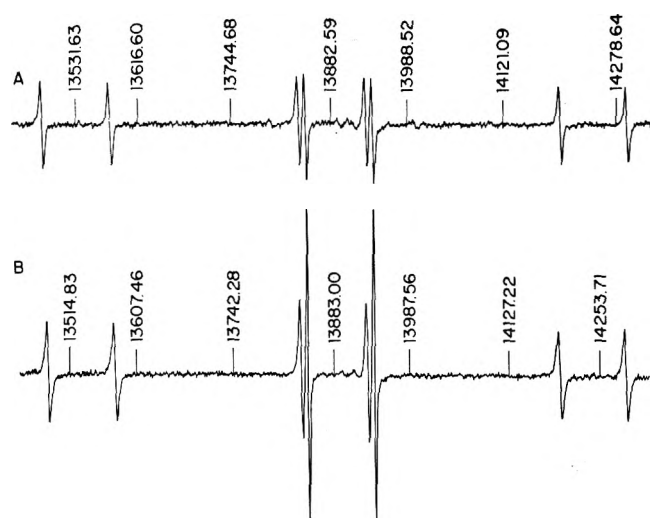


Figure 5. ESR spectrum of $F_2CH\cdot$ resulting from the reaction of tributylsilyl radicals with chlorodifluoromethane at (A) -50 and (B) -105° showing temperature-dependent line broadening.

In this expression A_{\parallel} is the parallel component of the anisotropic part of the hyperfine tensor in angular frequency units, $J_0 = 2\tau_r$, $J_\omega = 2\tau_r(1 + \omega^2\tau_r^2)^{-1}$, and τ_r is the correlation time for the rotational tumbling. In these calculations, A_{\parallel} for the trifluoromethyl radical was taken to be 108 G^{18} and T_{20} (eq 8) was chosen to give best agreement with the experimental spectra ($T_{20} = 75 \times 10^{-9} \text{ sec}$).

Several generalities and practical consequences of the dipolar broadening are noteworthy. From eq 9 it is seen that the dipolar contribution to the line widths will be largest for the lines corresponding to the maximum values of I and M_I , that is for the outermost lines of a hyperfine multiplet. In the case of fluoroalkyl radicals with one α fluorine, $R_1R_2\dot{C}F$, both lines of the fluorine doublet will be equally broadened. In the presence of additional hyperfine structure, dipolar broadening will effect equally all lines of the spectrum and contribute to each line an excess line width of $(A_{\parallel}^2/40)(7/2J_0 + 5J_\omega)$. For radicals with two α fluorines, RCF_2 , the central line of the triplet corresponding to the nondegenerate nuclear state with $I^F = 0$ and $M_I^F = 0$ will not be affected at all by dipolar broadening, while the wing lines with $I^F = 1$ and $M_I^F = \pm 1$ will have an additional width of $(A_{\parallel}^2/40)(11J_0 + 13J_\omega)$ and will appear, consequently, with reduced amplitudes (Figure 5). The downfield second-order component of the central line ($M_I = 0, I = 1$) is also broadened but less than the wing lines [$2T_{2d}^{-1} = (A_{\parallel}^2/40)(6J_0 + 14J_1)$]. If the rotational correlation time is sufficiently long, this effect can be so pronounced as to make the outermost lines completely undetectable. The dipolar broadening will be particularly severe for radicals of large molecular volume in viscous media as can be seen by consideration of the Debye relationship¹⁹

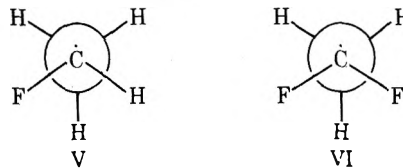
$$\tau_r = 4\pi r^3 \eta / 3kT \quad (10)$$

valid for a sphere of radius r in a fluid medium of viscosity η . In order to observe the whole spectrum for radicals strongly affected by dipolar broadening it is helpful to use an inert solvent of low viscosity such as cyclopropane or mixtures of cyclopropane and ethane. This expedient is preferable to raising the temperature to increase the molecular tumbling rate since higher temperatures usually also lead to lower radical concentrations and to spectra of poorer signal-to-noise ratios.

An interesting example of the usefulness of a solvent of low viscosity (cyclopropane-ethane) in allowing a low temperature study which would not be otherwise feasible is provided by the 1,1,3,3-tetrafluoro-2-chloroallyl radical.²⁰ This radical, in dramatic contrast to the parent allyl radical which has a barrier to rotation in excess of 17 kcal mol^{-1} ,²⁰ undergoes a fast stereoisomerization even at temperatures as low as -70° as judged by the observation of a quintet spectrum with partially resolved second-order structure appropriate for four equivalent fluorine atoms ($a^F = 43.3 \text{ G}$). Lowering the temperature to slow the dynamic process to its slow-exchange limit resulted in the obliteration of the outermost lines ($M_I = \pm 2, I = 2$) and the severe broadening of the next pair of composite lines ($M_I = \pm 1, I = 2$ and $M_I = \pm 1, I = 1$), while the central group of lines remained sharp. The relative dipolar contributions to the line widths of all the components of the multiplet can again be obtained from eq 9. For example, if axial symmetry of the A tensor is assumed, the excess width for the outermost lines is given by $(A_{\parallel}^2/40)(38J_0 + 38J_\omega)$. The $M_I = 0, I = 0$ line of the central group is, of course, unaffected by dipolar relaxation. Generation of the radical in cyclopropane-ethane mixtures allowed the slow-exchange limit to be reached at about -100° without undue complications from dipolar broadening. At this temperature the spectrum consisted of a triplet-of-triplets ($a^{F1} = 40.7 \text{ G}$, $a^{F2} = 44.9 \text{ G}$) for two pairs of nonequivalent fluorines.

From the foregoing description, it is apparent that one of the major differences in the nature of the hyperfine interactions for α protons and α fluorines is the much larger anisotropy of the latter. Another difference worthy of note is that the α -fluorine isotropic coupling is positive, as revealed by single crystal work,⁵ even in systems constrained to planarity at the α carbon by resonance effects. By contrast, it is well known that the α -proton isotropic coupling in planar systems is negative since it arises from spin polarization of the electrons in the σ CH bond by the unpaired π spin density on the α carbon. Recently, it has been suggested^{15c} that positive spin density in the 2s and 1s orbitals of α fluorines arises primarily by spin polarization caused by the unpaired spin density in the 2p fluorine orbitals (cf. structure IVb).

Conformations of α -Fluoroalkyl Radicals. The conformations V and VI for $CH_3\dot{C}HF$ and $CH_3\dot{C}F_2$ were deduced



by optimizing the experimental values of the proton and fluorine hyperfine splittings to the ones calculated by the LCAO-SCF molecular orbital method in the semiempirical INDO approximation.²¹ Interestingly, the geometry resulting from the optimization listed in Table IV is also close to a minimum for the total energy.²² Furthermore, the geometries of best-fit at C_α for $CH_3\dot{C}HF$ and $CH_3\dot{C}F_2$ show the same trend to bending as a result of the introduction of successive α -fluorine substituents as those obtained experimentally and theoretically for $H_2\dot{C}F$ and $H\dot{C}F_2$, respectively.^{14,15}

The extraordinarily small value of the proton hfs in $CH_3\dot{C}F_2$ ($a_H = 13.99 \text{ G}$) is striking for an α -methyl group in comparison with those of other alkyl radicals which have values of a^{HCH_3} in the range 23–26 G.²³

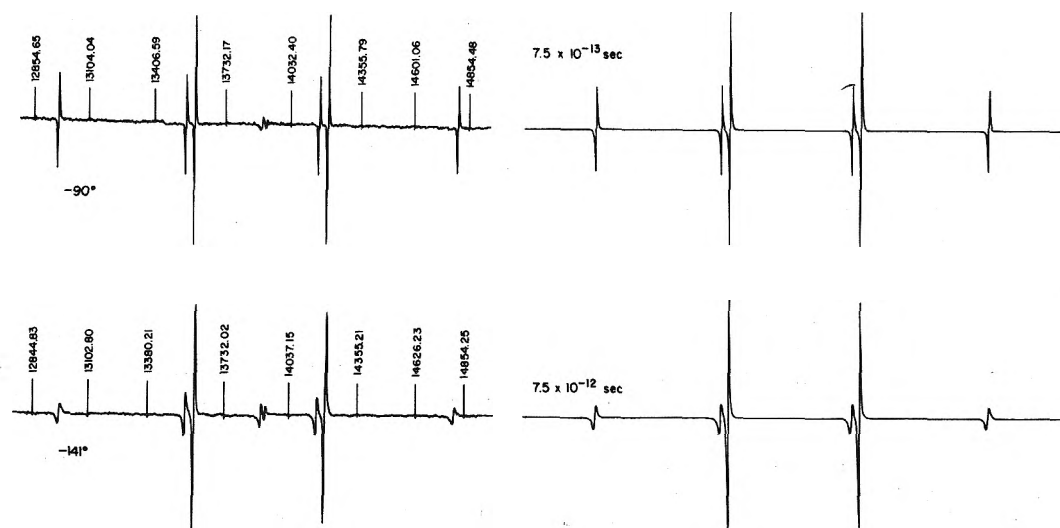


Figure 6. Esr spectra of the trifluoromethyl radical at two temperatures with the calculated spectra (Redfield relaxation matrix theory) for two rotational correlation times. The radical was generated by photolysis of a solution containing di-*tert*-butyl peroxide, dimethylphosphite, and bromotrifluoromethane (1:1:5 v/v/v).

TABLE IV: Conformational Dependence of Esr Parameters for α -Fluoroalkyl Radicals by INDO-MO^a

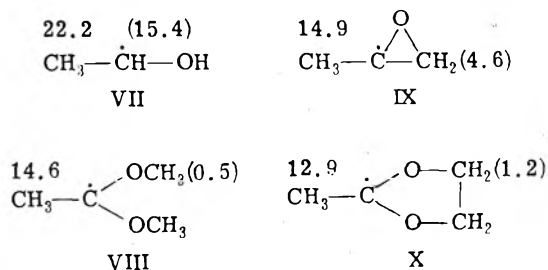
Parameters ^b and hfs	α, α -Difluoroethyl radical		α -Fluoroethyl radical
$\angle C_{\beta}C_{\alpha}F(H)$	115°	120°	119° (121°)
$\angle FC_{\alpha}F(H)$	106°	120°	(119°)
$r(C_{\alpha}-C_{\beta})$	1.51 Å	1.50 Å	1.52 Å
$a_{\beta H}$	(1) 37.21	49.90	52.28
	(2) 2.92	13.51	11.10
	(3) 2.92	13.51	13.64
	$\frac{1}{2} \sum a_i$	25.64	25.67 (24.48 ^c)
$a_{\alpha H}$			-18.58 (17.31 ^c)
a_F	93.69 (94.01 ^c)	49.89	61.95 (59.21 ^c)
$a_{\alpha C}$	142.50	36.86	44.56
$a_{\beta C}$	0.89	-11.80	-11.22
Total energy, au	-68.7374	-68.7258	-43.0303

^a Reference 21. ^b $r(C_{\alpha}-H_{\alpha}) = 1.08 \text{ \AA}$, $r(C_{\alpha}-F_{\alpha}) = 1.35 \text{ \AA}$, $r(C_{\beta}-H_{\beta}) = 1.08 \text{ \AA}$, $C_{\beta} = \text{tetrahedral}$; others listed below were optimized. Hfs in gauss. ^c Experimental values (absolute).

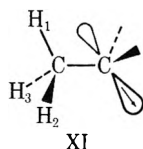
The INDO results of Table IV indicate that this diminution in the CH_3 proton coupling is solely attributable to the bent structure at the α carbon induced by the presence of two α fluorines. Thus, this coupling increases from 14 to 26 G (which compares with the CH_3 splitting for ethyl of 26.99 G), simply by constraining the radical site in CH_3CF_2 to be planar. A single fluorine on the α carbon in $CHFCH_3$ produces a much smaller diminution in $a^{H_{CH_3}}$ (24.48 G vs. 26.99 G) in accord with the much smaller bending influence of a single fluorine at the radical site as was seen for $\dot{C}H_2F$ (Table III).

Reductions in the values of the proton splitting for α - CH_3 groups has been observed for other radicals with pyramidal geometry at the radical site.²⁴ Thus, α -oxy substituents (with lone pairs of electrons on oxygen) are also effective in bending the configuration of the trigonal carbon. Similarly to α -fluoroalkyl radicals, two oxygen substituents produce a much greater degree of bending than one such substituent as established from ¹³C studies.^{24a} Angle strain by itself can also produce bending, as in the cyclopropyl ra-

dical,^{23a} which is enhanced in the presence of α oxygens. In all these cases the proton splitting of α - CH_3 groups diminishes in proportion to the bending as illustrated below for the α -hydroxyethyl radical VII,²⁵ for the α, α -dimethoxyethyl radical VIII,^{24a, 26} and for the radicals derived from propylene oxide,²⁷ IX, and methyldioxolane,^{24a} X. The re-



duction in the values of the α - CH_3 proton splittings in these radicals is mainly due to reduced hyperconjugative interactions afforded by structure XI.²⁸ In this structure,



XI

the spatial characteristics of the hybrid orbital containing the impaired electron compared to a pure $2p_z$ orbital afford less favorable overlap with the $1s$ orbitals of all three β protons. A situation which can also be described by a structure similar to XI obtains for the α -methylvinyl radical,^{23a} $\text{CH}_3\text{-}\dot{\text{C}}=\text{CH}_2$ for which the CH_3 proton coupling is also anomalously low (19.5 G). The nonlinear nature of the radical site is clearly indicated by the nonequivalence of the two β vinylic protons. In this case, an incipient line width effect affecting the central lines of the 1:3:3:1 quartets at -175° shows that the rotation of the methyl group is hindered by a threefold barrier to rotation whose height was estimated to be $1300 \text{ cal mol}^{-1}$.

A conformation analogous to VI is also obtained for the perfluoroethyl radical (XII) by minimization of the INDO energy with respect to the nonplanarity angle ϕ and the torsional angle θ of the CF_3 group.⁹ The resulting structure

	Exptl ($T = -170^\circ$)	Calcd
	$a_{\alpha\text{F}} = 87.6$	96.7
	$a_{\beta\text{F}_1} = 40.4$	184.6
	$a_{\beta\text{F}_{2,3}} = -3.14$	6.9
	$\frac{1}{3}\sum a_{\beta\text{F}_i} = 11.4$	66.1

with $\phi = 15^\circ$ accounts reasonably well for the α -fluorine coupling constant. The geometry at the trigonal carbon is thus comparable to that in $\dot{\text{C}}\text{F}_2\text{H}$ (cf. Table III) and in $\dot{\text{C}}\text{F}_2\text{CH}_3$. The lack of agreement between the calculated and experimental β -fluorine coupling constants is noteworthy and appears to be an intrinsic limitation of the INDO program. Variations in the $\text{C}_\alpha\text{-C}_\beta$ bond length and distortions at C_β did not significantly lower the calculated value of the single β -fluorine splitting in conformation XII. The INDO calculations also fail to predict a negative value for $a_{\beta\text{F}_{2,3}}$. The line width effect displayed by the perfluoroethyl radical at low temperatures (*vide infra*) unequivocally establishes opposite signs for $a_{\beta\text{F}_{2,3}}$ and $a_{\beta\text{F}_1}$ and it is reasonable to assign the negative sign to the smaller of the two couplings.

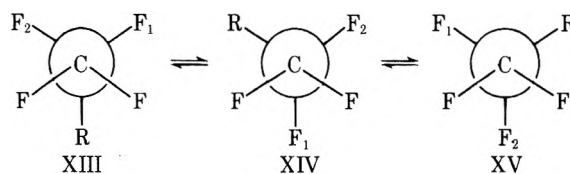
The average CF_3 fluorine coupling in this radical (11.4 G) is remarkably small when compared to the analogous splitting of 29.6 G (Table I) in $\dot{\text{C}}\text{H}_2\text{CF}_3$. The situation is similar to that in $\dot{\text{C}}\text{F}_2\text{CH}_3$, and it can be safely inferred that the reduction is due largely to the bending of the radical site, that is, to the hybrid nature of the orbital containing the unpaired electron (cf. structure XI). The α - CF_3 fluorine hfs responds to the geometry of the trigonal carbon in a manner analogous to the CH_3 proton splitting as can be seen in the series $\dot{\text{C}}\text{H}_2\text{CF}_3$ (29.6 G), $\dot{\text{C}}\text{HCF}_3$ (25.3 G), and $\dot{\text{C}}\text{F}_2\text{CF}_3$ (11.4 G). The same trend is also apparent for the radicals $\text{CF}_3\dot{\text{C}}\text{HCF}_3$ (22.6 G) and $\text{CF}_3\dot{\text{C}}\text{FCF}_3$ (19.2 G). A further decrease in this coupling for $\dot{\text{C}}(\text{CF}_3)_3$ (17.9 G) may well be due to a nonplanar radical structure for this radical, although ^{13}C studies are needed to confirm this expectation. Unfortunately, the dependence of the α - CF_3 fluorine hfs on the radical geometry makes it impossible at present to assess the electron-withdrawing capacity of each CF_3

group as can be done for simple alkyl radicals^{23a} (e.g., $\dot{\text{C}}\text{H}_2\text{CH}_3$, $\dot{\text{C}}\text{H}(\text{CH}_3)_2$, and $\dot{\text{C}}(\text{CH}_3)_3$).

The esr spectrum of the perfluoropropyl radical at -60° consists of a triplet-of-triplets caused by the two α fluorines (86.2 G) and the two β fluorines (15.1 G) split into quartets by the γ fluorines (3.61 G) (Figure 7). The radical was generated from the corresponding bromide by reaction 6b in a cyclopropane solution. At room temperature the spectrum of the perfluoroheptyl radical generated from the corresponding bromide by reaction 6b, is also a triplet-of-triplets (86.0 and 16.4 G, $g = 2.0041$). An inadequate signal-to-noise ratio coupled with the relative broadness of the lines precluded an interpretation of the additional long-range hyperfine structure (which resembles a quintet of about 1.5-G splitting).

The α -fluorine couplings indicate radical sites of comparable geometry to that in perfluoroethyl radical. In both radicals the magnitudes of the β -fluorine couplings increase notably as the temperature is raised. Except for the dipolar broadening of the wing lines, which are particularly severe for the larger heptyl radical, no additional line shape effect was apparent down to -80° . Studies at lower temperatures were complicated by dipolar broadening and by the second-order effects of the central group of lines (cf. Figure 7). We were able, nevertheless, to record the spectrum of the perfluoropropyl radical at -100° . At this temperature the triplet structure due to the two β fluorines is still apparent although not quite with 1:2:1 amplitudes. The central lines of the 1:3:3:1 quartets due to the γ fluorines, however, were severely broadened and appeared with strongly reduced amplitudes indicating that the rotation of the β - CF_3 group is hindered.

The temperature dependence of the β -fluorine couplings indicates the presence of a barrier to rotation about the $\text{C}_\alpha\text{-C}_\beta$ bonds. It is reasonable to suppose that the potential function governing this internal rotation has a dominant threefold term with minima corresponding to configurations XIII, XIV, and XV for both these radicals and indeed, by natural extension, for all unsubstituted primary perfluoroalkyl radicals. Rapid interconversion among these



rotamers can cause both a temperature dependence of the β -fluorine coupling constant as well as line width effects for sufficiently slow exchange rates (*i.e.*, nonmutual exchange, *vide infra*). Conformation XIII, by analogy with the perfluoroethyl radical in its slow-exchange limit (cf. XII), should lead to the smallest value for the β -fluorine coupling. The observation of a positive temperature coefficient for $a_{\beta\text{F}}$ must then mean that this rotamer is the more populated at low temperatures hence it is the more stable. This question will be pursued further in the next section.

Barriers to Hindered Internal Rotation about the $\text{C}_\alpha\text{-C}_\beta$ Bond in Fluoroalkyl Radicals. I. Effect of α -Fluorine Substitution. The esr spectrum of $\text{CH}_3\text{-}\dot{\text{C}}\text{HF}$ shows no selective line broadening in the temperature range from -20 to -140° . On the other hand, the esr spectrum of the α,α -difluoro analog, $\text{CH}_3\text{-}\dot{\text{C}}\text{F}_2$, shows the pronounced line width behavior illustrated in Figure 8.²¹ The outstanding feature of the spectra in Figure 8 is the broadening of the inner two

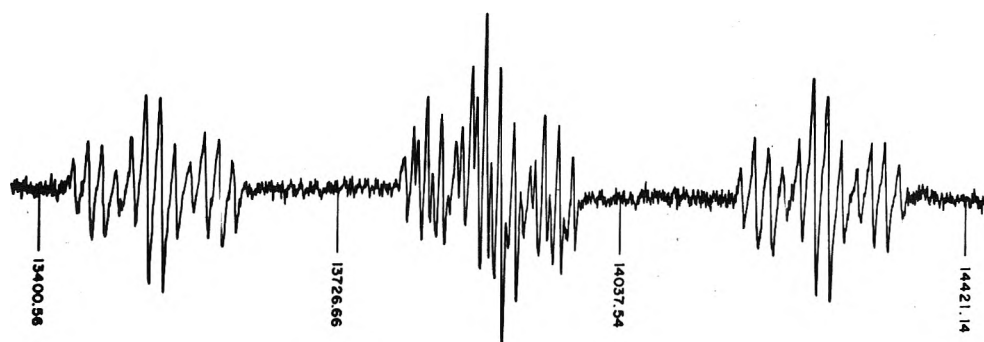


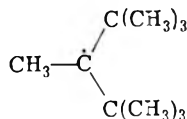
Figure 7. Esr spectrum of $\text{CF}_3\text{CF}_2\text{CF}_2\cdot$ at -60° generated by bromine atom abstraction from perfluoropropyl bromide in cyclopropane solution.



Figure 8. Experimental and simulated esr spectra of the α,α -difluoroethyl radical in a cyclopropane solution at -37 and -122° . The calculated rate constant k is for exchange in eq 8 (see text).

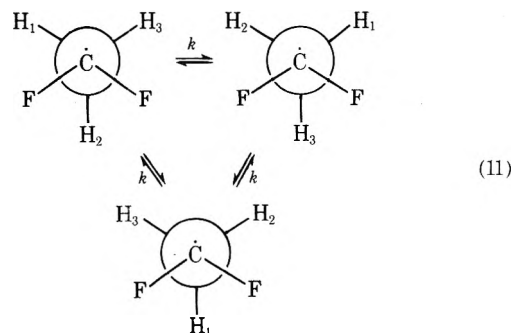
lines of the CH_3 quartets due to the modulation of the hfs of the three methyl protons resulting from hindered internal rotation about the $\text{C}_\alpha\text{-C}_\beta$ bond. The broadening beyond detection of the two outermost quartets as well as the downfield second-order components in the central region of the spectrum is due to dipolar broadening.

Hindered rotation of a methyl group is an unusual occurrence. In more or less planar radicals the rotation of a methyl group is unhindered even in the presence of bulky groups. Thus, the spectrum of the α,α -di-*tert*-butylethyl radical²⁹ shows no significant line width effects over a



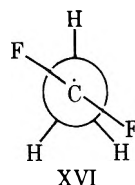
broad temperature range. Unusual hydrogen-fluorine interactions must also be excluded since there is no evidence for restricted rotation of the CH_3 group in the $\text{CH}_3\dot{\text{C}}\text{HF}$ radical. The presence of a substantial threefold barrier to rotation in $\dot{\text{C}}\text{F}_2\text{CH}_3$ is, therefore, a consequence of the py-

ramidal geometry at the α carbon. The line shape effect is caused by a rapid interconversion among the three equivalent conformations shown below which exchanges one of the two equivalent β protons with the unique β proton. The



simulated spectra of Figure 8 were calculated as a function of the exchange rate k using the method of the modified Bloch equations.³⁰ The two sets of proton hyperfine split-

tings at the slow limit required for these calculations were obtained from the INDO calculations in Table IV, since we were experimentally unable to obtain the spectrum at the slow exchange limit.²¹ The dipolar contribution to the line widths was also included in these calculations using eq 8 and 9. A value of 2.2 ± 0.5 kcal mol⁻¹ was obtained for the rotation barrier in CH₃CF₂ from an Arrhenius plot of the temperature dependence of k . The exchange mechanism shown above implies that the inversion barrier at the radical site is much larger than the threefold rotational barrier. A motion of coupled inversion and rotation with barriers of comparable heights (2.2 kcal mol⁻¹) and proceeding through a common transition state XVI would also produce



the same line width effects and cannot be rigorously excluded at present.

The esr spectrum of the perfluoroethyl radical⁹ is remarkably similar to the spectrum of the α,α -difluoroethyl radical (Figure 1). The same line width effects are observed as the temperature is lowered: first, the broadening of the inner two lines of the quartets associated with the β fluorines and, second, the broadening of the outer lines of the triplet and of the downfield second-order components ($M_I^{\alpha F} = 0$, $I^{\alpha F} = 1$ lines) associated with the two α fluorines. The latter effect has a strong viscosity dependence (Figure 1c) as expected for dipolar broadening.

The viscosity independent broadening of the central lines of the quartets ($M_I^{\beta F} = \pm \frac{1}{2}$ lines) is caused by hindered rotation of the trifluoromethyl group about the C-C bond axis and is shown as a function of temperature in Figure 9. The spectrum at -170° shows the incipient formation of two triplets of 3.14 G separated by 40.4 G indicating two equivalent β fluorines and a unique β fluorine in the most stable conformation of the radical. *Opposite signs* for these two coupling constants must be taken for their weighted average to be 11.37 G, in close agreement with 11.48-G quartet splitting at higher temperatures. Knowledge of the spectral parameters in the slow-exchange limit allows the spectra to be fitted by the density matrix method³¹ (Figure 9). An activation energy of 2.85 kcal mol⁻¹ is obtained for the rate process which exchanges one of the two equivalent β fluorine. This activation energy can be taken as a measure of the threefold barrier to rotation causing the existence of three equivalent interconverting rotamers in complete analogy with the α,α -difluoroethyl radical (*cf.* eq 11). Once again a motion of coupled inversion and rotation cannot be excluded.

It is noteworthy that neither the α,α -difluoroethyl nor the perfluoroethyl radical exhibits any measurable temperature dependence of the β nuclear spin hyperfine couplings ($a_{\beta H}$ and $a_{\beta F}$) over a very broad temperature range. This observation is entirely consistent with the presence of a threefold barrier to internal rotation

$$V(\theta) = \frac{V_3}{2}(1 - \cos 3\theta) \quad (12)$$

If it is assumed that the i th β nuclear spin coupling in either the $\dot{C}F_2CH_3$ radical (*cf.* eq 11) or the $\dot{C}F_2CF_3$ radical (*cf.* XII) has an angular dependence which can be repre-

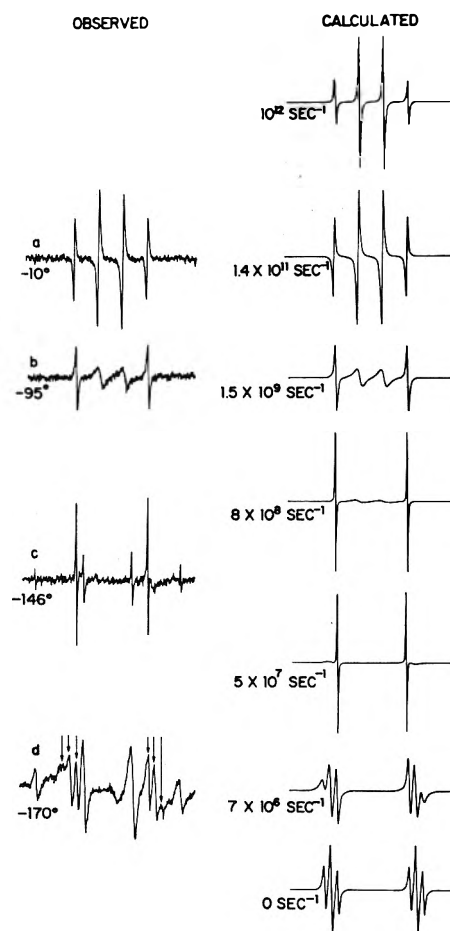


Figure 9. Line shape changes with temperature in the spectrum of perfluoroethyl radical due to hindered internal rotation of the CF₃ group. Spectra a and b were obtained by photolysis of perfluoropropionyl peroxide in CCl₂F₂ and represent the downfield $M_I^{\alpha F} = 1$ lines. Spectra c and d were obtained by photolysis of *tert*-butyl perfluoropropionyl perester in CClF₃ at -146° and -170° and show the central region of the spectrum containing the $M_I^{\alpha F} = 0$ lines. At these temperatures, the wing lines are broadened beyond detection. Spectra c and d are complicated by the presence of a quartet of 22.86 G attributed to the methyl radical of unknown provenance. At -146° the downfield $I^{\alpha F} = 1$ lines (second-order components) are obliterated by dipolar line broadening. The calculated spectra were obtained by the density matrix method.

sented by a truncated Fourier expansion of even cosine terms

$$a_\beta(\theta) = A_0 + A_2 \cos 2(\theta + \theta_0) = A + B \cos^2(\theta + \theta_0) \quad (13)$$

where θ is the torsional angle measured from the plane which bisects the F _{α} CF _{α} angle and contains the hybrid half-filled orbital on C _{α} , the temperature dependence of a_β can be approximated by^{7,31a}

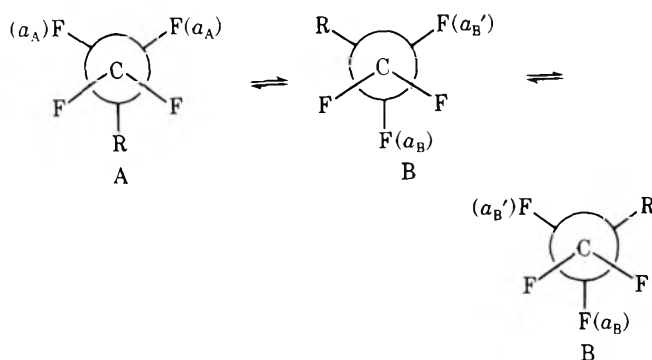
$$a_\beta(T) = \frac{\int_{-\pi}^{\pi} a_\beta(\theta) \exp[-V(\theta)/RT] d\theta}{\int_{-\pi}^{\pi} \exp[-V(\theta)/RT] d\theta} \quad (14)$$

The above integral is independent of the temperature for a threefold potential $V_3(\theta)$ as can be established by numerical integration. This result is quite reasonable since the positive contributions to $a_\beta(T)$ due to torsional oscillations around the two positions leading to a small β coupling are

cancelled by the negative contribution from torsional oscillations around the position leading to the largest β coupling. The same result will apply to the threefold component of a more complicated potential function and, as will be seen below, also to the fourfold component which must be considered for the β -fluoroethyl and β,β -difluoroethyl radicals.

There is an additional factor involved in the temperature dependence of α -CH₃ proton and α -CF₃ fluorine couplings which should be considered, namely, the inversional motion in a bent CH₃-C[•] and CF₃-C[•] structure. It was seen above that the magnitudes of the α -CH₃ proton and α -CF₃ fluorine couplings depend on the degree of pyramidality at C _{α} . An umbrella inversion of sufficiently low frequency can then produce a temperature dependence of these couplings. Recently, such a temperature dependence has been studied for the CH₃ groups in the *tert*-butyl radical which is apparently pyramidal but with a very low inversion barrier.³² The absence of any measurable temperature dependence for $a_{\alpha\text{CH}_3}^{\text{H}}$ and $a_{\alpha\text{CF}_3}^{\text{F}}$ in $\dot{\text{C}}\text{F}_2\text{CH}_3$ and $\dot{\text{C}}\text{F}_2\text{CF}_3$ is then indicative of a larger inversion barrier for these radicals.

If one of the β fluorines in $\dot{\text{C}}\text{F}_2\text{CF}_3$ is replaced by a substituent R [R = H, alkyl, fluoroalkyl, or CF₃ as in perfluoropropyl], the β fluorine coupling becomes temperature dependent. A substitution of this kind does not materially affect the structure at the α carbon as indicated by the very small changes in the α -fluorine coupling in the series $\dot{\text{C}}\text{F}_2\text{CF}_3$, $\dot{\text{C}}\text{F}_2\text{CF}_2\text{CF}_3$, and $\dot{\text{C}}\text{F}_2\text{CF}_2(\text{CF}_2)_4\text{CF}_3$. The threefold potential function can no longer have equivalent minima, and two distinct rotamers A and B become possible with fractional populations X_A and X_B which are temperature



dependent. For sufficiently fast rates of interconversion among these rotamers, the β fluorines will give rise to a triplet structure whose splitting will be an average of the limiting coupling constants for A and B weighted by the fractional populations of each rotamer.

$$a_{\beta\text{F}}(T) = X_A a_A + 2X_B \frac{a_B + a_B'}{2} \quad (15)$$

Changes in the fractional populations with temperature will lead to a change in $a_{\beta\text{F}}$. Since $X_A + 2X_B = 1$, the β -fluorine splitting can also be written as

$$a_{\beta\text{F}}(T) = 2X_B \left[\left(\frac{a_B + a_B'}{2} \right) - a_A \right] + a_A \quad (16)$$

If it is assumed, as is quite reasonable, that a_B' will not be much different from a_A , the β -fluorine coupling will be given approximately by

$$a_{\beta\text{F}}(T) = X_B (a_B - a_A) + a_A \quad (17)$$

whose high-temperature limit ($X_B = 1/3$) is given by

$$a_{\beta\text{F}}(\text{HT}) = (1/3)(a_B + 2a_A) \quad (18)$$

The fractional population X_B can then be written in terms of $a_{\beta\text{F}}(\text{HT})$ as follows

$$3X_B = \frac{a_{\beta\text{F}}(T) - a_A}{a_{\beta\text{F}}(\text{HT}) - a_A} \quad (19)$$

A positive temperature coefficient is observed experimentally for $a_{\beta\text{F}}$ for both the perfluoropropyl and perfluoroheptyl radicals ($a_{\beta\text{F}}(\text{HT}) > a_{\beta\text{F}}(T)$ assuming a positive β coupling). Therefore the right side of eq 19 is less than one and $X_B < 1/3$, provided the observed coupling constant is greater than a_A . Comparison with $\dot{\text{C}}\text{F}_2\text{CF}_3$ (*cf.* XII) supports the latter assumption. It is concluded that rotamer A is the more populated and therefore the more stable.

Knowledge of the limiting couplings for the perfluoropropyl radical would allow the determination of the fractional populations at each temperature and hence the equilibrium constant for the $A \rightleftharpoons B$ equilibrium as a function of the temperature. The enthalpy difference between A and B could then be determined experimentally. These limiting couplings, however, cannot be obtained experimentally. An alternative approach would seem to be, at first sight, to assume that the limiting couplings for perfluoroethyl radical (*cf.* XII) could be applied to the perfluoropropyl radical. Unfortunately, this cannot be done as seen by consideration of the expected high temperature limits of $a_{\beta\text{F}}$ for these two radicals. If this transfer were allowed, both radicals would exhibit the same high temperature limit, given by eq 18, which for $\dot{\text{C}}\text{F}_2\text{CF}_3$ amounts to 11.4 G. For $\dot{\text{C}}\text{F}_2\text{CF}_2\text{CF}_3$ this limit must be greater than the room-temperature value of 16.9 G since the experimental $a_{\beta\text{F}}(T)$ curve has a positive slope at this temperature. It appears that in radicals of the type $\dot{\text{C}}\text{F}_2\text{R}_F$ the average β fluorine coupling, $a_{\beta\text{F}}(\text{HT})$, is very sensitive to the number of fluorine atoms on the β carbon. It is smallest for three fluorines ($\dot{\text{C}}\text{F}_2\text{CF}_3$), larger for two fluorines (*e.g.*, $\dot{\text{C}}\text{F}_2\text{CF}_2\text{CF}_3$), and presumably larger yet for one fluorine. A similar trend obtains for the average $a_{\beta\text{F}}$ for β -fluoroethyl radicals which will be discussed below. Studies of the radicals $\dot{\text{C}}\text{F}_2\text{CHF}_2$ and $\dot{\text{C}}\text{F}_2\text{CH}_2\text{F}$ are now in progress to clarify this point. These radicals are also ideally suited for the study of line shape effects due to rapid interconversions between the nonequivalent isomeric species A and B above (nonmutual exchange).

II. Effect of β -Fluorine Substitution. The presence of substantial barriers to hindered internal rotation in $\text{CH}_3\dot{\text{C}}\text{F}_2$ and $\text{CF}_3\dot{\text{C}}\text{F}_2$ should be contrasted with the essentially free rotation in $\text{CH}_3\dot{\text{C}}\text{H}_2$ and $\text{CF}_3\dot{\text{C}}\text{H}_2$.^{23,33} In the latter species, the radical sites are planar and the molecules possess sixfold axis of internal rotation. Sixfold barriers³⁴ typically have magnitudes of only a few hundred calories mole⁻¹ or less. Barriers of 2–3 kcal mol⁻¹ are, therefore, indicative of a threefold axis of rotation which obtains in species such as $\text{CH}_3\dot{\text{C}}\text{F}_2$ with strongly pyramidal radical centers. This conclusion is entirely consistent with the magnitude of the α -fluorine coupling and is also borne out by INDO calculations described above.

In order to examine the effects of β -fluorine substitution more closely, the esr spectra of β -fluoroethyl, β,β -difluoroethyl, and β,β,β -trifluoroethyl radicals were studied and are reported separately in the following discussion.

A. β,β,β -Trifluoroethyl Radical. The esr spectrum of the β,β,β -trifluoroethyl radical is essentially invariant over a broad range of temperatures, both with regard to the

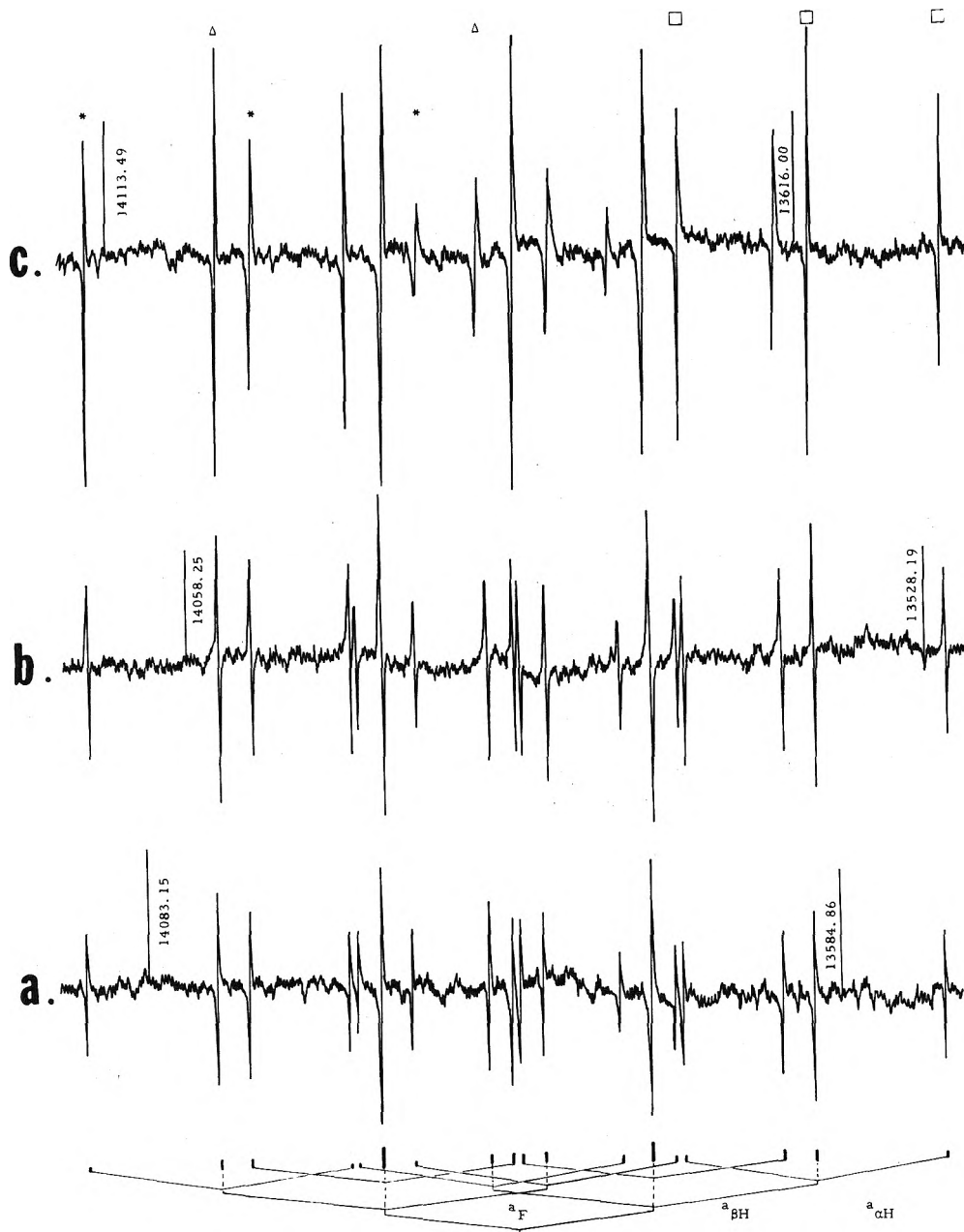


Figure 10. ESR spectrum of $FCH_2CH_2\cdot$ in cyclopropane solutions at (a) -59° , (b) -72° , and (c) -109° . The line spectrum is based on binomial intensities.

widths of the hyperfine lines as well as the magnitudes of the coupling constants.³³ The three β fluorines give rise to a quartet (with resolved second-order splittings expected for three equivalent spins of $\frac{1}{2}$), which persists unaltered down to temperatures as low as -180° . Furthermore, the proton and fluorine coupling constants vary only slightly with solvent. We deduce that the trifluoromethyl group rotates freely (with preexchange lifetimes shorter than 10^{-11} sec). The free rotation is consistent for a radical with a planar radical site and possessing a sixfold axis of internal rotation. The situation is, therefore, entirely analogous to that of the ethyl radical.^{23,35}

On the other hand, the spectra behavior of both the β -fluoroethyl and β,β -difluoroethyl radicals is more complicated. At low temperatures both radicals give rise to an unusual type of selective line broadening in the ESR spectra (*vide infra*). Furthermore, the magnitudes of the coupling

constants for the β protons and the β fluorines are not only strongly temperature dependent (as expected in the presence of hindered rotation about the $C_\alpha-C_\beta$ bond), but they also show an unusually strong dependence on relatively minor changes in the solvent.

B. β -Fluoroethyl Radical. The spectrum of the β -fluoroethyl radical at -59° in Figure 10a consists of a triplet of triplets of doublets assignable to the presence of two α hydrogens (22.16 G), two β hydrogens (27.83 G), and one fluorine (46.17 G). The relative amplitudes of the lines associated with the β protons and the β fluorine become anomalous as the temperature is lowered as shown by the accompanying stick diagram calculated on the basis of binomial relative intensities.

At the low temperature (-109° , Figure 10c), the β -proton triplets on the left side of the spectrum undergo progressive broadening from left to right (*cf.* triplet denoted

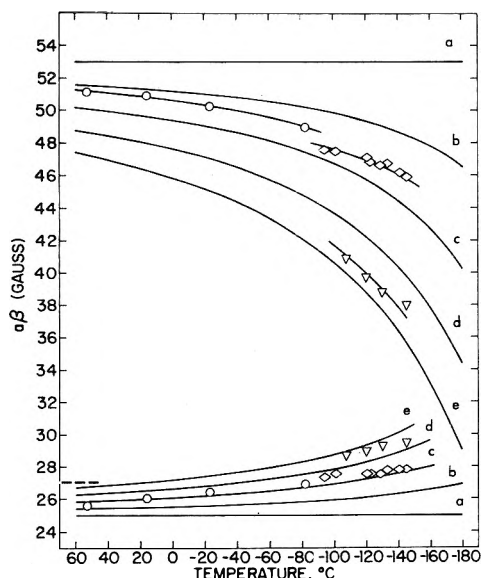


Figure 11. Experimental and calculated temperature dependences of $a_{\beta F}$ (upper part) and $a_{\beta H}$ (lower) for $FCH_2CH_2\cdot$ generated from $BrCH_2CH_2F$ by reaction with (O) $(EtO)_2PO$ in cyclopropane, (\diamond) $Et_3Si\cdot$ in cyclopropane, and (Δ) $Et_3Si\cdot$ in ethane. The calculated curves were obtained from eq 14 using the potential function of eq 29 with $V_4 = 1150 \text{ cal mol}^{-1}$ and $V_2 = 0$ (curves a), 50 (curves b), 100 (curves c), 150 (curves d), and 200 (curves e) cal mol^{-1} . The parameters of eq 23 and 24 were adjusted for optimum fit: $B_F = 106 \text{ G}$, $A_H = 1.2 \text{ G}$ (assumed), and $B_H = 47.6 \text{ G}$.

with asterisks) which is mirrored by an identical right-to-left broadening of the corresponding triplet on the right side of the spectrum. The doublets associated with the fluorine show a similar left-to-right and right-to-left broadening on each side of the spectrum (marked with triangles). The α -proton triplets show normal 1:2:1 relative amplitudes throughout the spectrum (marked with squares). Moreover, the total spread of the spectrum remains temperature invariant.

The line width effect described above depends ostensibly on the signs as well as the magnitudes of the M_I quantum numbers. In contrast, the more usual selective line width effect associated with intramolecular *mutual exchange* processes (in which the initial and final states are identical except for interchanged nuclear spins) gives rise to line widths which are independent of the signs of the M_I quantum numbers. Selective line broadening for mutual exchange is therefore always symmetric with respect to the center of each hyperfine multiplet.

The temperature dependence of the β -proton and -fluorine coupling constants for the β -fluoroethyl radical have opposite signs as shown in Figure 11. It should be noted that the β -proton splitting at the higher temperatures is smaller than that of the ethyl radical denoted in the figure by a dashed line.

We ascribe the temperature variations in the line widths and the hyperfine couplings to hindered internal rotation about the $C_\alpha-C_\beta$ bond in the β -fluoroethyl radical.³⁶ However, rotation of the FCH_2 group in a twofold potential with minima corresponding to two equivalent equilibrium conformations separated by a rotation of 180° is ruled out for the reasons cited above for processes involving mutual exchange. The observation of a selective line width effect which cannot be accounted for by mutual exchange suggests that a rapid interconversion takes place between

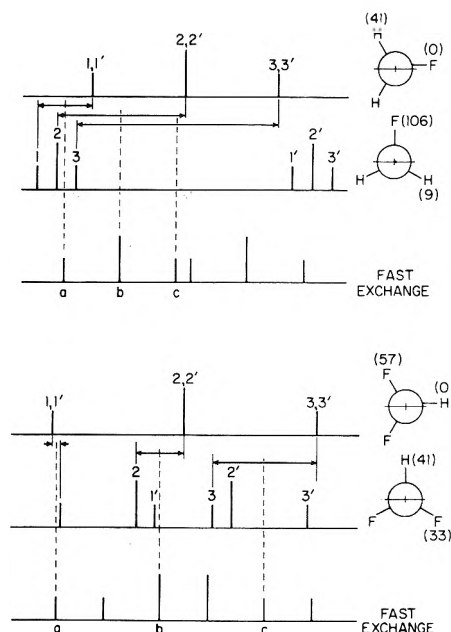
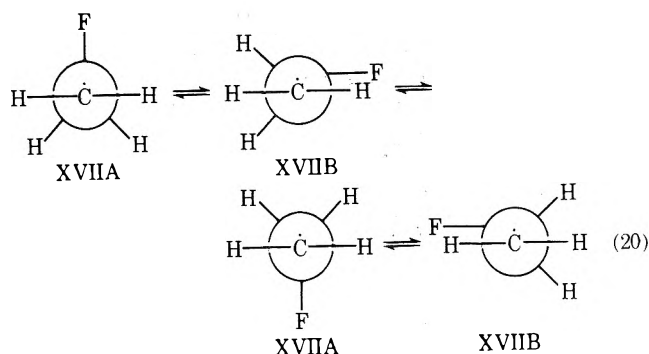


Figure 12. Correlation diagrams explaining the selective line broadening due to rapid interconversions among the stable rotamers of $FCH_2CH_2\cdot$ and $F_2CHCH_2\cdot$. The invariant hyperfine structures due to the α proton (1:2:1 triplets) are not included for clarity. At the slow exchange rates the resultant spectrum is a superposition of the spectra of each rotamer with relative intensities which are proportional to the fractional populations. At the fast exchange rates an averaged spectrum appears, the position of each line being the center of gravity of the correlated pair of lines. At intermediate rates the lines which move over a wider interval of field are broadened more than those moving over a narrower interval. Thus, lines c are broadened more than lines b which in turn are broader than lines a as observed experimentally.

two or more *nonequivalent* equilibrium conformations. If at least one of the stable conformations has a plane of symmetry, the potential energy function can be expanded as a Fourier series of only cosine terms, e.g.

$$V(\theta) = \frac{1}{2} \sum V_n (1 - \cos n\theta)$$

with a plane of symmetry at $\theta = 0$. Since the V_2 term must be relatively small and all V_n with n odd must vanish by virtue of the twofold symmetry of the planar α - CH_2 group, the simplest case would be represented by V_4 as the largest term in the torsional potential. One such representation is given by the stable rotamers XVIIA and XVIIIB which are separated by rotations of $\theta = 90^\circ$ as shown in eq 20.



The dynamic model presented in eq 20 can account for the unusual selective line broadening in the esr spectrum of

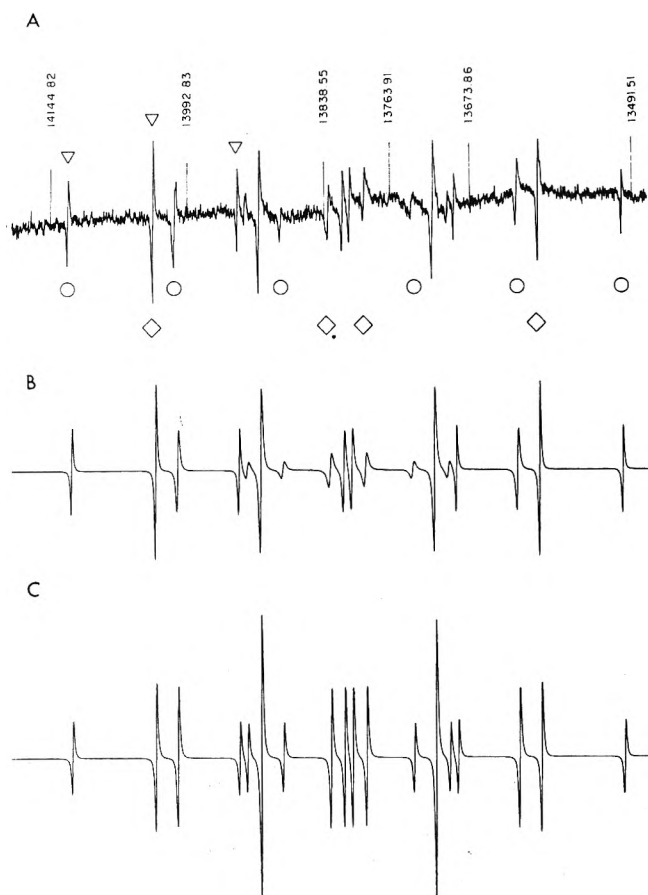


Figure 13. (A) ESR spectrum of $\text{FCH}_2\text{CH}_2\cdot$ at -140° in cyclopropane solution. The α -proton triplets (Δ) show normal 1:2:1 amplitudes while the β -proton triplets (O) and β -fluorine doublets (\diamond) show an asymmetric line width effect. (B) Calculated spectrum by the density matrix method based on nonmutual exchange. See text. (C) Calculated spectrum in the limit of fast exchange showing binomial amplitudes.

the β -fluoroethyl radical and the temperature dependences of the β -proton and -fluorine hyperfine coupling constants.³⁶⁻³⁸ Each of these phenomena will be described separately in the following sections.

1. *Selective Line Broadening in the ESR Spectrum of the β -Fluoroethyl Radical.* In the slow exchange limit, a superposition of the individual spectra of conformations XVIIIA and XVIIB, shown in the correlation diagram of Figure 12, would be observed with relative intensities proportional to the population of each conformer, which is determined by the free energy difference between the two. The barrier heights separating XVIIIA and XVIIB are not sufficiently high for this situation to arise in the β -fluoroethyl radical at experimentally accessible temperatures.

Above the slow exchange limit, the β -proton and -fluorine hyperfine splittings are given by the averages of the limiting splittings for XVIIIA and XVIIB weighted by their populations according to

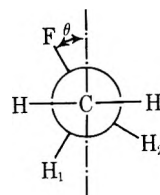
$$a_{\text{H}_B}(T) = 2X_A(T)a_{\text{H}}(A) + 2X_B(T)a_{\text{H}}(B) \quad (21)$$

and

$$a_{\text{F}}(T) = 2X_A(T)a_{\text{F}}(A) + 2X_B(T)a_{\text{F}}(B) \quad (22)$$

where $X_A(T)$ and $X_B(T)$ are the relative populations of XVIIIA and XVIIB, respectively, so that $2X_A(T) + 2X_B(T)$

= 1. The hyperfine coupling constants a_i for a given conformation of the β -fluoroethyl radical can be calculated from



two $\cos^2 \theta$ relationships given in eq 23 and 24, which have been derived by a combination of an INDO calculation and semiempirically.³⁶ In the ESR spectrum, the lines which

$$a_{\text{F}} = 106 \cos^2 \theta \quad (23)$$

$$a_{\text{H}_1} = 1.2 + 45.8 \cos^2 (\theta - 66.5) \quad (24a)$$

$$a_{\text{H}_2} = 1.2 + 45.8 \cos^2 (\theta + 66.5) \quad (24b)$$

move over broader intervals of field will be broadened more than others and will appear with reduced amplitudes. The line correlations in Figure 12 show that this model gives rise to the progressive broadening from left-to-right in each multiplet, mirrored by an equivalent right-to-left broadening on the other end of the spectrum which is indeed that observed experimentally.

The ESR line shapes in the β -fluoroethyl radicals can be calculated using the phenomenological density matrix equation of motion for a system undergoing nonmutual intramolecular exchange, *i.e.*, between several sites with different populations and spin Hamiltonians.³⁶ The low-temperature spectrum at -140° shown in Figure 13a can be readily fitted (Figure 13c) by this method using the V_4 model of eq 20 together with a knowledge of X_A and X_B and the proton and fluorine coupling constants. A good fit is obtained for a rate of conversion of XVIIIA to XVIIB of $5 \times 10^{10} \text{ sec}^{-1}$. The reverse rate is then 3×10^{10} based on the equilibrium constant of 1.6 at -140° (*vide infra*). These rates can be converted to activation energies using the Eyring equation³⁹

$$R(T) = \kappa \frac{kT}{h} \exp(-\Delta G^*/RT) \quad (25)$$

where κ is the transmission coefficient assumed to have the value of 1. An activation energy of $1.0_6 \text{ kcal mol}^{-1}$ is obtained for the conversion of conformation XVIIIA to XVIIB and an energy of $1.1_6 \text{ kcal mol}^{-1}$ for the reverse process.

2. *Temperature Dependence of the β -Proton and -Fluorine Coupling Constants in the β -Fluoroethyl Radical.* The temperature dependence of the magnitudes of the coupling constants shown in Figure 11 can also be readily understood according to the scheme in eq 20, if conformer XVIIB is more stable than XVIIIA. Thus, conformation XVIIB will be preferentially populated at low temperatures and will contribute a large β -proton (39.72 G) splitting and a negligibly small fluorine splitting. As the population of XVIIIA increases at higher temperatures, it will contribute a small β -proton (8.48 G) and a large fluorine (106 B) splitting and cause the experimentally observed overall increase in the fluorine splitting and a concomitant decrease in the β -proton splitting (*cf.* Figure 11).

Thus, the observed β -proton coupling can be considered as an average of the limiting coupling constants for XVIIIA and XVIIB in a predominantly fourfold potential weighted by their relative populations according to eq 21. If we take the coupling constants from the INDO calculation in eq 24,

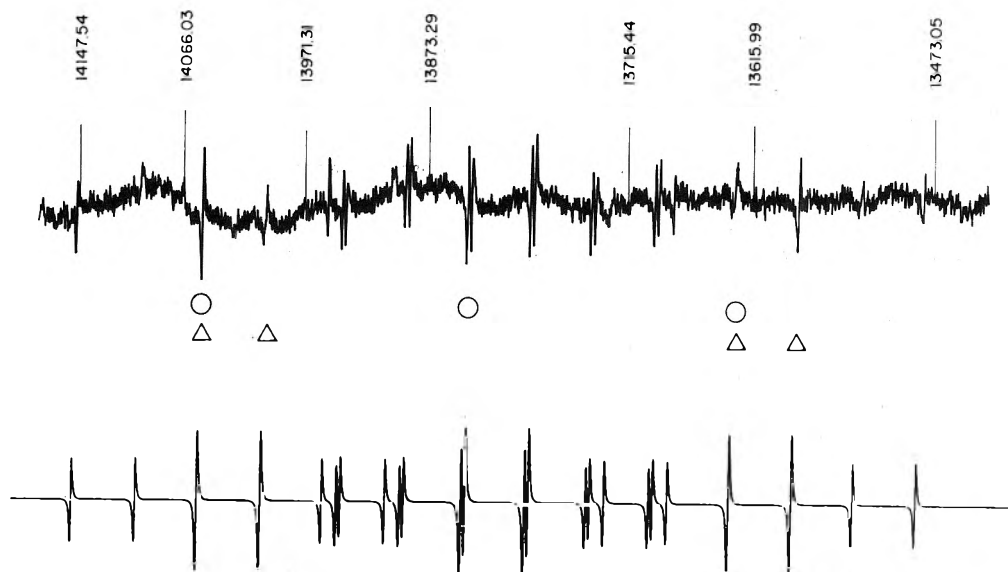


Figure 14. Esr spectrum of $F_2CHCH_2\cdot$ at -107° in cyclopropane solution. The doublets associated with the β protons (e.g., lines marked with Δ) and the triplets associated with the β fluorines (e.g., O) show an asymmetric line width effect as seen by comparison with the calculated spectrum below which includes second-order effects but no form of spin exchange.

the relative population at each temperature is given by eq 26 and 27. By this procedure the equilibrium constant K

$$X_B(T) = (a_{\beta H}(T) - 8.48)/62.48 \quad (26)$$

$$X_A(T) + X_B(T) = 0.5 \quad (27)$$

for the interconversion of XVIIIA and XVIIIB can be calculated at each temperature of the experiment and for each solvent system. The construction of plots of $\ln K$ vs. $1/T$ affords an average enthalpy difference between XVIIIA and XVIIIB of 100 cal mol^{-1} favoring XVIIIB.

The angular dependence of the fluorine coupling constant in eq 23 can also be used to express the observed fluorine couplings as averages of fluorine couplings in XVIIIA and XVIIIB weighted by their population in a manner similar to that carried out for the β -proton splittings. The temperature dependence for the fluorine coupling constant is given by eq 28.³⁶ If the values of $X_B(T)$ determined for

$$a_F(T) = 106[1 - 2X_B(T)] \quad (28)$$

each temperature and each solvent system from the experimental β -proton couplings (eq 26) are used in this equation, all the measured fluorine couplings can be reproduced within a standard deviation of $\pm 5 \text{ G}$.

An alternative approach to the temperature dependence of $a_{\beta H}$ and a_F consists in the application of eq 14 with $a_\beta(\theta)$ given by eq 23 and 24 and with

$$V(\theta) = \frac{V_2}{2}(1 - \cos 2\theta) + \frac{V_4}{2}(1 - \cos 4\theta) \quad (29)$$

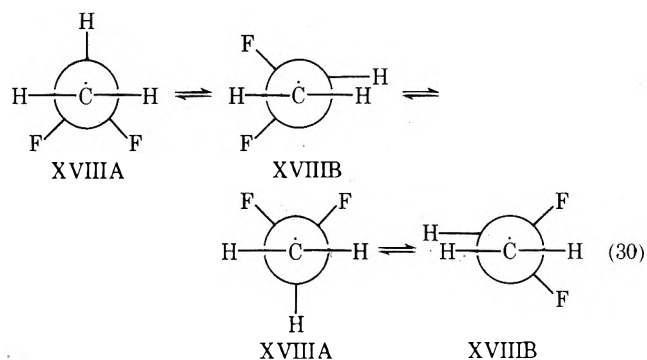
Numerical integration reveals that the value of the integral of eq 14 is independent of V_4 . Thus, the magnitudes of a_β 's are determined solely by the twofold term of the potential function which in turn determines the relative stabilities of the two conformers XVIIIA and XVIIIB supporting the above approach in terms of fractional populations. The calculated curves for $a_{\beta H}(T)$ and $a_{\beta F}(T)$ using eq 14 and 29 are shown in Figure 11 for five values of V_2 . The excellent agreement afforded by both treatments reinforces our confidence in eq 20 as a dynamic model for the β -fluoroethyl radical. It is particularly noteworthy that the singularly

pronounced solvent effects can be quantitatively attributed to slight changes in V_2 and therefore to slight redistributions of the fractional populations of rapidly interconverting conformations XVIIIA and XVIIIB in different media.

C. β,β -Difluoroethyl Radical. The esr spectrum of the β,β -difluoroethyl radical at -107° shown in Figure 14a consists of a large triplet (with resolved second-order splittings) of triplets of doublets attributable to two fluorines (49.51 G), two α protons (23.23 G), and a single β proton (11.81 G). A line width effect which is entirely analogous to that observed in the β -fluoroethyl radical is again apparent by comparison with the calculated spectrum in Figure 14b on the assumption of no form of nuclear spin exchange. The selective line broadening in the esr spectrum of β,β -difluoroethyl radical occurs at higher temperatures than that of the β -fluoroethyl radical.

The β -proton and -fluorine coupling constants in the β,β -difluoroethyl radical are also strongly temperature dependent, but the β -proton splitting increases and the fluorine splitting decreases as the temperature is raised, in trends which are exactly opposite to those of the β -fluoroethyl radical shown in Figure 11.

A dominant fourfold potential involving the stable conformations XVIIIA and XVIIIB in eq 30 is again employed



to account for the temperature dependences of the hyperfine splittings and the selective line broadening in the spectrum.³⁶ The average enthalpy difference between conformations

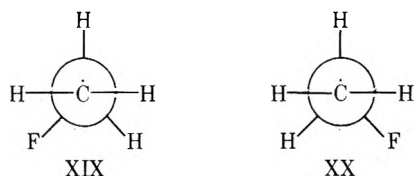
mations XVIII A and XVIII B is calculated from the temperature dependence of the equilibrium constant to be 250 cal mol⁻¹ favoring XVIII B; and the equilibrium constant at -107° is 2.5. The first-order rate constant for interconversion of XVIII A and XVIII B can be obtained by line shape analysis and its temperature dependence affords an activation energy of 1.4₀ kcal mol⁻¹ for the conversion of XVIII A to XVIII B and 1.7₀ kcal mol⁻¹ for the reverse process.

D. Angular Dependences of β -Hyperfine Splittings in β -Fluorine Substituted Ethyl Radicals. In the β -fluoroethyl and β,β -difluoroethyl radicals, the fittings of the temperature dependences of (a) the β -proton and -fluorine coupling constants and of (b) the line shapes in the esr spectra depend on our choice of a dynamic model for the radicals involving hindered internal rotation in a fourfold potential with the angular dependences for the β splittings following a $\cos^2 \theta$ relationship. The general form for these dependences given by eq 31 and 32 are confirmed by INDO

$$a_{\beta H} = A_H + B_H \cos^2(\theta + \theta_0) \quad (31)$$

$$a_{\beta F} = A_F + B_F \cos^2(\theta + \theta_0') \quad (32)$$

calculations.³⁶ For protons, the values of A , B , and θ_0 obtained by fitting eq 31 to the INDO calculations (Table V) are consistent with the experimental data and have been used unchanged in our treatment. For fluorines, the INDO values of B_F for CH₂CH₂F, CH₂CHF₂, and CH₂CF₃ are systematically too large²² while those for A_F are negligibly small. We have chosen to disregard the A_F terms and to treat the B_F terms as adjustable parameters to be fitted by the experimental data. The best values for the B_F 's are given in Table V. The values of θ_0 which differ from $\pm 60^\circ$ are a result of the asymmetry in XIX and XX.



It is interesting to note that the values of B_F and B_H listed in Table V, and therefore the isotropic averages (high-temperature limits) for the β interactions, are not constant but vary with the extent of β -fluorine substitution. Thus, B_H decreases proportionally with the number of β fluorines in going from ethyl ($B_H = 51$ G), to fluoroethyl ($B_H = 46$ G), to difluoroethyl radicals ($B_H = 41$ G), and B_F also decreases from fluoroethyl ($B_F = 106$ G), to difluoroethyl ($B_H = 92$ G), to trifluoroethyl ($B_F = 59$ G) radicals. The bearing of this trend on the hyperfine interactions of β fluorines in these radicals will be discussed separately.³⁶

III. γ -Fluorine Hyperfine Splittings. Long-range hyperfine splittings due to fluorine have been observed in perfluoropropyl and perfluoroheptyl radicals. The three equivalent γ -fluorines in the perfluoropropyl radical have a coupling of $a_F = 3.61$ G (quartet). The pronounced broadening of these inner two lines of this quartet below -100° indicates hindered rotation of the β -CF₃ group. Insufficient resolution does not allow an unequivocal interpretation of the long-range interactions in the perfluoroheptyl radical. An apparent quintet of about 1.5-G splitting may be due to two γ and two δ fluorines with similar hyperfine coupling constants. The presence of appreciable δ -fluorine splittings in fluoroalkyl radicals should be contrasted with vanishing-

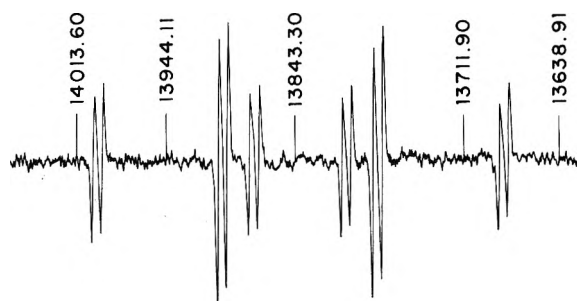
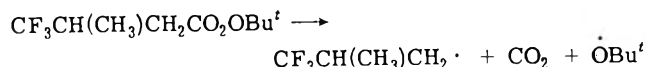


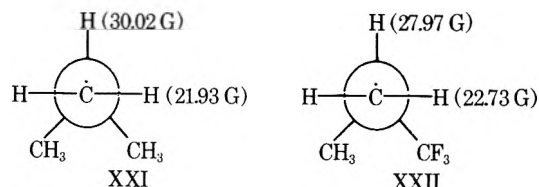
Figure 15. Esr spectrum of CF₃CH(CH₃)CH₂· produced during the photolysis of *tert*-butyl peroxy- γ,γ,γ -trifluoroisovalerate in cyclopropane solution at -120°. At this temperature only one of the three fluorines displays hyperfine interaction (small doublets).

ly small δ -proton couplings in unbranched aliphatic alkyl radicals.

The esr spectrum of the γ,γ,γ -trifluoroisobutyl radical obtained at -120° from the photolysis of the perester con-



sists of a triplet (22.82 G) of doublets (28.56 G) of doublets (1.68 G) as shown in Figure 15. As the temperature is raised, the triplet splitting due to the α protons remains invariant, but the large doublet decreases (27.97 G at -90° and 27.03 G at -60°). More significantly, the small doublets gradually changes until it develops into a quartet with a splitting of 0.8 G at -60°. The detailed observation of these spectral changes was unfortunately limited by the poor signal-to-noise ratio in the spectra at the higher temperatures. Both the magnitude and the temperature dependence of the β -proton hyperfine splitting in CF₃CH(CH₃)CH₂ are similar to those of the analogous isobutyl radical. Since the latter exists preferentially in the stable conformation XXI,⁷ we judge that CF₃CH(CH₃)CH₂ also exists in a similar conformation XXII. Since the isobu-

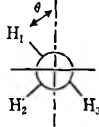
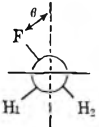
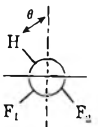
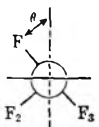


tyl radical did not give rise to resolvable proton hyperfine structure, we attribute the long-range splitting (doublet at -90° which changes to a quartet at -60°) to the fluorines of the CF₃ group whose rotation is strongly hindered. Examination of molecular models indicates considerable crowding of the CF₃ group, which may be sufficient to hinder its internal rotation and to place only one γ fluorine (1.68 G) in a favorable position relative to the radical center at the lowest temperatures studied.

Experimental Section

Materials. Di-*tert*-butyl peroxide was obtained from Shell Chemical Co., washed with water, dried, passed through an alumina column, and redistilled at reduced pressure prior to use. Triethylsilane was obtained from Columbia Chemicals Co., refluxed over molecular sieve, and redistilled prior to use. Bis(trifluoromethyl) peroxide was obtained from PCR, Inc. 1,1,1-Trifluoro-2-bromoethane (obtained from Pierce Chemical Co.) was washed with

TABLE V: INDO β -Proton and Empirical Fluorine Hyperfine Coupling Constants (Gauss) for the Ethyl and the β -Fluoroethyl Radicals Fitted to $A + B \cos^2 \theta$

			
$\cdot\text{CH}_2\text{CH}_3$	$\cdot\text{CH}_2\text{CH}_2\text{F}$	$\cdot\text{CH}_2\text{CHF}_2$	$\cdot\text{CH}_2\text{CF}_3$
$a_{H_1} = 2.2 + 50.9 \cos^2 \theta$	$a_F = (106^b) \cos^2 \theta$	$a_H = 0.25 + 40.7 \cos^2 \theta$	$a_{F_1} = (59.4^b) \cos^2 \theta$
$a_{H_2} = 2.2 + 50.9 \cos^2 (\theta - 60)$	$a_{H_1} = 1.2 + 45.8 \cos^2 (\theta - 66.5)$	$a_{F_1} = (92^b) \cos^2 (\theta - 52.5)$	$a_{F_2} = (59.4^b) \cos^2 (\theta - 60)$
$a_{H_3} = 2.2 + 50.9 \cos^2 (\theta + 60)$	$a_{H_2} = 1.2 + 45.8 \cos^2 (\theta + 66.5)$	$a_{F_2} = (92^b) \cos^2 (\theta + 52.5)$	$a_{F_3} = (59.4^b) \cos^2 (\theta + 60)$
$\langle a_{\beta H} \rangle = 27.7 (26.8^b)$	$\langle a_{\beta H} \rangle = 24.1$	$\langle a_{\beta H} \rangle = 20.6$	
	$\langle a_F \rangle = (53^b)$	$\langle a_F \rangle = (46^b)$	$\langle a_F \rangle = (29.7^b)$
$\langle a_{\alpha H} \rangle = -21.4 (22.4^b)$	$\langle a_{\alpha H} \rangle = -21.4 (22.2^b)$	$\langle a_{\alpha H} \rangle = -21.4 (23.2^b)$	$\langle a_{\alpha H} \rangle = -21.5 (23.7^b)$

^a The brackets () represent the isotropic average (i.e., $A + B/2$ for β hfs). ^b Experimental values.

water, dried, and redistilled prior to use. Perfluoropropyl and perfluoroheptyl bromides were from PCR, Inc., and used as received. 1,1-Difluoroethane (Genetron 152A) and 1,1-difluoro-1-chloroethane (Genetron 142B) were obtained from Pierce Chemical Co.

tert-Butyl hexafluoroisobutyl perester was prepared via the acid chloride⁴⁰ [nmr δ 1.31 (s), 403 (septet)]. *tert*-Butyl β,β,β -trifluoro- α -fluoropropionyl perester was prepared via the anhydride [nmr δ 1.31 (s), 4.17 (d \times q)]. *tert*-Butyl perfluoropropionyl perester was also prepared via the acid chloride [nmr δ 1.31 (s)].

Ethyl methanesulfonylacetate was prepared by the method of Crossland and Servis:⁴¹ yield 95% [nmr δ 1.32 (t), 1.58 (d), 3.07 (s), 4.25 (q), 5.04 (q)]. The lactate (20 g) and 12 g of anhydrous potassium fluoride in 65 ml of hexamethylphosphoric triamide were heated and stirred at 100° over a period of 24 hr. The reaction mixture was cooled, diluted with cold water, and extracted with anhydrous ether. The extracts were washed with water, dried over anhydrous magnesium sulfate, and distilled: bp 51° (93 mm), yield 50% [nmr δ 1.30 (t), 1.50 (d \times d), 4.20 (q), 4.87 (d \times q)]. Ethyl α -fluoropropionate (15 g) and 100 ml of 10% potassium hydroxide aqueous solution were stirred at room temperature over a period of 3 hr. The reaction mixture was extracted with ether, dried, and distilled: bp 84–85° (54 mm), yield 70% [nmr δ 1.62 (d \times d), 5.06 (d \times q)]. *tert*-Butyl α -fluoropropionyl perester was prepared via the acid chloride [nmr (δ 1.31 (s), 1.63 (d \times d), 5.14 (d \times q))].

2-Fluoropropane was prepared by the method of Edgell and Parts⁴² via the mesylate [nmr δ 1.32 (d \times d), 4.86 (d \times septet)].

2-Fluoroethanol and 2,2-difluoroethanol were obtained from Columbia Organic Chemicals Co. and were converted to the corresponding ethyl bromides by the method developed by Hoffman.⁴³ *tert*-Butyl β -fluoropropionyl perester was prepared from the acid chloride.

Esr Measurements. The modified Varian X-band spectrometer, microwave frequency measurements, light source, and sample tubes are as described previously.^{31a,33}

To minimize the error in the g value determinations, all measurements were made on spectra recorded on the same day for increasing magnetic field. Perylene cation radical $g = 2.002583$ ⁴⁴ was used as standard in the configuration employed. The accuracy of the measurements is estimated as ± 0.00003 . Hyperfine splittings were corrected for second-order shifts and confirmed by computer simulation.

For photolytic reduction of alkyl halides, equal volumes

of di-*tert*-butyl peroxide and triethylsilane were diluted with sufficient cyclopropane (and ethane) to give a final ratio of approximately 1:1:1:4 (v/v).

For the photolysis of acyl peresters, a small amount of the peroxide (ca. 100 mg) was dissolved in a relatively large volume (15:1) of cyclopropane or cyclopropane-ethane mixtures.

For the photolytic abstraction of hydrogen atom from the fluorohydrocarbons, a solution with a half a volume of di-*tert*-butyl peroxide or bis(trifluoromethyl) peroxide was diluted with cyclopropane or Freon-12 (CF₂Cl₂) to give a final ratio of approximately (1:0.5:4). For the generation of 1,1-difluoroethyl radical from 1,1-difluoroethane, bis(trifluoromethyl) peroxide was used, since di-*tert*-butyl peroxide under the same conditions did not afford sufficiently high concentrations of radicals for esr measurements. For the generation of 2-fluoropropyl radical from the photolytic abstraction of hydrogen from 2-fluoropropane, spectra of radicals with good signal-to-noise ratios could only be observed at temperatures higher than -80° .

Acknowledgment. K. S. C. wishes to thank the National Science Foundation for financial support. P. J. K. and P. M. are grateful to Mr. B. Gordon for experimental assistance. We also thank Dr. W. J. Middleton for a sample of 1-bromo-2-fluoroethane.

References and Notes

- (1) (a) E. I. du Pont de Nemours and Company. (b) Department of Chemistry, Indiana University. (c) Contribution No. 2390 from the Department of Chemistry, Indiana University. (d) Contribution No. 2132 from E. I. du Pont de Nemours and Co.
- (2) H. Fischer, "Free Radicals," J. K. Kochi, Ed., Vol. II, Wiley, New York, N. Y., 1973, Chapter 19.
- (3) W. A. Sheppard and C. M. Sharts, "Organic Fluorine Compounds," W. A. Benjamin, New York, N. Y., 1969.
- (4) A. P. Stefani, *Fluorine Chem. Rev.*, **5**, 115 (1971).
- (5) (a) M. Iwasaki, *Fluorine Chem. Rev.*, **5**, 1 (1971); (b) A. Hudson and K. D. J. Root, *Advan. Magn. Resonance*, **5**, 1 (1971).
- (6) P. D. Sullivan and J. R. Bolton, *Advan. Magn. Resonance*, **4**, 39 (1970); A. Hudson and G. R. Luckhurst, *Chem. Rev.*, **69**, 191 (1969).
- (7) J. K. Kochi and P. J. Krusic, *Chem. Soc., Spec. Publ.*, **24**, 147 (1969).
- (8) R. A. Sheldon and J. K. Kochi, *J. Amer. Chem. Soc.*, **92**, 4395, 5175 (1970).
- (9) P. Meakin and P. J. Krusic, *J. Amer. Chem. Soc.*, **95**, 8185 (1973).
- (10) J. K. Kochi and P. J. Krusic, *J. Amer. Chem. Soc.*, **91**, 3940 (1969).
- (11) (a) A. Hudson and R. A. Jackson, *J. Chem. Soc., Chem. Commun.*, 1327 (1969); (b) A. G. Davies, D. Griller, and B. P. Roberts, *J. Amer. Chem. Soc.*, **94**, 1782 (1972).
- (12) R. V. Lloyd and M. T. Rogers, *J. Amer. Chem. Soc.*, **95**, 1512 (1973).
- (13) (a) J. H. Freed and G. K. Fraenkel, *J. Chem. Phys.*, **39**, 326 (1963); (b) A. D. McLachlan, *Proc. Roy. Soc., Ser. A.*, **280**, 271 (1964); (c) J. Cooper, A. Hudson, R. A. Jackson, and M. Townson, *Mol. Phys.*, **23**, 1155 (1972).

- (14) R. W. Fessenden and R. H. Schuler, *J. Chem. Phys.*, **43**, 2704 (1965).
 (15) (a) K. Morokuma, L. Pederson, and M. Karplus, *J. Chem. Phys.*, **48**, 4801 (1968); (b) D. L. Beveridge, P. A. Dobosh, and J. A. Pople, *ibid.*, **48**, 4802 (1968); (c) H. Konishi and K. Morokuma, *J. Amer. Chem. Soc.*, **94**, 5603 (1972); (d) See also L. Pauling, *J. Chem. Phys.*, **51**, 2767 (1969).
 (16) J. K. Kochi, P. Bakuzis, and P. J. Krusic, *J. Amer. Chem. Soc.*, **95**, 1516 (1973), and references cited therein.
 (17) (a) H. Fischer and H. Hefter, *Z. Naturforsch. A*, **23**, 1763 (1968); (b) I. A. Zlochower, W. R. Miller, and G. K. Fraenkel, *J. Chem. Phys.*, **42**, 3339 (1965).
 (18) M. T. Rogers and L. D. Kispert, *J. Chem. Phys.*, **46**, 3193 (1967).
 (19) N. Bloembergen, E. M. Purcell, and R. V. Pound, *Phys. Rev.*, **73**, 679 (1948).
 (20) P. J. Krusic, P. Meakin, and B. Smart, to be submitted for publication.
 (21) K. S. Chen and J. K. Kochi, *J. Amer. Chem. Soc.*, **96**, 794 (1974).
 (22) The β -fluorine splittings are less reliably calculated by INDO (*vide infra*).
 (23) (a) R. W. Fessenden and R. H. Schuler, *J. Chem. Phys.*, **39**, 2147 (1963); (b) For a review, see J. E. Wertz and J. R. Bolton, "Electron Spin Resonance," McGraw-Hill, New York, N. Y., 1972.
 (24) (a) A. J. Dobbs, B. C. Gilbert, and R. O. C. Norman, *J. Chem. Soc. A*, 124 (1971); (b) P. J. Krusic, T. A. Rettig, and P. v. R. Schleyer, *J. Amer. Chem. Soc.*, **94**, 995 (1972).
 (25) R. Livingston and H. Zeldes, *J. Chem. Phys.*, **44**, 1245 (1966).
 (26) A. Hudson and K. D. J. Root, *Tetrahedron*, **25**, 5311 (1969).
 (27) P. J. Krusic, unpublished results.
 (28) INDO calculations as a function of the configuration at the α carbon for VII and IX predict normal CH_3 proton splittings for the planar structures (~ 25 G). Unpublished results.
 (29) K. S. Chen and J. K. Kochi, unpublished results.
 (30) K. S. Chen and N. Hirota, "Investigation of Rates and Mechanisms," G. Hammes, Ed., Wiley, New York, N. Y., 1973, Chapter 13, Part II.
 (31) (a) P. J. Krusic, P. Meakin, and J. P. Jesson, *J. Phys. Chem.*, **75**, 3438 (1971); (b) P. Meakin, E. L. Muetterties, F. N. Tebbe, and J. P. Jesson, *J. Amer. Chem. Soc.*, **93**, 4701 (1971).
 (32) (a) D. E. Wood, L. F. Williams, R. F. Sprecher, and W. A. Lathan, *J. Amer. Chem. Soc.*, **94**, 6241 (1972); (b) D. E. Wood, private communication.
 (33) D. J. Edge and J. K. Kochi, *J. Amer. Chem. Soc.*, **94**, 6485 (1972).
 (34) E. B. Wilson, Jr., *Advan. Chem. Phys.*, **2**, 367 (1959); J. Dale, *Tetrahedron*, **22**, 3373 (1966); G. J. Karabatsos and D. J. Fenoglio, *Top. Stereochem.*, **5**, 167 (1970).
 (35) R. W. Fessenden, *J. Chim. Phys.*, **61**, 1570 (1964).
 (36) P. J. Krusic, K. S. Chen, P. Meakin, and J. K. Kochi, to be submitted for publication.
 (37) A dynamic model based on a dominant sixfold component for the potential function can also account for the spectral behavior of the $\text{CH}_2\text{CH}_2\text{F}$ radical. The resulting barrier height of 1–2 kcal mol $^{-1}$, however, is too large for a sixfold potential function.³⁴
 (38) A recent study of the temperature dependence of $a_{\beta\text{H}}$ and $a_{\beta\text{F}}$ in $\text{CH}_2\text{CH}_2\text{F}$ and CH_2CHF_2 failed to recognize the importance of the four-fold term of the potential function (I. Biddles, J. Cooper, A. Hudson, R. A. Jackson, and J. T. Wiffen, *Mol. Phys.*, **25**, 225 (1973)).
 (39) W. F. K. Wynne-Jones and H. Eyring, *J. Chem. Phys.*, **3**, 492 (1935).
 (40) P. D. Bartlett and R. R. Hiatt, *J. Amer. Chem. Soc.*, **80**, 1398 (1958).
 (41) R. K. Crossland and K. L. Servis, *J. Org. Chem.*, **35**, 3195 (1970).
 (42) W. F. Edgell and L. Parts, *J. Amer. Chem. Soc.*, **77**, 4899 (1955).
 (43) F. W. Hoffman, *J. Org. Chem.*, **15**, 425 (1950).
 (44) B. G. Segal, M. Kaplan, and G. K. Fraenkel, *J. Chem. Phys.*, **43**, 4191 (1965).

Electron Spin Resonance Studies of Fluoroalkyl Radicals in Solution. II. Adducts to Fluoroolefins

Kuang S. Chen, Paul J. Krusic,^{*1a} and Jay K. Kochi^{*1b}

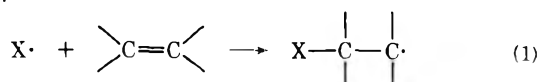
Department of Chemistry,^{1c} Indiana University, Bloomington, Indiana 47401 and The Central Research Laboratory,^{1d} E. I. du Pont de Nemours and Company, Wilmington, Delaware 19898 (Received January 2, 1974; Revised Manuscript Received April 23, 1974)

Publication costs assisted by E. I. du Pont de Nemours and Company

The addition of chlorine, oxygen, sulfur, and silicon-centered radicals to fluoroolefins such as vinyl fluoride, vinylidene fluoride, and tetrafluoroethylene is examined. The structure and conformations of fluoroalkyl adducts with β -heteroatom substituents are deduced from the magnitude of the nuclear hyperfine splittings and their temperature dependences as well as the selective line broadening in the esr spectra. These adducts exist in symmetric conformations XIIIa and b, in which the β heteroatom is located in the plane described by the principal axis of the half-filled orbital and the $\text{C}_\alpha\text{--C}_\beta$ bond. There are ambiguities associated with the assignment of conformations in radicals with pyramidal centers especially those with β -heteroatom substituents such as sulfur and chlorine which are distorted at the β carbon. Qualitative arguments are put forth which favor the conformation XIIIa in which the β heteroatom eclipses the half-filled orbital and presents the possibility of bridging such as that observed in the alkyl analogs.

Introduction

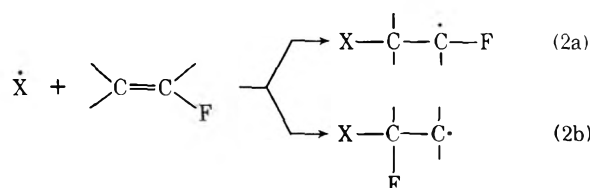
Free-radical addition to unsaturated molecules, such as alkenes and alkynes, constitutes an important route to the formation of C–C bonds in synthesis and polymerization or telomerization processes.^{2a} In particular, the formation of carbon–heteroatom bonds results by addition of heteroatom-centered free radicals $\dot{\text{X}}$ to carbon–carbon multiple bonds, e.g.



The formation of these radical adducts is tantamount to

substitution of heteroatoms in the β position of alkyl radicals and has important stereochemical consequences, as studies of bridged free radicals have shown.^{2b,c}

Additions to fluoroolefins raise additional questions regarding the orientations in free-radical additions.³



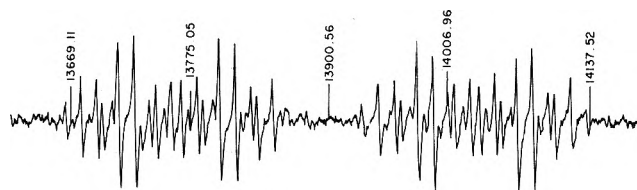


Figure 1. ESR spectrum of the adduct radical $\text{CF}_3\text{OCH}_2\dot{\text{C}}\text{HF}$ resulting from the reaction of trifluoromethoxy radical with vinyl fluoride. Proton nmr field markers are in kHz.

TABLE I: ESR Parameters of Oxy Radical Adducts to Fluoroolefins in Solution^a

Radical	T, °C	Hyperfine splitting, G			
		$a_{\alpha\text{H}}$	$a_{\alpha\text{F}}$	$a_{\beta\text{H}}$	$a_{\delta\text{F}}$
$\text{CF}_3\text{O}-\text{CH}_2\dot{\text{C}}\text{H}_2^b$	-72	22.71		28.13	2.01
	-129	22.72		29.39	1.86
$\text{CF}_3\text{O}-\text{CH}_2\dot{\text{C}}\text{HF}$	-70	21.42	63.47	8.10	3.37
	-114	21.42	62.27	7.73	3.36
$\text{CF}_2\text{O}-\text{CH}_2\dot{\text{C}}\text{F}_2$	-73		90.61	12.10	0.91
$\text{CF}_3\text{O}-\text{CH}_2\dot{\text{C}}\text{HCl}$	-128	21.65	3.47 ^c	9.70	2.99
$\text{HO}-\text{CH}_2\dot{\text{C}}\text{HF}^d$		19.1	57.6	11.2	
$\text{HO}-\text{CH}_2\dot{\text{C}}\text{HCl}^d$		17.7	3.0 ^e	14.4	
$\text{CH}_3\dot{\text{C}}\text{H}_2^e$	-113	22.37		26.99	
$\text{CH}_3\dot{\text{C}}\text{HF}^e$	-106	17.31	59.21	24.48	
$\text{CH}_3\dot{\text{C}}\text{F}_2^e$	-78		94.01	13.99	

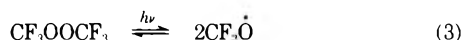
^a In olefin as solvent. ^b See also ref 6. ^c αC splitting. ^d In aqueous solutions at ambient temperatures, W. E. Griffiths, G. F. Longster, J. Myatt and P. F. Todd, *J. Chem. Soc. B*, 530 (1967). ^e From ref 4.

With the background developed in the foregoing study of the structure and conformation of fluoroalkyl radicals,⁴ we examined in this study the esr spectra of various transient fluoroalkyl radicals derived from the addition of heteroatom-centered free radicals to fluoroolefins, especially vinyl fluoride and vinylidene fluoride.

Since there are numerous product studies of a variety of adducts,³ we are mainly concerned with the information which esr can provide about the structural and conformational properties of the adduct radicals. Four classes of heteroatom-centered radicals involving oxygen, chlorine, sulfur, and silicon are examined by the photochemical technique described in the previous paper.⁴⁻⁶

Results

Oxygen-Centered Radical Adducts to Fluoroolefins. The uv photolysis of bis(trifluoromethyl) peroxide generates trifluoromethoxy radicals. In the absence of substrates the trifluoromethoxy radicals recombine in solution, and no esr spectrum is obtained.⁷



However, in the presence of fluoroolefins, intense and well-resolved esr spectra of adducts are observed. For example, the spectrum in Figure 1 obtained from vinyl fluoride at -70° consists of a doublet (21.42 G) of doublets (63.47 G) split further into a triplet (8.10 G) of quartets (3.37 G). The spectrum is readily assignable to hyperfine couplings to the single α -proton, α -fluorine, the pair of β -protons, and the three equivalent δ -fluorine nuclei, respectively, in the adduct I.

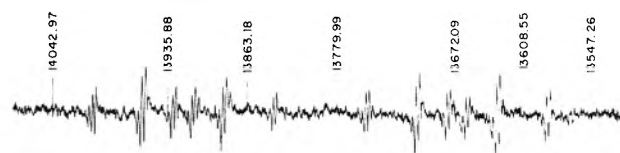


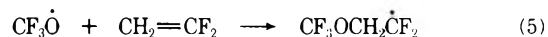
Figure 2. ESR spectrum of the adduct radical $\text{CH}_3\text{SCH}_2\dot{\text{C}}\text{HF}$ resulting from the reaction of methylthiyl radical with vinyl fluoride at -65° .

TABLE II: ESR Parameters of Thiyl Adducts to Fluoroolefins in Solution^a

Radical	T, °C	Hyperfine splitting, G			
		$a_{\alpha\text{H}}$	$a_{\alpha\text{F}}$	$a_{\beta\text{H}}$	$a_{\delta\text{F}}$
$\text{CH}_3\text{S}-\text{CH}_2\dot{\text{C}}\text{H}_2$	-70	21.60		14.89	NR
$\text{CH}_3\text{S}-\text{CH}_2\dot{\text{C}}\text{HF}$	-72	17.41	59.06	10.8	0.69 ^b
$\text{CH}_3\text{CH}_2\text{S}-\text{CH}_2\dot{\text{C}}\text{HF}$	-75	17.49	58.95	11.04	0.9 ^c
$\text{CH}_3\text{S}-\text{CH}_2\dot{\text{C}}\text{F}_2$	-50		88.4	4.3	1.0 ^b
$\text{CH}_3\text{S}-\text{CH}_2\dot{\text{C}}\text{HCH}_3^e$	-81	21.36	24.13 ^d	12.94	
$\text{CH}_3\text{S}-\text{CH}_2\dot{\text{C}}(\text{CH}_3)_2^e$	-84		22.37 ^d	11.20	

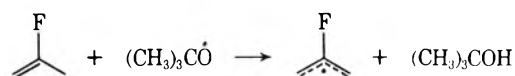
^a Either cyclopropane or olefin as solvent. ^b CH_2 quartet. ^c δ - CH_2 triplet. ^d α - CH_3 splitting. ^e From ref 6. NR = not resolved (<0.2 G).

A well-resolved spectrum is also obtained when a solution of bis(trifluoromethyl) peroxide in vinylidene fluoride is irradiated. The esr parameters for the adducts are collected

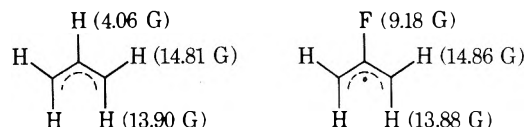


in Table I, together with the chloro and hydrocarbon analogs also listed for comparison.

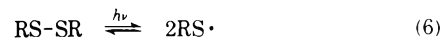
The reactions of trifluoromethoxy radical with 1,1,1-trifluoropropene and 2-fluoropropene were also examined, but the adducts were formed in insufficient concentrations for esr examination. Interestingly, no allylic radicals could be observed from 2-fluoropropene, although the same reaction with *tert*-butoxy radicals (photochemically generated from di-*tert*-butyl peroxide) afforded the well-resolved spectrum of 2-fluoroallyl radical.



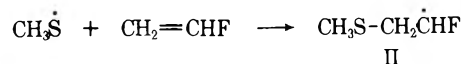
The proton hyperfine splittings in allyl⁸ and 2-fluoroallyl radicals are comparable.



Sulfur Radical Adducts to Fluoroolefins. Thiyl radicals are generated from the uv irradiation of dialkyl disulfides.⁶



The esr spectrum of the methylthiyl adduct (R = CH_3) to vinyl fluoride is shown in Figure 2. As expected, the hyperfine splitting pattern of the thiyl adduct II is the same as



the trifluoromethoxy adduct I, and the values of the splitting constants are listed in Table II, together with those of the vinylidene fluoride adduct and related species.

The presence of a resolvable splitting (0.7–1.0 G) of the methylmercapto group in the adducts to vinyl fluoride and vinylidene fluoride is remarkable in view of the absence of resolvable CH_3 splitting in the ethylene adduct,

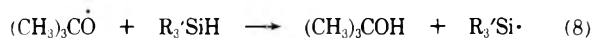
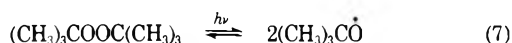


Figure 3. ESR spectrum of the adduct radical $\text{Et}_3\text{SiCH}_2\dot{\text{C}}\text{HF}$ resulting from the reaction of triethylsilyl radical with vinyl fluoride at -45° .

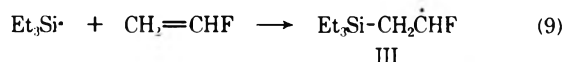
$\text{CH}_3\text{SCH}_2\dot{\text{C}}\text{H}_2$.⁶ Furthermore, the splitting of 4.3 G in the vinylidene fluoride adduct, $\text{CH}_3\text{SCH}_2\dot{\text{C}}\text{F}_2$, is unusually small for a β -proton splitting.⁵

The addition of methylthiyl radical to tetrafluoroethylene and 1,1,1-trifluoropropene was also examined, but the adducts were formed in insufficient concentrations to examine their ESR spectra.

Silicon Radical Adducts to Fluoroolefins. Trialkylsilyl radicals are generated in solution by hydrogen abstraction from trialkylsilanes with photochemically generated *tert*-butoxy radicals.⁹

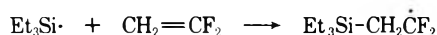


The ESR spectra of adducts are observed when the photolysis is carried out in the presence of fluoroolefins. The spectrum of the triethylsilyl adduct ($\text{R}' = \text{CH}_3\text{CH}_2$) to vinyl fluoride is shown in Figure 3 and the ESR parameters are

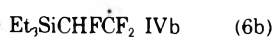
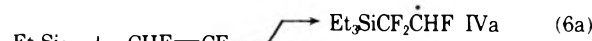


listed in Table III. The line widths are slightly broader in the silyl adducts compared to the oxygen and sulfur analogs, and we were unable to resolve the δ -proton splittings in the methylene groups of the β -triethylsilyl substituent.

Triethylsilyl radicals add to the methylene carbon of vinylidene fluoride in much the same manner as oxy and thyl radicals.

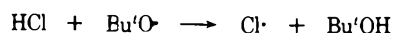


The ESR spectrum obtained from the addition of $\text{Et}_3\text{Si}\cdot$ to trifluoroethylene shown in Figure 4 consists of a single species with a doublet (20.30 G) of doublets (63.39 G) split further into triplets of 52.51 G. The intensities of the $M_I^F = 0$ lines in the spectrum are diminished by the partially resolved second-order splitting and possibly by selective line broadening. Two isomeric adducts IVa and IVb are possible as shown in eq 6. If the adduct were IVb, we would



expect the α -fluorine splitting to be in the range 85–90 G, characteristic of other α,α -difluoroalkyl radicals.⁴ On the other hand, an α -fluorine splitting of 60–65 G and an α -proton splitting of 16–20 G are expected for an α -fluoroalkyl radical as comparisons in Tables I–III indicate.⁴ We suggest, therefore, that the vinylidene fluoride adduct has structure IVa.

Addition of Chlorine Atom to Fluoroolefins. Chlorine atoms can be generated from hydrogen chloride and *tert*-butoxy radicals.¹⁰ In the presence of vinylidene fluoride,



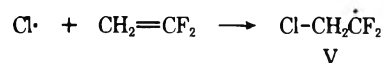
the spectrum shown in Figure 5 is obtained. The hyperfine splitting in the spectrum at -31° (Figure 5b) consists of a triplet (83.59 G) of triplets (2.04 G) of 1:1:1 quartets (8.41

TABLE III: ESR Parameters for Silyl Radical Adducts to Fluoroolefins in Solution

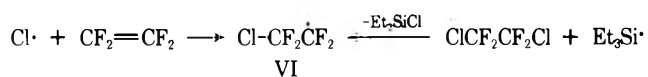
Radical	T, °C	Hyperfine splitting, G			
		$\alpha_{\alpha\text{H}}$	$\alpha_{\alpha\text{F}}$	$\alpha_{\beta\text{H}}$	$\alpha_{\beta\text{F}}$
$\text{Et}_3\text{Si}-\text{CH}_2\dot{\text{C}}\text{H}_2$	-119	21.01		17.67	
$\text{Et}_3\text{Si}-\text{CH}_2\dot{\text{C}}\text{HF}$	-54	15.78	59.74	20.70	
$\text{Et}_3\text{Si}-\text{CH}_2\dot{\text{C}}\text{F}_2$	-70		98.11	10.85	
$\text{Et}_3\text{Si}-\text{CF}_2\dot{\text{C}}\text{HF}$	-48	20.30	63.39		52.51
$\text{Et}_3\text{Si}-\text{CH}_2-\text{C}(\text{F})\cdot$ ^b	-98			9.36	48.72 <3.0 ^c
$\text{Et}_3\text{Si}-\text{CH}_2\dot{\text{C}}\text{HCH}_3$ ^e	-101	21.10	24.26 ^d	16.74	
$\text{Et}_3\text{Si}-\text{CH}_2\dot{\text{C}}(\text{CH}_3)_2$ ^e	-101		22.25 ^d	15.35	

^a In cyclopropane or olefin as solvent. ^b Adduct to methylene-hexafluorocyclobutane. ^c γ -F triplet, within line width. ^d α -CH₃ splitting. ^e From ref 6.

G) as shown by the accompanying "stick" diagram which includes second-order effects. The adduct clearly has the structure V, and the ESR parameters are included in Table IV.



Chlorine atom generated from hydrogen chloride also adds to tetrafluoroethylene to afford adduct VI. The same

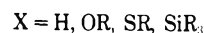
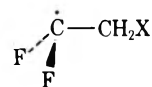


spectrum is obtained when 1,2-dichlorotetrafluoroethane (Freon 114) is treated with triethylsilyl radicals by a procedure described earlier.^{9,10} The outstanding feature in the spectra of both adducts V and VI is the unusually small value of the β -chlorine splitting. The splitting of 2.04 G in the vinylidene fluoride adduct is also exceptionally small for a pair of β protons.

Discussion

The ESR spectrum of only one principal isomeric adduct is observed during the addition of chlorine, oxygen, sulfur, and silicon-centered radicals to vinyl fluoride, vinylidene fluoride, and trifluoroethylene. The anti-Markovnikov orientation in these adducts coincides with the extensive product studies carried out on additions to fluoroolefins.³ Moreover, the low temperatures at which these reactions are carried out allow an examination of the ESR spectrum of the primary adduct with minimal interference from higher telomeric species.

ESR studies provide a unique insight into the structure and conformation of these adduct radicals. Thus, the magnitudes of the α -fluorine splittings in all of the adducts I–III to vinyl fluoride are in the range of 60 G observed for the hydrocarbon analog, $\text{CH}_3\dot{\text{C}}\text{HF}$.¹¹ Similarly, the splittings due to the pair of equivalent α fluorines in the adducts VII to vinylidene fluoride fall in the neighborhood of



90 G found in $\text{CH}_3\dot{\text{C}}\text{F}_2$.¹¹ The pyramidal configurations of the radical centers at C_α in $\text{CH}_3\dot{\text{C}}\text{HF}$ and $\text{CH}_3\dot{\text{C}}\text{F}_2$ were discussed in the foregoing study,⁴ and they also undoubtedly apply to the fluoroolefin adducts, judging from the similar

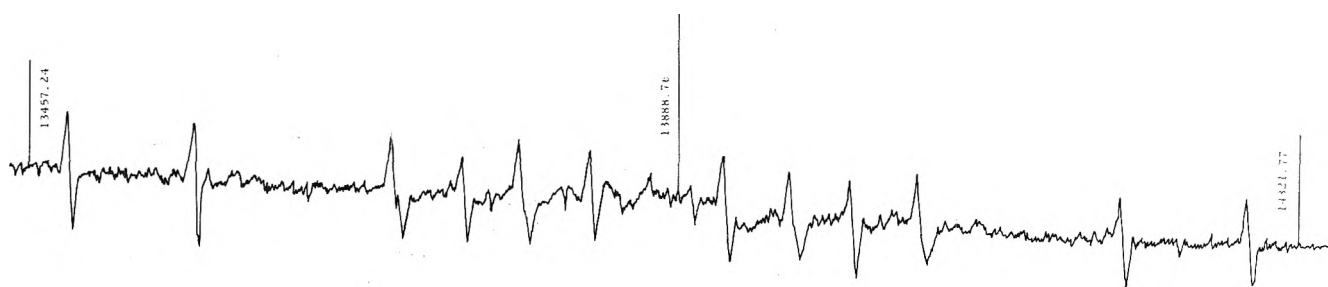


Figure 4. Esr spectrum of the adduct radical IV resulting from the reaction of triethylsilyl radical with trifluoroethylene at -47° .

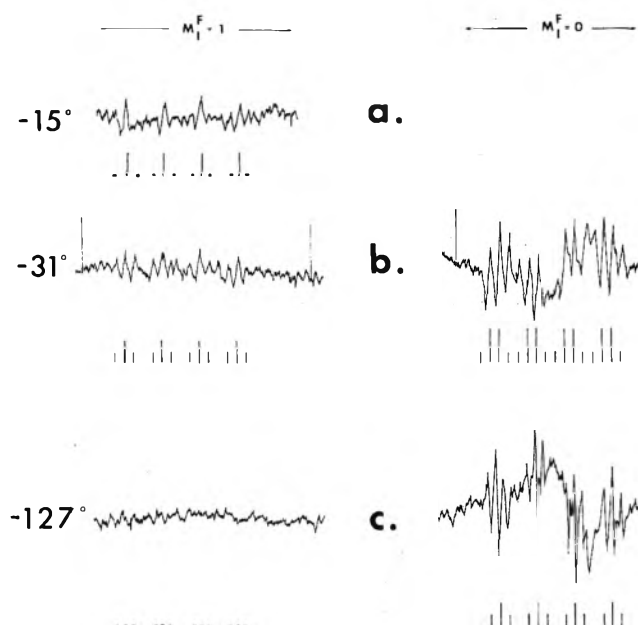


Figure 5. High-field and central multiplets of the esr spectrum of the adduct radical ClCH_2CF_2 resulting from the addition of chlorine atom to vinylidene fluoride: (a) at -15° , (b) at -31° , and (c) at -127° in cyclopropane solutions. Stick diagram below each experimental spectrum based on esr parameters in Table IV showing selective line broadening (horizontal bars) due to (a) in-phase modulation of the β -proton triplet and (c) dipolar broadening due to F anisotropy.

values of $a_{\alpha\text{F}}$ and $a_{\alpha\text{H}}$. Furthermore, all of the spectra of adducts VII like that of CH_3CF_2 show dipolar broadening of the lines due to the modulation of the α -fluorine anisotropic hyperfine tensor by rotational Brownian motion.⁴ The partial spectrum of the triethylsilyl adduct shown in Figure 6 is a relevant example, in which the $M_1^{\text{F}} = \pm 1$ lines (outer multiplet) and the low-field component of the second-order splitting in the $M_1^{\text{F}} = 0$ multiplet are broadened. The same dipolar broadening is also observed in the chlorine adduct V to vinylidene fluoride at -127° as shown in Figure 5c.

Conformations of the Adducts to Fluoroolefins. The addition of heteroatom centers to C_β of vinyl fluoride and vinylidene fluoride affords adducts which can exist in several conformations about the $\text{C}_\alpha\text{-C}_\beta$ bond. In alkyl radicals, the conformation about the $\text{C}_\alpha\text{-C}_\beta$ bond has been deduced from the magnitude of the β -proton splitting and its temperature dependence.⁶ If θ describes the dihedral angle

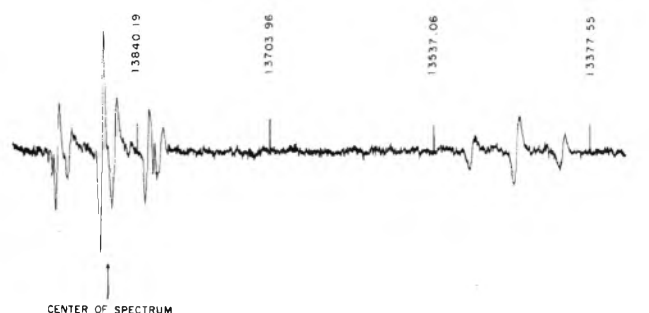
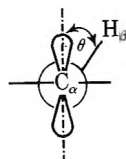


Figure 6. Low-field half of the esr spectrum of the adduct radical $\text{Et}_3\text{SiCH}_2\text{CF}_2$ from the reaction of triethylsilyl radical with vinylidene fluoride at -57° showing the selective line broadening due to the anisotropies of the fluorine hyperfine tensors.

TABLE IV: ESR Parameters for Chlorine Atom Adducts to Fluoroolefins^a

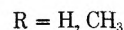
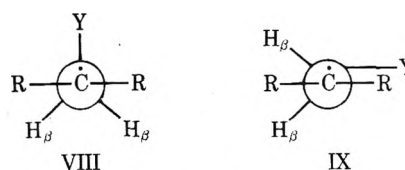
Radical	T, °C	$\langle g \rangle$	Hyperfine splitting, G			
			$a_{\alpha\text{F}}$	$a_{\beta\text{F}}$	$a_{\beta\text{H}}$	a_{Cl}
ClCH_2CF_2	-48	2.00501	83.59		2.04	8.41
ClCF_2CF_2	-97	2.00461	<i>b</i>	1.09		3.93

^a In cyclopropane solutions containing HCl, di-*tert*-butyl peroxide, and fluoroolefin. ^b $M_1^{\text{F}} \pm 1$ lines broadened beyond detection due to dipolar broadening; at higher temperatures tetrafluoroethylene polymerized.

between the β -CH bond and the p orbital at the radical center at C_α , then the instantaneous hyperfine splitting for the β proton is given by

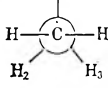
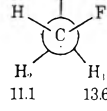
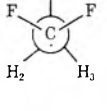
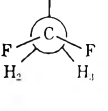
$$a_{\beta\text{H}} = A + B \cos^2 \theta \quad (10)$$

where *A* and *B* are constants. Alkyl radicals with β heteroatoms such as $\text{R}_2\text{C-CH}_2\text{Y}$ ($\text{R} = \text{H}, \text{CH}_3$) exist in essentially two stable conformations VIII and IX which can be described as symmetric and unsymmetric, respectively.^{6,12}



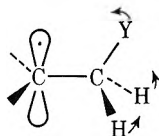
The value of the hyperfine splitting for the pair of β protons in species such as β -methoxyethyl radical ($\text{R} = \text{H}, \text{Y} = \text{OCH}_3$), which exists in conformations IX is typically 25–30 G and shows a *negative* temperature coefficient. On the other hand, $a_{\beta\text{H}}$ for radicals such as β -thiylethyl ($\text{R} = \text{H}, \text{Y} = \text{CH}_3\text{S}$) which exists in a stable conformation VIII is in the range of 15–18 G and has a *positive* temperature dependence. Radicals in conformation VIII place the heteroatom Y directly behind the p orbital at the radical center

TABLE V: Proton Hyperfine Splittings for the Symmetric Conformations of Fluoroethyl Radicals by the INDO Method

X^a	XI^b	$XIIa^b$	$XIIb^b$
$\angle HC\alpha H = 180^\circ$	$\angle HC\alpha F = 119^\circ$	$\angle FC\alpha F = 106^\circ$	
$a_{H_1} = 53.5 \text{ G}$	$(52.3 \text{ G}) H_1$	$(37.2 \text{ G}) H_1$	$(19.3 \text{ G}) H_1$
			
$a_{H_{2,3}} = 14.7 \text{ G}$	12.4	2.9	12.0
$1/3 \sum a_1(\beta H) = 27.6$	25.7	14.3	14.4
Exptl = 26.8	24.5	14.0	14.0

^a From ref 15. ^b From ref 11.

and optimally located to interact with it. The extent to which a "bridging" of Y between C_α and C_β occurs in VIII

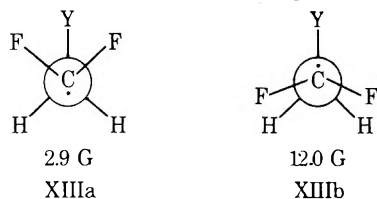


is reflected in values of $a_{\beta H}$ lower than 15 G, and barriers to hindered rotation about the $C_\alpha-C_\beta$ bond in excess of about 1 kcal mol⁻¹.^{12,13} Bridging in this context has been discussed in radicals having β heteroatoms such as Cl, S, Sn, and P.^{6,13,14}

The formulation given above cannot be applied directly to the α -fluorinated analogs, since there are significant differences in the configurations at the radical sites. In order to evaluate the values of $a_{H\beta}$ expected for the conformation VII in these α -fluorinated radicals, we employed the INDO method to calculate each value of $a_{H\beta}$ in the stable conformations XI and XII of $CH_3\dot{C}HF$ and $CH_3\dot{C}F_2$, respectively, after optimizing the parameters to the experimental values.¹¹ The individual β -proton hyperfine splittings are listed in Table V, together with those of the ethyl radical X.¹⁵

The results in Table V show that the hyperfine splittings for H_1 located at $\theta = 0^\circ$ and for $H_{2,3}$ located at $\theta = \pm 120^\circ$ decrease with increasing α -fluorine substitution, and the effect is most pronounced with α,α -difluoro substitution. This decrease in $a_{\beta H}$ with an increasing pyramidal configuration at the radical site reflects a decreased hyperconjugative interaction⁴ between the half-filled hybrid orbital on the α carbon and the β -CH bonds.

A β substitution of a heteroatom Y without distortion into conformations X, XI, and XII, thus, would result in radicals with characteristic values for the β -proton splittings. There are, however, some ambiguities associated with the assignments of conformations in radicals with pyramidal centers. For example, in the adducts to vinylidene fluoride there are two eclipsed conformations XIIIa and XIIIb, in which the β -proton splittings should be 2.9 and



12.0 G, respectively, on the basis of the INDO results shown in Table V.

Indeed, the esr parameters of the adducts to vinylidene

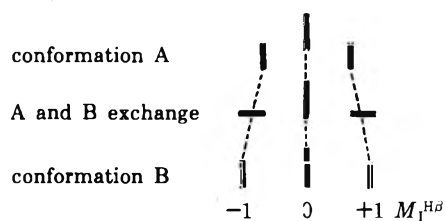
fluoride listed in Tables I–IV fall into two classes. The adducts in which Y is hydrogen, trifluoromethoxy, and triethylsilyl have values of the β -proton splittings of 14.0, 12.1, and 10.9 G, respectively. On the other hand, where Y is methylthiyl or chlorine the value of the β -proton splitting is significantly smaller, being 4.3 and 2.0 G, respectively.

On a simplistic analysis based only on the observed β -proton splittings, it would be attractive to assign the stable conformation of the chloro and sulfur adducts of vinylidene fluoride to conformation XIIIa, and that of the other analogs to XIIIb. However, threefold potential functions governing internal rotation about the C–C bond were deduced for both $CH_3\dot{C}F_2$ ¹¹ (with a barrier height of about 2.2 kcal mol⁻¹) and for $CF_3\dot{C}F_2$ ¹⁶ (with a barrier height of about 2.9 kcal mol⁻¹) with minima corresponding to the staggered conformation (cf. XIIa) and maxima corresponding to the eclipsed configuration (cf. XIIb) in which the α fluorines eclipse two β hydrogens or two β fluorines, respectively. Such eclipsing is, therefore, endoenergetic for approximately tetrahedral geometries at both the α and β carbons. The situation is not unlike that prevailing in ethane and perfluoroethane where similar barriers to internal rotation of the order of 3 kcal mol⁻¹ exist with minima for the *gauche* conformations. It would, therefore, seem that configuration XIIIb without substantial distortion at the β carbon could not arise unless the interaction between the β heteroatom and the half-filled orbital is sufficiently exoenergetic to overcome the unfavorable eclipsing of the α fluorines with the β hydrogens. Furthermore, it should be borne in mind that the calculations of Table V refer to an idealized *rigid* structure. In reality, however, there will be torsional motions the effect of which will be to add a *positive* contribution to the β -proton splitting.^{6,12} This torsional motion may also be coupled with the inversion at the radical site complicating the internal dynamics even further.

Bearing in mind these considerations we favor configuration XIIIa as the most stable conformation for all these adducts of vinylidene fluoride. The larger couplings to the β protons for Y = H, CF_3O , and R_3Si would then be a consequence of torsional motions of larger amplitudes compared to Y = Cl and RS. The latter may well be partially bridged, as was deduced for the CH_2CH_2Cl and CH_2CH_2SR , but the evidence in hand cannot be interpreted as readily because of the complications brought about by the pyramidal nature of the α carbon. It should be noted, however, that the adducts of RS· to vinyl and vinylidene fluorides, in contrast to their nonfluorinated analogs, give rise to resolved hyperfine interaction with the δ protons on the alkylmercapto groups (Table II). These appreciable long-range couplings might result from enhanced partial bridging in the $RSCH_2\dot{C}F_2$ radicals compared to their nonfluorinated analogs.

A previous study¹³ showed that chlorine bridging in a series of β -chloroethyl radicals increased with methyl substituents. The unusually small value of the ³⁵Cl splittings in $ClCH_2\dot{C}F_2$, however, cannot be used directly to evaluate the extent of chlorine bridging in these radicals, since the configurations at C_α are pyramidal, unlike the planar configuration at C_α in the hydrocarbon analogs. The change to a pyramidal configuration at the radical center is sufficient, by itself, to significantly lower the ³⁵Cl hyperfine splitting due to decreased hyperconjugative (and homoconjugative) interaction of the β chlorine,^{14a} as discussed earlier with regard to the β proton (in Table V).

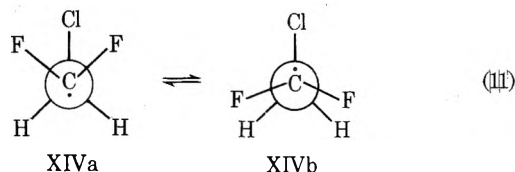
The absence of any temperature-dependent line width effect involving the β methylene triplets in $\text{CF}_3\text{OCH}_2\dot{\text{C}}\text{F}_2$, $\text{R}_3\text{SiCH}_2\dot{\text{C}}\text{F}_2$, and $\text{RSCH}_2\dot{\text{C}}\text{F}_2$ suggests the presence of only one distinct conformer which we believe to be represented by XIIIa rather than XIIIb for the reasons discussed above. Scrutiny of the esr spectra of $\text{ClCH}_2\dot{\text{C}}\text{F}_2$ at higher temperatures, however, reveals a selective broadening affecting the β -proton triplets of a kind expected if a second, distinct conformer with a pair of equivalent β protons became appreciably populated at these temperatures. Thus, in Figure 5a the partial spectrum (with its "stick" diagram) at -15° shows the $M_I^F = +1$ multiplet, in which only the $M_I^H = \pm 1$ lines of the β -proton triplet are broadened. The alternation of line widths in the spectrum at -15° is associated with *in-phase* modulation of the β -proton hyperfine splitting. The modulation diagram below shows that if the two β pro-



(horizontal bar represents broadened lines)

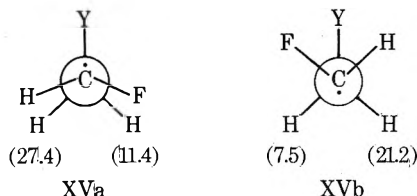
tons have hfs which are instantaneously equivalent at all times, but modulated between two limiting values the line widths would be proportional to $(M_I^H)^2$.^{2b,17} The latter would lead to selective broadening of only the "outer" pair of lines of the triplet corresponding to the β protons as indicated by the horizontal lines in the modulation diagram and the "stick" spectrum in Figure 5a.

A dynamic process in which the β protons are exchanged in a pairwise manner between XIVa and XIVb is given in eq 11. Thus, it would appear that for the β substituent ex-

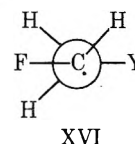


pected to lead to the most pronounced partial bridging, namely Cl, the less favorable conformation involving the eclipsing of the α fluorines and the β protons can be populated at sufficiently high temperatures. This is not surprising if it is considered that a consequence of partial bridging is a distortion at the β carbon tending to displace the β protons in conformation XIVb toward the nodal plane and away from the α fluorines reducing thus the unfavorable steric interaction of the eclipsed α and β substituents.⁶

The complexity of the situation increases markedly in the adducts to vinyl fluoride. For example, the β -proton hyperfine splittings, which were extracted from the INDO results from the α -fluoroethyl radical in the two eclipsed conformations XVa and XVb, show changed magnitudes.



Furthermore, a variety of less symmetric conformers, such as XVI, become *a priori* equally likely and cannot be ex-



cluded from consideration. It may not be surprising, therefore, that the esr parameters (particularly the β -hyperfine splittings) listed in Tables I-IV for the vinyl fluoride adducts form no consistent pattern such as those deduced for the vinylidene fluoride adducts or for β -substituted ethyl radicals discussed earlier.^{6,12-14}

Experimental Section

Materials. Dimethyl disulfide was obtained from Columbia Organic Chemicals and passed over neutral alumina before use. 2-Fluoropropene and 1,1,1-trifluoropropene were obtained from PCR. Ethylene, vinyl fluoride, vinylidene fluoride, trifluoroethylene, and tetrafluoroethylene were commercial samples from Du Pont Co. Methylene perfluorocyclobutane was kindly donated by Dr. D. C. England. The other chemicals were obtained as described previously.⁴

Esr Measurements. The technique for the preparation of the samples for irradiation and the esr measurements were as described previously.^{4,6}

Acknowledgment. K. S. C. thanks the National Science Foundation for financial support of this work.

References and Notes

- (1) (a) E. I. du Pont de Nemours and Company. (b) Department of Chemistry, Indiana University. (c) Contribution No. 2391 from the Department of Chemistry, Indiana University. (d) Contribution No. 2133 from E. I. du Pont de Nemours and Co.
- (2) (a) W. A. Sheppard and C. M. Shorts, "Organic Fluorine Chemistry," W. A. Benjamin, New York, N. Y., 1969, Chapter 6; (b) P. S. Skell and K. J. Shea in "Free Radicals," J. K. Kochi, Ed., Vol. II, Wiley, New York, N. Y., 1973, Chapter 26; (c) L. Kaplan, "Bridged Free Radicals," Marcel Dekker, New York, N. Y., 1972.
- (3) (a) W. Stacey and J. F. Harris, Jr., *Org. Reactions*, **13**, 150 (1963); (b) C. Walling and E. S. Huyser, *ibid.*, **13**, 91 (1963); (c) R. N. Haszeldine, *et al.*, *J. Chem. Soc. C* 414 (1970); 2800 (1957); (d) D. A. Ashton, A. F. Mackay, J. M. Tedder, D. C. Tipney, and J. C. Walton, *J. Chem. Soc., Chem. Commun.*, 496 (1973).
- (4) K. S. Chen, P. J. Krusic, P. Meakin, and J. K. Kochi, **78**, 2014 (1974).
- (5) J. K. Kochi and P. J. Krusic, *Chem. Soc., Spec. Publ.*, **247** 147 (1969).
- (6) P. J. Krusic and J. K. Kochi, *J. Amer. Chem. Soc.*, **93**, 846 (1971).
- (7) Cf. M. C. R. Symons, *J. Amer. Chem. Soc.*, **91**, 592 (1969).
- (8) J. K. Kochi and P. J. Krusic, *J. Amer. Chem. Soc.*, **90**, 7157 (1968).
- (9) A. Hudson and R. A. Jackson, *J. Chem. Soc., Chem. Commun.*, 1327 (1969).
- (10) D. J. Edge and J. K. Kochi, *J. Amer. Chem. Soc.*, **94**, 6485 (1972).
- (11) K. S. Chen and J. K. Kochi, *J. Amer. Chem. Soc.*, **96**, 794 (1974).
- (12) P. J. Krusic, P. Meakin, and J. P. Jesson, *J. Phys. Chem.*, **75**, 3438 (1971).
- (13) K. S. Chen, I. H. Elson, and J. K. Kochi, *J. Amer. Chem. Soc.*, **95**, 5341 (1973).
- (14) (a) T. Kawamura, D. J. Edge, and J. K. Kochi, *J. Amer. Chem. Soc.*, **94**, 1752 (1972); (b) T. Kawamura, P. Meakin, and J. K. Kochi, *ibid.*, **94**, 8065 (1972); (c) T. Kawamura and J. K. Kochi, *J. Organometal. Chem.*, **47**, 79 (1973); (d) A. R. Lyons and M. C. R. Symons, *J. Chem. Soc., Faraday Trans. 2*, 622 (1972); (e) W. Damerou, G. Lassman, and K. H. Lohs, *Z. Naturforsch. B*, **25**, 152 (1970).
- (15) J. A. Pople and D. L. Beveridge, "Approximate Molecular Orbital Theory," McGraw-Hill, New York, N. Y., 1970, p 144.
- (16) P. Meakin and P. J. Krusic, *J. Amer. Chem. Soc.*, **95**, 8185 (1973).
- (17) G. K. Fraenkel, *J. Phys. Chem.*, **71**, 139 (1967); P. D. Sullivan and J. R. Bolton, *ibid.*, **73**, 4387 (1969); *Advan. Magn. Resonance*, **4**, 39 (1970).

Electron Spin Resonance Studies of Fluoroalkyl Radicals in Solution. III. Photolysis of Perfluoroketones and Adduct Formation

Paul J. Krusic,*^{1a} Kuang S. Chen, Paul Meakin, and Jay K. Kochi*^{1b}

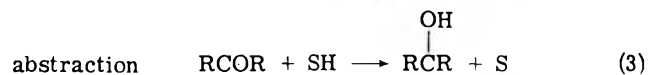
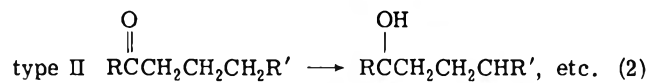
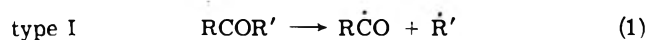
Central Research Department,^{1c} E. I. du Pont de Nemours and Company, Wilmington, Delaware 19898 and Department of Chemistry,^{1d} Indiana University, Bloomington, Indiana 47401 (Received January 2, 1974; Revised Manuscript Received June 13, 1974)

Publication costs assisted by E. I. du Pont de Nemours and Company

The esr spectra of paramagnetic species formed during the ultraviolet photolysis of various fluorinated ketones are examined directly in the cavity of the spectrometer. The production of fluoroalkyl radicals by Norrish type I photocleavage is observed in inert solvents. The fluoroalkyl and fluoroacyl radicals produced in the primary photochemical process add to the oxygen atom of the fluoroketones forming α -alkoxy- and α -acyloxyfluoroalkyl radicals. Fluoroacyl radicals have been detected by hydrogen atom abstraction from fluoroaldehydes. In cyclopropane solutions, α -hydroxyfluoroalkyl radicals resulting from hydrogen transfer from the solvent to the photoexcited ketone are observed, and their identity is verified by generating them by an independent procedure from the corresponding fluoroalcohol. The susceptibility of fluoroketones to addition of other radicals is also probed by the examination of the esr spectra of various adducts with silyl radicals. Addition of silyl radicals to sterically crowded perfluoroketones produces fluoroalkyl radicals of unusual stability. The esr spectrum of the carbonyl fluoride adduct $\text{Et}_3\text{SiOCF}_2$ like other α, α -difluoroalkyl radicals shows a pronounced line width effect due to dipolar broadening, which is simulated by the relaxation matrix method assuming a correlation time in the region of 10^{-11} sec for the tumbling motion of the free radical in solution.

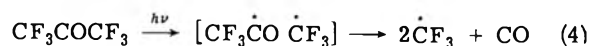
Introduction

The irradiation of the $n-\pi^*$ band of ketones leads to a rich array of photochemical reactions including homolysis of the acyl carbon bonds and intramolecular and intermolecular hydrogen atom transfer reactions.^{2a-d}



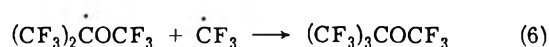
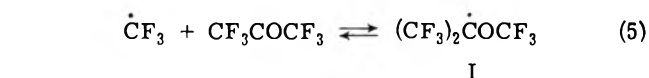
A variety of free-radical intermediates formed by such processes have been observed by esr techniques.^{2e,f}

Perfluoroketones represent an interesting class of compounds with an exceptionally electron-deficient carbonyl function.^{3,4} Their photochemical behavior has not been investigated as thoroughly as that of their hydrocarbon analogs, and there is uncertainty concerning the chemical processes following photoexcitation. Chemical studies indicate that the ultraviolet irradiation of hexafluoroacetone (HFA) in the gas phase affords principally carbon monoxide and perfluoroethane as the recombination product of two trifluoromethyl radicals.⁵ The latter have been detected by esr as stabilized adsorbed species following the photolysis of HFA on zeolites at 77°K.⁶ In one gas-phase study,⁷ however, significant amounts of perfluoro-*tert*-butyl methyl ether were also found, particularly at higher vapor pressures, in addition to carbon monoxide and perfluoroethane. A reversible addition of the trifluoromethyl radicals to the oxygen atom of an HFA molecule was postulated followed by the coupling of the resulting α -trifluoromethoxy radical



I with another trifluoromethyl radical to yield the perfluoro ether. Although this finding has been questioned,^{5c} it is in

harmony with the results of a recent investigation which shows that this perfluoro ether is in fact the major product (50–70% yield) obtained after prolonged exposure of liquid HFA to ultraviolet light.⁸



The role and stability of trifluoroacetyl radicals during photolysis of HFA is also controversial. The notable absence of hexafluorobiacetyl among the products of photolysis has been taken to imply a direct dissociation of HFA into carbon monoxide and two trifluoromethyl radicals, or the kinetically equivalent formation of a "hot" trifluoroacetyl radical which dissociates spontaneously by virtue of its excess energy.^{5b} The sole chemical indication extant so far of a stepwise decomposition consists in the observation of trifluoroacetyl halides from the photolysis of HFA in the presence of bromine or chlorine,⁹ but it has been given alternative explanations.^{3a,5b}

Chemical studies have also shown that HFA enters into a rich array of reactions *via* addition of various radicals to both the carbon and oxygen atoms of the carbonyl group.^{3,10,11} The radical reactions of other perfluoroketones have received much less attention so far. In this study, we examined the esr spectra of several types of fluorinated radical species in order to describe the paramagnetic intermediates in the photolysis of fluoroketones. The pertinent points we wish to describe are (a) radicals formed by uv photolysis of fluoroketones in inert fluorocarbon solvents with particular emphasis on hexafluoroacetone, (b) perfluoroacyl radicals obtained by hydrogen atom abstrac-

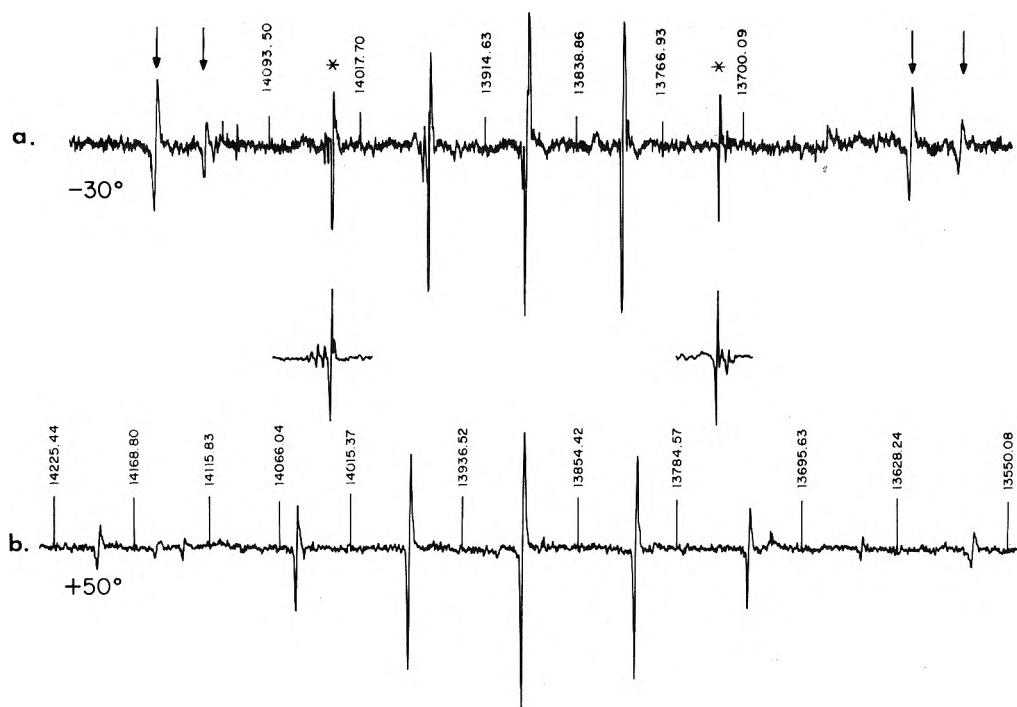


Figure 1. ESR spectra obtained during ultraviolet irradiation of hexafluoroacetone in dichlorodifluoromethane at -30° and in perfluoro-1,2-dimethylcyclobutane at $+50^\circ$. The groups of lines denoted with asterisks are shown on an expanded scale in the inserts. The major septet spectrum belongs to $(\text{CF}_3)_2\text{COCF}_3$. The lines denoted with arrows are the $M_I = \pm \frac{1}{2}$ lines of the CF_3 radical. The proton nmr field markers are in kHz.

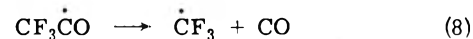
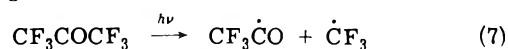
tion from perfluoroaldehydes, (c) α -hydroxyfluoroalkyl radicals derived by intermolecular photoreduction of fluoro ketones as well as by independent methods, and (d) species formed by addition of silyl radicals to the electron-deficient carbonyl functions.

Results and Discussion

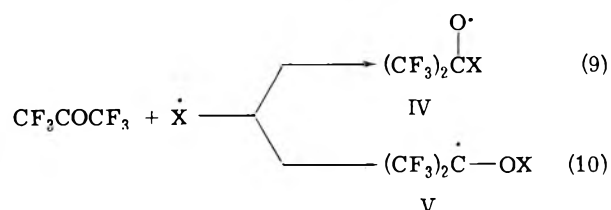
I. Photolysis of Fluoro ketones in Inert Solvents. A. Photolysis of Hexafluoroacetone (HFA). Ultraviolet irradiation of a dilute solution of HFA in dichlorodifluoromethane (1:10 v/v) at -30° affords, at low microwave power levels and low modulation amplitudes, the esr spectrum shown in Figure 1a which indicates the presence of three radical species: (a) the trifluoromethyl radical¹²⁻¹⁴ (only the $M_I^F = \pm \frac{1}{2}$ lines, denoted by arrows, are shown in Figure 1a), (b) a radical II giving rise to a septet spectrum ($a = 18.74$ G) with partially resolved second-order splittings, and (c) a third radical species III in lower concentration with a slightly larger septet splitting (19.30 G) and a small quartet splitting (0.84 G, see inserts in Figure 1a). The same composite spectrum is obtained under similar conditions using a variety of inert fluorinated solvents such as 1,2-dichlorotetrafluoroethane, perfluorocyclobutane, and perfluoro-1,2-dimethylcyclobutane. The relative concentrations of the last two species are temperature dependent, with species III becoming less important at higher temperatures. Thus, photolysis of HFA in perfluoro-1,2-dimethylcyclobutane at $+50^\circ$ gives only the spectra of $\dot{\text{C}}\text{F}_3$ and of species II (Figure 1b). The major septet spectrum is not affected by any selective line broadening effects down to -120° .

Attempts to identify the esr spectrum of the trifluoroacetyl radical during the photolysis of HFA gave ambiguous results. Paul and Fischer^{2e} had shown earlier that the esr spectra of acyl radicals can be observed during the photolysis of alkyl ketones at high microwave powers. Photolysis of

HFA in various fluorinated solvents over a wide temperature range under conditions of high microwave power brings out additional broad lines which form a complex pattern and decay slowly upon shuttering the light. These lines cannot be attributed to the trifluoroacetyl radical, since they do not coincide with the esr spectrum of $\text{CF}_3\dot{\text{C}}\text{O}$ generated at low temperatures by hydrogen abstraction from trifluoroacetaldehyde (*vide infra*). Since the trifluoroacetyl radical is highly unstable, the observation of $\dot{\text{C}}\text{F}_3$ is not inconsistent with a stepwise decomposition of HFA by type I cleavage.



The unambiguous identification of radicals II and III poses several problems. The known propensity of HFA to enter into radical addition reactions^{10,11} suggests that these species should be formed by addition of a radical X to the carbonyl function as shown in eq 9 and 10. Fluoroalkoxy radicals IV, resulting from the addition of X \cdot to carbon, can



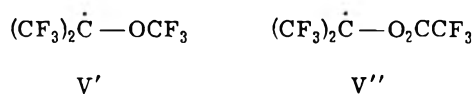
almost certainly be excluded from consideration since the large g tensor anisotropy expected for such radicals is inconsistent with the unusually narrow line widths observed for radicals II and III ($\Delta H = 0.18$ G for III at -30°). Indeed, it is doubtful that reactive alkoxy radicals can be detected in solution.¹⁵ ESR studies cannot, therefore, evaluate

TABLE I: ESR Parameters of α -Hydroxy- and α -Fluoroalkoxyfluoroalkyl Radicals in Solution

Radical	T, °C	(g)	Proton and fluorine isotropic coupling constants, G			
$\dot{\text{C}}\text{H}_2\text{OH}^a$	-50	2.00336			α -H: 17.84	OH: 1.75
$\text{CH}_3\dot{\text{C}}\text{H}(\text{OH})^a$	-33	2.00321	CH_3 : 22.27		α -H: 15.50	OH: 0.98
$(\text{CH}_3)_2\dot{\text{C}}\text{OH}^a$	26	2.00317	CH_3 : 19.66			OH: 0.70
$(\text{CH}_3)_3\dot{\text{C}}\text{OH}^a$	-23	2.00309	19.57			OH: 0.0
$\text{CF}_3\dot{\text{C}}\text{H}(\text{OH})^b$	-44		CF_3 : 29.82		α -H: 19.52	OH: 1.20
$\text{CF}_3\dot{\text{C}}(\text{CH}_3)\text{OH}^b$	-40		CF_3 : 29.43	CH_3 : 21.22		OH: c
$\text{CF}_3\dot{\text{C}}(\text{CH}_3)\text{OH}^b$	-109		29.00	21.38		
$(\text{CF}_3)_2\dot{\text{C}}\text{OH}^d$	-13		CF_3 : 23.15			OH: 1.16
$(\text{CF}_3)_2\dot{\text{C}}\text{OH}^d$	-55	2.00284	CF_3 : 23.94			OH: 1.72
$(\text{CF}_3)_2\dot{\text{C}}\text{OH}^d$	-130		$(\text{CF}_3)_a$: 26.49	$(\text{CF}_3)_b$: 22.28	$(\text{CF}_3)_{av}$: 24.39	OH: 2.41
$(\text{CF}_3)_2\dot{\text{C}}\text{OCH}(\text{CF}_3)_2^c$	-36		α - CF_3 : 20.3		γ - CF_3 : 2.2	
$(\text{CF}_3\text{CF}_2)_2\dot{\text{C}}\text{OH}^e$	-40		CF_2 : 30.74		CF_3 : 3.68	OH: 1.15
$(\text{CF}_3)_2\dot{\text{C}}\text{F}(\text{CF}_3)\text{OH}^e$	-35		CF : 16.78	α - CF_3 : 26.70	β - CF_3 : 2.61	OH: c
$(\text{CF}_3)_2\dot{\text{C}}\text{OCF}_3^d$	50		α - CF_3 : 18.81		β - CF_3 : c	
$(\text{CF}_3)_2\dot{\text{C}}\text{OCF}_3^d$	-42	2.00257	α - CF_3 : 18.74		β - CF_3 : c	
$(\text{CF}_3)_2\dot{\text{C}}\text{O}_2\text{CCF}_3^d$	-42		α - CF_3 : 19.30		γ - CF_3 : 0.84	
$(\text{CF}_3)_2\dot{\text{C}}\text{O}_2\text{CCH}_3$	-48		α - CF_3 : 21.23			
$(\text{CF}_3\text{CF}_2)_2\dot{\text{C}}\text{OCF}_2\text{CF}_3^d$	-70		α - CF_2 : 24.00		β - CF_3 : 3.20	OCF_2CF_3 : 0.6'
$(n\text{-Bu})_3\text{SiCF}_2\dot{\text{C}}\text{F}(\text{OCF}_3)$	-21	2.00397	α - CF_2 : 12.23	α -F: 91.2	OCF_3 : c	
$(n\text{-Bu})_3\text{SiCF}_2\dot{\text{C}}\text{F}(\text{OCF}_2\text{CF}_3)$	-10		α - CF_2 : 12.4	α -F: 89.9	OCF_2CF_3 : 0.5'	
$\text{CF}_3\dot{\text{C}}\text{F}_2^g$	-10	2.00386	CF_3 : 11.43	α -F: 87.7		
$(\text{CF}_3)_2\dot{\text{C}}\text{F}$	+30	2.00321 ^h	CF_3 : 19.75	α -F: 70.48		
$(\text{CF}_3)_2\dot{\text{C}}\text{H}^i$	-113	2.00221	CF_3 : 22.64	α -H: 24.61		
$\text{CF}_3\dot{\text{C}}\text{H}_2^i$	-113	2.00234	CF_3 : 29.61	α -H: 23.77		
$(\text{CF}_3)_3\dot{\text{C}}^j$	-60	2.0015	CF_3 : 17.9			
$(\text{CF}_3)_2\dot{\text{C}}\text{-O}^{-k}$	25	2.00397	CF_3 : 34.7			

^a From R. Livingston and H. Zeldes, *J. Chem. Phys.*, **44**, 1245 (1966). In aqueous solution. ^b In alcohol as solvent. ^c Unresolved. ^d In dichlorodifluoromethane. ^e In cyclopropane. ^f Nearly equivalent CF_2 and CF_3 fluorines (sextet). ^g From ref 13. ^h Corrected for second-order shifts and for nmr probe placement. ⁱ From ref 14. ^j From ref 20. ^k From E. G. Janzen and J. L. Gerlock, *J. Phys. Chem.*, **71**, 4577 (1967).

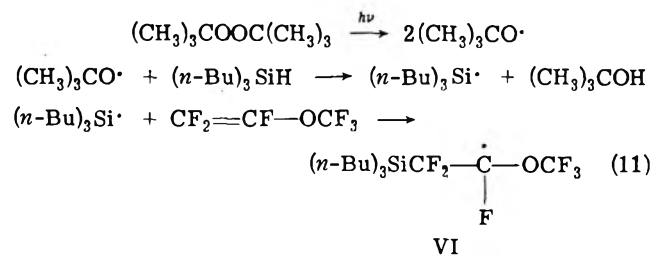
the importance of such additions in the radical reactions of fluoroketones. Radical addition to oxygen to afford α -oxyperfluoroalkyl radicals V, on the other hand, is plausible. Indeed, the available evidence strongly supports the assignment of the major septet spectrum of Figure 1 to the α -trifluoromethoxyhexafluoroisopropyl radical V' (X = CF_3 , eq 10).^{15a} The weaker spectrum consisting of a septet-of-quartets is attributed to the α -trifluoroacetoxyhexafluoroisopropyl radical V'' (X = CF_3CO , eq 10).



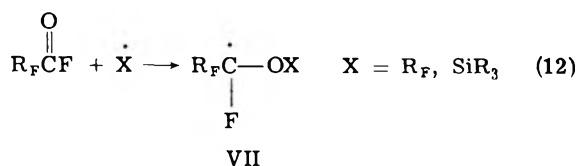
The formation of the ether radical V' is in harmony with the chemical studies of Gordon⁷ and Resnick,⁸ since it is the direct precursor of perfluoro-*tert*-butyl methyl ether (eq 6) found by these authors among the products of photolysis of HFA at high vapor pressures and in the liquid phase, respectively. The septet hyperfine structure (Figure 1) is due to the six equivalent β fluorines. Their coupling constant ($A_{\beta}^F = 18.74$ G) compares remarkably well with the β -fluorine coupling in the perfluoroisopropyl radical (19.75 G, Table I). The latter represents the proper comparison since α -fluoro and α -alkoxy groups exert similar out-of-plane bending influences on the trigonal carbon atom by virtue of the destabilizing interaction between the lone pairs of electrons on fluorine or oxygen and the adjacent half-filled p orbital on carbon.^{14,16} The most remarkable feature of the spectrum of species V', however, is the absence of any resolvable fluorine hyperfine structure due to the CF_3O group. For comparison, the methyl protons in methoxymethyl radical, $\dot{\text{C}}\text{H}_2\text{OCH}_3$, give rise to a splitting of about 2 G,¹⁷ and one would assume that the analogous

fluorine atoms would give rise to a comparable or larger interaction. We sought to confirm this unexpected effect by examining other α -perfluoroalkoxyalkyl radicals.

Indeed, the spectrum of radical VI, obtained by photolysis of a mixture of perfluorovinyl methyl ether, tri(*n*-butyl)silane, and di-*tert*-butyl peroxide in cyclopropane,¹⁸ is also devoid of any resolvable structure ($\Delta H = 0.70$ G) due to the ethereal CF_3 fluorines. The spectrum of radical VI ($g = 2.00397$, corrected for second-order effects) at -25° con-



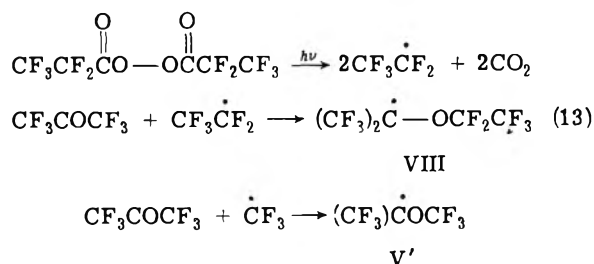
sists of a large doublet due to the α fluorine (91.20 G) further split into triplets by the two β fluorines (12.23 G). The magnitude of the doublet compares well with the α -fluorine coupling in $\text{CF}_3\dot{\text{C}}\text{F}_2$ (87.3 G), again demonstrating that $-\text{CFOR}$ and $-\text{CF}_2$ fragments have similar geometries at the radical sites. Analogous α -fluorine couplings in the region of 90 G have also been observed for a series of radicals VII formed by radical addition to perfluoroacyl fluorides.¹⁹ The



triplets associated with the β protons in VI display a pronounced broadening of the central lines ($M_1 = 0$ lines) below -40° , indicating hindered rotation about the $C_\alpha-C_\beta$ bond. This effect is also common for radicals such as VII and must be attributed to the strong pyramidity of a $-\dot{C}FOR$ radical site.¹⁴

The radical analogous to VI from perfluorovinyl ethyl ether and tri(*n*-butyl)silane ($a_\alpha^F = 89.9$ G; $a_\beta^F = 12.4$ G, $T = -10^\circ$) is also interesting in that each line of the basic doublet-of-triplets is further split into an apparent sextet of 0.5 G. Thus, while the fluorines of an α -trifluoromethoxy groups in a fluoroalkyl radical give no resolvable hyperfine structure, the CF_2 fluorines of an α -pentafluoroethoxy group give a small splitting of nearly the same magnitude as the splitting of the CF_3 fluorines one carbon atom further removed from the radical site.

This observation is confirmed by additional experiments which also demonstrate the ready addition of perfluoroalkyl radicals to the oxygen atom of HFA. Photolysis of a solution of HFA and perfluoropropionyl peroxide in 1,2-bis(trifluoromethyl)perfluorocyclobutane at room temperature leads to a spectrum consisting of at least four species. The $\dot{C}F_3$ and $CF_3\dot{C}F_2$ ^{13,20} radicals can be immediately recognized. The remaining two species, in comparable concentrations, give rise to overlapping septets of very similar splitting. Slow scans under conditions of low microwave power and modulation reveal that one septet has no additional resolved structure and is identical with the major septet of Figure 1, while the second septet is further split into apparent sextets of 0.7 G. This septet of small sextets must belong to the adduct VIII of a perfluoroethyl radical to the oxygen of HFA in which the five OCF_2CF_3 fluorines are again almost equally coupled to the unpaired electron despite their different positions. These small couplings to



etheral fluorines adjacent to the α -oxygen atom are surprising not only in view of the much larger coupling of the analogous etheral protons, as was pointed out above, but also in comparison with radicals such as $CF_3OCH_2\dot{C}H_2$,¹⁸ in which the fluorine splitting is 2.0 G despite the trifluoromethyl groups being one carbon further removed from the radical center. To add to the complexity of the situation, the radical $(CF_3)_2\dot{C}OCH(CF_3)_2$, obtained by hydrogen removal from bis(hexafluoroisopropyl) ether with *tert*-butoxy radicals in cyclopropane, shows no indication of a splitting by the etheral proton. Its spectrum consists of a large septet of 20.3 G (α - CF_3 fluorines) further splitting into small septets of 2.2 G by six equivalent δ fluorines. Clearly, much remains to be learned about long-range fluorine hyperfine interactions.

The trend displayed by the g factors for the series of radicals listed below (Table I) provides some insight into the possible causes for the small unresolvable hyperfine inter-

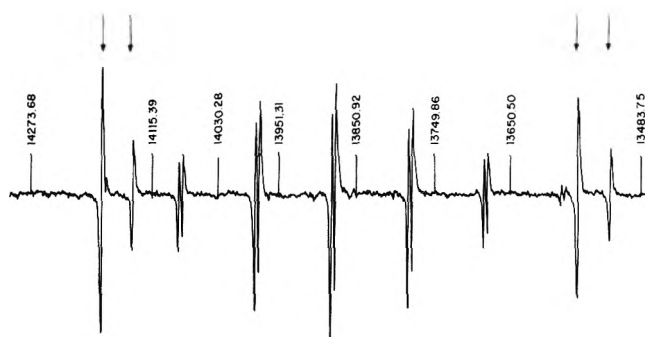
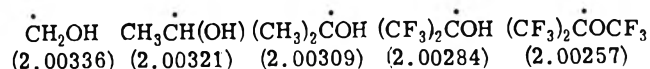
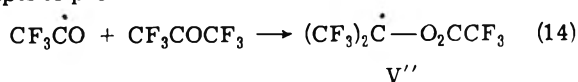


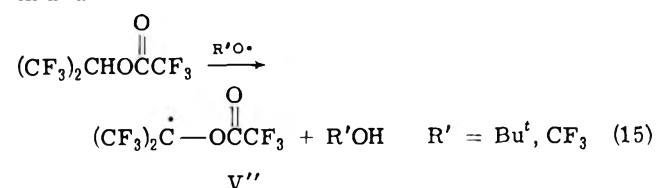
Figure 2. Esr spectrum of the $(CF_3)_2\dot{C}OH$ radical (0°) obtained by photolysis of a dichlorodifluoromethane solution containing hexafluoroacetone and trifluoroacetaldehyde. The lines denoted with arrows belong to the $\dot{C}F_3$ radical.

action to the OCF_3 fluorines in $(CF_3)_2\dot{C}OCF_3$. The smooth decrease in the g factors, from the highest value of 2.00336 for the hydroxymethyl radical to the lowest value of 2.00257 for the $(CF_3)_2\dot{C}OCF_3$ radical, indicates a steadily decreasing spin density on oxygen in this series. The latter is the major source for the increase in the g factors for α -hydroxyalkyl radicals over the values typical for alkyl radicals (2.0022–2.0026). Since the hyperfine interaction to the freely rotating CH_3 protons in $\dot{C}H_2OCH_3$ is determined by the spin density on oxygen through the combined effects of hyperconjugation and spin polarization, it is perhaps not surprising that the interaction to the etheral CF_3 fluorines in $(CF_3)_2\dot{C}OCF_3$ will be small if the spin density on oxygen is greatly reduced as evidenced by the unusually low g factor for this radical. Another interesting deduction can be made by comparing the hydroxylic proton splittings for $(CH_3)_2\dot{C}OH$ and $(CF_3)_2\dot{C}OH$ (Table I). The small magnitudes of these splittings implies a more or less planar structure.¹⁷ However, this splitting for the $(CH_3)_2\dot{C}OH$ radical must be *positive*, judging by the positive temperature coefficient of its absolute value (Table I), while the corresponding coupling in $(CF_3)_2\dot{C}OH$ must be *negative* since the temperature coefficient of its absolute value is negative in Table I (*cf.* ref 17).

The identification of the minor radical species in the photolysis of HFA as radical V'' is less certain. Our direct attempts to prove the structure of V'' have been unsuccessful as yet.



Thus, hydrogen atom abstraction from hexafluoroisopropyl trifluoroacetate (eq 15), under conditions well established to generate *tert*-butoxy or trifluoromethoxy radicals, afforded no esr spectrum of V''. Part of the difficulty is due to absorption of irradiation by the ester, even in dilute solutions.



Another approach also failed to provide support for V'' but led to interesting information. It was hoped that photolysis of HFA in the presence of trifluoroacetaldehyde, which produces the trifluoroacetyl radical by loss of the hydrogen atom (*vide infra*), would lead to an enhanced spectrum of V''. The spectrum of Figure 2, obtained by photoly-

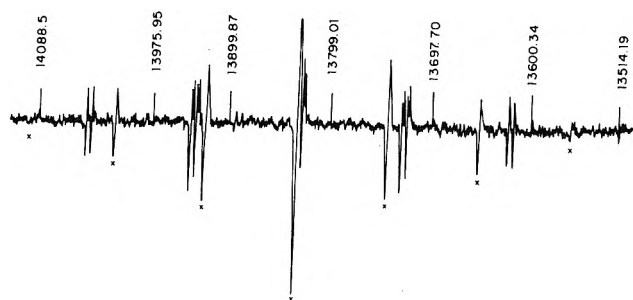
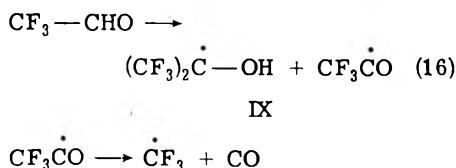
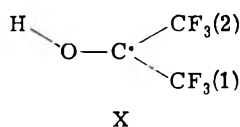


Figure 3. ESR spectrum obtained by photolysis of a mixture of hexafluoroacetone and acetaldehyde in a cyclopropane solution at -48° . Two radical species are present: the $(\text{CF}_3)_2\text{COCOCCH}_3$ radical (septet*) and the $(\text{CF}_3)_2\text{COH}$ radical (septet-of-doublets).

sis of these substances in dichlorodifluoromethane at 0° , however, shows only the presence of the trifluoromethyl radical, produced by decarbonylation of the trifluoroacetyl radical, and of the hydroxyhexafluoroisopropyl radical IX clearly produced by photoreduction of HFA. Raising the



temperature to 25° causes the appearance of an additional septet (18.81 G) identical with that of Figure 1, indicating that at higher temperatures radical V' is also formed in sufficient concentration for detection. Lowering the temperature steadily decreases the importance of the $\dot{\text{C}}\text{F}_3$ radical and produces alternating line shape effects in the spectrum of $(\text{CF}_3)_2\dot{\text{C}}\text{OH}$ symptomatic of hindered rotation of the OH fragment.¹⁷ At -140° , this rotation is slow on the ESR time scale and the two CF_3 groups appear inequivalent ($a_1^{\text{CF}_3} = 26.49$ G, $a_2^{\text{CF}_3} = 22.28$ G, $a^{\text{H}} = 2.41$ G) indicating a more or less planar equilibrium structure X. This effect will be de-



scribed fully in another context.²¹ The magnitudes of the fluorine and proton coupling constants are also notably temperature dependent. At the lowest temperature (-140°) and under conditions of high microwave power, the trifluoroacetyl radical can also be detected (*vide infra*). These experiments again underscore the low activation energy for decarbonylation of the trifluoroacetyl radical. Furthermore, the appearance of minor amounts of V' only at relatively high temperatures is consistent with its formulation as $(\text{CF}_3)_2\dot{\text{C}}\text{OCF}_3$ rather than $(\text{CF}_3)_2\dot{\text{C}}-\text{O}_2\text{CCF}_3$, since the steady-state concentration of $\dot{\text{C}}\text{F}_3$ increases with temperature within the range studied while the concentration of $\text{CF}_3\dot{\text{C}}\text{O}$ decreases. The failure to observe V' and V'' at lower temperatures is attributed to the high reactivity of the aldehydic proton toward abstraction and thus promoting an efficient radical chain reaction.

The adduct of acetyl radicals to HFA, however, can be observed together with $(\text{CF}_3)_2\text{COH}$ in the photolysis of a mixture of HFA and acetaldehyde in Freon 12 or cyclopropane (Figure 3). The septet of doublets is readily assigned to $(\text{CF}_3)_2\text{COH}$. The broader septet lines (starred, $a^{\text{F}} = 21.23$ G) are associated with the acetyl adduct

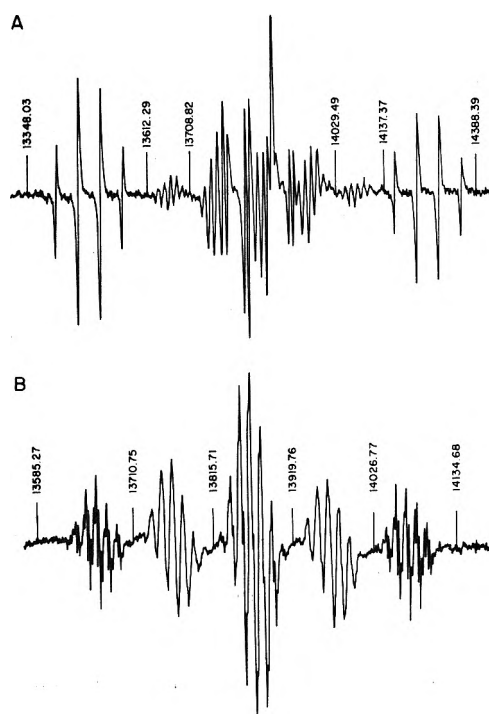
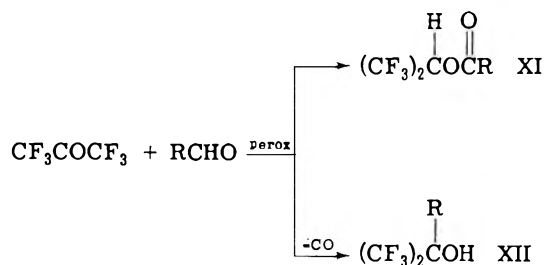
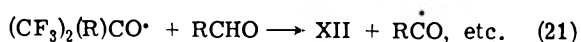
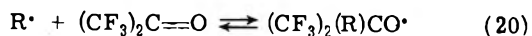
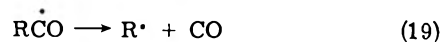
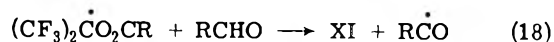
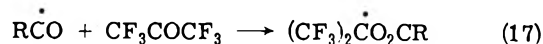


Figure 4. ESR spectra recorded during photolysis of perfluoroethyl ketone in dichlorodifluoromethane: (A) -30° , wide scan at relatively high microwave power showing the perfluoroethyl radical (note the unencumbered outer quartets) and radical XIII, (B) -70° , radical XIII at low microwave power and low modulation amplitude (expanded scale) showing selective line broadening.

$(\text{CF}_3)_2\dot{\text{C}}\text{O}_2\text{CCH}_3$ in eq 17 ($\text{R} = \text{CH}_3$). Indeed, chemical studies¹¹ have shown that 1:1 adducts XI can be isolated in high yields during the free-radical chain reaction of aldehydes and hexafluoroacetone, e.g.



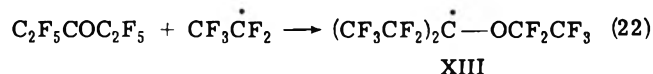
In addition, carbon monoxide and tertiary alcohols XII are formed. The structures of XI and XII suggest that acyl radicals as intermediates add to the perfluoroacetone at the oxygen terminus, whereas alkyl radicals resulting from de-



carbonylation add to carbon. The quantitative delineation of these processes is made difficult by the reversibility in the latter instance. The ready observation of the acetyl adduct contrasts with our inability to observe the trifluoroacetyl adduct under similar conditions. One of the factors responsible for the contrasting behavior is no doubt ascri-

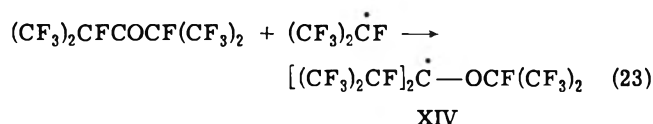
able to the longer lifetime of the acetyl radical prior to decarboxylation compared to the trifluoroacetyl radical.

B. Photolysis of Higher Fluoroketones. Type I cleavage (eq 1) followed by addition of the resulting fluoroalkyl radical to the carbonyl oxygen appears to be a general sequence of events in the photochemistry of fluoroketones in inert fluorocarbon solvents. Photolysis of a dilute solution of perfluoroethyl ketone in dichlorodifluoromethane (1:10 v/v) at -30° leads to the spectrum of Figure 4A in which two radical species are apparent: the $\text{CF}_3\dot{\text{C}}\text{F}_2$ radical, recognized by the outer quartets and by their separation, and a second species giving rise to a quintet of small septets. The latter spectrum can be recorded without interference from the $\text{CF}_3\dot{\text{C}}\text{F}_2$ radical using low microwave powers, low modulation amplitudes, and slow scans. Under these conditions the spectrum of this species at -70° (Figure 4B) reveals additional hyperfine structure and the presence of selective line broadening affecting the $M_1 = \pm 1$ lines and, to a lesser extent, the $M_1 = 0$ lines of the major quintet. This spectrum is assigned to radical XIII resulting from the addition of a $\text{CF}_3\dot{\text{C}}\text{F}_2$ radical to the oxygen of perfluoroethyl ketone.



The quintet structure (24.00 G) is associated with the four β fluorines and the septets (3.20 G) with the six equivalent γ fluorines. The additional partially resolved hyperfine structure (0.6 G) is believed to consist of sextets associated with five nearly equivalent OCF_2CF_3 fluorines. Although the wing lines of the sextets are too weak to be clearly discerned and are also obscured by overlap, this interpretation is consistent with similar results for the α -perfluoroethoxyalkyl radicals discussed above. The observed line width effect affecting the inner lines of major quintet indicates that the rotation about the two $\text{C}_\alpha-\text{C}_\beta$ bonds is hindered and that each $\alpha\text{-CF}_2$ group exists in a preferred conformation relative to the axis of the central trigonal carbon atom in which the two β fluorines are nonequivalent. Unfortunately better quality spectra could not be obtained at sufficiently low temperatures to observe the spectrum in the slow exchange limit where the four β fluorines would presumably appear nonequivalent in pairs and give rise to a triplet-of-triplets spectrum.

Photolysis of a dilute solution of perfluoroisopropyl ketone in perfluoro-1,2-dimethylcyclobutane at room temperature produces an intense spectrum of the perfluoroisopropyl radical²⁰ formed by a type I cleavage ($a^{\text{F}}(\text{CF}_3) = 19.75$ G, $a_\alpha^{\text{F}} = 70.48$ G, $g = 2.00321$ corrected for second-order shift), together with the spectrum of a second radical species (Figure 5A) which can be best recorded under conditions of low microwave power (Figure 5B). By analogy with the simpler fluoroketones, we believe that this spectrum is also associated with an adduct radical such as XIV,



although we have been unable to analyze it in detail. A doublet splitting of about 20 G, however, is definitely part of this spectrum and constitutes the largest splitting, indicating that the two α -perfluoroisopropyl groups cannot be conformationally equivalent. Examination of molecular models also suggests that these groups should be locked in nonequivalent orientations with respect to the axis of the

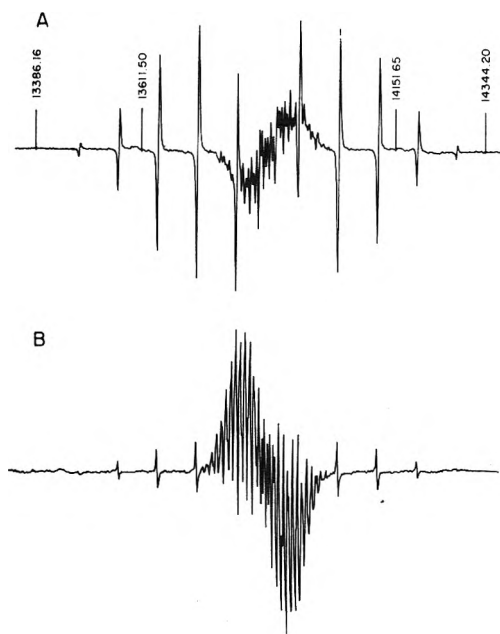
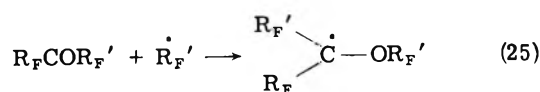
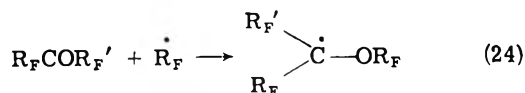


Figure 5. ESR spectra at high (A) and low microwave power levels (B) resulting by photolysis of a dilute solution of perfluoroisopropyl ketone in perfluoro-1,2-dimethylcyclobutane showing the spectra of the perfluoroisopropyl radical (doublet-of-septets) and of the adduct radical XIV (room temperature).

central trigonal carbon by the steric requirements of the bulky CF_3 groups. The steric crowding around the carbon radical center is also responsible, no doubt, for the unusually long life of this radical. Additional examples of extraordinarily stable fluoroalkyl radicals with bulky substituents will be mentioned below.

Several asymmetric fluoroketones were also irradiated in inert fluorocarbon solvents, and in all cases adduct formation appeared to be an important radical process attending photolysis. Unfortunately, the resulting spectra were complicated by the presence of more than one radical species. The occurrence of at least two adducts in the photolysis of an asymmetric fluoroketone $\text{R}_\text{F}\text{COR}_\text{F}'$ is, of course, expected since either R_F or R_F' , resulting by type I cleavage, can add to the oxygen of a ground-state ketone molecule (eq 24 and 25). Indeed, the superposed spectra are often quite



similar with regard to the major splitting pattern which is determined by the nature of the fluoroalkyl groups directly attached to the central carbon atom. Thus, photolysis of $(\text{CF}_3)_2\text{CFCOCF}_3$ produces a very intense and complex spectrum of two adduct species with very similar hyperfine splittings. The major pattern for both species is a quartet of doublet of septets (approximately 20, 10, and 3 G, respectively), as required by the structure of the ketone, further split by additional small splittings. Under conditions of relatively high microwave power, the perfluoroisopropyl as well as the trifluoromethyl radicals can also be detected.

An intense spectrum of a relatively stable radical species can also be obtained after a short irradiation of a dilute so-

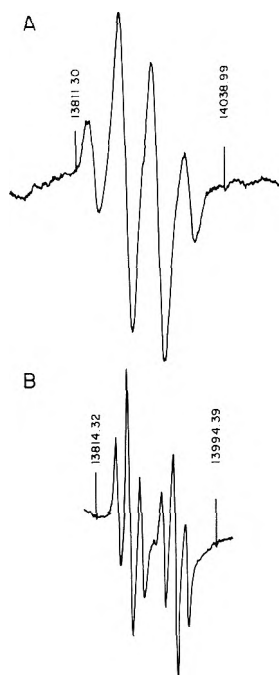
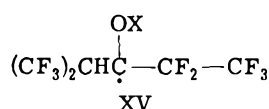


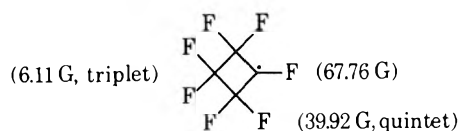
Figure 6. ESR spectra of the trifluoroacetyl radical (A, -97°) and of the perfluoropropionyl radical (B, -135°) obtained by photolysis of cyclopropane solutions containing di-*tert*-butyl peroxide and trifluoroacetaldehyde and pentafluoropropionaldehyde, respectively.

lution of $(\text{CF}_3)_2\text{CHCOCF}_2\text{CF}_3$ in dichlorodifluoromethane at room temperature. It consists of a well-separated triplet of 26.46 G further split into a complex pattern of many lines. Interestingly, the central pattern appears with reduced amplitude relative to the wing multiplets (selective line broadening) indicating a pair of exchanging spins of $1/2$. We believe this stable species to be radical XV in which X may be the $(\text{CF}_3)_2\text{CH}$ or the CF_3CF_2 group. The triplet is

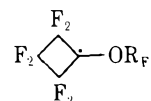


clearly associated with the two β - CF_2 fluorines which undergo exchange between two conformational positions.

We have also briefly examined the photolysis of perfluorocyclobutanone. This ketone is interesting since previous photochemical product studies²² have shown the formation of perfluorocyclopropane as well as tetrafluoroethylene. Photolysis in the esr cavity of this ketone dissolved in dichlorodifluoromethane at -30° produces an intense spectrum which clearly represents the superposition of two similar quintets of triplets of different intensities (approximately 2:1). For the major species the couplings are $a^{\text{F}}(\text{quintet}) = 50.91$ G and $a^{\text{F}}(\text{triplet}) = 11.22$ G, while for the minor species they are $a^{\text{F}}(\text{quintet}) = 49.06$ G and $a^{\text{F}}(\text{triplet}) = 10.32$ G ($\Delta H = 1.0$ G). Because of their large magnitudes, the quintets show second-order splittings for the $M_1 = \pm 1$ and $M_1 = 0$ lines. Product studies now in progress will be needed to identify these radicals. Our results are nevertheless noteworthy, since they show that the photolysis of perfluorocyclobutanone solutions at low temperatures afford radicals which retain the integrity of the cyclic carbon framework. This conclusion is reached by comparison with the fluorine couplings in the perfluorocyclobutyl radical²³ at -60° .

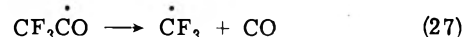
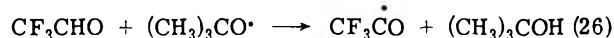


We propose that two types of adduct radicals such as XVI are involved with different R_F groups.

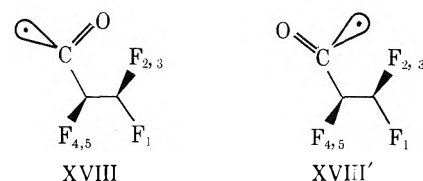
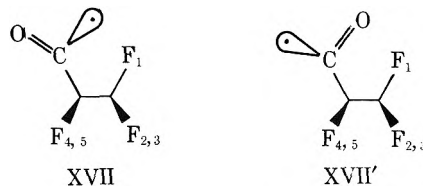


XVI

II. Perfluoroacyl Radicals. The stability of the trifluoroacetyl radical is a subject of considerable controversy.^{5,9} Our attempts to identify this radical in the low-temperature photolysis of HFA were hampered by the presence of other radical species. The esr spectrum of this radical can be obtained, however, by photolysis of a cyclopropane solution containing di-*tert*-butyl peroxide and trifluoroacetaldehyde below -80° and at high microwave powers (Figure 6A). The spectrum consists of a broad ($\Delta H = 4$ G) quartet of 11.54-G splitting with the unusually low g factor of 2.00104. Such low g factors are typical for acyl radicals^{2e,f} as well as for other σ radicals.²⁴ Above -80° , this spectra is replaced by that of the $\dot{\text{C}}\text{F}_3$ radical which becomes progressively more intense as the temperature is raised. Gas evolution can also be observed at higher temperatures. These observations are consistent with abstraction of the aldehydic hydrogen atom to give the trifluoroacetyl radical which readily decarbonylates above -80° .



The perfluoropropionyl radical can similarly be generated from perfluoropropionaldehyde in cyclopropane solutions below -100° . Above this temperature the spectrum is replaced by that of the $\text{CF}_3\dot{\text{C}}\text{F}_2$ radical formed from the acyl radical by loss of CO (bubbling accompanies experiments above -100°). The spectrum of the perfluoropropionyl radical (Figure 6B) is quite unusual in that it consists of a doublet of 16.1 G further split into triplets of 4.44 G (-124°). The low g factor of 2.00075 leaves little doubt that this spectrum indeed belongs to $\text{CF}_3\text{CF}_2\dot{\text{C}}\text{O}$. The doublet splitting could imply a CF_3 group "locked" in such a conformation as to allow only one of the three γ fluorines to interact appreciably with the unpaired electron localized in an sp^2 -hybrid orbital. Four conformations consistent with the equivalence of the β fluorines are depicted in projection below. Conformation XVII' can almost certainly be



excluded from consideration since space-filling models in-

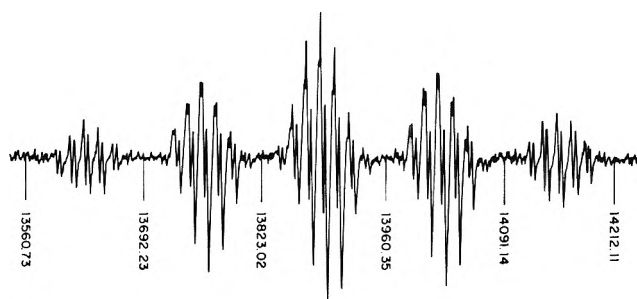
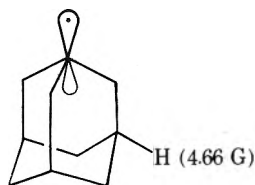


Figure 7. Esr spectrum of the radical $(\text{CF}_3\text{CF}_2)_2\dot{\text{C}}\text{OH}$ obtained by photolysis of perfluoroethyl ketone in cyclopropane at -40° .

dicates a severe steric interaction between the oxygen and the F_1 atom. Furthermore, the eclipsing of the two β fluorines with two of the γ fluorines in this conformation, as well as in conformation XVII, must surely represent an endoenergetic situation. The most likely equilibrium conformations for the radical appear to be XVIII and XVIII', which are related by a rotation of 180° of the carbonyl group about the $\text{C}_\alpha\text{-C}_\beta$ bond. These conformations may indeed interconvert rapidly. We propose that conformation XVIII is the more highly populated since this structure is more likely to give rise to the unusually large γ -hyperfine interaction (16.1 G). Indeed, a W bonding arrangement exists in this conformation comprising the axis of the sp^2 -hybrid orbital, the two C-C bonds, and the C-F₁ bond. In another σ radical, the adamantyl^{24b} radical shown below, a



similar W bonding arrangement also led to a large γ hyperfine interactions. Molecular orbital calculations are now underway to clarify this unusual effect. Interestingly, the magnitude of the β -fluorine coupling is temperature dependent, varying smoothly from 4.15 G at -135° to 4.71 G at -108° , while the doublet splitting is essentially constant (16.10 and 16.02 G, respectively). Torsional motions about the $\text{C}_\alpha\text{-C}_\beta$ bond must be responsible for this dependence. The positive sign of the temperature coefficient is also consistent with the magnitude of the fluorine coupling in $\text{CF}_3\dot{\text{C}}\text{O}$ (11.54 G), which could be taken as the high-temperature limit for a freely rotating $\beta\text{-CF}_2$ group in $\text{CF}_3\text{CF}_2\dot{\text{C}}\text{O}$.

It should be noted that the perfluoropropionyl radical could not be detected above -100° , while the trifluoroacetyl radical under identical experimental conditions, gave a rather good spectrum up to -80° . We believe that this observation implies a lower activation energy for decarbonylation in the perfluoropropionyl radical.

III. Photoreduction of Fluoroalkyl Radicals and α -Hydroxyfluoroalkyl Radicals. The formation of the α -hydroxyhexafluoroisopropyl radical IX (eq 16) during photolysis of HFA and trifluoroacetaldehyde has been discussed above. The intense esr spectra (Figure 2) obtained by this photochemical reaction no doubt reflect the ease with which the aldehydic hydrogen can be abstracted by the photoexcited HFA molecule. Much less reactive hydrogen atoms can also be abstracted by photoexcited HFA. Thus, photolysis of HFA in cyclopropane also produces the esr spectrum of the

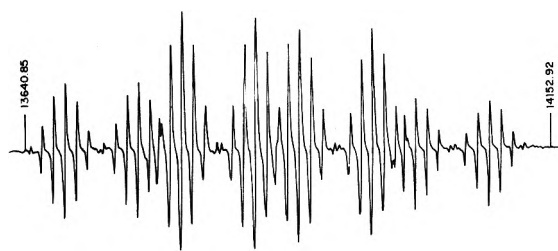
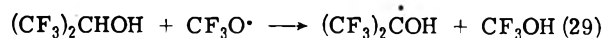


Figure 8. Esr spectrum of radical XX formed during irradiation of perfluoroisopropyl trifluoromethyl ketone in cyclopropane at -35° .

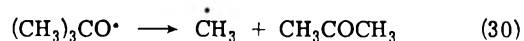
α -hydroxyperfluoroisopropyl radical (Table I) over a broad temperature range. No spectral evidence for the cyclopropyl radical was obtained, however, although it is necessarily formed in these experiments. Spectra of adducts formed by radical addition to the oxygen atom of ground-state HFA were also absent. The spectrum of the α -hydroxyperfluoroisopropyl radical can also be obtained by photolysis of HFA and hexafluoroisopropyl alcohol (HFIP) in Freon solvents, or by hydrogen abstraction from the same alcohol with trifluoromethoxy radicals generated photochemically



from bis(trifluoromethyl) peroxide. The α -hydroxytrifluoroisopropyl radical (Table I) can similarly be generated from 1,1,1-trifluoroisopropyl alcohol. Interestingly, *tert*-

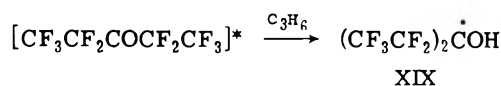


t-butoxy radicals are not capable of abstracting efficiently the two hydrogen atoms from HFIP, indicating that this alcohol is a poor hydrogen donor. Thus, photolysis of dilute solutions of HFIP and di-*tert*-butyl peroxide in dichlorodifluoromethane gives rise only to the spectrum of the methyl radical even at very low temperatures (-100°). With more concentrated solutions, a very weak spectrum of IX can be observed but the major radical species remains the $\dot{\text{C}}\text{H}_3$ radical. The latter can also be observed by irradiating di-*tert*-butyl peroxide alone in dichlorodifluoromethane. These observations are unusual since they imply β scission of *tert*-butoxy radicals which we have never observed di-



rectly in hydrocarbon solvents, including cyclopropane. We conclude that the absence of abstractable hydrogens in inert fluorocarbon solvents promotes β scission of *tert*-butoxy radicals as a favorable alternative to their recombination to regenerate the peroxide.

Photolysis of other fluoroalkyl radicals in cyclopropane produces the corresponding α -hydroxyfluoroalkyl radicals by photoreduction. Thus, photolysis of a dilute solution of



perfluoroethyl ketone in cyclopropane at -40° yields the spectrum of radical XIX (Figure 7) as the sole observable radical species, consisting of a quintet (30.74 G), from four α fluorines, of septets (3.68 G), from six CF_3 fluorines, further split into small doublets (1.15 G) by the hydroxylic proton. Similarly, photolysis of a dilute cyclopropane solution of perfluoroisopropyl trifluoromethyl ketone at -35° gives a particularly intense spectrum of radical XX (Figure 8) showing a quartet ($a_\alpha^{\text{CF}_3} = 26.70$ G) of doublets ($a^{\text{CF}} = 16.78$ G) of septets ($a_\gamma^{\text{CF}_3} = 2.61$ G). No observable splitting for the hydroxylic proton is observed in this case. It is

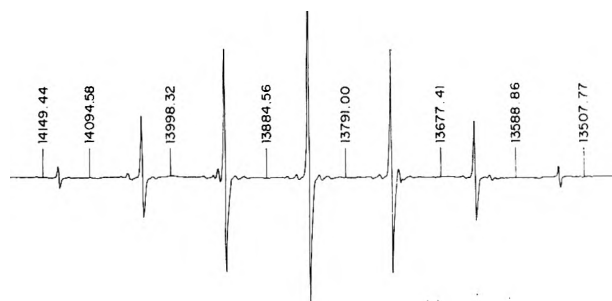
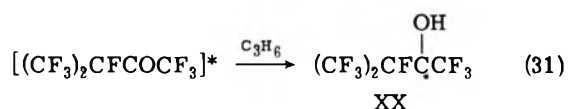


Figure 9. ESR spectrum (septet) of the $(\text{CF}_3)_2\dot{\text{C}}\text{OSiEt}_3$ radical resulting by addition of triethylsilyl radicals to hexafluoroacetone at -40° in a cyclopropane solution. Some of the minor peaks are due to hyperfine interaction with ^{29}Si .

TABLE II: ESR Parameters of Silyl Adducts to Fluoroketones and Related Radicals

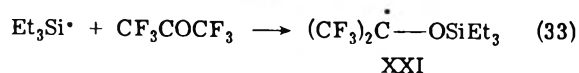
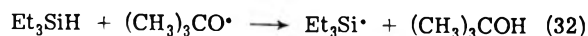
Radical	T, °C	Proton and fluorine isotropic coupling constants, G
$(\text{CF}_3)_2\dot{\text{C}}\text{OSiEt}_3$	-118	CF_3 : 23.24
$(\text{CF}_3)_2\dot{\text{C}}\text{OSiEt}_3$	-47	23.28
$\text{CF}_3\dot{\text{C}}(\text{CH}_3)\text{OSiEt}_3^a$	<i>b</i>	CF_3 : 28.8 CH_3 : 21.5
$(\text{CH}_3)_2\dot{\text{C}}\text{OSiEt}_3$	-121	CH_3 : 19.95
$(\text{CF}_3)_2\dot{\text{C}}\text{OH}$	-55	CF_3 : 23.94
$(\text{CH}_3)_2\dot{\text{C}}\text{OH}^c$	26	CH_3 : 19.66
$\text{F}_2\dot{\text{C}}\text{OSiEt}_3$	-86	$\alpha\text{-F}$: 147.6 ^{29}Si : 1.9
$(\text{CF}_3\text{CF}_2)_2\dot{\text{C}}\text{OSi}(n\text{-Bu})_3$	-60	CF_2 : 30.31 CF_1 : 3.65
$\text{F}-\dot{\text{C}}-\text{OSiEt}_3$	-63	$\beta\text{-F}$: 51.53 $\gamma\text{-F}$: 10.98
$\text{F}-\dot{\text{C}}-\text{F}^d$	-60	$\beta\text{-F}$: 39.92 $\gamma\text{-F}$: 6.11
		$\alpha\text{-F}$: 67.76
$\text{F}-\dot{\text{C}}-\text{O}^-^e$	+25	$\beta\text{-F}$: 82.9 $\gamma\text{-F}$: 37.33

^a From ref 26a. ^b Not given in ref 26a. ^c From R. Livingston and H. Zeldes, *J. Chem. Phys.*, **44**, 1245 (1966). ^d From ref 23. ^e J. L. Gerlock and E. G. Janzen, *J. Phys. Chem.*, **72**, 1832 (1968).



also noteworthy that radical XX decays after shuttering the light. A lifetime of about 6 sec for this radical underscores the already mentioned stabilizing effect of α -perfluoroisopropyl groups on fluoroalkyl radicals.

IV. Homolytic Additions to Fluoroketones. Silyl radicals generated from silanes and *tert*-butoxy radicals²⁵ add efficiently to fluoroketones at the oxygen site.^{10,26} The ESR spectrum of the adduct XXI (Figure 9) is obtained on pho-



tolysis of a dilute cyclopropane solution containing HFA, triethylsilane, and di-*tert*-butyl peroxide. The septet splitting ($a^{\text{CF}_3} = 23.28$ G at -47°) is relatively temperature independent as shown in Table II, and no line width effects were observed down to -120° .

Related α -siloxyfluoroalkyl radicals were also obtained in a similar manner from perfluoroethyl ketone and perfluorocyclobutanone with or without added di-*tert*-butyl peroxide (Table II). In the latter case, the photoexcited fluoroketone must abstract the hydrogen attached to silicon in

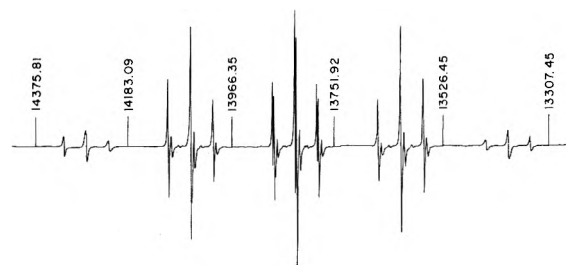


Figure 10. ESR spectrum of the radical resulting by addition of triethylsilyl radicals to perfluorocyclobutanone in a cyclopropane solution at -55° . The additional splittings of the inner triplets are due to second-order effects.

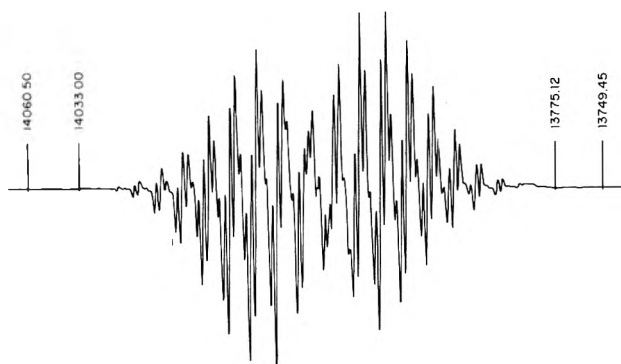
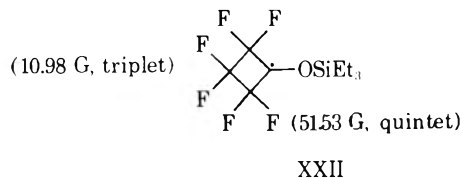


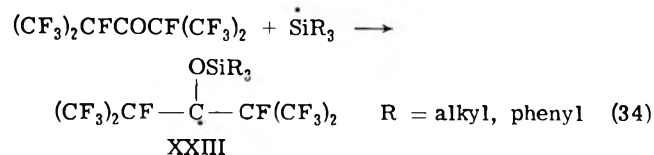
Figure 11. ESR spectrum of radical XXIII obtained by addition of tri-*n*-butylsilyl radicals to perfluoroisopropyl ketone at -28° in a cyclopropane solution.

the initial radical process. The resulting α -hydroxyfluoroalkyl radicals could not be observed, presumably because of their participation in a chain reaction. These spectra are unusually intense as seen in Figure 10 for radical XXII. No



indication of resolvable structure due to the protons of the siloxy groups was obtained for these radicals.

The most dramatic demonstration of the attenuation of radical reactivity by bulky fluoroalkyl substituents attached to a carbon radical center is afforded by the photochemical reaction between perfluoroisopropyl ketone and a variety of silanes. Thus, the intense spectrum of Figure 11 is obtained at -28° when a dilute cyclopropane solution containing perfluoroisopropyl ketone and tri-*n*-butylsilane (10:1:1 v/v) is briefly irradiated with uv light. The radical species giving rise to this spectrum is stable indefinitely in the original sealed tube. The doublet splitting of 16.5 G is the only feature of the spectrum which can be immediately recognized. By analogy with the simpler fluoroketones, we attribute this spectrum to the siloxy radical XXIII ($\text{R} = n$ -



butyl). The observation of only one doublet as the largest fluorine hyperfine splitting for the series of radicals XXIII,

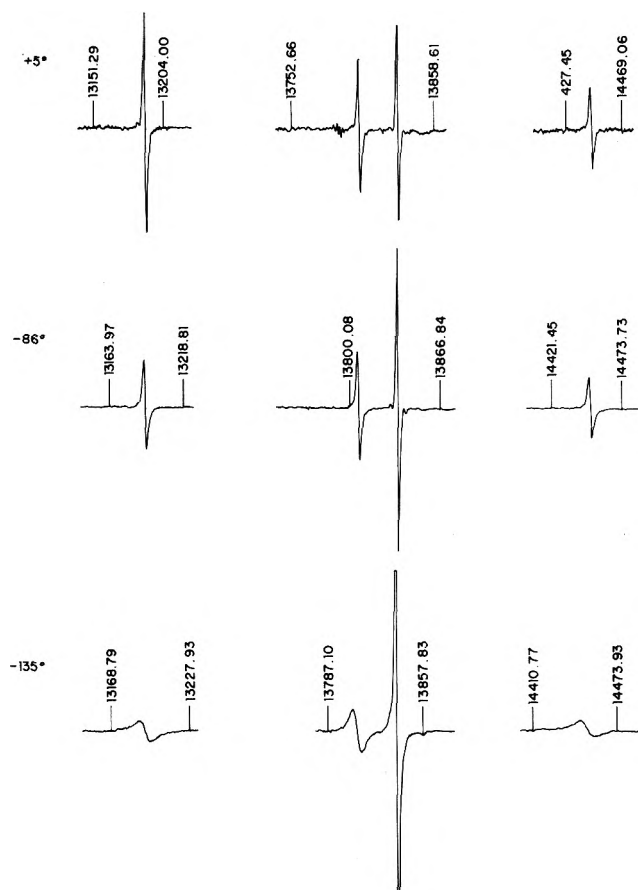
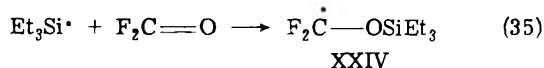


Figure 12. Temperature dependence of the line shapes in the esr spectrum of the $\text{CF}_2\text{OSiEt}_3$ radical.

indicates two conformationally nonequivalent perfluoroisopropyl groups. The two β fluorines are therefore locked in specific orientations relative to the half-occupied p orbital on the central carbon in such a manner that only one fluorine interacts appreciably (16.5 G) with the unpaired electron. A more complete account of the esr spectra of these uniquely stable fluoroalkyl radicals will be reported elsewhere.²⁷

Triethylsilyl radicals add to carbonyl fluoride in cyclopropane solutions to afford the $\alpha\alpha$ -difluoromethyl adduct XXIV shown in Figure 12. The hyperfine pattern at $+5^\circ$



consists of a triplet of 147.5 G, in which the $M_1 = 0$ line shows a large second-order splitting. The triplet splitting is essentially independent of temperature, being 147.6 G at -135° . It should be noted that this splitting is larger than the fluorine splitting in the trifluoromethyl radical¹²⁻¹⁴ (144.1 G at -90°) indicating that the siloxydifluoromethyl radical is slightly more pyramidal than the trifluoromethyl radical. At -86° satellite lines due to splitting by ^{29}Si can be seen flanking the narrowest line of the spectrum and separated by 1.9 G.

As the temperature is lowered, the two $M_1 = \pm 1$ lines are selectively broadened together with only the low-field $M_1 = 0$ line. Below -135° this broadening is so severe as to make these lines undetectable. In the absence of unusual relaxation effects, the four lines of the spectrum in Figure 12 should be of equal amplitude. Unfortunately, the steady-state concentration of $\text{F}_2\text{COSiEt}_2$ diminished rapidly at the

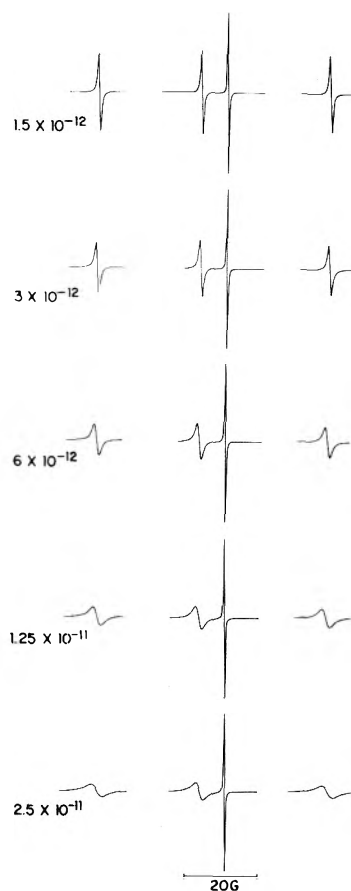
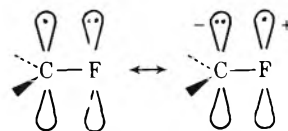


Figure 13. Calculated line shapes for the radical $\dot{\text{C}}\text{F}_2\text{OSiEt}_3$ as a function of the rotational correlation time in sec (see text).

highest temperature studied ($+5^\circ$) and the true intensities were difficult to record in the entire spectrum. This problem was less severe at lower temperatures and fairly accurate relative line intensities could be obtained. The spectra at -86 and -135° clearly show that the outer lines and the low-field second-order line become progressively broader as the temperature is lowered. The relatively small temperature dependence and the strong solvent (viscosity) dependence of this selective line broadening indicate a relaxation process which is dependent on the tumbling motion of the radical in solution as previously presented for $\dot{\text{C}}\text{F}_3$, $\text{CH}_3\dot{\text{C}}\text{F}_2$, and $\text{CF}_3\dot{\text{C}}\text{F}_2$.^{13,4,28}

Experimental studies on fluorinated radicals in single crystals and theoretical considerations indicate that the anisotropic component (dipolar component) of the hyperfine coupling tensor in α -fluoroalkyl radicals is very large relative to the anisotropy of the coupling to α protons.²⁹ The origin of this large dipolar interaction in α -fluoroalkyl radicals can be attributed to the presence of substantial unpaired spin density in nonbonding p orbitals on fluorine arising through the p- π interaction which confers to the trivalent carbon at the radical center some of the properties of carbanions including the pyramidal configuration typical of α -fluoroalkyl radicals.¹⁴ Modulation of this elec-



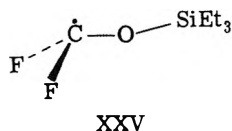
tron spin-nuclear spin dipolar interaction by the tumbling

of the radical in solution provides an efficient relaxation mechanism.

A relaxation-matrix analysis of a spin system undergoing dipolar relaxation was carried out by assuming that the two fluorine nuclei in a CF_2 fragment are completely equivalent (that is, that the anisotropic part of the hyperfine tensor has the same orientation for both fluorine nuclei) and that they have an axially symmetric hyperfine tensor. The dipolar contributions to the line widths of the wing lines ($M_1 = \pm 1$) and of the second-order line was given previously.^{13,14,30}

As can be seen from Figures 12 and 13, the calculated and observed spectra are in good qualitative agreement for this model. In these calculations the anisotropic component of the A tensor in $\text{CF}_2\text{OSiEt}_3$ was represented by $A_{\parallel} = 108$ G and $A_{\perp} = -54$ G. These values were obtained for the $\dot{\text{C}}\text{F}_3$ radical in a single crystal study.³¹

The temperature-dependent line width effect in the spectrum of $\text{F}_2\dot{\text{C}}\text{OSiEt}_3$, thus, can be attributed solely to dipolar broadening. The absence of other dynamic processes (in particular, modulation of the fluorine hyperfine splitting due to a mutual exchange process) suggests that the radical exists in a stable symmetric conformation such as XXV. Furthermore, the small γ - ^{29}Si splitting of 2 G con-



trasts with that observed in the alkyl analog, $\text{Et}_3\text{SiCH}_2\dot{\text{C}}\text{H}_2$ ($a^{\text{Si}} = 37.4$ G),³² and it may be due to the highly pyramidal radical center or an expanded $\text{C}_a\text{-O-Si}$ angle [compare also ref 18].

Conclusions

The esr study presented in this paper serves primarily to identify and characterize some of the transient paramagnetic species formed during ultraviolet irradiation of fluoroketones. We surmise that photolysis of perfluoroketones is similar to that of their hydrocarbon analogs with several outstanding exceptions. Thus, products of type I cleavage (eq 1) are observed in inert fluorocarbon solvents, and intermolecular processes (eq 3) are observed in protiated solvents. However, the formation of adducts, such as V' from hexafluoroacetone and the analogous species from higher perfluoroketones as the principal radical species in inert solvents, suggests that radical addition to perfluoroketones is a significantly more facile process than it is with alkyl ketones. Another major difference pertains to the greater thermal instability of perfluoroacyl radicals derived by type I scission of fluoroketones which lose carbon monoxide much more readily than their hydrocarbon analogs. Chemical studies have indicated that addition can occur at both the C and O termini of the carbonyl function. The observation of α -perfluoroalkoxyfluoroalkyl radicals is consistent with addition to oxygen. ESR studies in solution are unable to evaluate the importance of radical addition to C, since the fluoroalkoxy radicals so formed cannot be detected by esr. Photoexcited fluoroketones in their triplet states are powerful hydrogen abstracting agents as evidenced by their photoreduction in the presence of even poor hydrogen donors such as cyclopropane. Silicon-centered radicals are particularly prone toward addition to the oxygen terminus of fluoroketones. Addition of silyl radicals to sterically

crowded ketones results in the formation of extraordinarily stable fluoroalkyl radicals. Additional chemical studies would be highly desirable to elucidate further the apparent diversity of radical processes in the photochemistry of fluoroketones in solution.

Experimental Section

The fluoroketones in this study were kindly supplied by Drs. D. C. England, E. G. Howard, W. J. Middleton, and J. E. Nottke. Bis(hexafluoroisopropyl) ether was donated by W. J. Middleton. 1,2-Bis(trifluoromethyl)perfluorocyclobutane was a gift from Dr. P. R. Resnick. The remaining fluoroorganic compounds were either Du Pont materials or were obtained from P.C.R. Inc. and the Aldrich Chemical Co.

Hexafluoroisopropyl trifluoroacetate was prepared by adding a 10% excess of trifluoroacetic anhydride dropwise to hexafluoroisopropyl alcohol at 0° followed by a similar addition of pyridine (10% excess). The mixture was allowed to stand for 1 day and worked up by diluting with ice water, washing the upper phase with water, and drying it over anhydrous magnesium sulfate. Distillation afforded 30% of hexafluoroisopropyl trifluoroacetate boiling at 44.5° . The proton nmr spectrum consisted of a binomial septet at δ 5.77 ppm.

Trifluoroacetaldehyde was generated by dropwise addition of trifluoroacetaldehyde methyl hemiacetal (P.C.R. Inc.) to polyphosphoric acid at 150° . Essentially pure trifluoroacetaldehyde distilled off and was used immediately. Perfluoropropionaldehyde was similarly prepared from the corresponding hemiacetal.

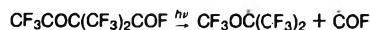
The technique for sample preparation and the esr instrumentation were described previously.^{18a}

Acknowledgments. We are grateful to Drs. D. C. England, E. G. Howard, W. Mahler, W. J. Middleton, J. E. Nottke, W. A. Sheppard, and P. R. Resnick (Du Pont) for many samples and useful discussions and to Mr. B. F. Gordon for technical assistance. K. S. C. wishes to thank the National Science Foundation for financial support.

References and Notes

- (1) (a) E. I. du Pont de Nemours and Company. (b) Department of Chemistry, Indiana University. (c) Contribution No. 2135 from E. I. du Pont de Nemours and Co. (d) Contribution No. 2392 from the Department of Chemistry, Indiana University.
- (2) (a) P. J. Wagner and G. S. Hammond, *Advan. Photochem.*, **5**, 21 (1968); (b) P. J. Wagner, *Accounts Chem. Res.*, **4**, 163 (1971); (c) D. Bryce-Smith, "Special Periodical Reports on Photochemistry," Vol. I, II, III, Chemical Society, London, 1970, 1971, 1972; (d) J. C. Dalton and N. J. Turro, *Annu. Rev. Phys. Chem.*, **21**, 499 (1970); (e) H. Paul and H. Fischer, *J. Chem. Soc., Chem. Commun.*, 1038 (1971); *Helv. Chim. Acta*, **56**, 1575 (1973); (f) H. E. Chen, S. P. Vaish, and M. Cocivera, *J. Amer. Chem. Soc.*, **95**, 7586 (1973).
- (3) (a) C. G. Krespan and W. J. Middleton, *Fluorine Chem. Rev.*, **1**, 145 (1967); (b) H. P. Braendlin and E. T. McBee, *Advan. Fluorine Chem.*, **3**, 1 (1963); (c) J. Heicklen, *Advan. Photochem.*, **7**, 57 (1969).
- (4) W. A. Sheppard and C. M. Sharts, "Organic Fluorine Chemistry," W. A. Benjamin, New York, N. Y., 1969, p 437 ff.
- (5) (a) P. S. Ayscough and E. W. R. Steacie, *Proc. Roy. Soc., Ser. A*, **234**, 476 (1956); (b) J. S. McIntosh and G. B. Porter, *Trans. Faraday Soc.*, **64**, 119 (1968); (c) S. L. Chong and S. Toby, *J. Phys. Chem.*, **74**, 2801 (1970).
- (6) P. Svejda, *J. Phys. Chem.*, **76**, 2690 (1972).
- (7) A. S. Gordon, *J. Chem. Phys.*, **36**, 1330 (1962).
- (8) P. R. Resnick, personal communication.
- (9) B. G. Tucker and E. Whittle, *Proc. Chem. Soc.*, 93 (1963); *Trans. Faraday Soc.*, **61**, 484 (1965).
- (10) E. G. Howard, P. B. Sargeant, and C. G. Krespan, *J. Amer. Chem. Soc.*, **89**, 1422 (1967).
- (11) W. H. Urry, A. Nishihara, and J. H. Y. Niu, *J. Org. Chem.*, **32**, 347 (1967).
- (12) R. W. Fessenden and R. H. Schuler, *J. Chem. Phys.*, **43**, 2704 (1965).

- (13) P. Meakin and P. J. Krusic, *J. Amer. Chem. Soc.*, **95**, 8185 (1973).
 (14) K. S. Chen, P. J. Krusic, P. Meakin, and J. K. Kochi, *J. Phys. Chem.*, **78**, 2014 (1974).
 (15) M. C. R. Symon, *J. Amer. Chem. Soc.*, **91**, 5924 (1969).
 (15a) *Note Added in Proof*. This assignment has recently been confirmed by the detection of radical V' formed by type I cleavage during the photolysis of $\text{CF}_3\text{OC}(\text{CF}_3)_2\text{COF}$ in inert fluorocarbon solvents.



We thank Dr. P. R. Resnick for suggesting this experiment and a sample of the fluoroacyl fluoride. ESR studies of the radicals involved in the photolysis of fluoroacyl halides are in progress.

- (16) R. C. Bingham and M. J. S. Dewar, *J. Amer. Chem. Soc.*, **95**, 7182 (1973); *cf.* also A. J. Dobbs, B. C. Gilbert, and R. O. C. Norman, *J. Chem. Soc. A*, 124 (1971).
 (17) P. J. Krusic, P. Meakin, and J. P. Jessor, *J. Phys. Chem.*, **75**, 3438 (1971).
 (18) (a) P. J. Krusic and J. K. Kochi, *J. Amer. Chem. Soc.*, **93**, 846 (1971); (b) K. S. Chen, P. J. Krusic, and J. K. Kochi, *J. Phys. Chem.*, **78**, 2030 (1974).
 (19) P. J. Krusic, manuscript in preparation.
 (20) R. B. Lloyd and M. T. Rogers, *J. Amer. Chem. Soc.*, **95**, 1512 (1973).
 (21) P. J. Krusic and P. Meakin, manuscript in preparation.
 (22) (a) D. England, *J. Amer. Chem. Soc.*, **83**, 2205 (1961); (b) D. Phillips, *J. Phys. Chem.*, **70**, 1235 (1966).
 (23) B. S. Smart and P. J. Krusic, manuscript in preparation.
 (24) (a) P. J. Krusic and T. A. Rettig, *J. Amer. Chem. Soc.*, **92**, 722 (1970); (b) P. J. Krusic, T. A. Rettig, and P. v. R. Schleyer, *ibid.*, **94**, 995 (1972).
 (25) P. J. Krusic and J. K. Kochi, *J. Amer. Chem. Soc.*, **91**, 3938 (1969).
 (26) A. J. Bowles, A. Hudson, and R. A. Jackson, *J. Chem. Soc. B*, 1947 (1971); J. Cooper, A. Hudson, and R. A. Jackson, *J. Chem. Soc., Perkin Trans. 2*, 1933 (1973).
 (27) P. J. Krusic, manuscript in preparation.
 (28) K. S. Chen and J. K. Kochi, *Chem. Phys. Lett.*, **23**, 233 (1973); *J. Amer. Chem. Soc.*, **96**, 794 (1974).
 (29) (a) M. Iwasaki, *Fluorine Chem. Rev.*, **5**, 1 (1971); (b) A. Hudson and K. D. J. Root, *Advan. Mag. Resonance*, **5**, 1 (1971).
 (30) J. Cooper, A. Hudson, R. A. Jackson, and M. Townson, *Mol. Phys.*, **23**, 1155 (1972).
 (31) M. T. Rogers and L. D. Kispert, *J. Chem. Phys.*, **46**, 3193 (1967).
 (32) P. J. Krusic and J. K. Kochi, *J. Amer. Chem. Soc.*, **91**, 6161 (1969).

Electron Spin Resonance Measurement of Ammonia Condensed at 77°K after Reaction with Discharge Products and after High-Frequency Discharge

F. W. Froben¹

Max-Planck-Institut für Biophysikalische Chemie Abteilung Spektroskopie, D 34 Göttingen-Nikolausberg, Germany

(Received March 22, 1974)

Publication costs assisted by the Max-Planck-Gesellschaft

Amino radicals are condensed at 77°K from the vapor of a fast flow system. The esr spectra are somewhat different for the discharge (where their shape depends on HF discharge energy and pressure) and for the reaction of discharge products from N_2 , H_2 , and Ar with ammonia, added through an inlet between the discharge and the detection system. The differences can be caused by the environment of the radicals and by signals from other radicals.

Introduction

Electron impact excitation of ammonia at 2×10^{-5} to 5×10^{-3} Torr yield NH radicals as primary products.^{2a} Above 10^{-2} Torr is a small contribution of NH_2 radicals, visible by emission of the α bands of ammonia (2A_1). In gas-phase photolysis,^{2b} pulse radiolysis,³ and in reaction of atoms with ammonia⁴ NH radicals have been found as well as NH_2 radicals. By condensation of the radicals from a fast flow system and subsequent esr measurement it was possible to obtain further information on this system. For better identification deuterated ammonia is used as well.

Esr spectra of ammonia at 77°K have been measured after γ -irradiation,⁵⁻⁹ photolysis,^{5,6,10} and electron impact.^{5,11} The spectra have been ascribed to amino radicals with one exception, which has been corrected by private communication. NH radicals have been observed only by their uv spectra¹² and the lack of esr spectra is explained by broadening of the resonance lines even at 4°K. The present investigation deals with the measurement of amino radicals at 77°K and the variation of the esr spectra found for different experimental conditions.

Experimental Section

The apparatus is shown in Figure 1. Radicals are produced in a fast flow system by a microwave discharge (Microtron 200, 2.45 GC) and condensed on a cold finger at 77°K inside the esr cavity. The position of the discharge and the substrate inlet can be varied along the flow tube. The distance between cold finger and discharge varied from 50 to 100 cm and between substrate inlet and cold finger from 5 to 25 cm. That corresponds at the linear flow velocity of 1000 cm/sec (at the pressure used for most experiments and measured by the disappearance of esr signals in the gas phase with different positions of the discharge) to a time of 0.05–0.1 sec for the discharge products to reach the cold finger and for the added materials 0.005–0.025-sec flow time until they are condensed. The total pressure was varied between 5×10^{-3} and 1 Torr and the discharge energy between 15 and 150 W. The deposit was collected for a constant time of 10 min for all experiments, after checking the linear dependence of esr signal intensity with time of deposition.

The discharge in flowing ammonia is a very complex sys-

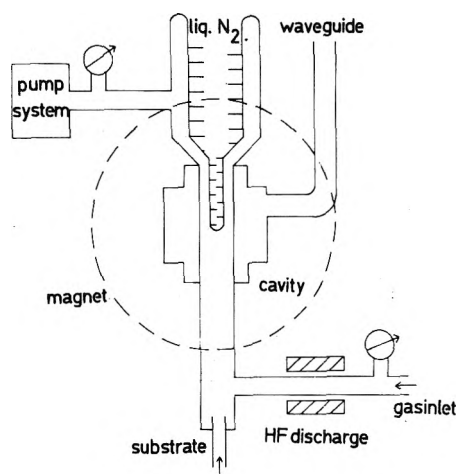


Figure 1. Experimental arrangement. The position of discharge and substrate inlet can be moved relative to the cold finger.

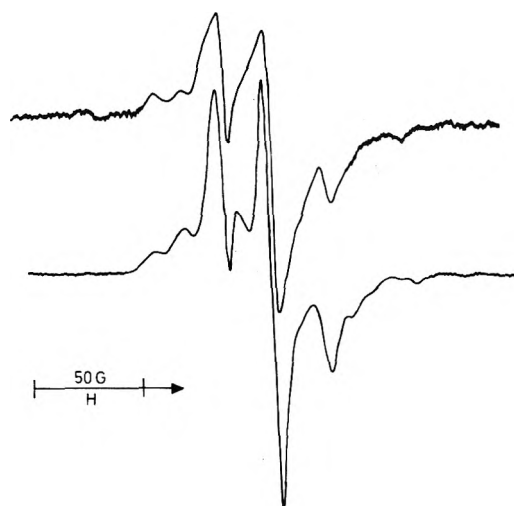


Figure 2. ESR spectra of deposition from NH_3 discharge at 0.3 Torr and 20-W discharge energy (upper trace) and from N_2 discharge (20 W) with addition of ammonia (lower trace): $\text{N}_2:\text{NH}_3 = 2:1$, total pressure 0.3 Torr, relative intensities 1:2.5.

tem. End products¹³ are, besides ammonia, hydrazine (up to ~10%), H_2 , and N_2 . In the gas phase H and N atoms can be observed by esr.

Esr spectra are measured using a Varian X-Band spectrometer with cylinder cavity V-4135 and 100 kHz modulation.

NH_3 (Matheson Anhydrous 99.99%), ND_3 (Stohler Isotope Chemicals 99% D), N_2 (L'Air liquide 99.9992%), H_2 , and Ar (Messer Griesheim >99.998% purity) were used as received.

Results

A. Reaction of Discharge Products with Ammonia. The 77°K esr spectra obtained by discharge in N_2 , H_2 , or Ar and addition of ammonia to the flowing gas are due to amino radicals.

By moving the discharge and the ammonia inlet position it can be shown that the reaction of the N_2 discharge products is due to excited N_2 molecules (within an experimental error of 10%). For H_2 discharge it is due to H atoms and for Ar discharge to excited Ar molecules and electrons. The g value and hyperfine splitting constants of the radicals pro-

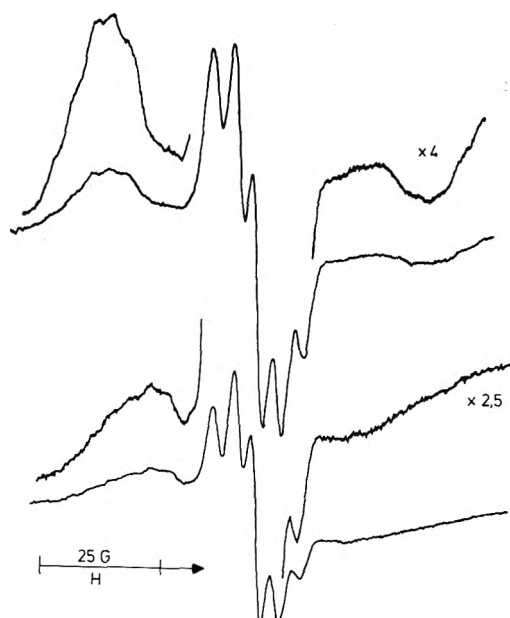


Figure 3. ESR spectra of deposition from ND_3 discharge (20 W) at 0.3 Torr (upper trace) and from the reaction of the N_2 discharge (20 W) with added ND_3 (lower trace): $\text{N}_2:\text{NH}_3 = 2:1$, total pressure 0.2 Torr, relative intensities 1:1.

duced by this method (Figures 2 and 3 bottom) are the same as given in the literature for NH_2 (ND_2). Their relative concentrations under the same experimental conditions are $\text{H}_2:\text{N}_2:\text{Ar} = 1:20:20$. Variation of pressure and HF energy change only the intensity but not the shape of the spectra. Variation of the position of the discharge relative to the cold finger shows a linear dependence of the intensity, but for the N_2 discharge only a 10% change in the 77°K spectra compared to the gas-phase N atom intensities.

B. Discharge in Ammonia. At low discharge energy and "medium" pressure the esr spectra (Figures 2 and 3 top) of the deposit are similar to the spectra produced by method A. The difference for NH_3 is that the two most intense lines are broadened and for ND_3 the outer lines are further apart from the center.

The result of discharge energy variation on the spectra is shown in Figures 4 and 5. For energies above 50 (NH_3) and 80 W (ND_3) respectively the shape of the spectra does not change.

Only at low discharge energy and a pressure below 0.4 Torr can the hyperfine structure be resolved. With increasing power it decreases steadily and vanishes first on the high-field side of the spectrum (Figure 5, two lower recordings).

A similar behavior is observed when the pressure is changed. Above 0.5 Torr at 20-W discharge energy the hyperfine structure disappears. This pressure limit goes down for increasing power. Above 60-W discharge energy the fine structure is not resolved even at the lowest pressure of 5×10^{-3} Torr at which the discharge burns steadily.

Variation of the distance between the discharge and the cold finger causes no effect on the structure but only on the intensity. For maximum variation the intensity is changed by a factor of 2.

C. Reaction of N_2 Discharge on the Deposit (for ND_3 only because of the Fine Structure). At low discharge energy the spectrum is identical with the ammonia discharge. Starting around 40 W some additional features appear on the position of the maximum of the outer lines in the N_2

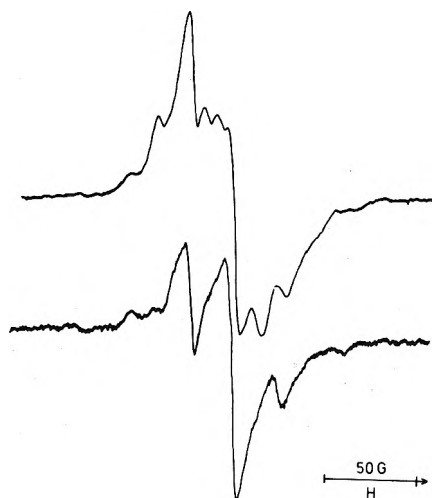


Figure 4. ESR spectra of deposition from NH_3 discharge at 0.1 Torr: upper spectrum, 50-W discharge energy; lower spectrum, 20 W; relative intensities (50 W):(20 W) = 4:1.

discharge plus ammonia case (compare Figure 3). The center is not affected and the fine structure is not changed even for prolonged treatment with active nitrogen. The intensity increases first linearly with time and shows, for times longer than 20 min, a saturation behavior.

D. Discharge in a Mixture of Nitrogen and Ammonia (for ND_3 only). The epr spectra of the deposit from these experiments are very small (less than 10% of the intensity without nitrogen for the same conditions). Treatment of the condensate with active N_2 produces the fine structure of ND_2 as in the experiments on N_2 discharge with addition of ND_3 (part A, Figure 2, bottom). Prolonged treatment causes the fine structure to disappear simultaneously on both sides of the center.

E. Discharge in Ammonia and Addition of N_2 Prior to Condensation. The epr spectra intensity is only 1% of the spectra without addition of N_2 . Reaction of active nitrogen produces ND_2 signals with less resolution on the high-field side. The spectra are comparable to the ammonia discharge signals (Figure 2 top) but their final intensity is a factor of 4 smaller.

Discussion

Solids formed by vapor deposition on a cold surface occur often in different modifications from those obtained by cooling the liquid. The ratio of amorphous material to polycrystalline aggregates depends mostly on the deposition speed, which is different for experiments at low and high pressure and can cause different structures of the solid. X-Ray diffraction studies¹⁴ on condensed ammonia show that there are four different forms at 4°K, including an amorphous modification. The hydrogen bonded structure of ammonia is stable at low temperature⁵ and affects the shape of the spectra.

High pressure condensation can cause a temperature gradient on the surface of the cold finger producing a structure difference perpendicular to the surface.

Two effects found in the experiments need further discussion. First the change in spectra with different discharge energy (Figure 5) especially the difference in the hyperfine splitting on the low- and high-field side and second the difference in the spectra for discharge and for the reactions.

The change in spectra with different discharge energy

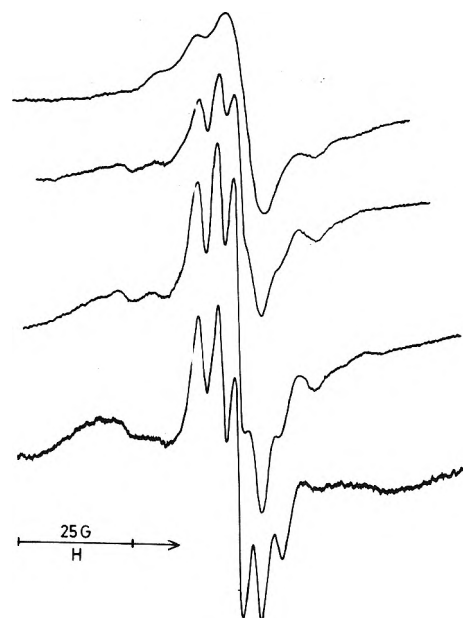


Figure 5. ESR spectra of deposition from ND_3 discharge at 0.4 Torr: discharge energy from top to bottom 80, 65, 50, 20 W; relative intensities 2, 2, 1.5, 1.

can be partly explained by an environment effect. At low discharge energy only ~10% of the ammonia is dissociated (depending on the pressure) and at energies higher than 60 W more than 20% is destroyed in the discharge. This may cause broadening of the lines because of interaction of radicals close to each other.⁵ But this cannot be the only explanation because the spectra in part C still show fine structure.

The difference at low and high field can be explained by the presence of another radical (a singlet or triplet signal with $g = 2.002$). This could be ND_3^+ .¹⁵ The superposition of the observed ND_2 signals at low discharge energy and the ND_3^+ spectra reported affect the splitting at the high-field lines more than the low-field side and cause a growing in of a line between the center and the outer lines which is observed in the experiments (Figure 5).

The second effect (the difference in the spectra for discharge and reactions) has been observed similarly for samples with large differences in the water content.^{6,9} This cause can be excluded for the experiments reported here since the ammonia is the same and the N_2 does not show any epr signal originating from water. However again this difference could be explained by ND_3^+ lines and by hydrogen bonding effects in the environment of the radicals. The most likely explanation is a different modifications of the solid which has been shown to exhibit such differences in the spectra.⁵

The difference in intensity of the signals for varied distance between the production of radicals and condensation is small, compared to the variation in atom intensities and lifetime of radicals under similar conditions. This is important for the ammonia discharge and could be explained by the existence of a long-lived precursor of the amino radical, which can be an excited ammonia molecule.¹⁶ If this is true, the addition of gases could destroy this precursor without generating the radical. The experiments (part E) support this view.

In the discharge through ammonia a number of other radicals, such as, N_2H_3 and more complicated radicals, can be formed, but the spectra for these radicals, which have

been reported in the literature,^{17,18} are different. NH radicals are certainly formed in the gas phase but their stability at 77°K seems unlikely. It is therefore desirable to extend the measurements to lower temperatures.

Acknowledgment. Thanks are due to Professor A. Weller and Dr. E. Sackmann from the MPI in Göttingen for critical reading of the manuscript and valuable comments.

References and Notes

- (1) Address correspondence to Institut für Molekülphysik, Freie Universität Berlin, 1 Berlin 33, Germany.
- (2) (a) H. Bubert and F. W. Froben, *J. Phys. Chem.*, **75**, 769 (1971); (b) K. A. Mantei and E. J. Bair, *J. Chem. Phys.*, **49**, 3248 (1968).
- (3) G. A. Meaburn and S. Gordon, *J. Phys. Chem.*, **72**, 1592 (1968).
- (4) D. C. Carbaugh, F. J. Mumo, and J. M. Marchello, *J. Chem. Phys.*, **47**, 5211 (1967).
- (5) R. Marx and J. Maruani, *J. Chim. Phys.*, **61**, 1604 (1964).
- (6) B. S. Al-Naimy, P. N. Moorthy, and J. J. Weiss, *J. Phys. Chem.*, **70**, 3654 (1966).
- (7) V. A. Roginskii and A. G. Kotov, *Russ. J. Phys. Chem.*, **40**, 88 (1966).
- (8) D. R. Smith and W. A. Seddon, *Can. J. Chem.*, **48**, 1938 (1970).
- (9) I. S. Ginns and M. C. R. Symons, *J. Chem. Soc., Faraday Trans. 2*, **68**, 631 (1972).
- (10) E. L. Chochran, F. J. Adrian, and V. A. Bowers, *J. Chem. Phys.*, **51**, 2759 (1969).
- (11) G. Beuermann, *Z. Phys.*, **247**, 25 (1971).
- (12) L. F. Keyser and G. W. Robinson, *J. Amer. Chem. Soc.*, **82**, 5245 (1960).
- (13) R. Barker, *J. Chem. Soc., Faraday Trans. 1*, **68**, 315 (1972).
- (14) H. S. Peiser in A. M. Bass and H. P. Broida, "Formation and Trapping of Free Radicals," Academic Press, New York, N. Y., 1960, p 301 ff.
- (15) J. K. S. Wan, *Ber. Bunsenges. Phys. Chem.*, **72**, 245 (1968).
- (16) R. Barker, *J. Chem. Soc., Faraday Trans. 2*, **68**, 421 (1972).
- (17) K. V. S. Rao and M. C. R. Symons, *J. Chem. Soc. A*, 2163 (1973).
- (18) R. Fantechi and G. A. Helcké, *J. Chem. Soc., Faraday Trans. 2*, **68**, 924 (1972).

Computer-Recorded Gouy Interferometric Diffusion and the Onsager-Gosting Theory

T. A. Renner and P. A. Lyons*

Department of Chemistry, Yale University, New Haven, Connecticut 06520 (Received April 22, 1974)

Publication costs assisted by Yale University

Using computer-recorded data, a method for the determination of the intensity distribution in Gouy interference patterns has been devised, and the Onsager-Gosting theory for this distribution has been verified. A procedure for obtaining diffusion coefficients from the complete fit of intensity data has been developed. An improved method for determining diffusion coefficients from intensity measurements at a fixed position in the Gouy focal plane has been described and tested.

Introduction

The effect of an index of refraction gradient on slightly convergent light is sketched in Figure 1. If the gradient is produced by diffusion across an initially sharp boundary on the optic axis, an interference pattern will be produced at the focal plane. This Gouy phenomenon was recognized to provide a means for the determination of diffusion coefficients.¹ Soon thereafter, theories were developed which made this possible.²⁻⁴ It was quickly established that accurate values for the diffusion coefficients could be obtained from measurements of the positions of the lower fringe minima as a function of time.⁵ Onsager and Gosting later developed a general theory for the intensity distribution in a Gouy pattern.⁶ An experimental study verified that the O-G theory correctly predicted (1) the ratio of intensities of maxima in the fringe pattern, (2) the linear variation of the intensity of a given maximum with time, and (3) the correct values of D from measurement of the positions of maxima as well as minima.⁷ Instrumental limitations resulted in some questions being left unanswered. Does the O-G theory correctly predict intensities at positions other than maxima? Given the intensity data at all positions, can diffusion coefficients be computed exploiting all the infor-

mation? (The latter question might be pertinent for dealing with skewed boundaries.)

To answer these questions, an experiment was devised which involved rapid photomultiplier scanning of the focal plane. High-speed recording of the photomultiplier output voltage with a computer produced the raw data upon which the subsequent analyses were based. During the work, it became apparent that extremely precise diffusion data could be obtained from recording the time dependence of the intensity at a fixed position in the focal plane. This experimental variation was explored.

Experimental Section

The basic interferometer design used in these experiments has already been described.^{8,9} The equipment for photoelectric scanning was a modification of an earlier study.⁷ A 1P21 RCA photomultiplier tube was enclosed in a light-tight brass housing which in turn was fastened to the carriage of a Gaertner traveling microscope. The brass housing was provided with an adjustable slit set at an opening of about 20 μ for all experiments. (Typical fringe widths in the patterns during observations were about 500 μ .) The carriage was driven up or down by a reversible, di-

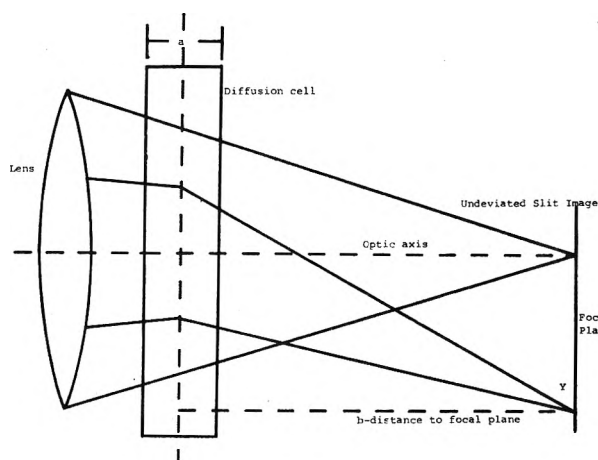


Figure 1. Convergence of light rays for Gouy interference phenomenon: $a = 2.54$ cm; $b = 305.5$ cm; focal length of lens = 60.96 cm.

rectly-coupled, 60 rpm, synchronous motor (Bodine Model KYC-24A2A1). The traveling microscope was fixed to a massive brass mount and the entire assembly was supported on a vibration-free bench.

A Fluke Model 402M power supply was the source of voltage for the photomultiplier. Data were collected with the photomultiplier voltage being typically 900 V dc. The photocurrent was passed through a 100K load resistor and the voltage drop across the resistor was amplified using an operational amplifier with a range of 5 to 50.

After amplification, the output voltage was fed into the analog-to-digital converter of a PDP-12 digital computer. The signals were simultaneously stored on magnetic tape and displayed on an oscilloscope, permitting constant monitoring of the experiment in progress.

The light source was the 5460.7-Å line obtained by use of a Wratten No. 77 filter with an AH4 Hg arc lamp. This lamp was chosen for several reasons: it is remarkably stable and it has rather high intensity. Unfortunately, since it is an ac lamp, the output photomultiplier voltage had considerable ripple. Several features of the PDP-12 were crucial for a solution of the ripple problem. The computer is equipped with a KW12-A crystal clock which may be set to vibrate at a chosen fixed frequency between 100 Hz and 400 kHz. The clock may then control the rate of sampling through the use of appropriate clock-control statements in the general computer program used for data collection. Furthermore, the clock may also be activated with an external signal by means of a Schmitt trigger arrangement which can be used to produce pulses which set the clock flag and allow the analog-to-digital conversion to be performed.

The source for the trigger was the 60-Hz house voltage. At each passage of the wall voltage through zero amplitude with positive slope the trigger was fired. Since the same 60-Hz source was used for the lamp supply, the computer served as a phase-sensitive detector. In fact, the ripple was eliminated from the intensity data. Signals could then be collected at each $\frac{1}{60}$ of a second and be either stored or averaged. Some of the results reported derive from the average of 60 signals recorded each second.

For the scanning experiments, the fringe pattern was recorded from the lowest fringe upward to the optic axis. One revolution of the drive motor corresponded to a 0.10-cm motion of the slit. One intensity point was recorded at each $\frac{1}{60}$ of a second. Since the distance is related to the motor

drive rate, both the time, t , and the distance, Y , from the optic axis to a given fringe position were determined by counting data points on the printed computer output. In our mode of operation, the time interval between points was 0.0166 sec and the distance between points was 0.0017 cm. After the slit had scanned through the lower seven fringes (in about 3 sec), a reference Rayleigh fringe pattern was produced on the optic axis by masking the light source with a set of double-double slits.⁴ When the slit passed through the reference pattern, the position of the optic axis could be readily located.

In the fixed slit procedure, the slit was located at a position appropriate for recording the collapse of about the lower ten fringes, with data collection starting at 1500 sec after the boundary sharpening was completed. Intensities were recorded in phase with the lamp power frequency at $\frac{1}{60}$ -sec intervals. The average of 60 of these readings was recorded each second. The distance from the fixed slit to the optic axis was determined by employing the reference Rayleigh pattern and slowly moving the photomultiplier until the output voltage showed a maximum. The difference between readings on the Gaertner traveling microscope was then noted. Differences were reproducible to ± 5 μ .

Corrections for optical imperfections in the interferometer and the number of fringes in the Gouy patterns were all measured photographically in the usual fashion.⁴

Results and Discussion

The general expression derived by Onsager and Gosting for the relative intensity distribution in a Gouy interference pattern may be simplified for use with systems whose diffusion is ideal and where only the lower fringes are to be considered. From the Airy integral refinement of the quarter-wave approximation for the interference conditions, Onsager and Gosting⁶ proposed the following expression for the relative intensity distribution function

$$I(Y) = (16\pi^2 K^2 D t / \epsilon) \left\{ Ai(\alpha) \times \left[1 - \frac{2\alpha^2}{5\epsilon} + \frac{1}{\epsilon^2} \left(\frac{2\alpha^2}{7} + \frac{\alpha^5}{200} \right) - \frac{1}{\epsilon^3} \left(\frac{47}{675} + \frac{2347\alpha^3}{9450} + \frac{81\alpha^6}{14,000} + \dots \right) \right] + Ai(\alpha) \times \left[-\frac{\alpha^2}{10\epsilon} + \frac{1}{\epsilon^2} \left(\frac{17}{105} + \frac{8\alpha^3}{105} \right) - \frac{1}{\epsilon^3} \left(\frac{1223\alpha}{4725} + \frac{1163\alpha^7}{18,900} + \frac{\alpha^7}{6000} \right) + \dots \right] \right\}^2 \quad (1)$$

This function applies to the lower fringes of a Gaussian boundary when diffraction from the cell mask is neglected. $I(Y)$ is the intensity at position Y in the focal plane, D is the diffusion coefficient, t is the time, and K^2 is a constant which is typical of the instrumentation employed. ϵ and α are defined by the equations

$$\epsilon = (2\sqrt{\pi} j_m)^{2/3} \quad (2)$$

and

$$\alpha = \epsilon(Y/C_t - 1) \quad (3)$$

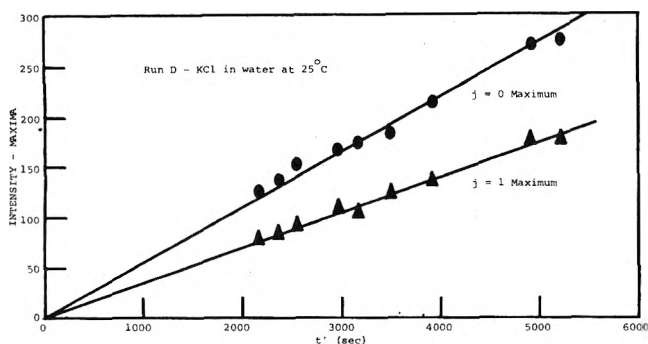


Figure 2. Linear variation of intensity, in the two lowest maxima of a Gouy interference pattern, as a function of time.

where j_m is the number of fringes in the Gouy pattern and C_t is the maximum downward displacement of light in the focal plane, which is given by the principles of geometric optics. $Ai(\alpha)$ and $Ai'(\alpha)$ are the Airy integral and its first derivative, respectively.

For the system KCl-water, and also for the nonaqueous system tetra-*n*-butylammonium tetraphenylboride in acetonitrile, the conditions for applying the simplified eq 1 are nicely met, so that only this form will be employed throughout this discussion. Since diffusion in KCl-water solutions has been well defined, this system was chosen as a reference with which to evaluate the new computer technique. The data of Gosting⁵ for KCl-water mixtures obtained by the Gouy photographic method are in excellent agreement with the conductimetric data of Harned and Nuttall¹⁰ in the region of overlap; thus, all Gouy computer results were referred to the work of Gosting for comparison. The average concentration of the final homogeneous solution was chosen to fall on the flat portion of the D vs. concentration curve. This selection ensured that differential diffusion coefficients were being determined. The concentration difference between diffusing solutions was fixed such that j_m was approximately equal to 100 fringes. All diffusion coefficients were measured at $25.00 \pm 0.01^\circ$.

\bar{c} , the average concentration of the KCl-water solution at homogeneity after a run, was $0.2250 M$ and the difference in concentration, Δc , was $0.2000 M$. The corresponding diffusion coefficient from Gosting's data was $1.838 \times 10^{-5} \text{ cm}^2/\text{sec}$. A value for D under the experimental conditions listed above was measured by the Gouy photographic method and found to be $1.839 \times 10^{-5} \text{ cm}^2/\text{sec}$, in excellent agreement with Gosting.

Equation 1 predicts that the intensity in any fringe should increase linearly with time. Figure 2 shows this linear variation of intensity observed in a KCl-water reference run with the PDP-12 computer. With the points obtained early in time, $t < 5000$ sec, the best linear fit of intensity against time was calculated by least squares for the $j = 0$ and the $j = 1$ maxima. These peaks were chosen, since they would later be used to normalize the intensity distribution. Each intensity was also corrected for background noise before any calculations were made.

Diffusion coefficients were first evaluated from computer-recorded data in the usual way, from the positions of the lowest five fringe minima. This was done to see whether or not the experiment would yield reasonable values of D in a straight-forward manner before trying to apply the Onsager-Gosting theory to the whole intensity distribution. These results are summarized in Table I. The extrapolated value of D' , $D(\text{final})$, is in excellent agreement with

TABLE I: Determination of Diffusion Coefficients from the Minima of a Gouy Interference Pattern Recorded with a PDP-12 Computer^a

t' , sec	$10^4(1/t')$	\bar{C}_t , cm	$10^5 D'$, cm^2/sec
2165.8	4.6172	2.1504	1.8421
2366.7	4.2253	2.0574	1.8415
2547.0	3.9262	1.9820	1.8438
2966.6	3.3709	1.8375	1.8417
3169.6	3.1550	1.7767	1.8441
3494.4	2.8617	1.6888	1.8511
3919.5	2.5513	1.6001	1.8384
4921.5	2.0319	1.4271	1.8405
5219.3	1.9160	1.3867	1.8381

^a Instantaneous scan of test run D, KCl in water; $\bar{c} = 0.2250 M$, $j_m = 90.89$, $\Delta c = 0.2000 M$; $NDS = +16 \mu$; \bar{C}_t averaged from $j = 0$ to $j = 4$ minima at time t' . From a linear least-squares analysis of D' vs. $1/t'$, $D(\text{final}) = 1.839 \times 10^{-5} \text{ cm}^2/\text{sec}$; $\Delta t = 5$ sec. $D(\text{Gosting}) = 1.838 \times 10^{-5} \text{ cm}^2/\text{sec}$. $D(\text{photographic, this study}) = 1.839 \times 10^{-5} \text{ cm}^2/\text{sec}$.

TABLE II: Comparison of Intensity Ratios Calculated from Eq 1 with Experimental Ratios Obtained from Instantaneous Scans

Run D, KCl in water; see Table I for experimental conditions
 $I(j = 0 \text{ max})/I(j = 1 \text{ max}) = 1.597$ (theoretical value)
 $I(j = 0 \text{ max})/I(j = 1 \text{ max}) = 1.612$ (experimental value)

Gosting's number and with the value determined photographically by us.

In order to test eq 1, another simple calculation was performed. The ratio of the intensity in the $j = 0$ maximum to that in the $j = 1$ maximum was determined from eq 1 and compared with experimental KCl-water computer results. These ratios are displayed in Table II.

Examination of the intensity distribution equation shows that the diffusion coefficient, D , is the only undetermined parameter, all others, in principle, determinable from direct measurements. The intensity of the $j = 0$ maximum was selected as the normalizing intensity for the whole envelope; the time at which this maximum was recorded was taken as the reference time to which all other experimental intensities were corrected. For each separate scan in a given run, values of $I(Y)/I(j = 0 \text{ max})$ were computed from the experimental data points. From the right-hand side of eq 1, the theoretical value for each intensity ratio was determined in the following way. An initial value of D was estimated and substituted into the theoretical expression. D was then iterated until the experimental and theoretical intensity ratios were identical for every point in the scan to within a preselected error limit. This may be expressed as

$$\frac{I(Y)/I(j = 0 \text{ max})}{\text{(experimental)}} = \frac{[f(\alpha_Y)]^2/[f(\alpha_0)]^2}{\text{(theoretical)}} \quad (4)$$

where α_Y and α_0 are functions of the iterated parameter D . The diffusion coefficients, D' , which satisfied condition 4, were then plotted against $1/t'$ in the usual way,⁵ in order to obtain the extrapolated value, $D(\text{final})$, for \bar{c} . The very good agreement between diffusion coefficients computed from eq 1 with condition 4 and those calculated from intensity minima only is demonstrated in Table III. It should be pointed out that the agreement might be improved somewhat by incrementing D in each iterative step by a smaller amount. However, the cost of computation would then become prohibitive; in any event the D values from the whole intensity distribution are already within 0.1–0.2% of those

TABLE III: Comparison of Diffusion Coefficients Calculated from Minima with Those Determined by the Iterative Computer Method

Run D, KCl in water; see Table I for experimental conditions $D(\text{final}) = 1.839 \times 10^{-5} \text{ cm}^2/\text{sec}$; $\Delta t = 5.0 \text{ sec}$ (minima only)
$D(\text{final}) = 1.840 \times 10^{-5} \text{ cm}^2/\text{sec}$; $\Delta t = 4.9 \text{ sec}$ (determined by the iterative computer calculation using the $j = 0$ maximum as the normalizing intensity)
Run F, KCl in water; same experimental conditions as run D above
$D(\text{final}) = 1.840 \times 10^{-5} \text{ cm}^2/\text{sec}$; $\Delta t = 23.4 \text{ sec}$ (minima only)
$D(\text{final}) = 1.842 \times 10^{-5} \text{ cm}^2/\text{sec}$; $\Delta t = 19.7 \text{ sec}$ (determined by the iterative computer calculation using the $j = 0$ maximum as the normalizing intensity)
$D(\text{final}) = 1.842 \times 10^{-5} \text{ cm}^2/\text{sec}$; $\Delta t = 24.4 \text{ sec}$ (determined by the iterative computer calculation using the $j = 1$ maximum as the normalizing intensity)

determined from minima alone. A good example of the compatibility of theory and experiment may be seen in Figure 3. This displays a set of data for a single scan in a run subjected to the iterative computer analysis outlined above.

It was decided to further test the Onsager-Gosting theory to see if there was any significant difference in the final value of D when the $j = 1$ maximum was chosen as the normalizing intensity. By analogy to eq 4, one may write

$$\frac{I(Y)/I(j = 1 \text{ max})}{(\text{experimental})} = \frac{[f(\alpha_Y)]^2/[f(\alpha_1)]^2}{(\text{theoretical})} \quad (5)$$

Reference to Table III shows that there is no difference, within experimental error, between extrapolated values of $D(\text{final})$ calculated from intensity distributions normalized by either the $j = 0$ or the $j = 1$ maximum.

One last severe test was made of the Onsager-Gosting equation. It was already known⁷ that the zeros of eq 1 correctly predicted positions of the minima in Gouy interference patterns; however, what would happen if one were to move away from these turning points? Data from the negatively sloping side of the $j = 0$ maximum were analyzed by the iterative procedure used before to obtain a value of the diffusion coefficient characteristic of the reference time, t' . These results are summarized in Table IV. It is very interesting to see that a quite decent value of D was calculated from data sets which contain no maxima or minima of intensity. Furthermore, these data sets came from the lowest fringe for which the theory might be expected to be least secure.

The instantaneous scan Gouy computer method, described above, permits determination of diffusion coefficients to about $\pm 0.2\%$; however, the computing time required to fit the experimental intensity distributions to theory is excessive. As a result, a second direct-recording technique with a fixed distance Y was developed. The fixed position of the slit was chosen to be between 1.7 and 2.0 cm from the optic axis for all runs. Approximately 10 or 11 fringes passed by the fixed slit in a 30-min period. From a visual inspection of the printed computer output of the intensities recorded in this way, the maxima and the minima could easily be located. Since the first point was recorded at 1500 sec and each point thereafter at 1-sec intervals, the exact times when minima and maxima passed by the slit

TABLE IV: Computation of Diffusion Coefficients from Intensity Data Obtained from the Negatively-Sloping Side of the $j = 0$ Maximum Away from the Turning Points of the Intensity Distribution

Run D, KCl in water $D' = 1.844 \times 10^{-5} \text{ cm}^2/\text{sec}$ for $t' = 2163.7 \text{ sec}$; this value was obtained using data from the whole relative intensity distribution packet
$D' = 1.844 \times 10^{-5} \text{ cm}^2/\text{sec}$ for $t' = 2163.7 \text{ sec}$; an identical value for D' using only 25 points from the downslope of the $j = 0$ intensity maximum; no turning points included
Run F, KCl in water $D' = 1.856 \times 10^{-5} \text{ cm}^2/\text{sec}$ for $t' = 2630.0 \text{ sec}$; this value was obtained using data from the whole relative intensity distribution packet
$D' = 1.855 \times 10^{-5} \text{ cm}^2/\text{sec}$ for $t' = 2630.0 \text{ sec}$; excellent agreement with the above value for D' at the same t' , and calculated using only 21 points from the downslope of the $j = 0$ intensity maximum; no turning points included

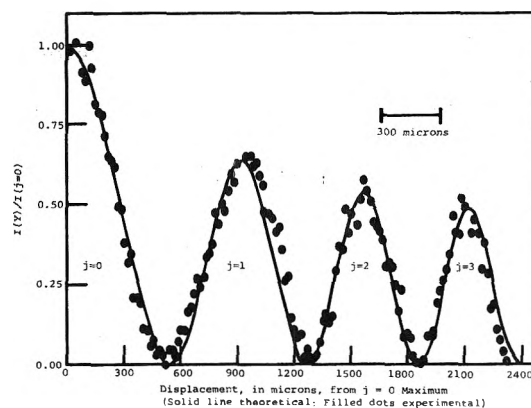


Figure 3. Comparison of intensity data from the instantaneous scan Gouy technique with intensities predicted by the Onsager-Gosting theory: run D, KCl in water at 25° ; one scan at $t' = 2545.4 \text{ sec}$; $j = 0$ maximum was the normalizing peak.

could be computed. Direct application of the equation⁸

$$D' = (j_m^2 \lambda^2 b^2) / 4\pi C_t^2 t' \quad (6)$$

yielded values for the diffusion coefficient as a function of time, subject to the extrapolation procedure mentioned before and expressed by

$$D' = D[1 + (\Delta t/t')] \quad (7)$$

where D is the extrapolated value of D' . Δt for a good run normally lies between 5 and 40 sec. This small Δt takes account of the fact that it is not possible to obtain an infinitely sharp boundary at $t' = 0$. It should be noted that both maxima and minima were employed in this method, whereas the photographic technique depends only on the minima.

KCl-water, $\bar{c} = 0.2250 M$, $\Delta c = 0.2000 M$, was again the reference system. The results of three repetitive runs are shown in Table V. Agreement of the fixed slit results with Gosting's value and with our photographic value of the diffusion coefficient is again excellent.

Three runs were also made on the system tetra-*n*-butylammonium tetraphenylboride in acetonitrile. These results are shown in Table VI. For this system, plots of D' vs. $1/t'$ are included in Figure 4 and illustrate the precision of

TABLE V: Summary of Fixed-Slit Experiments for Runs G, H, and I^a

Run	Y(fixed), cm	$10^4 D(\text{final})$, cm ² /sec	Δt , sec	$j_m(\text{no. of fringes})$
G	1.6793	1.841	16.4	91.03
H	1.6797	1.837	22.4	91.07
I	1.9989	1.840	13.8	91.08

^a KCl in water; $\bar{c} = 0.2250 M$; $\Delta c = 0.2000 M$. $D(\text{final})$, average value of three runs, 1.839×10^{-6} cm²/sec. Average deviation of the mean, 0.11%.

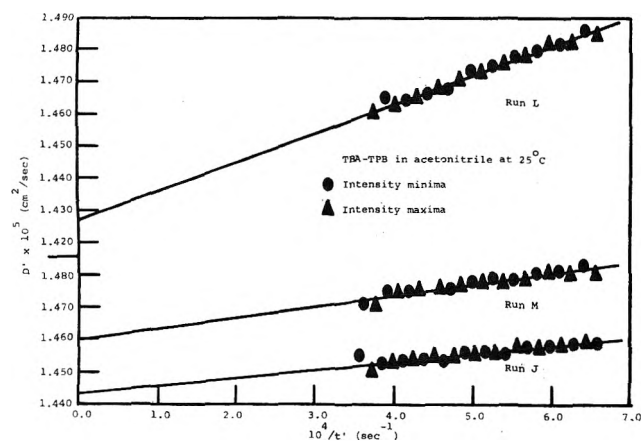


Figure 4. D' vs. $1/t'$ for data obtained by the fixed-slit Gouy computer method.

the fixed slit computer method, compared with the usual photographic technique. The error is estimated to be between 0.05 and 0.10% in the final value of D , depending on the run, contrasted with an error of about 0.2% or greater for the photographic method.

It was of some interest to see whether or not intensity ratios for various pairs of maxima would correspond to those predicted by theory, as was the case in the instantaneous scan experiments. It was found that calculated ratios deviated enormously from experimental ratios and that there seemed to be no systematic trend to these deviations. (This might have been anticipated from the data presented in Figure 2. In that figure the ratio of the slopes of the least-squares fits is the theoretical value (1.60) but individual intensity values vary substantially and randomly from the least-squares lines.)

This can be at least partially accounted for by a consideration of the conditions under which intensities were recorded. For the instantaneous scans, data for the first six or seven fringes were obtained over a period of about 3–4 sec, which amounted to several hundred intensity points at the chosen sampling rate. However, fixed slit scans required about 30 min to collect all the data needed to calculate diffusion coefficients from the same number of fringes. Over 3 sec the mercury arc lamp seems to be stable but, over a 30 min period, this same source might very well have exhibited substantial fluctuations in output depending on random variations in the line voltage and on random move-

TABLE VI: Determination of Diffusion Coefficients in a Nonaqueous System by the Fixed-Slit Computer Technique^a

Run	Y(fixed), cm	$10^4 D(\text{final})$, cm ² /sec	t , sec	\bar{c} , M	$j_m(\text{no. of fringes})$
J	2.0003	1.443	17.9	0.01201	90.24
L	2.0001	1.427	63.5	0.01563	90.00
M	2.0006	1.460	23.1	0.00810	90.08

^a TBA-TPB in acetonitrile.

ment if the arc across the horizontal source slit. This would be reflected in values of experimental intensity ratios. Since it was already firmly established by Riley⁷ and by the instantaneous scan method developed in this study that intensity ratios are indeed correctly given by the Onsager-Gosting theory, it was not considered crucial to try to resolve this problem in the fixed slit experiments.

A systematic study of the diffusion coefficient-concentration behavior of a binary mixture as a function of temperature allows the evaluation of an activation energy for diffusive flow. The improved accuracy and precision of the fixed slit Gouy technique would lend itself nicely to such an application. To date, such energies are only known to within a few per cent; these uncertainties could probably be reduced by direct-recording Gouy experiments.

Conclusions

It has been possible to verify the Onsager-Gosting theory for the entire intensity distribution in a Gouy pattern produced by a Gaussian boundary. An iterative method for evaluating diffusion coefficients from the Gouy envelope (or any fraction thereof) has been devised and tested. With considerable effort, this procedure might be adapted for the case of skewed boundaries. A simple and extremely precise fixed slit method for determining diffusion coefficients has been described and compared with other procedures.

Acknowledgments. Our thanks go to B. Ellison and to T. Netzel who aided in the writing of the PDP-12 data-collecting programs. Financial support in the form of a Graduate Fellowship from the National Science Foundation is gratefully acknowledged by one of us (T.A.R.).

References and Notes

- (1) L. G. Longworth, *J. Amer. Chem. Soc.*, **69**, 2510 (1947).
- (2) L. J. Gosting and M. S. Morris, *J. Amer. Chem. Soc.*, **71**, 1998 (1949).
- (3) G. Kegeles and L. J. Gosting, *J. Amer. Chem. Soc.*, **69**, 2516 (1947).
- (4) C. A. Coulson, J. T. Cox, A. G. Ogston, and J. StL. Philpot, *Proc. Roy. Soc., Ser. A*, **192**, 382 (1948).
- (5) L. J. Gosting, *J. Amer. Chem. Soc.*, **72**, 4418 (1950).
- (6) L. Onsager and L. J. Gosting, *J. Amer. Chem. Soc.*, **74**, 6066 (1952).
- (7) J. F. Riley, Dissertation, Yale University, 1954.
- (8) L. J. Gosting, E. M. Hansen, G. Kegeles, and M. S. Morris, *Rev. Sci. Instrum.*, **20**, 209 (1949).
- (9) M. S. Lyons and J. C. Thomas, *J. Amer. Chem. Soc.*, **72**, 4506 (1950).
- (10) H. S. Harned and R. L. Nuttall, *J. Amer. Chem. Soc.*, **69**, 736 (1947); **71**, 1460 (1949).

Structure, Energetics, and Dynamics of the Water Dimer¹

Lester L. Shipman,^{2a} John C. Owicki,^{2b} and Harold A. Scheraga*

Department of Chemistry, Cornell University, Ithaca, New York 14850 (Received May 17, 1974)

The Shipman-Scheraga empirical intermolecular potential energy function for water (SS potential) has been applied to a study of the structure, energetics, and dynamics of the water dimer. The entire six-dimensional potential energy surface of the water dimer has been searched for minima and saddle points. Only one minimum-energy structure, the trans near-linear dimer (TNLD), has been found, while several important saddle points that serve as transition states for interconversions between TNLD configurations have been found. The TNLD's of (H₂O)₂ and (D₂O)₂ have been characterized by calculating the following properties: potential energy and O...O distance at the minimum, internal energy at absolute zero temperature, frequencies and dipole moment derivatives of the intermolecular normal vibrational modes, zero-point energy for intermolecular vibrations, principal moments of inertia, location of the center of mass, directions of the principal axes for the moments of inertia, and components of the total dipole moment along the principal axes. The important transition states for interconversion between the TNLD's have been characterized by calculating the following properties: potential energy, intermolecular vibrational frequencies, intermolecular vibrational zero-point energy, internal energy at absolute zero temperature, and internal energy relative to the TNLD at absolute zero temperature. The familiar cyclic and bifurcated dimers have been found to be saddle points, not minima, on the six-dimensional potential energy surface. The importance of motion through the various transition states for interconversion between the TNLD's has been considered. Implications of the computed results for future spectroscopic studies are discussed.

I. Introduction

The water dimer is the smallest unit with which to gain an understanding of the energetics and dynamics of water-water interactions. The intermolecular potential energy surface of the water dimer has six dimensions corresponding to three translations and three rotations of one water relative to the other. Because the potential energy surface is so extensive, previous studies have found it economical to study only a small part of it. The present study is aimed at extending our knowledge of the entire six-dimensional potential energy surface with particular attention to the role of the features of the surface which determine the dynamics of the water dimer. An extensive search of the potential energy surface was made to locate minima and low-energy saddle points, which correspond to transition states for interconversion between minima. An empirical intermolecular potential energy function for water, recently derived by Shipman and Scheraga³ (SS potential), was used to calculate the potential energy as a function of the six dimensions. H₂O and D₂O are assumed to interact according to the same isotope-independent potential. For the one minimum-energy structure located, the following properties were calculated for (H₂O)₂ and (D₂O)₂: the potential energy, O...O distance, frequencies and dipole moment derivatives of the intermolecular normal vibrational modes, intermolecular vibrational zero-point energy, internal energy at absolute zero temperature, location of the center of mass, principal moments of inertia, directions of the principal axes for the moments of inertia, and components of the dipole moment along the principal axes. For each saddle point located, the following properties were calculated: potential energy, intermolecular vibrational frequencies, intermolecular vibrational zero-point energy, internal energy at absolute zero temperature, and height above the minimum at absolute zero temperature.

II. Search for Minima and Saddle Points

Water dimer structures in six-dimensional space were generated using the set of spherical coordinates and Euler angles described in section X of ref 3. The potential energy was minimized with respect to all six degrees of freedom starting from many points in six-dimensional space. Two methods were used to generate starting structures: (1) starting structures were chosen from among possible minima considered in previous studies⁴ and (2) starting points were generated randomly from the set of all relative molecular orientations with O...O distances between 2.0 and 4.0 Å using the RANDU subprogram from the IBM Scientific Subroutine Package. The tetrahedral linear dimer (TLD), cyclic dimer (CD), perpendicular plane bifurcated dimer (PePBD), parallel plane bifurcated dimer (PaPBD), perpendicular plane opposed dimer (PePOD), and perpendicular plane linear dimer (PePLD) constituted our set of dimers considered as possible minima in previous studies.⁴ See Figure 1 for a schematic representation of these dimers. Roughly 100 randomly generated water dimer structures were also considered as starting points for minimizations. A program using a minimization technique developed by Powell⁵ and modified by Zangwill⁶ was used to perform the minimizations.

The aforementioned energy minimization program minimized the potential energy to points on the potential energy surface having zero gradients and positive diagonal elements in the matrix of second derivatives with respect to the set of six variables used to generate the water dimer structures. In some cases, these two conditions were satisfied, but the point was a saddle point having a negative second derivative with respect to one or more directions involving two or more of the six variables simultaneously. At the end of each minimization all distances and rotation angles had converged to at least six significant figures.

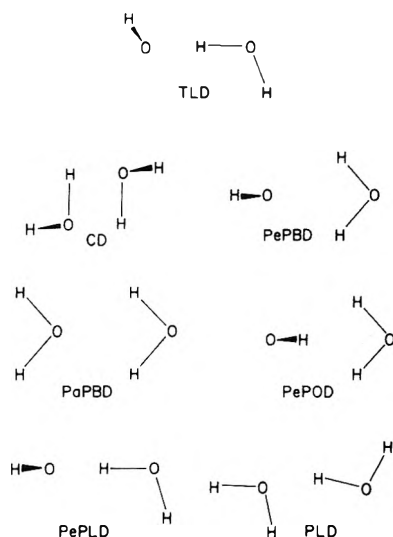


Figure 1. Water dimers considered: tetrahedral linear dimer (TLD), cyclic dimer (CD), perpendicular plane bifurcated dimer (PePBD), parallel plane bifurcated dimer (PaPBD), perpendicular plane opposed dimer (PePOD), perpendicular plane linear dimer (PePLD), and planar linear dimer (PLD). The first six were considered as possible minimum-energy structures from earlier studies;⁴ the last was obtained from the random generation procedure.

The combination of randomly generated starting points and the set of six water dimers above as starting points for energy minimizations should have been sufficient to locate all important minima and saddle points, but it should be noted that there is no mathematical or physical guarantee that all have been found. Only one minimum-energy structure and various saddle points were located; these will be characterized in sections III and IV, respectively. Implications of the results obtained here for future spectroscopic studies of the water dimer will be discussed in section V.

III. Computed Results: Trans Near-Linear Dimer

The minimum-energy configuration for the dimer, calculated using the SS empirical intermolecular potential,³ has a nearly linear hydrogen bond and the remaining hydrogens trans to each other across the hydrogen bond. The structure has therefore been termed the trans near-linear dimer (TNLD). The $(\text{H}_2\text{O})_2$ and $(\text{D}_2\text{O})_2$ TNLD's are shown in Figure 2 in the (cartesian) coordinate system of the principal axes of their respective inertia tensors. Geometrically, the H_2O and D_2O TNLD's are identical; the differences in their coordinates in Figure 2 result from the differences in the two coordinate systems, arising from the different centers of mass and principal axes of inertia in the two dimers. The TNLD minimum occurs eight times on the six-dimensional potential energy surface corresponding to the eight possible hydrogen bonds involving hydrogens of one molecule and lone-pair electrons of the other (see section V.A); all such TNLD's are superimposable structures. We found no other minima on the energy surface.

The potential energy of the TNLD is -5.76 kcal/mol relative to infinitely separated molecules. The $\text{O}\cdots\text{O}$ distance is 2.85 Å, the $\text{H}\cdots\text{O}$ distance is 1.90 Å, and the $\text{O}-\text{H}\cdots\text{O}$ angle along the hydrogen bond is 171.3° (this compares to a value of 180° for a linear hydrogen bond). The moments of inertia of the TNLD have been calculated and are given in section V.D. The six intermolecular vibrational frequencies were calculated using the method outlined in a previous study⁷ of the intermolecular vibrational modes of

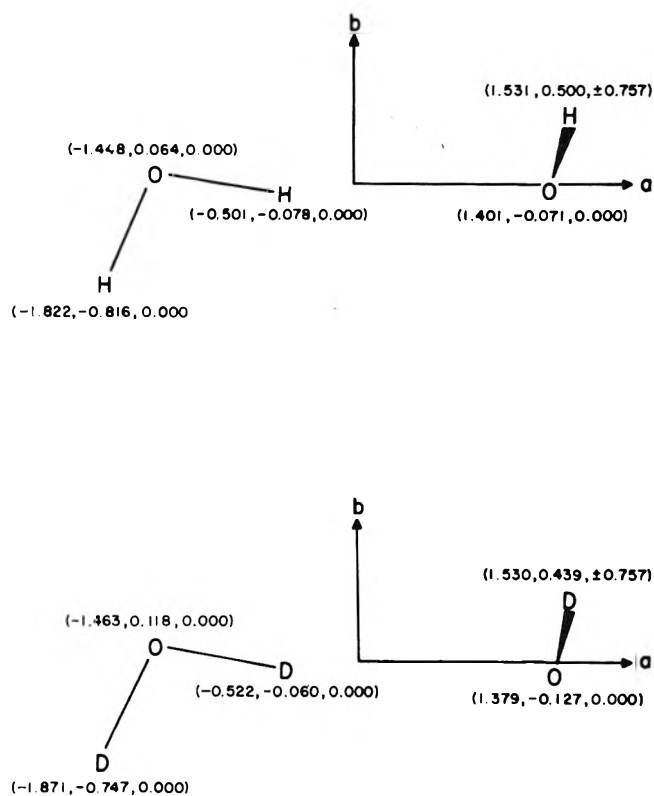


Figure 2. $(\text{H}_2\text{O})_2$ and $(\text{D}_2\text{O})_2$ in their principal-axes systems. Atomic coordinates are (a, b, c) in Ångströms.

ice I_h and are given in Table I. From these frequencies, zero-point energies of 2.28 and 1.71 kcal/mol were calculated for $(\text{H}_2\text{O})_2$ and $(\text{D}_2\text{O})_2$, respectively (zero-point energies were calculated by taking $hc/2$ times the sum of the six intermolecular vibrational frequencies in cm^{-1}). The internal energy of the TNLD at absolute zero (taken as the sum of the potential energy and zero-point energy) was calculated to be -3.48 and -4.05 kcal/mol for $(\text{H}_2\text{O})_2$ and $(\text{D}_2\text{O})_2$, respectively. Using the atom-atom induced dipole moment model for induced dipoles⁷ and a permanent dipole moment of 1.884 D⁸ for each monomer, the components of the total dipole moment (permanent plus induced dipole moments) in the principal-axes coordinate system are $\mu_a = 1.72$, $\mu_b = 0.18$, and $\mu_c = 0.00$ D for $(\text{H}_2\text{O})_2$ and $\mu_a = 1.73$, $\mu_b = 0.11$, and $\mu_c = 0.00$ D for $(\text{D}_2\text{O})_2$ (these differ because of the difference in the two coordinate systems). The total dipole moment has a magnitude of 1.73 D for both $(\text{H}_2\text{O})_2$ and $(\text{D}_2\text{O})_2$. The integrated infrared absorptivity of the i th normal mode, Q_i , is directly proportional to the quantity $d\mu/dQ_i \cdot d\mu/dQ_i$. The values of this quantity, computed as indicated in ref 7, for the various intermolecular normal modes are given in Table I.

IV. Computed Results: Transition States

Five classes of transition states for interconversion of TNLD's were found, each type occurring at several points on the potential energy surface just as the TNLD minimum appeared eight times. These transition states (mathematically, saddle points on the potential energy surface) correspond to the cyclic dimer (eight total), planar linear dimer (eight total), perpendicular plane opposed dimer (two total), perpendicular plane bifurcated dimer (four total), and parallel plane bifurcated dimer (four total) shown in Figure 1. Thus 26 transition states were found for intercon-

TABLE I: Intermolecular Normal Vibrational Modes of Trans Near-Linear Water Dimer

Vibration mode i	Freq ω_i^a		$d\mu/dQ_i \cdot d\mu/dQ_i^b$		Character of normal mode ^{c,d}
	(H ₂ O) ₂	(D ₂ O) ₂	(H ₂ O) ₂	(D ₂ O) ₂	
1	681	487	2.1	1.2	Hydrogen-bond bend out of donor plane (primarily motion of donor)
2	451	332	0.7	0.2	Hydrogen-bond bend in donor plane (primarily motion of donor)
3	183	175	1.5	1.1	Hydrogen-bond stretch
4	113	82	3.6	1.9	Torsion about hydrogen bond
5	106	77	6.8	3.6	Hydrogen-bond bend in donor plane (primarily motion of acceptor)
6	63	45	0.6	0.3	Hydrogen-bond bend out of donor plane (primarily motion of acceptor)

^a Units are cm⁻¹. ^b Units are D² amu⁻¹ Å⁻². ^c "Donor" and "acceptor" refer to proton (or deuteron) donor and acceptor, respectively. ^d From examination of eigenvectors of the vibrational force constant matrix.



Figure 3. Labeled water monomer. H and L denote hydrogens and lone pairs, respectively.

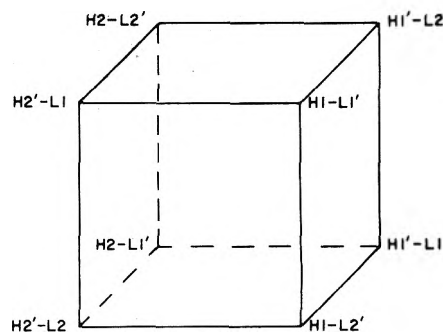


Figure 4. Schematic relationships between the eight trans near-linear dimers. See Figure 3 for the meaning of labels and section V.A for a discussion of the interconversion of TNLD's.

versions among the eight TNLD's. The first four types of transition states have been characterized by calculating the following properties (see Table I): nuclear geometry, O...O distance, potential energy, intermolecular vibrational frequencies, intermolecular vibrational zero-point energy, internal energy at absolute zero temperature, and internal energy relative to the TNLD at absolute zero temperature. The parallel plane bifurcated dimer was not characterized because it is a saddle point on paths connecting the more stable perpendicular plane bifurcated dimer and planar linear dimer transition states and should therefore be unimportant to TNLD interconversion. The cyclic dimer, planar linear dimer, and perpendicular plane bifurcated dimers are single transition states. In other words, five normal modes are vibrations and the sixth, whose force constant is negative, is a transition coordinate; the structures are unstable with respect to motion along the direction of the sixth normal mode. The perpendicular plane opposed dimer is a double transition state (i.e., four normal modes are vibrations and two are transition coordinates). Double transition states involve interconversions among four TNLD's, while single transition states connect only two.

V. Discussion

A. Relationships between the Trans Near-Linear Dimers and the Transition States for Their Interconversion. On the six-dimensional potential energy surface of (H₂O)₂ and (D₂O)₂ there are eight minima corresponding to TNLD's. As an aid to understanding the relationships between the TNLD's and the transition states for interconversion of TNLD's, hydrogens and lone pairs have been artificially labeled as shown in Figure 3. If one water is labeled with primed and the other with unprimed labels, each TNLD can be uniquely identified by specifying the lone pair and hydrogen making the closest approach in the near-linear hydrogen bond. The eight TNLD's, represented in this way, are shown schematically in Figure 4 at the corners of a cube. Examination of the pathway from each TNLD to the nearest transition state (with the aid of a

computer program) shows that each nearest-neighbor pair of TNLD's connected by an edge of the top or bottom face of the cube is connected by a path in six-dimensional space having a cyclic dimer transition state. Each nearest-neighbor pair of TNLD's connected by a vertical edge of the cube is connected by two paths in six-dimensional space having planar linear dimer transition states. Finally, each pair of TNLD's connected by a diagonal in the top or bottom face of the cube is connected by a path in six-dimensional space having a perpendicular plane bifurcated dimer transition state. As an aid to the visualization of the interconversion process, Figure 5 depicts the transition between two TNLD's through a CD. The eigenvector corresponding to the CD transition coordinate normal mode is consistent with the process described in Figure 5.

B. Dynamics of Trans Near-Linear Dimer Interconversions. As shown in Table II, for (H₂O)₂ the internal energies of the various transition states relative to the internal energy of the TNLD at absolute zero temperature are 0.54, 0.10, and 1.78 kcal/mol for the cyclic dimer, planar dimer, and perpendicular plane bifurcated dimer, respectively. For (D₂O)₂, on the other hand, the heights of the transition states above the TNLD's are 0.49, 0.21, and 2.10 kcal/mol, respectively. The barriers are so small that, at room temperature, the dimer can pass over (or through) the barriers. The motions that take the dimer from one TNLD to another involve primarily rotations of the two molecules relative to each other, which is mostly proton (or deuteron) motion. This light mass, in combination with the low height of the transition states, makes tunneling through the barriers

TABLE II: Characterization of Transition States

Properties	Cyclic dimer	Planar linear dimer	Perpendicular plane opposed dimer	Perpendicular plane bifurcated dimer
Coordinates of water no. 2 ^{a,b}				
O	(0.634, 2.351, 1.389)	(-1.706, -2.294, 0.000)	(3.239, 0.000, 0.000)	(-3.210, 0.000, 0.000)
H (or D)	(0.048, 3.108, 1.389)	(-2.651, -2.143, 0.000)	(2.653, 0.000, 0.757)	(-2.624, 0.000, 0.757)
H (or D)	(0.048, 1.594, 1.389)	(-1.323, -1.416, 0.000)	(2.653, 0.000, -0.757)	(-2.624, 0.000, -0.757)
O...O dist ^c	2.80	2.86	3.24	3.21
Potential energy ^d	-5.42	-5.25	-0.78	-2.78
Intermolecular vibr. freq ^{e,f}				
ω_1	848	540	444	355
ω_2	448	488	375	142
ω_3	167	169	375	127
ω_4	140	55	103	108
ω_5	132	53	97	26
Intermolecular vibrational zero-point energy ^{d,e}	2.48	1.87	1.85	1.08
Internal energy at absolute zero temp ^{d,e,f}	-2.94	-3.38	1.07 ^g	-1.70
Internal energy rel to TNLD at absolute zero temp ^{d,e,h}	0.54	0.10	4.55 ^g	1.78
			4.62 ^g	2.10

^a Cartesian coordinates (x, y, z) in Å. ^b In all cases the coordinates of water no. 1 are as follows: O (0.000, 0.000, 0.000); H (or D) (0.586, 0.757, 0.000); H (or D) (0.586, -0.757, 0.000). ^c Units are Å. ^d Units are kcal/mol. ^e For each transition state, (H₂O)₂ results are on the left and (D₂O)₂ results are on the right. ^f Units are cm⁻¹. ^g Sum of potential energy and intermolecular vibrational zero-point energy. ^h Internal energy of transition state minus internal energy of TNLD at absolute zero temperature (-3.48 kcal/mol for H₂O and -4.05 kcal/mol for D₂O). ⁱ FePOD would actually dissociate rather than assume a state of positive internal energy. See section V.B for explanation.

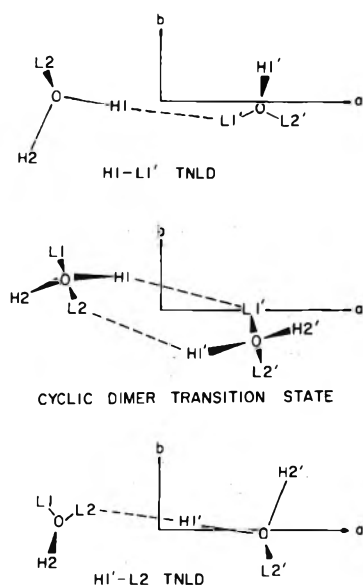


Figure 5. Picture of the interconversion of TNLD's H1-L1' and H2'-L1 through a CD transition state. See Figure 3 for the meaning of the labels and section V.A for a discussion of the interconversion of TNLD's.

very likely. The sum of the potential energy and intermolecular vibrational zero-point energy (*i.e.*, the internal energy) for the perpendicular plane opposed dimer is greater than zero (see Table II). Therefore, the water dimer will supply dissociate (to reach an internal energy equal to zero) rather than pass through this high-energy transition state.

C. Implications for the Infrared Spectrum of Water Dimer. The integrated absorptivity for each TNLD normal mode has been calculated with the dipole moment model described in section III (see Table I). Within the limits of the harmonic oscillator approximation, the 100–120-cm⁻¹ region has the largest value of the integrated absorptivity and, therefore, should be the most prominent in the infrared spectrum. The data in Table I also indicate that, for the same concentration of water dimers, the sum of the integrated absorptivities is ~50% smaller for (D₂O)₂ than (H₂O)₂; hence, the infrared spectrum of (D₂O)₂ would be expected to have an integrated absorptivity approximately 50% that of (H₂O)₂ in the region of the intermolecular vibrations. From the higher frequencies of the normal mode vibrations involving motions of the hydrogen (or deuterium) donor molecule (as characterized in the last column of Table I), it is clear that, under the constraint of a hydrogen bond, the donor molecule is more hindered in its motions than the acceptor molecule.

D. Implications for the Microwave Spectrum of the Water Dimer. The microwave spectrum of the water dimer can give the values for the principal moments of inertia for the TNLD, and the Stark shift (in the microwave spectrum) can give the components of the total dipole moment along the principal axes. For a possible future comparison with such data, we present here the calculated values. The principal moments have been calculated to be $I_a = 2.48$, $I_b = 74.41$, and $I_c = 74.59$ amu Å² for (H₂O)₂ and $I_a = 4.70$, $I_b = 83.98$, and $I_c = 84.06$ amu Å² for (D₂O)₂. The large change of 90% for I_a in going from (H₂O)₂ to (D₂O)₂ as compared to changes of only 11% for both I_b and I_c should be noted. According to second-order perturbation theory, the Stark shift is given by the quantity⁹ $C_a\mu_a^2 + C_b\mu_b^2 + C_c\mu_c^2$, where C_a , C_b , and C_c are different coefficients for

each transition. The calculated values for μ_a^2 , μ_b^2 , and μ_c^2 are 2.96, 0.03, and 0.00 D², respectively, for (H₂O)₂ and 2.99, 0.01, and 0.00 D², respectively, for (D₂O)₂. It follows that none of the Stark shift arises from the μ_c^2 component (because μ_c^2 is identically zero) and that, if μ_b^2 is to be determined accurately, some transitions for which $C_b/C_a \gg 1$ will have to be studied.

E. A "Picture" of the Dynamics of the Water Dimer. At very low temperatures, the water dimer vibrates in its ground vibrational state in a six-dimensional TNLD potential well. As the temperature is increased, the water dimer begins tunneling first through the planar linear dimer barrier and then through the cyclic dimer barrier. Tunneling through the perpendicular plane bifurcated dimer barrier would not be expected to be as important because it is higher in energy than the cyclic and planar linear dimer transition states, and it is possible to interconvert any pair of the eight TNLD's by tunneling through a succession of these more stable transition states (see Figure 4). The normal vibrational frequencies given in Table II have been calculated under the assumption of vibrations in harmonic wells and it is clear from the transition-state heights that this approximation cannot be valid beyond the ground state. In fact, at room temperature, water dimers should move quite freely among the TNLD wells. The picture of this motion which emerges is of a fairly stable O...O internuclear distance in the range of 2.8–2.9 Å (based on the structures of the TNLD and the low-lying CD and PLD) while the hydrogen atoms of the two molecules are rapidly rotating in a concerted fashion as the dimer passes through transition states among the eight TNLD minima. This implies that any experiment carried out on a time scale much longer than that for molecular rotation will give information only about an average dimer structure with contributions from all TNLD's.

F. Concluding Remarks. Since an empirical potential was available,³ it was possible to explore the complete six-dimensional surface of the dimer. Now that one minimum-energy structure and several transition-state structures have been located, it is desirable that a test be made of the stabilities of these structures by large basis set *ab initio* calculations with configuration interaction included. It is also desirable to obtain experimental spectroscopic data on the water dimer as a check on the quantities computed here.

A promising technique^{10,11} combining molecular beam electric deflection and microwave spectroscopy is being applied to the water dimer by Muentner and Dyke. The final results (structure and dipole moment of water dimer) of their study will be directly comparable to the calculated results in section V.D.

Note Added in Proof. Dyke and Muentner have very recently published preliminary results from their microwave study of the water dimer;¹² their observed structure of the water dimer is *trans* and near-linear, in agreement with our calculated structure. The microwave spectrum of the water dimer indicates the presence of large-amplitude tunneling motions such as those discussed in our section V.E. Dyke and Muentner note that *averages* of large-amplitude hydrogen motions are observed; thus it follows that the observed structural parameters may differ slightly from the structural parameters corresponding to the TNLD minimum in the potential energy surface of the water dimer. The observed structure has an O...O distance of 2.98 ± 0.04 Å, and the

hydrogen bond is within 10° of being linear. This compares with our calculated O...O distance of 2.85 Å and an 8.7° deviation from linearity of the hydrogen bond. The hydrogen bond stretch is anharmonic (see curve h of Figure 3 in ref 3) to such an extent that the observed O...O distance would be expected to be larger than the O...O distance at the potential energy minimum. In this regard, it is significant that the observed O...O distance is approximately 4% greater than the calculated value of the O...O distance at the SS potential energy minimum. The observed angle (θ) between the plane of the acceptor molecule and the oxygen-oxygen axis is $60 \pm 10^\circ$, and this compares with the calculated value of 80° at the SS potential minimum. Although these values appear to be in disagreement, the SS potential energy curve for variation of θ is very flat (see Figure 4 in ref 3; the minimum in this curve is not at the 80° value of the six-dimensional minimum because the O...O distance was constrained to be 3.00 Å and the hydrogen bond was constrained to be linear), with a shape that suggests that averaging would make the observed θ smaller than the value of θ at the potential energy minimum. However, we feel that all of the 10 – 30° difference is not due to anharmonicity alone and that some of it may be attributed to a defect in the SS potential (see ref 3 for a discussion of the approximations made in the derivation of the SS potential). Dyke and Muentner report a value of 2.60 D for μ_a , and this compares with the calculated value of 1.72 D. This difference is primarily a direct result of the aforementioned

difference between the calculated and observed values for θ (μ_a increases as θ decreases). Our calculations on the transition states for TNLD interconversions should be useful input to a study of the effects of tunneling on the microwave spectrum of the water dimer.

A comparison of our computed results for the water dimer with those just published by Kistenmacher, *et al.*,¹³ will be presented in a forthcoming paper.

References and Notes

- (1) This work was supported by research grants from the National Science Foundation (GB-28469X3) and from the National Institute of General Medical Sciences of the National Institutes of Health, U. S. Public Health Service (GM-14312).
- (2) (a) NIH Postdoctoral Fellow, 1972–1974. (b) NSF Predoctoral Fellow, 1968–1969 and 1972–1974.
- (3) L. L. Shipman and H. A. Scheraga, *J. Phys. Chem.*, **78**, 909 (1974).
- (4) (a) K. Morakuma and L. Pederson, *J. Chem. Phys.*, **48**, 3275 (1968); (b) P. A. Kollman and L. C. Allen, *ibid.*, **51**, 3286 (1969); (c) G. Dierckson, *Theor. Chim. Acta*, **21**, 335 (1971).
- (5) M. J. D. Powell, *Comput. J.*, **7**, 155 (1964).
- (6) W. I. Zangwill, *Comput. J.*, **10**, 293 (1967).
- (7) L. L. Shipman and H. A. Scheraga, *J. Phys. Chem.*, submitted for publication.
- (8) M. Lichtenstein, V. E. Derr, and J. J. Gallagher, *J. Mol. Spectrosc.*, **20**, 391 (1966).
- (9) S. Golden and E. B. Wilson, *J. Chem. Phys.*, **16**, 669 (1948).
- (10) T. R. Dyke and J. S. Muentner, *J. Chem. Phys.*, **57**, 5011 (1972).
- (11) J. S. Muentner and T. R. Dyke, Abstracts, Fifth Northeast Regional Meeting of the American Chemical Society, Oct 1973.
- (12) T. R. Dyke and J. S. Muentner, *J. Chem. Phys.*, **60**, 2929 (1974).
- (13) H. Kistenmacher, G. C. Lie, H. Popkie, and E. Clementl, *J. Chem. Phys.*, **61**, 546 (1974).

Charge Neutrality in Electrolytic Solutions and the Liquid Junction Potential

Julius L. Jackson*

Wayne State University, Detroit, Michigan 48202 (Received January 31, 1974; Revised Manuscript Received April 29, 1974)

Publication costs assisted by Wayne State University

An ideal two-component liquid junction is treated theoretically by a method due to Howard J. Hickman. The results, which are correct for times greater than times of the order of magnitude of 10^{-9} sec, are derived formally without recourse to the assumption of charge neutrality or any other unproved physical assumption. For this simple two-component case, the well-known formula for the liquid junction potential is obtained as well as closed-form expressions for the charge densities and electric field.

I. Introduction

One of the basic problems in the physical chemistry of electrolytic solutions relates to the seemingly paradoxical use of the assumption of charge neutrality in the theoretical derivations of the electrical potentials in such solutions when a concentration gradient has been established. The assumption was first used by Planck¹ in 1890 to derive the famous formula for the liquid junction potential. The apparent inconsistency between the existence of a potential difference and the vanishing of the net charge, which gives rise to that potential difference, has been a source of con-

tention and puzzlement to physicists and chemists since Planck's original paper.

In 1970, in a remarkable paper, a general solution of the problem was presented by Hickman.² In the present article, we will work out the details of the solution for the simplest case, two univalent ions. For this simple case the mathematics is not as complicated and one can more easily see through it to the underlying physical meaning of what is going on. In addition one gets closed-form expressions for the leading terms in the charge densities and the electric field so that one can see in detail how the quantities go and

how the paradox stated in the previous paragraph is resolved. We hope also by means of this paper to make Hickman's general results better known. The reader interested in these results as well as discussions of other important aspects of the problem is referred to his paper.

The case which we will consider is that of two solutions of the same simple salt, say NaCl, which are initially at different concentrations and which are kept from mixing by a barrier. At a given time the barrier is removed and the ions diffuse between the compartments (see Figure 1). We call n_c and n_d the initial concentrations of the ions in the two compartments, with the subscripts c and d standing for concentrated and dilute, respectively.

When the barrier is removed, an electric potential difference is created between the right side of the right compartment and the left side of the left compartment. That potential, which we will write V_p (P for Planck), is called the liquid junction potential. Planck's result is

$$V_p = - \frac{(D_+ - D_-)kT}{(D_+ + D_-)e} \ln \frac{n_c}{n_d} \quad (1)$$

Here D_+ is the diffusion constant of the positive ions and D_- that of the negative ions, k Boltzmann's constant, T the absolute temperature, and e the electronic charge. The sign may be seen to make sense as when D_+ is greater than D_- , there is a faster flow of positives from the right compartment in Figure 1, leaving the right side negative and the left side positive. Thus the right side is at a lower potential than the left side in accord with the sign in eq 1.

II. The Classical Derivation

In the classical derivation of eq 1, which somehow works even though it involves the seemingly contradictory use of the neutrality hypothesis, the positive and negative currents are equated. These currents are

$$j_+ = -D_+ \frac{\partial n_+}{\partial x}(x, t) + \mu_+ e E(x, t) n_+(x, t) \quad (2a)$$

$$j_- = -D_- \frac{\partial n_-}{\partial x}(x, t) - \mu_- e E(x, t) n_-(x, t) \quad (2b)$$

Here μ_+ and μ_- are the mobilities of the positive and negative ions and $E(x, t)$ is the x component in the electric field. It is assumed that we are dealing with a one-dimensional problem, all quantities depending only on x , the coordinate perpendicular to the partition between the compartments. The mobilities satisfy the Einstein relationship

$$D_{\pm}/kT = \mu_{\pm} \quad (3)$$

It is argued now that once transients (of unspecified duration) die out, the positive and negative currents must be equal. If they were not, there would be a continuous build-up of charge in the compartments. Using the Einstein relations (eq 3) and setting j_+ equal to j_- we get

$$-D_+ \frac{\partial n_+}{\partial x} + D_+ \frac{eE}{kT} n_+ = -D_- \frac{\partial n_-}{\partial x} - \frac{D_- eE n_-}{kT} \quad (4)$$

Assuming charge neutrality we may set $n_+ = n_- = n$ and eq 4 may be rewritten

$$(D_+ - D_-) \frac{\partial n}{\partial x} = \frac{(D_+ + D_-)eEn}{kT} \quad (5)$$

If we now integrate eq 5 with respect to x from the left of

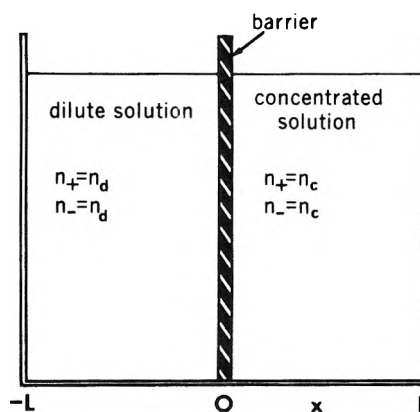


Figure 1. Initial condition of a liquid junction.

the left compartment ($x = -L$) to the right of the right compartment ($x = L$), we get

$$V_p = - \int_{x=-L}^{x=L} E dx \quad (6)$$

$$= - \frac{(D_+ - D_-)}{(D_+ + D_-)} \left(\frac{kT}{e} \right) \ln \frac{n(L)}{n(-L)}$$

Setting the concentrations of the ions at the extreme ends of the cell equal to their initial values, we obtain the liquid junction potential formula, eq 1.

III. Questions

Perhaps the skepticism in the discussion of the derivation in the preceding section is exaggerated. Indeed, there are good physical reasons why the steady-state currents may be equated and why charge neutrality is a good approximation. Were this not so the electrostatic energies would be enormous. Indeed, presumably the correct answer is obtained from these arguments because they are physically correct. Apart from this, however, the question is, how can one prove that they are correct? The system after all is not indeterminate. There are, in point of fact, three equations in three unknowns with well-defined initial and boundary conditions. The three unknown functions are n_+ , n_- , and E . The three equations are the continuity equations for the two charge species and Maxwell's first equation. Using eq 2a and 2b, the Einstein relations, the continuity equation, and Maxwell's equation, these three equations are

$$\frac{1}{D_+} \frac{\partial n_+}{\partial t} = \frac{\partial^2 n_+}{\partial x^2} - \frac{\partial}{\partial x} \left(\frac{eE n_+}{kT} \right) \quad (7a)$$

$$\frac{1}{D_-} \frac{\partial n_-}{\partial t} = \frac{\partial^2 n_-}{\partial x^2} + \frac{\partial}{\partial x} \left(\frac{eE n_-}{kT} \right) \quad (7b)$$

$$\frac{\partial E}{\partial x} = \frac{4\pi e}{\epsilon} (n_+ - n_-) \quad (7c)$$

Here ϵ is the dielectric constant of water, ~ 80 . The initial conditions are

$$n_+(x, 0) = n_-(x, 0) = \begin{cases} n_c & (0 \leq x \leq +L) \\ n_d & (0 \geq x \geq -L) \end{cases} \quad (8)$$

$$E(x, 0) = 0$$

The boundary conditions are simply that the ion currents are zero at $x = \pm L$, but for a cell of reasonable laboratory dimensions and for times less than days, it is sufficient to have the concentrations go to n_c and n_d as x approaches $+L$ or $-L$, respectively.

If the physical reasoning used in going from eq 2a and 2b to eq 6 is correct, how can one see it from the equations for the system, eq 7 and 8? If the result is a "very good approximation," what is the nature of the approximation? What is the small parameter, if any? How does one get the next term in the approximation, and how large is the next term? In spite of an enormous amount of work involving the use of the liquid junction potential formula and many papers discussing the theory,³ before the 1970's there was no correct explanation of how the fundamental equations (eq 7) led to the liquid junction potential formula or justified the assumptions used in the heuristic derivation presented in the previous section.

IV. The Search for a Small Parameter

It should be said at the outset that there is no apparent way to obtain an analytical solution of eq 7. The major source of the difficulty is the nonlinear conduction current terms in (7a) and (7b) which are products of the electric field with the ion densities. If we cannot find an exact solution, then we must find an approximate method of solving the basic equations—an approximate method which, we hope, will lead to an understanding of the liquid junction potential formula. In order to find an approximate method, we must attempt to find a small parameter which is characteristic of the process and which will lead to an expansion procedure. To see how we must proceed toward this objective we introduce transformations in the variables which make the equations dimensionless. We call the average density

$$\bar{n} = \frac{n_c + n_d}{2} \quad (9)$$

and introduce dimensionless densities according to

$$N_+ = \frac{n_+}{\bar{n}} \quad N_- = \frac{n_-}{\bar{n}} \quad (10)$$

These dimensionless densities are generally of order of magnitude unity. It is also convenient to introduce an "effective" diffusion constant, \bar{D} , according to

$$\frac{1}{\bar{D}_+} = \frac{1}{\bar{D}}(1 - \Delta) \quad \frac{1}{\bar{D}_-} = \frac{1}{\bar{D}}(1 + \Delta) \quad (11)$$

where Δ is a dimensionless parameter proportional to the difference between D_+ and D_- . The inverse relations are

$$\bar{D} = \frac{2D_+D_-}{D_+ + D_-} \quad \Delta = \frac{D_+ - D_-}{D_+ + D_-} \quad (12)$$

We may also introduce units of length, time and electric field which we can choose at our convenience to make the equations as simple as possible. If we write these units as x_0 , t_0 , and E_0 , we may introduce dimensionless coordinates according to

$$y = \frac{x}{x_0} \quad \tau = \frac{t}{t_0} \quad \xi = \frac{E}{E_0} \quad (13)$$

With eq 10, 11, and 13, the basic equations, eq 7a-c, become

$$\frac{\partial^2 N_+}{\partial y^2} - \frac{eE_0x_0}{kT} \frac{\partial}{\partial y}(\xi N_+) = \frac{x_0^2}{t_0\bar{D}}(1 - \Delta) \frac{\partial N_+}{\partial \tau} \quad (14a)$$

$$\frac{\partial^2 N_-}{\partial y^2} + \frac{eE_0x_0}{kT} \frac{\partial}{\partial y}(\xi N_-) = \frac{x_0^2}{t_0\bar{D}}(1 + \Delta) \frac{\partial N_-}{\partial \tau} \quad (14b)$$

$$\frac{\partial \xi}{\partial y} = \frac{4\pi ex_0\bar{n}}{\epsilon_0}(N_+ - N_-) \quad (14c)$$

We may now choose the units to eliminate as many parameters in the equations as possible. Accordingly, we take

$$eE_0x_0/kT = 1 \quad (15a)$$

$$x_0^2/t_0\bar{D} = 1 \quad (15b)$$

$$4\pi e\bar{n}x_0/\epsilon_0 = 1/2 \quad (15c)$$

In the last equation, the left-hand side is set equal to $1/2$ (rather than 1) so that we arrive at the conventional definition of the Debye length for x_0 . Solving for the unit sizes we have

$$x_0 = \left(\frac{\epsilon kT}{8\pi\bar{n}e^2} \right)^{1/2} \quad (16a)$$

$$E_0 = \frac{kT}{ex_0} = \left(\frac{8\pi\bar{n}kT}{\epsilon} \right)^{1/2} \quad (16b)$$

$$t_0 = \frac{x_0^2}{\bar{D}} = \frac{\epsilon kT}{8\pi\bar{n}e^2\bar{D}} \quad (16c)$$

Equations 14a-c then become

$$\frac{\partial^2 N_+}{\partial y^2} - \frac{\partial}{\partial y}(\xi N_+) = (1 - \Delta) \frac{\partial N_+}{\partial \tau} \quad (17a)$$

$$\frac{\partial^2 N_-}{\partial y^2} + \frac{\partial}{\partial y}(\xi N_-) = (1 + \Delta) \frac{\partial N_-}{\partial \tau} \quad (17b)$$

$$\frac{\partial \xi}{\partial y} = \frac{1}{2}(N_+ - N_-) \quad (17c)$$

The equations are now bare of all constants except Δ , which although it must be less than unity in absolute magnitude, does not have to be particularly small. An expansion of the solution in powers of Δ is not the procedure for which we have been looking. It does not converge rapidly enough and it does not yield the correct result to first order in Δ .

If the small parameter is not in the equations, where then is it? We can see which way to proceed if we evaluate the units x_0 and t_0 for representative experimental conditions. The Debye length under typical conditions ($n \approx 0.1 M$ and $T \approx 300^\circ K$) is of the order of 10^{-7} cm. As ionic diffusion constants are of the order of 10^{-5} cm² sec⁻¹, we get for the unit of time

$$t_0 = \frac{x_0^2}{\bar{D}} \cong \frac{10^{-14}}{10^{-5}} \cong 10^{-9} \text{ sec}$$

Thus in eq 17 the time t is measured in units of 10^{-9} sec. One second after the barrier has been removed $\tau = 10^9$. In an experimental situation we want the asymptotic form of the solution for $\tau \rightarrow \infty$. Thus, the small parameter for which we are looking is the reciprocal of the elapsed time measured in units of t_0 , which is of order 10^{-9} sec. Our conclusion therefore is that we must in some way search for a solution of the system of equations that is an expansion in powers of τ^{-1} .

V. The Solution

The reason for saying "in some way" at the end of the last section is that we still have to find the proper form of the expansion. An expansion of the form $N = N_0(y) + (1/\tau)N_1(y) + (1/\tau^2)N_2(y) + \dots$ cannot describe an on-going diffusion process. In view of the fact that there is diffusion going on it is natural to introduce an appropriate variable

$$z = y/\sqrt{\tau} \tag{18}$$

An expansion of the densities of the form $N = N_0(z) + N_1(z)/\tau + N_2(z)/\tau^2 + \dots$ makes sense. It yields solutions which for large times satisfy the differential equations and are consistent with the initial conditions. In terms of the new variable z , the partial differential equations become

$$\frac{1}{\tau} \frac{\partial^2 N_+}{\partial z^2} - \frac{\partial}{\partial z} \left(\frac{N_+ \xi}{\sqrt{\tau}} \right) = (1 - \Delta) \frac{\partial N_+}{\partial \tau} - \frac{z}{2\tau} \frac{\partial N_+}{\partial z} \tag{19a}$$

$$\frac{1}{\tau} \frac{\partial^2 N_-}{\partial z^2} + \frac{\partial}{\partial z} \left(\frac{N_- \xi}{\sqrt{\tau}} \right) = (1 - \Delta) \frac{\partial N_-}{\partial \tau} - \frac{z}{2\tau} \frac{\partial N_-}{\partial z} \tag{19b}$$

$$\frac{\partial}{\partial z} \left(\frac{\xi}{\sqrt{\tau}} \right) = \frac{1}{2} (N_+ - N_-) \tag{19c}$$

It is convenient to introduce in place of the positive and negative charge densities (in dimensionless units), the total ion density and the net charge density

$$S = N_+ + N_- \tag{20a}$$

$$C = N_+ - N_- \tag{20b}$$

Here S stands for "sum" and C for "charge." Adding and subtracting eq 19a and 19b the set of equations becomes

$$\frac{1}{\tau} \frac{\partial^2 S}{\partial z^2} - \frac{\partial}{\partial z} \left(\frac{\xi}{\sqrt{\tau}} C \right) = \frac{\partial}{\partial \tau} (S - \Delta C) - \frac{z}{2\tau} \frac{\partial}{\partial z} (S - \Delta C) \tag{21a}$$

$$\frac{1}{\tau} \frac{\partial^2 C}{\partial z^2} - \frac{\partial}{\partial z} \left(\frac{\xi}{\sqrt{\tau}} S \right) = \frac{\partial}{\partial \tau} (C - \Delta S) - \frac{z}{2\tau} \frac{\partial}{\partial z} (C - \Delta S) \tag{21b}$$

$$\frac{\partial}{\partial z} \left(\frac{\xi}{\sqrt{\tau}} \right) = \frac{C}{2} \tag{21c}$$

We now introduce the large τ expansions of the functions. We write

$$S(z, \tau) = S_0(z) + \frac{S_1(z)}{\tau} + \frac{S_2(z)}{\tau^2} + \dots \tag{22a}$$

$$C(z, \tau) = C_0(z) + \frac{C_1(z)}{\tau} + \frac{C_2(z)}{\tau^2} + \dots \tag{22b}$$

$$\frac{\xi(z, \tau)}{\sqrt{\tau}} = \frac{\eta_1(z)}{\tau} + \frac{\eta_2(z)}{\tau^2} + \dots \tag{22c}$$

In eq 21a-c, $\tau^{-1/2}$ always occurs with ξ and we have introduced the expansion eq 22c accordingly. With regard to this expansion, there is no $\eta_0(z)$ as $\xi(z, \tau)$ would continue to increase with increasing time if such a term were present. The leading term in $\xi(z, \tau)$ is thus

$$\xi(z, \tau) \cong \eta_1(z)/\sqrt{\tau} \tag{23}$$

This makes very good sense in that it gives rise to a time-independent V_p , for we can then write (with eq 13 and 18)

$$V_p = E_0 \int_{x=-\infty}^{x=\infty} \frac{\eta_1(z) dx}{\sqrt{\tau}} \tag{24}$$

$$= -E_0 x_0 \int_{-\infty}^{\infty} \eta_1(z) dz$$

The procedure is now to insert eq 22 into eq 21 and equate like powers of τ . There is only one term of order τ^0 . From eq 21c this equation is

$$\tau^0: C_0(z) = 0 \tag{25}$$

The above result constitutes the derivation of charge neutrality. That is, the leading term in the charge density goes at most as τ^{-1} (recall that $\tau = t/t_0$, $t_0 \approx 10^{-9}$ sec).

Equating the coefficients of all terms of order τ^{-1} we get

$$\tau^{-1}: \frac{d^2 S_0}{dz^2} = -\frac{z}{2} \frac{dS_0}{dz} \tag{26a}$$

$$-\frac{d}{dz} [\eta_1(z) S_0(z)] = \frac{z \Delta}{2} \frac{dS_0}{dz} \tag{26b}$$

$$\frac{d\eta_1(z)}{dz} = \frac{C_1(z)}{2} \tag{26c}$$

In the above, eq 26a may be integrated directly with the constants of integration chosen to satisfy the boundary conditions. The result is

$$S_0(z) = (N_c + N_d) + \frac{(N_c - N_d)}{\sqrt{\pi}} \times \int_{z=0}^z dz' \exp\left(-\frac{z'^2}{4}\right) \tag{27}$$

Here N_c and N_d are respectively n_c/\bar{n} and n_d/\bar{n} . In writing eq 27 we have assumed that we are dealing with values of the time such that the quantity $L/(\bar{D}t)^{1/2}$ is much greater than unity. That means that in the integral in eq 27 at $z = Lt_0^{1/2}/x_0 t^{1/2} = L/(\bar{D}t)^{1/2}$ (corresponding to $x = L$) we may take the upper limit to be infinity and $S_0(L)$ becomes $2N_c$ as it should. Similarly at $x = -L$, $S_0(-Lt_0^{1/2}/x_0 t^{1/2}) = 2N_d$. This result shows that the total ion density diffuses with an effective diffusion constant equal to \bar{D} . That is

$$D_{\text{eff}} = \bar{D} = \frac{2D_+ D_-}{D_+ + D_-} \tag{28}$$

which is the well-known expression for the ambipolar diffusion constant.

If we now use the result of eq 27 in eq 26b and integrate from $-\infty$ to z we get

$$\eta_1(z) = \frac{\frac{\Delta}{\sqrt{\pi}} (N_c - N_d) \exp(-z^2/4)}{N_c + N_d + \frac{(N_c - N_d)}{\sqrt{\pi}} \int_{z=0}^z dz' \exp(-z'^2/4)} \tag{29}$$

Inserting this result in eq 24 and using eq 12 and 16 yield precisely the result for the liquid junction potential formula, eq 1.

The last of the equations for terms of order τ^{-1} , eq 22c, simply provides an expression for the charge density $C_1(z)$ that is consistent with the leading term in the electric field intensity.

VI. Conclusions

In effect the theory provides a formal derivation of the assumptions conventionally made in the study of ionic dif-

fusion in liquid junctions. It is shown that in a matter of fractions of 1 sec after ions are allowed to diffuse across a barrier, the net charge density approaches zero, the total ion density diffuses with a diffusion constant equal to the ambipolar diffusion constant $D_{\text{eff}} = 2D_+D_-/(D_+ + D_-)$, and the potential difference $V_P = V(L) - V(-L)$ is given by the liquid junction potential formula. Furthermore, explicit expressions are obtained for the leading terms of all of the quantities. The paradox of the existence of a potential while one has charge neutrality may now be resolved. The charge density at any point does indeed go to zero as t^{-1} . The spread of the charge however increases as $t^{1/2}$. Therefore the net charge per unit area decreases as $t^{-1/2}$. The potential difference is of the order of the product of the charge per unit area (proportional to the field), which goes as $t^{-1/2}$, with the separation, proportional to $t^{1/2}$. Hence the liquid junction potential is time independent as long as we are dealing with times large compared to t_0 ($\sim 10^{-9}$ sec) and small compared to the time for the ions to diffuse to the walls. It is interesting to note that in obtaining all of these results at no point did we have to make use of any argument relating to the magnitude of the electrostatic energy compared to thermal energies. Indeed, the actual basis of all of the results enumerated above depends on the physical fact that diffusion over a Debye length takes of the order of 10^{-9} sec in typical laboratory situations and on the subjective "fact" that for a human observer 10^{-9} sec is an extremely small time.

This calculation of course does not provide any information on what goes on at the junction for times less than 10^{-9} sec. The results of numerical integrations of the basic equations, which start from the initial stages of the process

and exhibit the growth of the liquid junction potential to its long time value, were presented by Hafeman⁴ in 1965. Hafeman carried out computer calculations under more general conditions than those we treat here but for large times his results are in general agreement with those of this analytic treatment, including the induction times of the order 10^{-9} sec.

Acknowledgments. The author thanks Drs. Lee Segel of the Weizmann Institute, Sam R. Coriell of the National Bureau of Standards, and Jacob Jorné of Wayne State University for their help and encouragement. This work originated while the author was a Senior Weizmann Fellow in the Polymer Research Department of the Weizmann Institute of Science during the academic year 1971–1972. He is indebted to many colleagues in the department for helpful discussions. In particular, he wishes to express his debt to the late head of the Polymer Research Department, Dr. Aharon Katchalsky, whose love of science and enthusiasm was an inspiration to all who knew him.

References and Notes

- * Deceased July 5, 1974. Address correspondence to Dr. Jacob Jorné, Department of Chemical Engineering and Material Sciences, Wayne State University, Detroit, Mich. 48202.
- (1) M. Planck, *Ann. Phys. (Leipzig)*, **39**, 161 (1890).
 - (2) H. J. Hickman, *Chem. Eng. Sci.*, **25**, 381 (1970).
 - (3) Reference 2 contains many references in which there are a variety of theoretical approaches to the liquid junction potential problem. More recent examples are as follows: R. N. Goldberg and H. S. Frank, *J. Phys. Chem.*, **76**, 1758 (1972); S. B. Maloedkar and M. D. Kosten, *J. Chem. Phys.*, **57**, 3263 (1972); E. C. Moreno and R. T. Zahradnick, *J. Electrochem. Soc.*, **120**, 641 (1973).
 - (4) D. R. Hafeman, *J. Phys. Chem.*, **69**, 4226 (1965).

Statistical Thermodynamic Consideration of Solvent Effects on Conformational Stability. The Supermolecule–Continuum Model

David L. Beveridge* and Gary W. Schnuelle

Chemistry Department, Hunter College of the City University of New York, New York, New York 10021 (Received April 23, 1974)

A theoretical analysis of solvent effects on the conformational stability of a dissolved molecule is presented in terms of statistical thermodynamics. The relationships among the various current approaches to the problem are discussed in this context, together with considerations on their capabilities and limitations. The union of these approaches into a "supermolecule-continuum" model is shown to accommodate the main factors which contribute to solute–solvent interactions. A progression of improved methods for supermolecule-continuum calculations are proposed and the prospects for quantum mechanical calculations in each case are discussed.

I. Introduction

The theoretical treatment of chemical bonding and molecular geometry in polyatomic molecules has reached a relatively high level of sophistication, with *ab initio* molecular quantum mechanics and well-parametrized approximate

quantum mechanical or classical potential function methods widely available. However, the use of these methods in many chemical and biochemical problems requires also a consideration of environmental effects, since the relative stability of molecular conformations and the relative ease of conformational changes for dissolved molecules can be

profoundly influenced by the presence of solvent. The main factors responsible are (a) bulk dielectric aspects of intermolecular solute-solvent interactions, (b) dielectric modulation of solute intramolecular interactions, and (c) specific solute-solvent binding and antibinding.

Theoretical studies of solvent effects on large molecules are currently proceeding mainly from two points of view: the continuum model and the supermolecule model. In the continuum model, the solute-solvent system is represented as a solute molecule in a cavity imbedded in a polarizable dielectric continuum. Bulk dielectric effects are calculated on a classical basis in terms of the electric multipole moments of the solute and induced reaction fields in the continuum as originally described by Onsager.¹ Applications of this approach to problems in biomolecular conformational stability have been described by Sinanoglu² and Beveridge, *et al.*,³ the latter study emphasizing intermolecular bulk dielectric effects. Intramolecular dielectric effects were included in studies of solvent effects on polymer structure by Scheraga⁴ and coworkers and by Hopfinger⁵ using an effective dielectric constant for interatomic coulombic interactions. Kirkwood⁶ described an elegant approach to the calculation of both intermolecular and intramolecular bulk dielectric effects using classical or quantum mechanics. Extensive studies of the thermodynamic properties of solutions using the continuum model have recently been reported by Huron and Claverie.⁷

The supermolecule approach involves explicitly including one or more solvent molecules along with the solute in a calculation and determining conformational energies and related properties for the molecular assembly. Here solute-solvent binding effects are explicitly introduced. Quantum mechanical supermolecule calculations for single solute-solvent interactions and the idea of solvation sites, *i.e.*, energetically preferred solute-solvent configurations, have been described in a series of papers by Pullman and coworkers.⁸ Techniques for the optimization of solvation sites for an entire solvation shell have been discussed by Mantione and Daudey.⁹ Classical and statistical thermodynamic approaches to this model are contained in the studies of Scheraga, *et al.*,⁴ and of Hopfinger;⁵ the basic idea involves a variation in solvation number and related energetics with solute conformation.

The specific studies referenced above each include one or another of the main factors responsible for solvent effects on conformational stability, but no one calculation includes all three factors. Furthermore the formal relationship between the various current methods has not previously been developed. We present herein a general theoretical analysis of relevant aspects of solvent effects on conformational stability in terms of statistical thermodynamics. The logical relations among the current methods are displayed and the path to improved theoretical treatment of the problem is clearly indicated. With a judicious use of the supermolecule model for short-range solute-solvent interactions and the continuum model for long-range effects, statistical thermodynamic calculations using quantum mechanically calculated energies appear to be tractable. A progression of improved methods are proposed and the prospects for quantum mechanical calculations in each case are discussed.

II. Theory, Present Models, and Methods

A theoretical framework for understanding the continuum and supermolecule models and a basis for improved theoretical treatments of solvent effects can be developed

in terms of statistical thermodynamics. A very dilute solution can be taken as a canonical ensemble of systems consisting of a solute molecule surrounded by a large number of solvent molecules. The thermodynamic properties of the system follow from the canonical ensemble partition function. The configurational part of the function is (within a constant factor)

$$Z = \sum_i e^{-E_i/kT} \rightarrow \int e^{-E(Q)/kT} dQ \quad (1)$$

where k is the Boltzmann constant, T is the absolute temperature, and the E_i are in principle the quantum mechanical energy states of the system. Replacing the summation by the integration in eq 1 can be effected if the energy states are sufficiently close together. Here Q represents the configurational coordinates of all N molecules of the system, $Q = (q_1, q_2, q_3, \dots, q_N)$ and $dQ = dq_1 dq_2 dq_3 \dots dq_N$. The configurational coordinates q_i for individual molecules include position v_i , orientation ω_i , and internal coordinates χ_i , so that $q_i = \{v_i, \omega_i, \chi_i\}$ and $dq_i = dv_i d\omega_i d\chi_i$. The internal coordinates χ_i for a molecule may be likewise factored to a first approximation into bond lengths r_i , bond angles θ_i , and dihedral angles τ_i . The configurational free energy of the system is given by

$$A = -kT \ln Z \quad (2)$$

To relate solute conformation to the configurational partition function, we write the reduced partition function for the solute molecule (taken as particle 1) as

$$Z(\tau_1) = \iiint \dots \int e^{-E(q_1, q_2, q_3, \dots, q_N)/kT} dq_1' dq_2 dq_3 \dots dq_N \quad (3)$$

where the integrations extend over all coordinate space of the solvent molecules 2, 3, ..., N and over all the coordinates of the solute molecule except those internal coordinates involved to first order in establishing molecular conformation and conformational changes, *i.e.*, the dihedral angles τ_1 of the solute molecule. A general statistical mechanical treatment of internal modes and statistical weights in conformational problems has been described by Go and Scheraga;¹⁰ we restrict our consideration here to aspects of the problem relevant to the various models for treating solvent effects. We note in passing that eq 3 could be evaluated in principle for a system by a Monte Carlo calculation. This method is used extensively for the calculation of liquid structure using classical energy functions. This would of course be presently intractable for an N of respectable size using quantum mechanical methods for the energy evaluations, but the path of theoretical development lies in this direction.

The continuum and supermolecule models can both be regarded as efforts to approximate the evaluation of the energy function $E(q_1, q_2, q_3, \dots, q_N)$. The continuum model follows from making the approximation

$$E(q_1, q_2, q_3, \dots, q_N) \cong E^{\text{eff}}(\tau_1) + E_{\text{solvent}} \quad (4)$$

and calculating $E^{\text{eff}}(\tau_1)$ as an effective energy treating all intramolecular solute interactions explicitly and calculating solute-solvent interactions with the solvent considered as a polarizable dielectric continuum. The evaluation of $E^{\text{eff}}(\tau_1)$ can be carried out directly as described by Kirkwood;⁶ the first quantum mechanical calculation of this type was recently reported by Hylton, Christoffersen, and Hall.¹¹ The Onsager reaction field approach is a specific

case of the Kirkwood method and is applicable with the additional approximation

$$E^{\text{eff}}(\tau_1) \cong E_{\text{solute}}(\tau_1) + E_{\text{solvation}}^{\text{eff}}(\tau_1) \quad (5)$$

where $E_{\text{solute}}(\tau_1)$ is the solute conformational energy computed in the free-space approximation and $E_{\text{solvation}}^{\text{eff}}(\tau_1)$ the solute-solvent interaction energy. The term E_{solvent} in eq. 4 represents solvent-solvent intermolecular interactions (the cohesive energy of the solvent). This term is independent of solute conformation to a high order of approximation and contributes a term to the configurational free energy which can be regarded as a constant for each solvent.

For the i th specific conformation of the solute molecule, the conformational partition function in the continuum model is then

$$Z_i(\tau_1) = e^{-E_i^{\text{eff}}(\tau_1)/kT} \quad (6)$$

The conformational free energy is

$$A_i(\tau_1) = -kT \ln Z_i(\tau_1) = E_i^{\text{eff}}(\tau_1) \quad (7)$$

i.e., the conformational energy calculated using the continuum model is a conformational free energy.

In spite of the familiar form of eq 5 and 6, the $A_i(\tau_1)$ are free energies only in a limited sense: each $A_i(\tau_1)$ is the free energy the system can have if the solute were frozen in the i th conformation. More generally we have

$$A = -kT \ln Z = -kT \ln \sum_i Z_i(\tau_1) = -kT \ln \sum_i e^{-A_i(\tau_1)/kT} \quad (8)$$

so that the conformational free energies do not sum linearly to the total free energy as required of an extensive property. Nevertheless, inspection of the $A_i(\tau_1)$ as a function of τ_1 (cf. the conformational maps of ref 3) permits a convenient visualization of the contributions to the configurational partition function and thus indicates which conformations make the heaviest contribution to the Helmholtz configurational free energy. Since the important conformations can be identified with one or another of the various energy minima in the τ_1 conformational space, a common way of examining results is to partition the summation over i into a double summation over the k minima and the i conformations in the immediate vicinity of the k th minimum

$$\sum_i Z_i = \sum_k \sum_{i \in k} Z_i = \sum_k W_k \quad (9)$$

where W_k is the statistical weight of the k th minimum. The probability of observing the j th minimum is then

$$P_j = W_j / \sum_k W_k \quad (10)$$

The conformational properties of the system in terms of the supermolecule model as used by Pullman⁸ can be considered in terms of the reduced partition for the solute and a single solvent molecule (taken as particle 2)

$$Z(\tau_1, q_2) =$$

$$\int \int \dots \int e^{-E(q_1, q_2, q_3, \dots, q_N)/kT} dq_1' dq_3 \dots dq_N \quad (11)$$

The supermolecule model corresponds to making the approximation

$$E(q_1, q_2, q_3, \dots, q_N) \cong E(\tau_1, q_2) + E_{\text{solvent}} \quad (12)$$

and calculating $E(\tau_1, q_2)$ in the free-space approximation using quantum mechanics or classical mechanics. For the i th conformation of the solute molecule and the j th relative position and orientation of the solvent molecule

$$Z_{ij}(\tau_1, q_2) = e^{-E_{ij}(\tau_1, q_2)/kT} \quad (13)$$

Analogous to eq 5 we may write the solute molecule conformational partition function using the supermolecule model as

$$Z_i(\tau_1) = \sum_j e^{-E_{ij}(\tau_1, q_2)/kT} \rightarrow \int e^{-E_i(\tau_1, q_2)/kT} dq_2 \quad (14)$$

where the sum and integral indicate configurational averaging over the coordinates of the solvent molecule.

A formal definition of solvation sites emerges from a partitioning of eq 14 into sums from the individual minima k in the $E(\tau_1, q_2)$ hypersurface. Then

$$Z_i(\tau_1) = \sum_k \sum_{j \in k} Z_{ij} = \sum_k W_{ik} \quad (15)$$

which serves to define W_{ik} , the statistical weight of the k th solvation site for a solute molecule in the i th conformation. The position of the k th solvation site is the geometry corresponding to the minimum in the $E_{ij}(\tau_1, q_2)$, $j \in k$, surface. The relative importance of a given solvation site depends on the magnitude of the statistical weight W_{ik} , a function of both the solute-solvent binding energy and the shape of the binding hypersurface. A tightly bound solvation site may be of little interest to the system if the binding force constants are high.

This analysis can be easily extended to accommodate an entire solvation shell. For this we write the reduced partition function for the solute molecule and $M - 1$ neighboring solvent molecules as

$$Z(\tau_1, q_2, q_3, \dots, q_M) = \int \int \dots \int e^{-E(q_1, q_2, \dots, q_M, \dots, q_N)/kT} dq_1' dq_{M+1} \dots dq_N \quad (16)$$

Explicit consideration of the solute and $M - 1$ solvent molecules in a calculation would amount to the approximation

$$E(q_1, q_2, \dots, q_M, \dots, q_N) \cong E(\tau_1, q_2, \dots, q_M) + E_{\text{solvent}} \quad (17)$$

Note that the results at this level would differ from results of calculations carried out at the level of eq 11 if cooperative effects among solvent molecules are important.

The solvation shell methods used in conjunction with classical energy calculations by Scheraga and by Hopfinger⁵ can be considered in the context of the supermolecule model and correspond to the approximation

$$E(\tau_1, q_2, q_3, \dots, q_M) \cong E_{\text{solute}}(\tau_1) + E_{\text{solvation}}(q_2, q_3, \dots, q_{M(\tau_1)}) \quad (18)$$

where the first term on the right-hand side is an isolated molecule solute energy and the second term is the solvation energy. The number of solvent molecules explicitly considered is written as $M(\tau_1)$ to emphasize dependence of solvation number on solute conformation. The solvation energy term is then considered in the form

$$E_{\text{solvation}}(q_2, q_3, \dots, q_{M(\tau_1)}) = \sum_j^{M(\tau_1)} V_j \quad (19)$$

where the individual solute-solvent molecule interaction energies V_j are determined theoretically or semiempirically on prototype cases.

Both the continuum and supermolecule models have specific advantages and disadvantages. The continuum model is suitable for solvent effects on conformational stability in systems where specific solute-solvent binding does not vary significantly with conformation, *i.e.*, when differential effects are negligible. This model would be inadequate in systems where conformational changes in the solute move potential solvent binding sites from protected to exposed regions or in systems where specific structures are stabilized by intramolecular hydrogen bonding. The supermolecule model can adequately treat solute-solvent binding but would be inadequate for systems where the electric moments of the solute are sharply varying functions of solute conformation and bulk dielectric effects are important.

III. Improved Model and Proposed Methods

Most of the shortcomings discussed above for the continuum and supermolecule models for solvent effects can be avoided by combining the best features of the two approximations. The union of the two models into a supermolecule-continuum model follows from the supermolecule partition function as written in eq 19, invoking the approximation

$$E(q_1, q_2, q_3, \dots, q_M, \dots, q_N) = E^{\text{eff}}(\tau_1, q_2, q_3, \dots, q_M) + E_{\text{solvent}} \quad (20)$$

and calculating $E^{\text{eff}}(\tau_1, q_2, q_3, \dots, q_M)$ as an effective energy of the solute and the $M - 1$ vicinal solvent molecules in a cavity imbedded in a polarizable dielectric continuum. A solute molecule conformational partition function may be formed by writing for the i th conformation of the solute molecule and the j th, k th, \dots , m th configuration of the solvent molecules explicitly considered

$$Z_{ijk\dots m}(\tau_1, q_2, q_3, \dots, q_M) = e^{-E^{\text{eff}}_{ijk\dots m}(\tau_1, q_2, q_3, \dots, q_M) / kT} \quad (21)$$

Analogous then to eq 4 and 17 we may write for the supermolecule-continuum model

$$Z_i(\tau_1) = \sum_j \sum_k \dots \sum_m e^{-E^{\text{eff}}_{ijk\dots m}(\tau_1, q_2, q_3, \dots, q_M) / kT} \rightarrow \iint \dots \int e^{-E_i^{\text{eff}}(\tau_1, q_2, q_3, \dots, q_M) / kT} dq_2, dq_3 \dots dq_M \quad (22)$$

where M may depend on the solute conformational variables τ_1 . Definitions of statistical weights and solvation sites can be written as straightforward analogs of eq 8 and 14.

The classical or quantum mechanical evaluation of the individual energies in this model follows directly from the original Kirkwood paper,⁶ but a consideration of cavity size and shape will require special attention. A classical calculation based on this idea was carried out by Kirkwood in a study of dielectric polarization in polar liquids.¹² This approach has also been used in theoretical accounts of the hydrated electron, and the recent *ab initio* quantum mechanical study of this system by Newton¹³ approaches a supermolecule-continuum calculation except for configurational

averaging. We consider herein the prospects for calculations based on this model for conformational studies.

The advantage of the supermolecule-continuum model for studies of solvent effects on molecular conformation is that both inter- and intramolecular bulk dielectric effects and specific solute-solvent binding are accommodated. Classical conformational energy calculations based on this model are clearly feasible combining Hopfinger's solvation shell method with an Onsager or Kirkwood treatment of the dielectric.¹⁴ The extent to which quantum mechanical calculations at especially the *ab initio* level are tractable for this model is a question of considerable interest, since the use of classical potential functions introduces more approximations. The details of self-consistent field molecular orbital continuum calculations are being reported by Hylton, *et al.*,¹¹ and the extension of the calculation to supermolecule-continuum is straightforward for individual energy grid points. The main problem in a quantum mechanical supermolecule-continuum calculation is the extent to which configurational averaging can be included in a computationally manageable manner for systems of chemical interest.

We mention in passing that the explicit presence of molecules in the first solvation shell may account for the most important intramolecular solvent dielectric effects in a supermolecule-continuum calculation. The remaining effects would then be adequately represented by additive terms as in eq 5 calculated classically. Prototype studies are required to assess the need actually to include solvent dielectric terms in the quantum mechanical Hamiltonians for these calculations.

With reference to eq 21, a progression of computational methods can be enumerated which have considerable possibilities for estimates of configurational averaging over the solvent molecules in quantum statistical mechanical calculations of solvent effects on conformational stability. These are described in the following paragraphs in terms of the shell method, the cell method, and the site method. Each of the methods involves a Monte Carlo calculation at some point, and the various variance reduction techniques as described in the monograph by Hammersley and Handscomb¹⁵ are of course relevant.

The Shell Method. The shell method is an obvious approach and is described here for completeness and the definition of terminology relevant to the other methods. Since the focus of the problem is on the solute and solvent effects on solute structure, the translational domain of the $M - 1$ solvent molecules can be restricted to regions of space immediately vicinal to the solute molecule. This region is then operationally partitioned into solvation shells, with the first shell containing first nearest neighbors, the second shell containing the second nearest neighbors, etc. The conformational partition function for the supermolecule-continuum method including first nearest neighbors in the shell model is

$$Z_i(\tau_1) = \int_{v_2}^{s_1} \int_{\omega_2} \dots \int_{v_M}^{s_1} \int_{\omega_M} e^{-E^{\text{eff}}(\tau_1, v_2, \omega_2, \dots, v_M, \omega_M) / kT} dv_2 d\omega_2 \dots dv_M d\omega_M \quad (23)$$

where s_1 indicates that the integration extends over the first solvation shell. While it is possible that the influence of shells beyond the first on solute conformational stability

will be adequately represented by the continuum, the sphere of influence of, e.g., an ionic functional group of the solute certainly extends beyond the first layer. Differential effects on conformation may still be negligible, but this point requires careful numerical study.

The Cell Method. In the statistical mechanics of pure liquids, an approach to tractability in the configurational partition function is represented by the cell theories. Here the overall integration is reduced to a product of integrals each involving the configurational coordinates of one molecule only by restricting the positional domain of each particle to a small region or "cell," with "walls" of the cell located at the van der Waals contact surface of nearest-neighbor molecules. Widely quoted examples of this genre of calculations are the studies of Lennard-Jones and Devonshire¹⁶ and Wentorf, Buehler, Hirschfelder, and Curtiss.¹⁷ The principal error in the model is quantified in terms of the communal free energy and entropy, which appear when the walls of all the cells are removed so that all molecules have access to the common total volume.

An analog of cell theory can be defined for calculation of conformational partition functions in the supermolecule-continuum model. The solvation shell described above is spatially partitioned into $M - 1$ cells each accommodating one solvent molecule. The partition function then reduces to

$$Z_i(\tau_1) = \int_{v_2}^{c_1} \int_{\omega_2} \cdots \int_{v_M}^{c_{M-1}} \int_{\omega_M} e^{-E^{\text{eff}}(\tau_1, v_2, \omega_2, \dots, v_M, \omega_M) / RT} dv_2 d\omega_2 \dots dv_M d\omega_M \quad (24)$$

where the volume integrations extend over the domains of the individual solvation cells of each solvent molecule. The extent to which communal free energies and entropies influence conformational stability can be determined by comparing the results of the shell method and cell method on prototype systems.

The methods for the computation of solvation energy in the classical energy calculations described at the end of section II can be considered supermolecule cell methods. Note also in this regard that the shell method is in a sense a supercell method, and communal effects upon including additional solvation shells in the calculation can be evaluated by comparing the results of a calculation by the shell method and analogously defined supershell method.

The Site Method. The logical extreme of the cell method is the total restriction of positional degrees of freedom. In the site method, the $M - 1$ solvent molecules are deployed on specific solvation sites in the solvation shell, and only orientation averaging is considered. The conformational partition function for the site method is simply

$$Z_i(\tau_1) = \int_{\omega_2} \cdots \int_{\omega_M} e^{-E^{\text{eff}}(\tau_1, \omega_2, \dots, \omega_M)} d\omega_2 \dots d\omega_M \quad (25)$$

The principal problem in the application of the site method is the reasonable determination of site positions and, as above, communal errors. A steric method of selecting solvation sites has been proposed by Mantione and Daudey.⁹ The tractability of the method is better than that of any approach involving positional averaging and the capabilities and limitations of the method are worth exploring on

prototype systems. The results of shell method or cell method calculations on individual functional groups may identify solvation sites with some degree of transferability, so that experience gained in these methods on small systems can be used to configure a reasonable form of site theory for large molecules. It should be recognized that positional reorganization within certain regions the first solvation shell is expected to be common in conformational studies and the choice of sites in the site method must depend on solute conformation.

IV. Summary and Conclusions

Statistical thermodynamics has been used to describe the relationships among the various current approaches to the calculation of solvent effects on conformational stability and their capabilities and limitations. The three main factors in solute-solvent interactions are seen to be accommodated by a union of existing models into the supermolecule-continuum model.

Overall the supermolecule-continuum model is directly adaptable to classical energy calculations with only a slight extension of current methodology. The prospects for quantum mechanical calculation of solvent effects on conformational stability depend on the techniques that can be devised for reasonable approximations to configurational averaging in the first solvation shell. Calculations at least at the approximate molecular orbital level and to some degree at the *ab initio* level are within reach of the method. Numerical calculations on solvent effects using the supermolecule-continuum model in conjunction with quantum mechanical energy calculations are currently in progress in this laboratory.

Acknowledgment. This study was supported by U. S. Public Health Service Research Career Development Award 6K04-GM21281-01A1 to D. L. B. from the National Institute of General Medical Sciences.

References and Notes

- (1) L. Onsager, *J. Amer. Chem. Soc.*, **58**, 1486 (1936).
- (2) O. Sinanoglu in "Molecular Associations in Biology," B. Pullman, Ed., Academic Press, New York, N. Y., 1968, p 427 ff.
- (3) D. L. Beveridge, M. M. Kelly, and R. J. Radna, *J. Amer. Chem. Soc.*, in press; D. L. Beveridge, R. J. Radna, G. W. Schnuelle, and M. M. Kelly in "Proceedings of the 7th Jerusalem Symposium on Molecular and Quantum Pharmacology," B. Pullman and E. Bergmann, Ed., Academic Press, New York, N. Y., in press.
- (4) H. A. Scheraga, *Chem. Rev.*, **71**, 195 (1971).
- (5) A. J. Hopfinger, "Conformational Properties of Macromolecules," Academic Press, New York, N. Y., 1973.
- (6) J. G. Kirkwood, *J. Chem. Phys.*, **2**, 351 (1934).
- (7) M. J. Huron and P. Claverie, *J. Phys. Chem.*, **76**, 2123 (1972); in press.
- (8) G. Alagona, A. Pullman, E. Scrocco, and J. Tomasi, *Int. J. Peptide Protein Res.*, **5**, 251 (1973); G. Alagona, A. Pullman, and J. Tomasi, *Theor. Chim. Acta*, in press; G. N. Port and A. Pullman, *FEBS (Fed. Eur. Biochem. Soc.) Lett.*, **31**, 70 (1973).
- (9) M. J. Mantione and J. P. Daudey, *Chem. Phys. Lett.*, **6**, 93 (1970).
- (10) N. Gö and H. A. Scheraga, *J. Chem. Phys.*, **51**, 4751 (1969). These authors discuss the contribution of the integration over momenta to the total partition function, which we are implicitly treating as a constant. They show that our approximation neglects the effect of the "kinetic entropy," which is on the order of 0.5 kcal/mol for polymers and is expected to be smaller still for solute molecules amenable to the present treatment.
- (11) J. Hylton, R. Christoffersen, and G. G. Hall, *Chem. Phys. Lett.*, **24**, 501 (1974).
- (12) J. G. Kirkwood, *J. Chem. Phys.*, **7**, 911 (1939).
- (13) M. Newton, *J. Chem. Phys.*, **58**, 5833 (1973). See also ref 4 of this paper.
- (14) Note that the Onsager treatment assumes a value of unity for the dielectric constant within the cavity and therefore ignores intramolecular dielectric effects. These could be included in a classical calculation in

the Kirkwood formulation, which allows a variable dielectric constant within the cavity.

- (15) J. M. Hammersley and D. C. Handscomb, "Monte Carlo Methods," Methuen, London, 1964.

(16) J. E. Lennard-Jones and A. F. Devonshire, *Proc. Roy. Soc., Ser. A*, **163**, 53 (1937); **165**, 1 (1938).

- (17) R. H. Wentorf, R. J. Buehler, J. O. Hirschfelder, and C. F. Curtiss, *J. Chem. Phys.*, **18**, 1484 (1950).

COMMUNICATIONS TO THE EDITOR

Surface Acidity of Co-Mo-Al₂O₃ Catalysts

Sir: The surface acidity of the Co-Mo-Al₂O₃ system has recently been reported by Kiviat and Petrakis.¹ The influence of two factors, namely, the sodium content of the alumina support and the order of impregnation of the cobalt and molybdenum salts on the acidity of the final product, was not indicated. In our work on the structural characterization of hydrodesulfurization catalysts, we have found that these two parameters play an important role in determining both the total acidity and the acid strength distribution in the final product. Our results relating to the surface acidity of these samples are reported below.

Sample A was obtained from Boehmite by calcination at 550° for 24 hr in air and consisted of γ -alumina as seen from XRD patterns. Sample B was prepared from sample A and contained 279 ppm of Na⁺ ions by weight. Samples C and D were prepared from sample B and contained 12.5% of MoO₃ and 2.0% of CoO by weight, respectively. Samples E-G were obtained from sample B and all of them contained 2.0% of CoO and 12.5% of MoO₃, by weight. In the preparation of sample E, the support was impregnated with

the cobalt nitrate solution, dried at 110° (24 hr), and calcined at 550° in air for 4 hr. The ammonium paramolybdate solution was then impregnated on the resulting material. This order of impregnation was reversed in preparing sample F. Both of the constituents were impregnated simultaneously on sample B to yield sample G. Ammonium paramolybdate was impregnated (12.5% by weight of MoO₃) on sample A to yield sample H. Mo and Co salts were impregnated (12.5 and 2.0% by weight of MoO₃ and CoO, respectively) simultaneously on sample A to yield sample I. Sample J contained 2% by weight of CoO (impregnated from a solution of cobalt nitrate) on sample A. Sample K was prepared by impregnating sample H with cobalt nitrate solution (2% by weight of CoO) and drying the resulting material at 110° for 24 hr. Samples B-K were calcined in air at 550° for 4 hr before use. Sample L was pure MoO₃ prepared by the decomposition of ammonium paramolybdate in air at 500° for 24 hr. The acidity measurements were made using *n*-butylamine and H₀ indicators.²

The acid strength distribution of the surface sites in the various samples is shown in Table I. The following features

TABLE I: Surface Acid Strength Distribution in the Co-Mo-Al₂O₃ System

Sample	Differences in <i>n</i> -butylamine titer values ^a for indicators of various pK _a values				
	5 > pK _a > 3.3	3.3 > pK _a > 2	2 > pK _a > -3	-3 > pK _a > -5.6	pK _a < -5.6
A (Al ₂ O ₃)	0.8	0	0	3.4	0
B (Al ₂ O ₃ -Na)	0	0	0	0.9	0
C (Mo-Al ₂ O ₃ -Na)	1.5	0	0	3.6	6.0
D (Co-Al ₂ O ₃ -Na)	0.8	0	0	6.2	0
E (Co-Mo-Al ₂ O ₃ -Na)	1.0	0	0.8	3.6	7.0
F (Mo-Co-Al ₂ O ₃ -Na)	0.7	0	0	3.9	5.0
G (CoMo-Al ₂ O ₃ -Na)	2.2	0	0	2.4	6.5
H (Mo-Al ₂ O ₃)	3.4	0	0	5.0	5.0
I (CoMo-Al ₂ O ₃)	1.0	0	5.0	1.6	9.4
J (Co-Al ₂ O ₃)	0.1	0	0	6.6	0
K (Mo-Co-Al ₂ O ₃)	2.7	0	0	5.1	4.5
L (MoO ₃)	18.1	0	22.1	20.1	64.2

^a Number of *n*-butylamine molecules consumed by 1000 Å² of the surface of the samples; the values are reproducible to about ±0.8.

can be noted from the data. (1) Strong-acid sites are generated when MoO_3 is deposited on alumina (compare samples A and H or B and C) in agreement with the results of Kiviat and Petrakis.² (2) When MoO_3 is supported on alumina, the absence or presence of Na^+ ions (samples H and C, respectively) does not alter significantly the concentration of the strong-acid sites ($\text{p}K_a < -5.6$). Weak-acid sites, however, are suppressed in the presence of Na^+ ions. (3) $\text{Co-Al}_2\text{O}_3$ samples do not contain strong-acid ($\text{p}K_a < -5.6$) sites (samples D and J). (4) When Co and Mo salts are impregnated simultaneously (samples G and I), both strong and medium acidities ($2.0 > \text{p}K_a > -5.6$) are suppressed by the presence of Na^+ . Alkali ions actually increase the proportion of weak-acid sites ($5 > \text{p}K_a > 3.3$). It is possible that some of the strong-acid sites are converted to weaker ones in the presence of Na^+ . (5) The sample obtained by depositing MoO_3 "on top" of preimpregnated Co (sample E) contains a larger number of strong-acid sites than the one wherein MoO_3 had been deposited first (sample F). (6) The last and what we consider to be the most significant point is the following. In the absence of Na^+ , the $\text{CoMo-Al}_2\text{O}_3$ catalyst is more acidic than $\text{Mo-Al}_2\text{O}_3$ (samples I and H). When Na^+ is present, however, they have similar acidic properties (samples G and C). In other words, the interaction between the cobalt and molybdenum moieties to generate strong-acid sites is inhibited by the Na^+ concentration of the alumina support. These results lend additional support to our earlier findings³ that in the $\text{Co-Mo-Al}_2\text{O}_3$ system, not only is there a structural interaction between the cobalt and molybdenum constituents but also the nature of this interaction itself is a function of the structural features of the support. Thus, all three constituents (Co, Mo, and Al_2O_3) form a true interacting system and it is not possible to discuss the nature of any one of them without reference to the other two.

Acknowledgment. We thank Drs. M. G. Krishna and K. K. Bhattacharya for encouragement and support.

References and Notes

- (1) F. E. Kiviat and L. Petrakis, *J. Phys. Chem.*, **77**, 1232 (1973).
- (2) A. E. Hirschler and A. Schneider, *J. Chem. Eng. Data*, **6**, 313 (1961).
- (3) (a) P. Ratnasamy, R. P. Mehrotra, and A. V. Ramaswamy, *J. Catal.*, **32**, 63 (1974); (b) P. Ratnasamy, A. V. Ramaswamy, K. Banerjee, D. K. Sharma, and N. Ray, submitted for publication in *J. Catal.*

India Institute of Petroleum
Dehradun (U. P.), India

P. Ratnasamy*
D. K. Sharma
L. D. Sharma

Received March 20, 1974

sion of the merits and limitations of the "indicator titration" method utilized by the authors, but rather we simply refer to the recent review article by Forri⁴ on the subject.

What is interesting are the additional data provided by these authors on the complexity of the system and the undisputed profound effects that dopants can have on the surface characteristics of Al_2O_3 .

It is pleasing, of course, that Ratnasamy and coworkers find, in agreement with our work,¹ that strong-acid sites are generated when MoO_3 is incorporated in alumina. However, one must be very careful in making comparisons, especially when the levels of dopant substitution and manner of preparation are not precisely defined. In a series of papers⁵⁻⁹ Petrakis and coworkers have demonstrated and quantified aspects of the vital role that the levels of MoO_3 substitution and pretreatment of the system have on the surface properties.

For example, it has been shown that the distribution of molybdenum valences depends importantly on the amount initially incorporated. Low levels of MoO_3 favor Mo(V), while at higher levels the Mo(V) is quenched in favor of Mo(IV) and Mo(VI). In fact, there is a dramatic decrease in the Mo(V) levels in going from 9% MoO_3 to the 12.5% MoO_3 utilized by the authors of the above communication.⁵ Thus, if it is assumed that molybdenum plays a critical role in the modification of the host surface, the distribution of molybdenum among the various valences and the type of sites they occupy are bound to have a determining effect on the observed surface modifications. Similar results have been obtained⁸ on the dependence of the distribution of the molybdenum species on the nature of host (alumina) and temperature and time of pretreatment. Thus, we reach the conclusion that cross-system comparisons must be made with the utmost care.

Another factor not considered by Ratnasamy, *et al.*, in comparing their results to those presented in ref 1 is that the alumina substrates differed. It is known that pyridine adsorbs differently on γ , η -, and δ -alumina surfaces, the differences being ascribed to differences in the numbers and relative strengths of the Lewis acid sites.¹ An investigation of MoO_3 supported on both an η - and δ -alumina indicated that these differences are maintained in the presence of Mo.¹ Hence, a quantitative comparison of surface acidities of systems where the substrate differs is subject to inherent differences in results.

Finally, with respect to the above authors' claim that in the absence of Na^+ the $\text{Co-Mo-Al}_2\text{O}_3$ catalyst is more acidic than the $\text{Mo-Al}_2\text{O}_3$, it must be said that that situation could occur without necessarily contradicting our earlier observations. Given the demonstrated great sensitivity of the systems on the factors discussed earlier, the same caution must be exercised in comparing ternary systems. As to the relative capacity of sodium and cobalt to quench the molybdenum-induced acidic sites of the host material, only a very careful series of experiments designed in the context discussed here could delineate that point.

References and Notes

- (1) F. E. Kiviat and L. Petrakis, *J. Phys. Chem.*, **77**, 1232 (1973).
- (2) J. H. Ashley and P. C. H. Mitchell, *J. Chem. Soc. A*, 2730 (1969).
- (3) J. M. J. G. Lipsch and G. C. A. Schit, *J. Catal.*, **15**, 174 (1969).
- (4) L. Forri, *Catal. Rev.*, **8**, 65 (1973).
- (5) K. S. Seshadri and L. Petrakis, *J. Phys. Chem.*, **74**, 4102 (1970).
- (6) L. Petrakis, *et al.*, paper presented at the 165th National Meeting of the American Chemical Society, Dallas, Tex., April 1973; to be submitted for publication in *J. Phys. Chem.*

Surface Acidity of Modified Alumina

Publication costs assisted by Gulf Research and Development Company

Sir: The preceding communication by Ratnasamy, *et al.*, presents some very interesting data pertaining to the effect of compositional and preparational factors on the acidity of $\text{Co-Mo-Al}_2\text{O}_3$ systems. Their results are not surprising and they are in general agreement with other findings.¹⁻³ This communication is not the appropriate vehicle for a discus-

- (7) L. Petrakis and K. S. Seshadri, *J. Phys. Chem.*, **76**, 1443 (1972).
 (8) K. S. Seshadri and L. Petrakis, *J. Catal.*, **30**, 195 (1973).
 (9) L. Petrakis and K. S. Seshadri, to be submitted for publication in *J. Phys. Chem.*

Gulf Research and Development Company
 Pittsburgh, Pennsylvania 15230

L. Petrakis*
 F. E. Kiviat

Received April 19, 1974

2537-Å Mercury-Sensitized Photochemical Decomposition of Perfluorocyclobutane

Publication costs assisted by The Robert A. Welch Foundation

Sir: The decomposition of perfluorocyclobutane, $c\text{-C}_4\text{F}_8$, has been studied by several methods including γ -radiolysis,¹ X-radiolysis,² Xe-sensitized photolysis,³ and hot ^{18}F atom recoil.^{4,5} We report some results of our work with 2537-Å mercury-sensitized decomposition of $c\text{-C}_4\text{F}_8$ for comparison.

The perfluorocyclobutane used was obtained from Peninsular ChemResearch, Inc., and further purified by bulb-to-bulb distillation until gas chromatograms showed no impurity peaks.

Irradiations (3-min) of $c\text{-C}_4\text{F}_8$ were carried out in a cylindrical 130 mm \times 20 mm o.d. quartz vessel at pressures ranging from 100 to 105 Torr and at a temperature of $43 \pm 1^\circ$. These conditions gave an overall decomposition of $5.6 \pm 1.9\%$. During irradiations, the reaction vessel was inserted within the coils of a Hanovia low-pressure mercury-resonance lamp of spiral configuration. The lamp intensity was determined by potassium ferrioxalate actinometry to be 2.8×10^{18} quanta sec^{-1} .

The products were analyzed on a Beckman GC72-5 gas chromatograph equipped with thermal conductivity detectors. A standard four stopcock by-pass loop injection system between a high vacuum manifold and the gas chromatograph was used for direct injection of the products from a given sample; therefore, only the volatile products from a given sample were analyzed in this work. The additional material not accounted for in the material balance was assumed to be nonvolatile polymeric material since a white residue was observed in the photolysis vessel following irradiations of longer than 3 min. Two columns were employed in the analysis: a KELF No. 3 oil on Chromosorb W for lower molecular weight products (<250 molecular weight) and a squalane on Chromosorb P column, temperature programmed, for higher molecular weight products.

The identification of low molecular weight products CF_4 , C_2F_6 , C_3F_8 , $n\text{-C}_4\text{F}_{10}$, and $c\text{-C}_4\text{F}_8$ was by comparison of retention times with reference gases. Our column does not separate perfluoropropene and perfluorocyclopropane; however, the mass spectral pattern of the peak eluting at this retention time was in reasonable agreement with that of the main product of 2537-Å mercury-sensitized photolysis of C_2F_4 , which is reported to be perfluorocyclopropane,⁶ and with the mass spectral pattern of perfluorocyclopropane reported by Fallgatter and Hanrahan.¹ In addition, since all other identified products in this work are saturat-

TABLE I: Products and Yields from 2537-Å Mercury-Sensitized Photolysis of $c\text{-C}_4\text{F}_8$

Product	Relative yield ($c\text{-C}_4\text{F}_8 = 100$)
CF_4	0.170 ± 0.018
C_2F_6	0.147 ± 0.018
C_3F_8	0.072 ± 0.005
$c\text{-C}_3\text{F}_8$	0.016 ± 0.004
$n\text{-C}_4\text{F}_{10}$	0.029 ± 0.006
$\text{CF}_3\text{-}c\text{-C}_4\text{F}_8$	0.713 ± 0.042
$\text{C}_2\text{F}_5\text{-}c\text{-C}_4\text{F}_8$	0.328 ± 0.022
$c\text{-C}_4\text{F}_7\text{-}c\text{-C}_4\text{F}_7$	0.629 ± 0.048
12 additional high molecular weight products	0.135

ed compounds, we have tentatively identified the C_3F_6 as the ring compound.

The higher molecular weight products perfluoromethylcyclobutane ($\text{CF}_3\text{-}c\text{-C}_4\text{F}_7$), perfluoroethylcyclobutane ($\text{C}_2\text{F}_5\text{-}c\text{-C}_4\text{F}_7$), and perfluorobicyclobutyl ($c\text{-C}_4\text{F}_7\text{-}c\text{-C}_4\text{F}_7$) were trapped out from the gas chromatograph effluent and analyzed mass spectrometrically. The identity assignments of $\text{CF}_3\text{-}c\text{-C}_4\text{F}_7$ and $\text{C}_2\text{F}_5\text{-}c\text{-C}_4\text{F}_7$ are tentative, since no comparison mass spectra or supplementary analysis was available; however, these assignments are reasonable based on the characteristics of perfluorocarbon mass spectra given by Majer⁷ (e.g., the highest mass peaks observed are the m/e 231(C_5F_9^+) and m/e 281($\text{C}_6\text{F}_{11}^+$), respectively, and both compounds exhibit additional m/e peak yields resembling that of $c\text{-C}_4\text{F}_8$). The identification of perfluorobicyclobutyl was based on a close agreement of the mass spectra with that reported by Banks, *et al.*⁸

Individual product yields were normalized to the residual $c\text{-C}_4\text{F}_8$ and are reported as relative yields in Table I. The CF_4 and C_3F_8 yields have been corrected for relative thermal conductivity by direct calibration, whereas C_3F_6 and $n\text{-C}_4\text{F}_{10}$ yields were corrected with the use of data from Askew, *et al.*⁹ All products of higher molecular weight than $c\text{-C}_4\text{F}_8$ were assumed to have the same thermal conductivity as $c\text{-C}_4\text{F}_8$. The imprecision reflects one standard deviation. Individual relative yields for the 12 higher molecular weight products (grouped together in Table I) were all less than 0.025.

As shown in Table I, we observed only saturated products to be produced (C_2F_4 , *cis*- and *trans*- $2\text{-C}_4\text{F}_8$, $c\text{-C}_4\text{F}_6$, and $1,3\text{-C}_4\text{F}_6$ are all separated on our columns) with 75% of the product yield accounted for by the CF_3 , C_2F_5 , and $c\text{-C}_4\text{F}_7$ derivatives of the parent $c\text{-C}_4\text{F}_8$. The fact that we observed only saturated products does not preclude the possibility of the transient formation and subsequent loss through internal radical scavenging of unsaturated products, although a series of irradiations in which the irradiation time was successively decreased to 5 sec produced no change in the product distribution within experimental error. Preliminary experiments with added isobutene scavenger, however, show the higher molecular weight products to be removed, indicating at least in part a mechanism of radical recombination. These results are similar to previously reported radiolysis results,^{1,2} although Davenport and Miller report *trans*- C_4F_8 as the major product in Xe-sensitized photolysis of $c\text{-C}_4\text{F}_8$.³ More quantitative scavenging experiments are being carried out in an attempt to determine the distribution of primary radical precursors indicated in this system.

Acknowledgments. We are grateful to Dr. L. B. Sims of the University of Arkansas for continued encouragement and counsel throughout the course of this study, for helpful suggestions regarding this communication, and for assistance with mass spectral analyses. We also wish to thank Dr. B. C. Musgrave of the Idaho Nuclear Corporation for suggesting this work, Dr. R. J. Hanrahan of The University of Florida for the use of his laboratory facilities for preliminary experiments, and Dr. C. G. Venier of Texas Christian University for assistance with mass spectral analyses. We are especially grateful to G. W. Beall¹⁰ for the mercury resonance lamp intensity measurements, and to G. K. Rogan¹⁰ and J. P. McAlister¹⁰ who did much of the preliminary work of establishing our research facilities. We gratefully acknowledge the support of this research by The Robert A. Welch Foundation for a generous grant, and the partial support of Tarleton State University for a Faculty Research Grant.

References and Notes

- (1) M. B. Fallgatter and R. J. Hanrahan, *J. Phys. Chem.*, **69**, 2059 (1965).
- (2) E. Heckel and R. J. Hanrahan, *Advan. Chem. Ser.*, No. **82**, 120 (1968).
- (3) J. E. Davenport and G. H. Miller, *J. Phys. Chem.*, **73**, 4430 (1969).
- (4) C. F. McKnight and J. W. Root, *J. Phys. Chem.*, **73**, 4430 (1969).
- (5) T. C. Hinkson, Ph.D. Thesis, The University of Arkansas, Fayetteville, Ark., 1970.
- (6) B. Atkinson, *J. Chem. Soc.*, 2684 (1952).
- (7) J. R. Majer, *Advan. Fluorine Chem.*, **2**, 55 (1961).
- (8) R. E. Banks, K. Mullen, and G. E. Williamson, *J. Chem. Soc.*, 2608 (1968).
- (9) W. C. Askew, T. M. Reed, III, and J. C. Mailen, *Radiat. Res.*, **33**, 285 (1968).
- (10) Robert A. Welch Undergraduate Scholar.

*Department of Chemistry
Tarleton State University
Stephenville, Texas 76402*

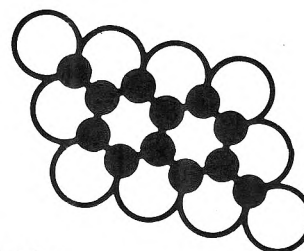
**Rodney L. Cate¹⁰
T. C. Hinkson***

Received March 18, 1974

Highly Recommended!

NEW TECHNICAL BOOKS
JOURNAL OF INORGANIC &
NUCLEAR CHEMISTRY
and other leading scientific
and technical journals

COMPREHENSIVE INORGANIC CHEMISTRY



The Editorial Board:

J C BAILAR Jr - Urbana

H J EMELEUS FRS - Cambridge

†Sir Ronald NYHOLM FRS - London

A F TROTMAN - DICKENSON - Cardiff (Executive Editor)

INDEPENDENT OPINION

"Highly Recommended" by CHOICE, which wrote, "Since the length and cost are not prohibitive, this set of books should be well within the budget of most libraries. Not only will professional chemists find these books useful but students and other readers will find them a valuable reference source. These should be in every graduate and undergraduate library, as well as industrial libraries. Many professional may even consider them for their personal libraries."

NEW TECHNICAL BOOKS asserts "the work deserves a place in all general science collections."

LEADING SCIENTISTS AGREE!

"a highly commendable collection of material which will be valuable to chemists of all kinds" commented Professor Sir Harold W. Thompson, F.R.S., Oxford.

"will undoubtedly remain the standard first source of information in this area for many years to come," wrote Prof. N.N. Greenwood, F.R.I.C., Leeds. Prof. C.C. Addison, F.R.S., concurs, "quite remarkable, in that they can justifiably claim to be comprehensive, yet at the same time remain interesting and readable; they are probably unique in this respect."

COMPREHENSIVE INORGANIC CHEMISTRY

Is the most modern and authoritative standard work and guide to research in Inorganic Chemistry published in a complete and readily accessible format. The physical basis of chemistry is emphasized throughout the 5 volumes. It includes contributions by 71 of the world's most eminent research workers, industrial practitioners, and teachers in the chemical sciences. Arrangement is by Element, in accordance with the Periodic Table. Each article includes the History and Discovery of each Element, its Occurrence and Distribution, Production, Industrial Uses and Processes, Preparation of Pure Material, Allotropes, Nuclear Properties, Physical Properties, Chemistry, Chemical Properties, Analytical Chemistry, and Compounds. Extensive use is made of illustrations, diagrams, tables, and footnotes. Each volume is indexed separately and a Master Index to the entire work appears in Volume 5.

Over 6000 pages in 5 volumes
Sturdy library-standard bindings
New Printing Now Available

Complete \$ 500.00

Orders and Inquiries to:

PERGAMON PRESS, INC.
Maxwell House, Fairview Park
Elmsford, New York 10523

PERGAMON PRESS, LTD.
Headington Hill Hall
Oxford, OX3 0BW, England

To: PERGAMON PRESS

I wish to order ___ copies of COMPREHENSIVE INORGANIC CHEMISTRY, at \$500.00 each.

Payment enclosed (Pergamon to pay shipping)

Please bill me, I have an account.

Diners Club No. _____ Exp. _____

Send your 2-color brochure with an extensive description

Att: _____

City _____ State _____ Zip _____

NICOLET nmr data systems... for routine research problems and advanced applications

The Nicolet 1080 and NMR-80 data acquisition and analysis systems are in use worldwide in solving not only routine research problems but also in advancing the frontiers of nmr knowledge. These data systems are highly regarded for their timing accuracy, sensitivity, continuous display capabilities and general versatility in the conception and execution for new experiments. Some of these are:

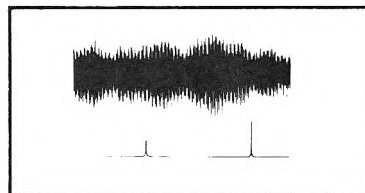
STOCHASTIC RESONANCE — This technique involves random noise modulation of the rf excitation frequency, leading to a broadband excitation whose response is measured and Fourier transformed much as in conventional pulsed-FT nmr. Its principal advantage lies in the fact that much less rf power is needed to excite the chemical shift range of interest and that it has the same Fellgett's advantage of FT nmr.

RAPID SCAN NMR — In this technique, a spectral region is swept at a rate much greater than allowed for by slow passage conditions and the resulting ringing spectrum correlated with a spectrum of a single ringing line or of a theoretical line. Its principal advantage lies in the ability to acquire data rapidly even in the presence of strong solvent lines, without requiring that these lines be part of the signal averaged data.

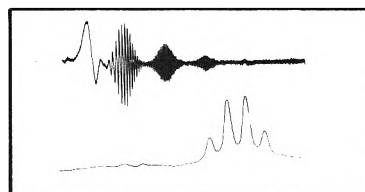
HOMOSPOIL T_1 SEQUENCE — This sequence allows the rapid measurement of long T_1 's without the long $5xT_1$ waiting period needed by the inversion-recovery sequence. It is accomplished by a $-(90\text{-spoil-}\tau\text{-}90\text{-sample-spoil})$ - sequence.

QUADRATURE DETECTION NMR — This technique allows $\sqrt{2}$ enhancement over conventional pulsed nmr since the rf carrier can be placed in the center of the spectral region and dual phase detectors used to receive the response. The two resulting free induction decays are Fourier transformed using a complex transform which results in a single frequency domain spectrum.

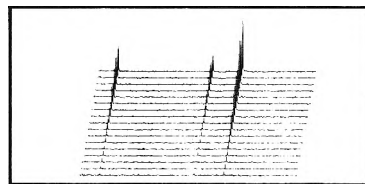
Please phone or write for details on these applications or to discuss how the versatile NMR-80 data system may be used for your experiments. Complete systems start at \$20,000. If you are already a Nicolet data system user, you may order free software for the above techniques from our Nicolet Users Society (NUS) library.



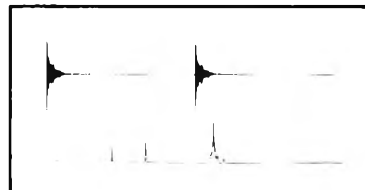
R. R. Ernst, *J. Mag. Res.* 3 10-27 (1970); R. Kaiser, *J. Mag. Res.* 3 28-40, (1970); J. Cooper and R. Addleman, 13th Experimental Nmr Conference (1972); E. Lippmaa, private communication.



J. Dadok and R. F. Sprecher, 13th and 14th Experimental Nmr Conferences (1972, 1973); E. Becker, paper in press.



J. L. Markley, W. J. Horsley and M. P. Klein *J. Phys. Chem.* 55 3604 (1971); R. Freeman and H. D. W. Hill, *Ibid.* 54 April (1971); G. G. McDonald and J. S. Leigh, Jr., *J. Mag. Res.* 9 358 (1973).



J. Schaeffer and E. O. Stejskal, 15th Experimental Nmr Conference (1974), and *J. Mag. Res.* March (1974) (in press); J. D. Ellett, et al., *Adv. Mag. Res.* 5 117 (1971)

**NICOLET
INSTRUMENT
CORPORATION**

5225 Verona Road
Madison, Wisconsin 53711
Telephone: 608/271-3333